Anthracene Based Colorimetric Molecular Sensors

Dissertation
zur Erlangung des mathematisch-naturwissenschaftlichen Doktorgrades
„Doctor rerum naturalium“
der Georg-August-Universität Göttingen

im Promotionsprogramm Chemie
der Georg-August University School of Science (GAUSS)

vorgelegt von Sebastian Wandtke
aus Zweibrücken

Göttingen, 2014

Betreuungsausschuss

Prof. Dr. Dietmar Stalke, Institut für Anorganische Chemie

Prof. Dr. Oliver S. Wenger, Department für Chemie der Universität Basel

Mitglieder der Prüfungskommission

Referent: Prof. Dr. Dietmar Stalke

Korreferent: Prof. Dr. Oliver S. Wenger

Weitere Mitglieder der Prüfungskomission

Prof. Dr. Konrad Koszinowski, Institut für Organische und Biomolekulare Chemie

Prof. Dr. Guido Clever, Institut für Anorganische Chemie

Prof. Dr. Dr. h.c. mult. Herbert W. Roesky, Institut für Anorganische Chemie

Dr. Michael John, Institut für Anorganische Chemie

Tag der mündlichen Prüfung: 15.12.2014

Danksagung

An erster Stelle danke ich meinem Betreuer Herrn Prof. Dietmar Stalke für die Begleitung und Unterstützung während meines Promotionsvorhabens. Die freie Ausgestaltung meines Arbeitens habe ich als große Chance gesehen, selbstständig Schwerpunkte zu setzten.
Danken möchte ich auch Herrn Prof. Oliver Wenger, der trotz seiner Berufung in die Schweiz nicht nur offiziell mein zweiter Betreuer blieb, sondern mir durch seine Expertise auf dem Gebiet der Lumineszenzspektroskopie viele generelle Fragen beantwortet, sowie Rückmeldung zu meinem Projekt gegeben hat.
Mein Dank geht auch an die weiteren Mitglieder meiner Prüfungskommission, die sich die Zeit genommen haben, meine Arbeit mit zu bewerten.
Dankbar bin ich Arne Visscher und David Dauer, die nicht nur die drei Jahre der Promotion meine Laborkollegen waren, sondern auch Korrekturen zu weiten Teilen dieser Arbeit vorgeschlagen haben. Neben Kollegen sind sie mir einfach zu Freunden geworden. Die praktische Arbeit im Labor ging einher mit der Betreuung von Bachelor- (Benjamin und Jerome) und Masterstudenten (Roman und Julian), sowie einer Auszubildenden (Julia). Bei diesen Helfern bedanke ich mich für ihre Zeit und ihr Engagement, das zum Gelingen dieses Projektes beitrug.
An dieser Stelle möchte ich dem gesamten Arbeitskreis Stalke für die kollegiale Atmosphäre und die allgegenwärtige Hilfsbereitschaft danken. Die Offenheit und Bereitschaft, Wissen weiterzugeben haben eine Einarbeitung in komplexe Zusammenhänge sehr erleichtert. Gerade auf dem Gebiet der Röntgenbeugung hatten erfahrene Kollegen immer Zeit zu helfen, zu erklären und zu vermitteln.
Ich danke Thomas Niklas für die Hilfe bei Durchführung und Auswertung von NMR Experimenten, sowie das Anmerken von Korrekturen zu dieser Arbeit. David Engelhard danke ich für die Unterstützung bei der Aufnahme von UV/Vis Spektren und die anregende Diskussion über dessen theoretische Grundlagen.
Zuletzt möchte ich meiner Frau Claudia für ihre Unterstützung während der Promotionszeit danken. Ihr offenes Ohr und ihre einfühlsame Begleitung auf der einen Seite und ihre ehrlichen kritischen Anmerkungen durch Korrekturen zu dieser Arbeit auf der anderen Seite zeigen mir, welch großes Glück ich mit einer solchen Frau an meiner Seite habe.

Table of Contents

List of Abbreviations

Å	Ångström
A_λ	absorbance at a certain wavelength
cf.	lat. *confer* meaning "compare" or "consult"
CIP	nomenclature for stereogenic center based on CAHN, INGOLD and PRELOG
conc.	concentrated
cps	counts per second
δ	chemical shift
DCM	dichloromethane
EET	electronic energy transfer
EI	electron ionization
eq.	equivalent(s)
ESI	electrospray ionization
FRET	fluorescence resonance energy transfer
HOMO	highest occupied molecular orbital
Hz	Hertz
I	intensity (detected)
I_0	intensity of incoming beam
ICT	intramolecular charge transfer
λ	wavelength
λ_{det}	detected wavelength
λ_{ex}	excitation wavelength
lg	logarithm to the base 10
LUMO	lowest unoccupied molecular orbital
M	molar
MeCN	acetonitrile
MeOH	methanol
MLCT	metal-ligand charge transfer
MS	mass spectrometry
m/z	mass/charge
NMR	nuclear magnetic resonance
Ns	nosyl
OLED	organic light emitting diode
OTs	tosyl
PET	photoinduced electron transfer
Pg	protection group
pK_A	negative lg of the acid dissociation constant
PMDTA	pentamethyldienthylene-triamine
ppm	parts per million
SES	*β*-trimethylsilyl-ethanesulfonyl
THF	tetrahydrofuran
TICT	twisted intramolecular charge transfer
TMEDA	tetramethylethylenediamine
ῡ	wavenumber
v. s.	lat. *vide supra* meaning "see above"

1 Introduction

1.1 Luminescence

The first written report of a luminescent appearance was handed down by the Spanish physician and botanist NICOLÁS BAUTISTA MONARDES.[1] His *Historica Medicinal* was translated in 1574 by CHARLES DE L'ÉCLUSE into Latin, a few years after the completion of its Spanish original.

This translation coined the name of a luminescent material that was discussed by scientists for centuries. The wood *lignum nephriticum* was used by the Aztecs as medicine long before the Spanish arrived in Central America. MONARDES reported in his book that an aqueous infusion of this wood can be used to treat kidney and urinary diseases.[2]

Figure 1-1: Images displaying the luminescent infusions of *lignum nephriticum*.[3,1]

The left part of Figure 1-1 displays an image published in 1915, which depicts the luminescence of an infusion of *lignum nephriticum* with its typical blue color. Indeed, the manufacture of a cup, made of this special wood around 1646, is reported "*which would color water poured into it a deep blue*"[4]. A modern photo is displayed in the right part of Figure 1-1 and shows also the blue luminescent radiation at the surface of the solution.

MONARDES recommended the preparation of such an infusion and mentioned interesting observations:[2]

> *"They take the wood and make slices of it as thin as possible, and not very large, and place them in clear spring water, that must be very good and transparent, and they leave them all the time the water lasts for drinking. Half an hour after the wood was put in, the water begins to take a very pale blue colour, and it becomes bluer the longer it stays, though the wood is of white colour"*

Especially the last sentence is noticeable, since it points towards an unusual process aside from a simple coloring of water by usage of a dye. This, with the knowledge of that time, not explainable process was investigated in the 17th century by famous scientists like BOYLE[5] and NEWTON[6] but they were also not able to explain the ongoing phenomenon properly. NEWTON, for example, reported that infusions of *lignum nephriticum* belong to "*substances apt to reflect one sort of light and transmit another*"[7].

It took around 450 years from the first reported luminescent observation of *lignum nephriticum* until 2009 a research group, also from Spain, published detailed information about the species responsible for that luminescence.[8] For instance, the structure of the emitting species was determined by NMR spectroscopy. Furthermore, a proposed formation out of a, in the wood naturally occurring, precursor by an oxidation reaction was recognized.

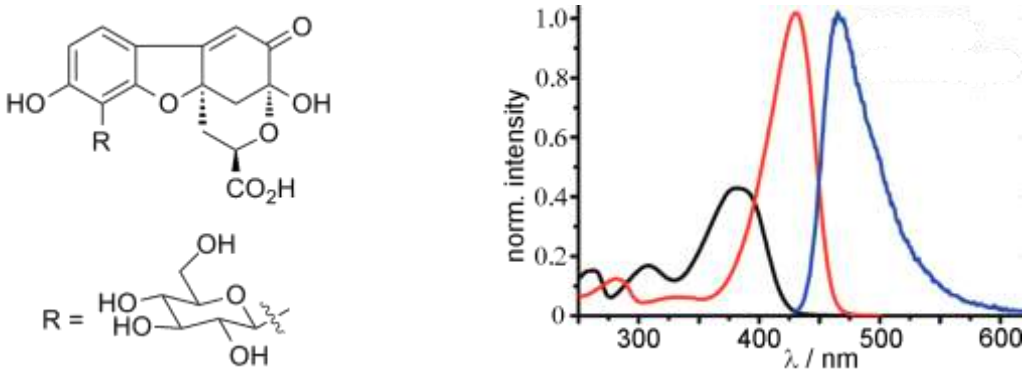

Figure 1-2: Left: Structure of the luminescent component (oxidized) of *lignum nephriticum*. Right: Normalized absorption (red) and emission (blue) spectra of the luminescent component as well as absorption of the non-oxidized precursor (black).[8]

The absorptive properties of the natural precursor (black) as well as the absorption (red) and emission (blue) characteristics of the resulting luminescent component were investigated and are displayed in the right part of Figure 1-2. While the precursor exhibits absorption but no luminescence, the oxidation product (Figure 1-2 left) is strongly luminescent and emits radiation with a wavelength of around 466 nm.

The today quite well elaborated description of emission processes after absorption of photons dates back to the work of HERSCHEL[9], STOKES[10] and other scientists of the 19th century, who established the basic concepts of fluorescence as well as the term itself.[11] In 1888 the German physicist and science historian EILHARD WIEDEMANN coined with the term *luminescenz* a predecessor of today's umbrella term for fluorescence and phosphorescence.[1]
Despite of known exceptions (e.g. persistent luminescence[12]), the qualitative distinction between fluorescence and phosphorescence by the lifetime of their excited states is in general valid. The typical time a photon takes to be absorbed by a chromophore is with around 10^{-15} s orders of magnitudes faster than numerical benchmarks for fluorescence (10^{-6}-10^{-9} s) or even phosphorescence (10^{-3}-100 s).[13]
These processes of absorption and emission are often displayed in a JABLOŃSKI[14] diagram, named after the prominent researcher in the field of fluorescence ALEKSANDER JABLOŃSKI. An example is shown in Figure 1-3.

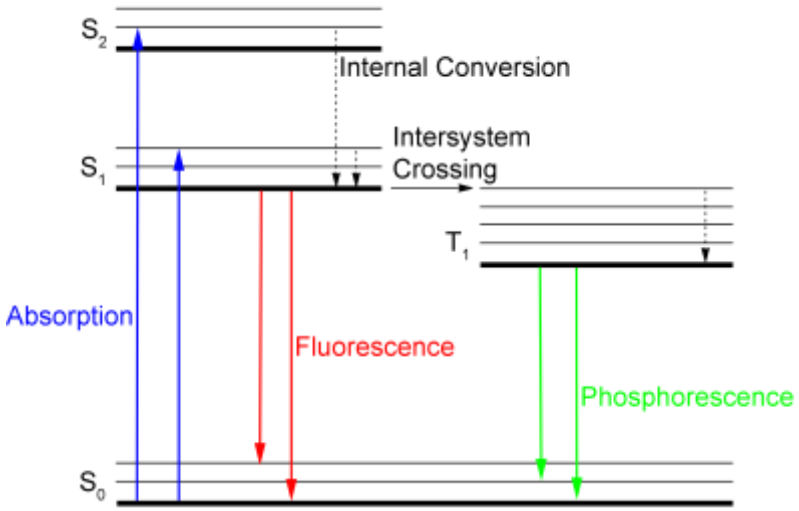

Figure 1-3: JABLOŃSKI diagram covering basic absorption and emission processes.

This visualized description is an intuitive representation of photoluminescence. Excitation occurs from the electronic ground state (S_0) to an electronically excited state (in this example S_1 or S_2) by absorption of a photon with an energetically suitable wavelength. Internal conversion is in general the subsequent process and means a thermal relaxation of excited vibrational states (thinner horizontal lines in Figure 1-3) to their ground state in the S_1 level. The radiative deactivation of this state is called fluorescence and accompanied with emission of a photon. The wavelength of this photon is typically longer than the one of the exciting photon. This phenomenon is called STOKES shift and is named after Sir GEORGE GABRIEL STOKES, a pioneer in the description of fluorescence processes.[15]
Another possibility for an electronically excited state is intersystem crossing. The excited molecule undergoes a change of its spin multiplicity and the first excited triplet state T_1 is populated. The relatively long lifetime of this state is caused by the spin-forbidden relaxation to the electronic ground state.[16] This radiative relaxation is called phosphorescence.

To understand which potential transitions are observable, a quantum mechanical interpretation of the FRANCK-CONDON[17] principle concerning the absorption of photons has to be considered. An exemplary depiction is shown in Figure 1-4.

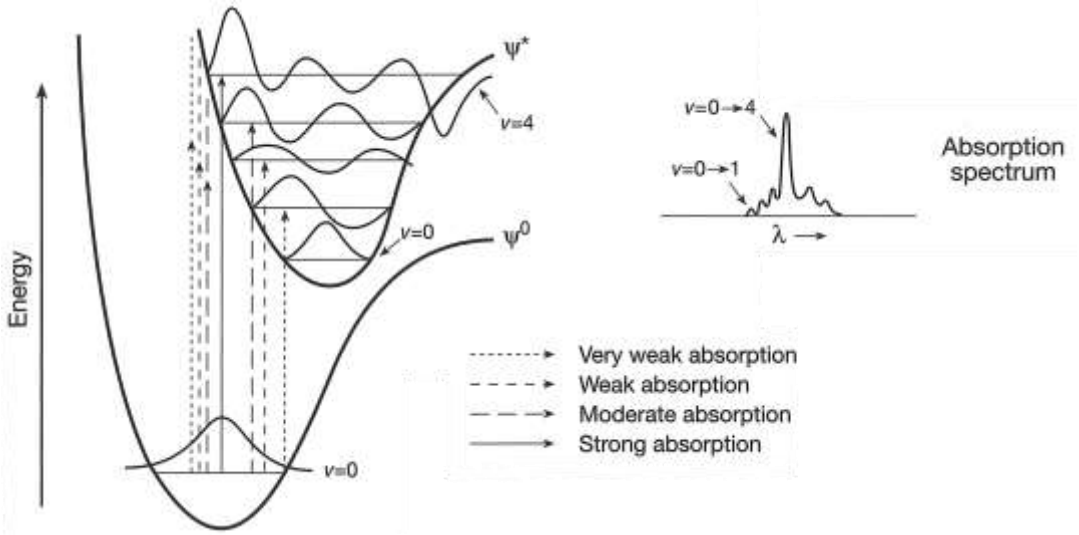

Figure 1-4: Quantum mechanical FRANCK-CONDON interpretation concerning absorption of light with associated absorption spectrum.[18]

Potentials of two anharmonic oscillators are displayed in the left part of Figure 1-4 corresponding to the electronic ground state (Ψ^0) and electronically excited state (Ψ^*). In Ψ^0 only one vibrational state is depicted, because the majority of the molecules is in this state at room temperature before excitation. In contrast, five vibration states of Ψ^* are shown, because excitation occurs to several states. The appropriate wave function is illustrated at each vibrational state. The probability of transitions is determined by the overlap integral of the wave functions of the initial state and the final state. For example, the vibronic transition from the electronic and vibrational ground state to the electronically and vibrationally excited state v = 4 results in strong absorption (solid arrow), because the values of the wave function are large in both states. It is important to note, that transitions can occur only vertical according to the FRANCK-CONDON principle.[18]

For emission processes, an analog picture could be presented. Again, the probability of a transition is determined by the wave functions of the initial and final states. The main difference is that emission occurs only from the vibrational ground state of Ψ^* (because of the rapid internal conversion) to various vibrational states of Ψ^0.

1.2 Anthracene

Polycyclic aromatic hydrocarbons and their fluorescent behavior are known for a long time. Anthracene is one member of this class and was discovered in the first half of the 19th century.[19] The reactive positions of this derivative were recognized early as well as the molecular formula but the idea about the bonding situation, especially in the middle anthracene ring, evolved over the years.

Figure 1-5: Structural ideas of 9-bromo-10-methylanthracene. Left: concept from 1926.[20] Right: current concept.

In former times the 9- and 10-position were believed to be linked by a direct bond (Figure 1-5 left), because these positions exhibit a chemical behavior reminiscent to a double bond. For instance, the reaction of anthracene and elemental bromine leads to an addition of bromine in the opposing positions. The subsequent elimination of hydrobromic acid restores the conjugated π-system of the six-membered ring.[21] This bromination by an addition/elimination mechanism is found for double bonds[22] but not in aromatic compounds like benzene.

After its discovery, the luminescence properties of anthracene have been studied intensively and its capability as a fluorophore was recognized.[23] The emission and absorption properties are displayed in the left part of Figure 1-6.

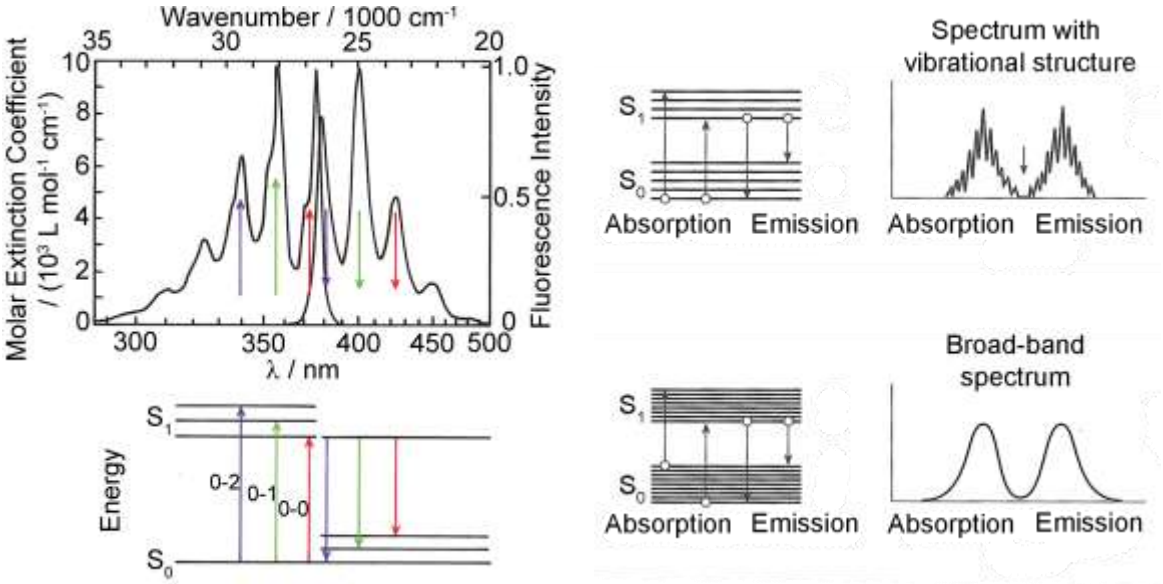

Figure 1-6: Left: Absorption and emission of anthracene with corresponding energetic states [24] (modified). Right: Influence of the energetic spacing between vibrational states on appearance (top) or absence (bottom) of vibrational structured emission and absorption bands.[25]

This representation enables an easy assignment between the observed peaks of the absorption and emission spectra (above) with the associated transition in the simplified JABLOŃSKI diagram (below). Every resolved peak belongs to an absorptive (upwards pointing arrows) or fluorescent transition (downwards pointing arrows). The emission spectrum looks like a mirror image of the absorption spectrum. This observation is valid for the majority of investigated fluorophores and is known as the mirror image rule.[24] It is also true for the luminescent compound of *lignum nephriticum* displayed in Figure 1-2. Besides this similarity, a fundamental difference

between these two discussed molecules can be found in the curve shape of their spectra. Anthracene exhibits a vibrational structured band, whereas *lignum nephriticum* shows just one broad band. The reason for these shapes can be found in the spacing of their vibrational states. Small energetic distances cause a broad band, whereas larger gaps induce the vibrational structured signals (Figure 1-6 right).

1.3 Luminescence sensors

During the last decades, luminescent materials were introduced to many fields of application (e.g. labeling[26], polymerization[27], OLEDs[28], microscopy[29]). One particular ongoing field of research has been the recognition of various target species (analytes) by systematic usage of derivatized fluorophores (sensors). Luminescence sensors change their emission properties in the presence of bonded analytes. To demonstrate the growing interest in this field and to point out the different used approaches, a search with the research discovery application *SciFinder*® was done and the results are displayed in Figure 1-7.

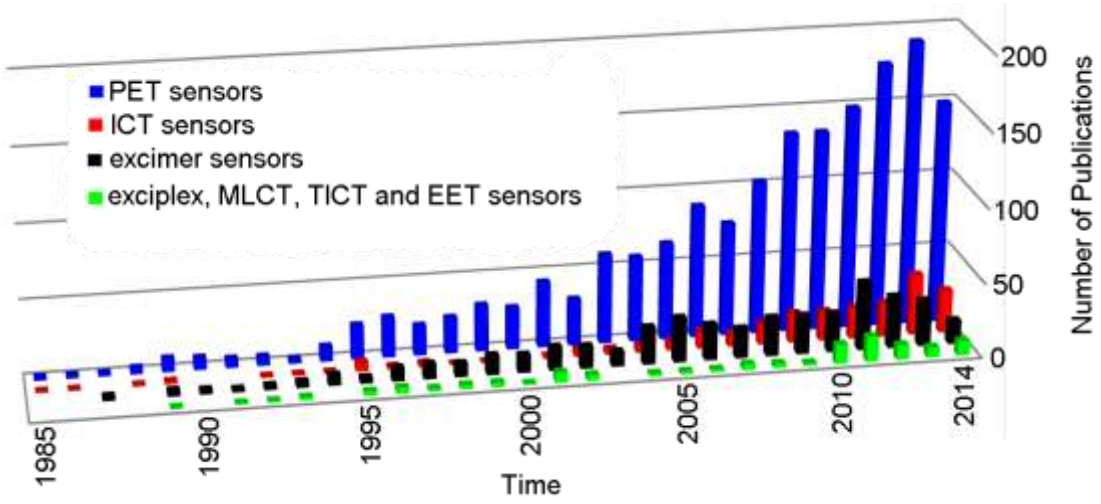

Figure 1-7: Results of a *SciFinder*® search covering the terms "PET sensor" (blue), "ICT sensor" (red), "excimer sensor" (black), as well as the summarized category of "exciplex sensor", "MLCT sensor", "TICT sensor", and "EET sensor" (green)(data collected at 17th September 2014).

The development of throughout the years established sensing mechanisms shows that the PET[30] (photoinduced electron transfer) effect is the most widespread principle for the construction of luminescent sensors (1675 publications found). But other mechanisms like the ICT[31] (intramolecular charge transfer, 238 pub.) or the

excimer formation[32] (435 pub.) show the same trend of increasing scientific effort. In addition, some areas with less published examples, for instance exciplex formation[33] (38 pub.), MLCT[34] (metal-ligand charge transfer, 30 pub.), TICT[35] (twisted intramolecular charge transfer, 24 pub.) or EET[36] (electronic energy transfer, 14 pub.) are known. This list includes the best known and explored sensing principles but is not a complete enumeration.[37]

A further important luminescent signaling mechanism is FRET (fluorescence resonance energy transfer). 1374 publications were found entering this search term. However, this is most likely an overestimating number, because in the area of protein research the term "FRET sensor" is sometimes related with the determination of distances or conformations in proteins.[38] Therefore, entries of this concept were not plotted in Figure 1-7. Nevertheless, numerous examples are known that use this principle for the detection of analytes.[39]

In the following sections, the most common luminescent sensing mechanisms (PET, ICT, excimer formation and FRET) are presented and their structural requirements as well as their functionality is explained. Furthermore, an in 2007 emerged mechanism called C=N isomerization is discussed.

1.3.1 Photoinduced electron transfer (PET)

The first recognition principle that comes in mind while thinking about detection of analytes via luminescence is the PET effect. Its manifold examples (Figure 1-7) are based on an electron transfer process.[40]

The ongoing processes can be illustrated with the help of a frontier orbital energy diagram (Figure 1-8). This includes the highest occupied molecular orbital (HOMO) and lowest unoccupied molecular orbital (LUMO) of the fluorophore as well as the HOMO* of the receptor (marked with a * for distinction) in their qualitative energetic arrangement.

When no analyte is bonded to the sensor (top), the HOMO* is located energetically between the HOMO and the LUMO of the fluorophore. After excitation, an electron of the non-bonded HOMO* is transferred to the HOMO and radiative relaxation from the LUMO to the HOMO cannot occur. The PET effect proceeds and only a poor luminescence is observed.

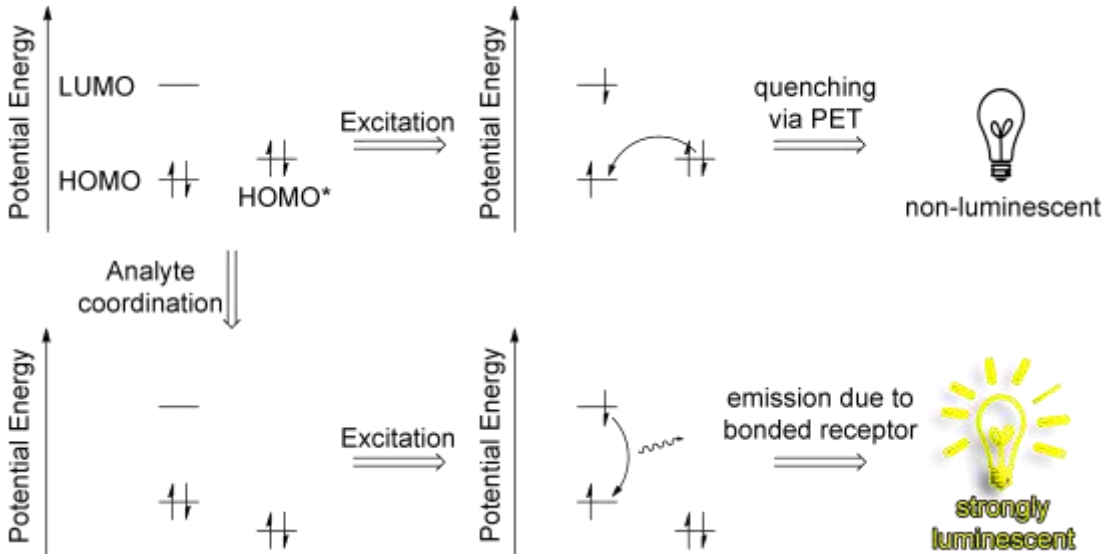

Figure 1-8: Energy diagram including the frontier orbitals of the fluorophore (HOMO, LUMO) and the receptor (HOMO*). Top: Feasible PET process. Bottom: Coordination of analytes suppresses the PET effect and enables luminescence.

The lower part of Figure 1-8 displays the situation when the electron pair of the receptor is involved in a bond to the analyte. This bonding decreases the energetic level of the HOMO*. Therefore, the PET is suppressed and emission can be detected.
A structural requirement of such a sensor is a spacer between the fluorophore and the receptor. This is demonstrated in an early publication of this field from 1988.[41]

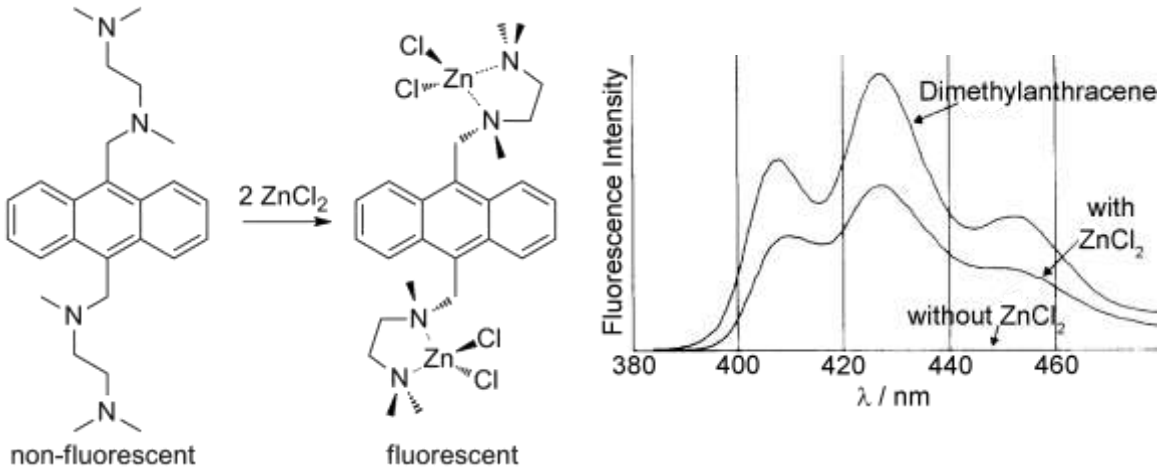

Figure 1-9: Proposed coordination of $ZnCl_2$ (left) and accompanied fluorescence spectra before and after addition of $ZnCl_2$ as well as the emission of 9,10-dimethylanthracene for comparison (right).[41]

In this example, the methylene spacer separates the anthracene fluorophore from the TMEDA-like receptor electronically. Hence, the PET effect proceeds and no fluorescent emission is observable in the absence of zinc chloride (Figure 1-9 right). The

picture changes upon addition of the mentioned metal salt. The TMEDA-derivatized anthracene restores its fluorescence by coordination of the zinc salt and becomes nearly as emissive as the reference compound 9,10-dimethylanthracene, where no PET effect was present. Although impressive for the date of publication, some, from a present-day perspective, interesting features were not investigated. For instance, the solvent in use was acetonitrile and no experiments in protic solvents like water were reported. The selectivity of the sensor would be interesting, too, testable by the usage of different other metal halides.

A variety of further PET sensors for cations[42], anions[43] or pH changes[44] was presented since this early example. Furthermore, so-called logic gates were introduced where the combination of different chemical inputs result in distinct luminescent outputs.[45] In 2005 a system for blood analysis was presented, which includes three fluorescence sensors for the detection of sodium, potassium and calcium cations.[46] There commercially available cassettes, called OPTI LION® and OPTI R®, are sold by the company *Optimedical Inc.* and reached in 2008 an estimated sales value of 50 million US$.[47]

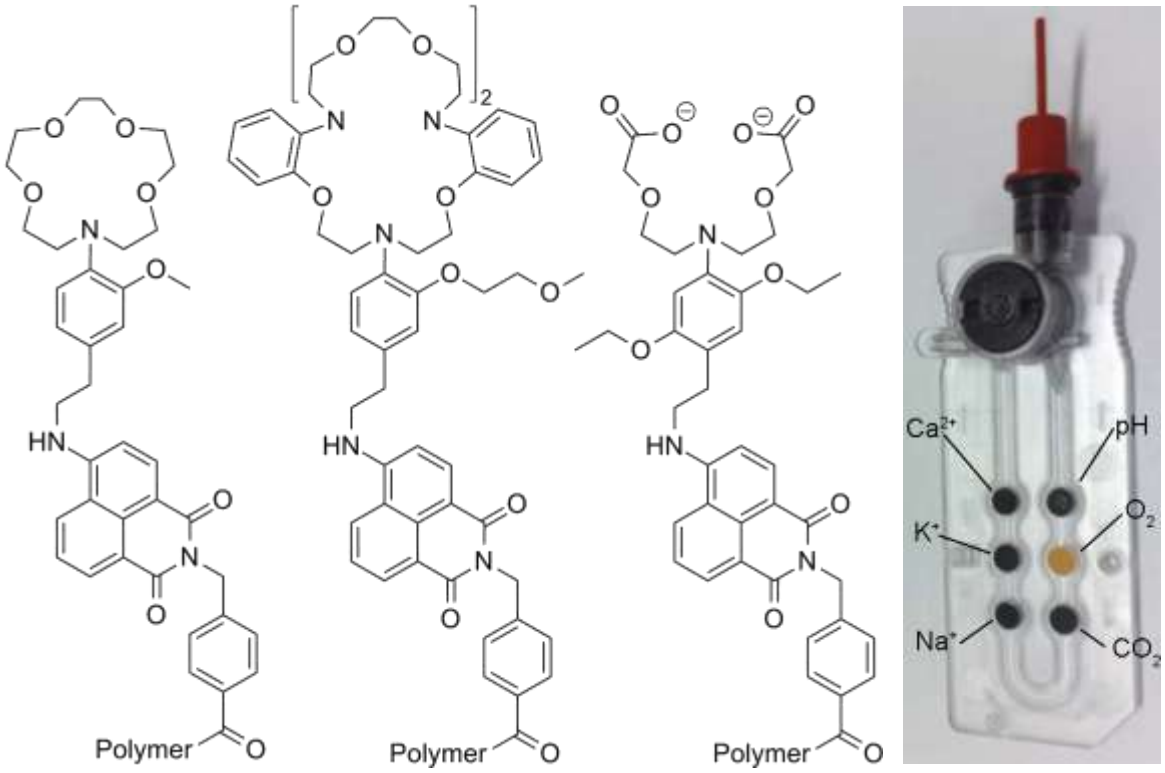

Figure 1-10: PET sensors for (from left to right) Na^+, K^+ and Ca^{2+} applied in the cassette OPTI R® (right), monitoring also the concentrations of protons, oxygen and CO_2 in blood.[46-47]

The sensors displayed in Figure 1-10 consist of a 4-aminonaphthalimide fluorophore that is covalently linked to a polymer. Additionally, different receptors are bonded to this fluorophore, electronically separated by an ethylene linker. The three sensors exhibit a selective and sensitive response to (from left to right) sodium, potassium and calcium ions. Typically in blood existing concentrations of these cations can be detected via a linear increase in fluorescence emission.[46] The examined blood can be used untreated, the red blood cells are filtered off by a polymer prior to the cassette and the almost colorless serum flows through the different immobilized sensors successively (Figure 1-10 right).

1.3.2 Intramolecular charge transfer (ICT)

Sensors, working on the basis of the ICT mechanism, exhibit clearly different dipole moments in their electronic ground state and their electronically excited state. Therefore, a charge transfer from one part of the molecule to another occurs after excitation of such chromophores. This influences the emission wavelength. A structural requirement for ICT sensors is that "*the fluorophore and the receptor share some critical atoms*"[48]. In contrast to sensors designed to work with the PET effect, ICT sensors must not have a spacer between the receptor and the fluorophore but a conjugated π-system is necessary for their performance.

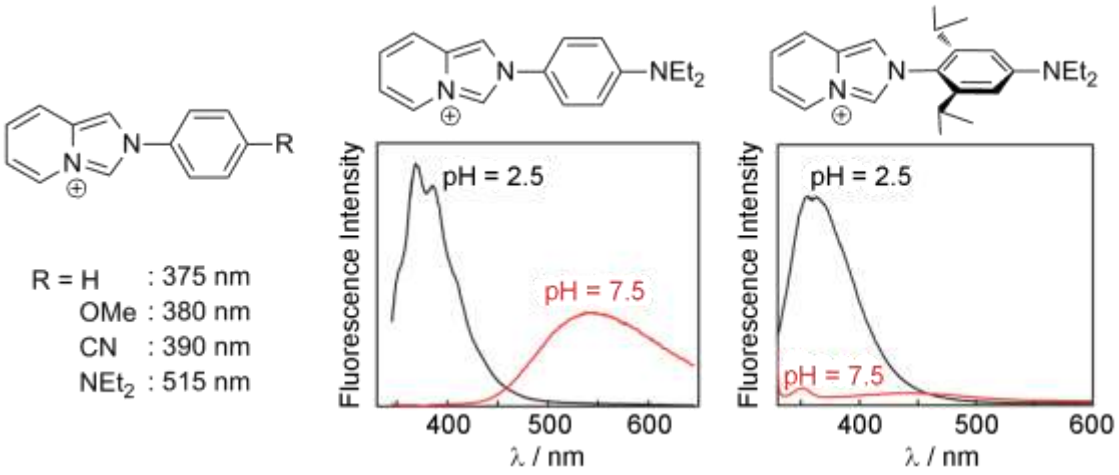

Figure 1-11: Left: Imidazo[1,5-*a*]pyridinium derivatives with corresponding emission maxima. Middle and right: Two examples and respective fluorescence spectra recorded at neural (pH = 7.5) and acidic (pH = 2.5) conditions.[49]

Both mentioned requirements are reflected in the fluorescence properties of imidazo[1,5-*a*]pyridinium ions published by ARON and coworkers in 2012.[49]
In the left part of Figure 1-11 one can recognize the structure of different imidazo[1,5-*a*]pyridinium ions with their fluorescence emission maxima. Noticeable is the large difference of the emission wavelength caused by the NEt_2 derivative compared to the other illustrated. Following the arguments of the authors, this shift is induced by an ICT-type transition. The charge transfer from the electron rich *N*-aryl unit to the electron deficient heterocycle causes this pronounced red shift. This is also reflected in the middle part of Figure 1-11 (red line). Upon protonation (black line), the charge transfer is hindered and the restored fluorescence is similar to that of derivatives without ICT. These findings allow the estimation, that the NEt_2 substituted derivative is a fluorescence sensor for protons.
In addition, a derivative bearing isopropyl groups in 2- and 6-position was prepared (Figure 1-11 right). Here, the fluorescence emission at neutral pH value (red line) exhibits no strong bathochromic shift but is barely detectable. In this case, the electronic conjugation between the fluorophore and the receptor is hampered by the steric demand of the isopropyl groups and the ICT does not proceed. Instead the PET effect leads to quenching of the emission. The twisted phenylene moiety acts as a spacer and so the regular PET assembly is present. Consequentially, protonation of this derivative disables the PET and emission is detectable around 360 nm like in the substances without electron or charge transfer.

1.3.3 Excimer formation

The formation of excited dimers (excimers) and their emission is known for a long time and was already reviewed 35 years ago.[50] This phenomenon is exemplified based on pyrene in Figure 1-12.
Lowering the concentration of pyrene results in a decrease of the signal around 480 nm, whereas the emission around 400 nm remains almost unchanged. In high concentrations (10^{-2} M till 10^{-3} M), pyrene forms an excimer that emits at higher wavelengths compared to its emission in low concentrations.

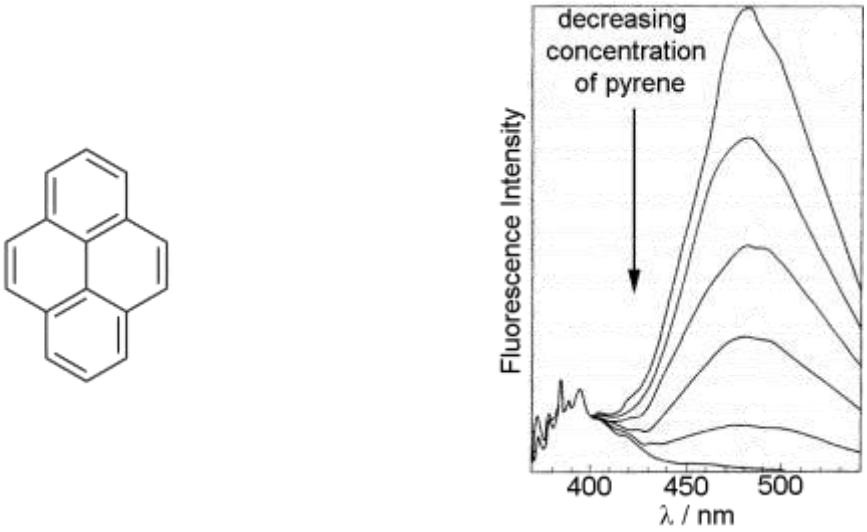

Figure 1-12: Structure (left) and emission of pyrene (right) with decreasing concentration (from top to bottom: 10^{-2} M, $7.75 \cdot 10^{-3}$ M, $5.5 \cdot 10^{-3}$ M, $3.25 \cdot 10^{-3}$ M, 10^{-3} M, 10^{-4} M) in cyclohexane.[51]

The reason for the fluorescence of excimers is the formation of an emitting species, "*produced by the collisional interaction of excited molecules and unexcited molecules*"[50].

Besides experimental results, the topic of excimer formation of aromatic hydrocarbons was explored by theoretical investigations, too.[52]

This formation of a new emitting species was transferred to the construction of luminescent sensors.[53] The formation or disintegration of excimers by coordination of analytes provides a sensing mechanism. For instance, the following pyrene derivative is capable to detect mercury ions.[54]

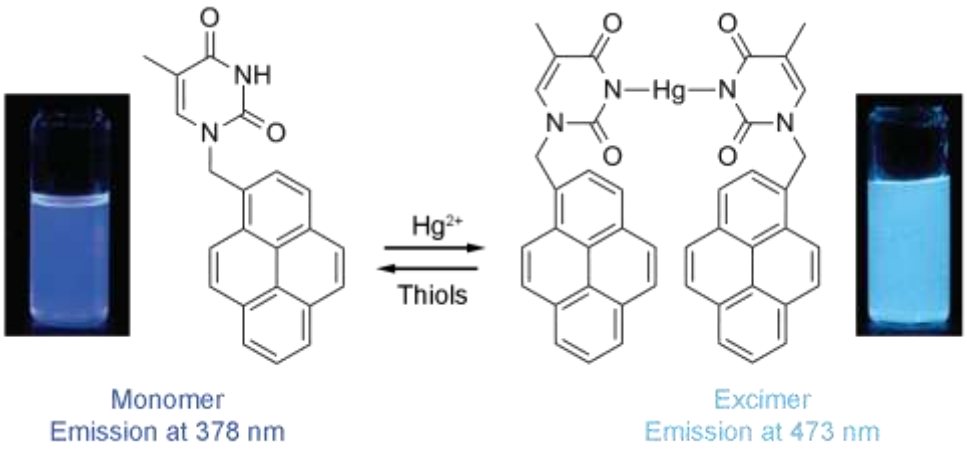

Figure 1-13: Emission of a pyrene derivative in the absence (left) and presence (right) of Hg^{2+} ions.[54]

Upon addition of mercury cations to the pyrene derivative displayed in the left part of Figure 1-13, the emission maximum is shifted from 378 to 473 nm. This process can be reversed by the addition of thiols like glutathione, cysteine or homocysteine that are found in living organisms. Therefore, the mercury complex can be used as a sensor for thiol-containing amino acids by restoring the emission at 378 nm to distinguish them from other amino acids.[54]

1.3.4 Fluorescence resonance energy transfer (FRET)

The usage of FRET dates back to the German physical chemist THEODOR FÖRSTER and is also called FÖRSTER resonance energy transfer to acknowledge his work in the discovery of this process.[55] This non-radiative process between two fluorophores is shown in Figure 1-14 exemplified by the donor fluorescein and the acceptor rhodamine.

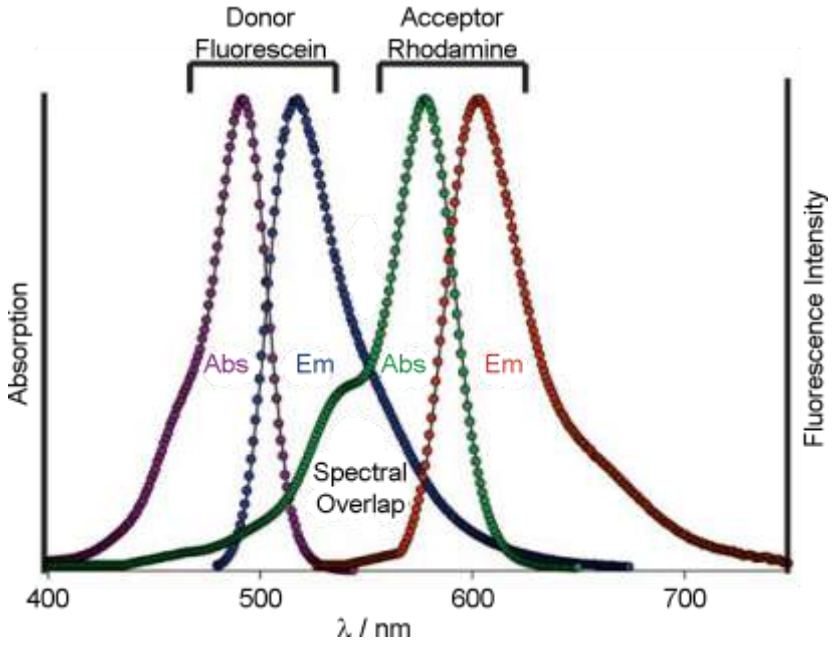

Figure 1-14: Absorption and emission spectra of fluorescein and rhodamine with a FRET process from the first to the second.[56]

When fluorescein is excited around 480 nm it becomes fluorescent and emits photons with a wavelength of approximately 520 nm. If an acceptor, for example rhodamine, is close to the excited fluorescein (1 to 10 nm)[57], a non-radiative relaxation path opens and the excited donor transfers its energy to the rhodamine mole-

cule. A spectral overlap between the emission spectrum of the donor and the absorption spectrum of the acceptor is necessary for an occurring FRET. However, the energy transfer is caused by a long-range dipole-dipole interaction instead of a subsequent emission/absorption process.[56]

Most sensor systems using FRET for the detection of analytes are based on proteins[58] or quantum dots[59]. Fewer examples of molecular FRET sensors are known for the detection of specific cations. One of them is shown in Figure 1-15.

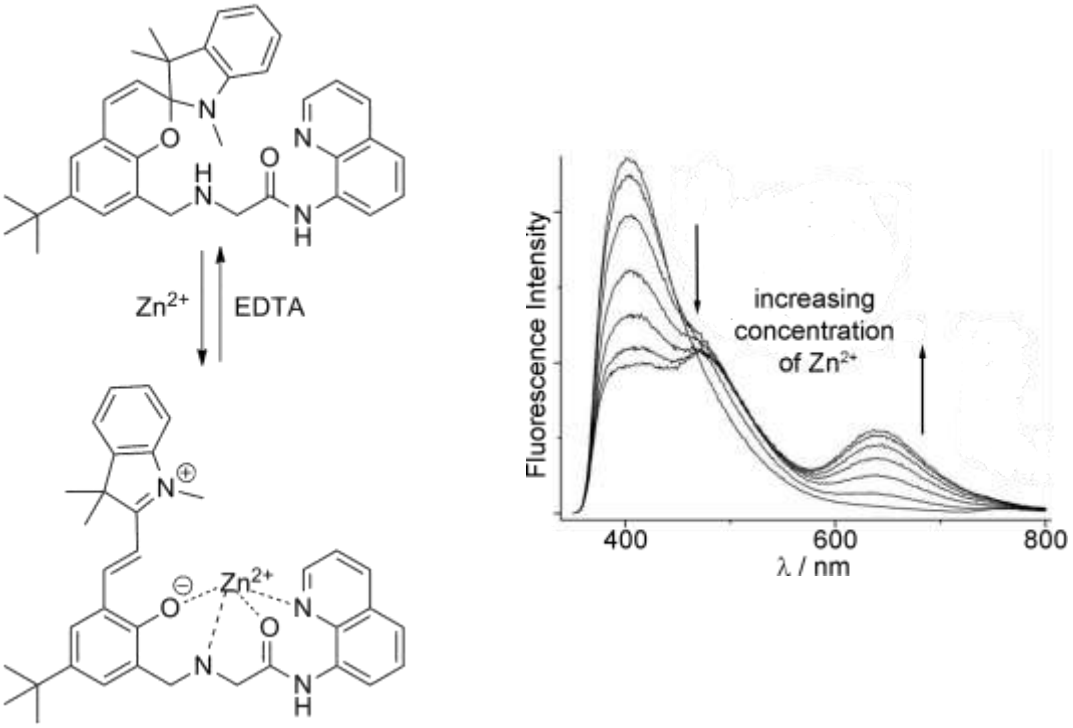

Figure 1-15: Left: Proposed binding motif upon addition of Zn^{2+}. Right: Fluorescence emission spectra at different equivalents of Zn^{2+} (0 eq., 0.1 eq., 0.3 eq., 0.5 eq., 0.7 eq., 0.9 eq. and 1.0 eq.).[60]

The spiropyran shown in the upper left part of Figure 1-15 undergoes a ring opening by addition of zinc cations. This leads to a merocyanine motif (lower left part) and results in a larger conjugated π-system. Besides this new fluorophore, the quinoline part of the molecule remains structurally unchanged. So after the complexation of zinc cations, two separated aromatic systems are present in this sensor. Excitation of the quinoline moiety now initiates a FRET to the merocyanine moiety, which is reflected in the corresponding fluorescence spectrum (Figure 1-15, right). Upon addition of zinc cations, the intensity around 400 nm decreases, whereas an increase at

around 625 nm is recognizable. The underlying ring opening can be reversed by addition of EDTA to restore the emission around 400 nm.[60]

1.3.5 C=N isomerization

This relatively new sensing mechanism emerged in 2007 and is named after the structural requirement for those sensors, the C=N double bond. Previous comparative work concerning the emissive properties of derivatives bearing bridged and non-bridged C=N double bonds showed interesting observations.[61]

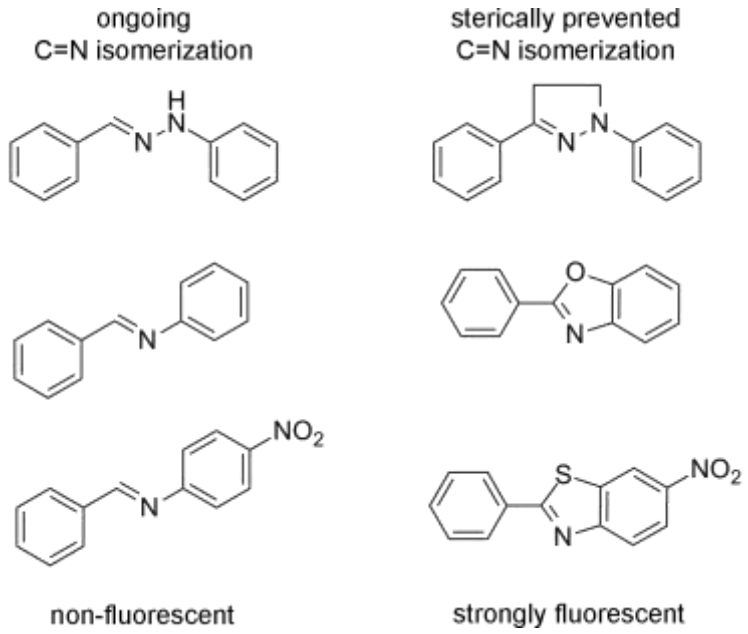

Figure 1-16: Structures and emission properties of derivatives bearing non-bridged (left) and bridged (right) C=N double bonds.

The molecules shown in the left part of Figure 1-16 consist of C=N double bonds that undergo isomerization between their *E* and *Z* isomers. No fluorescence emission of these derivatives can be detected. In contrast, the molecules displayed on the right side cannot isomerize, because the C=N double bonds are bridged covalently. Consequentially, these derivatives exhibit strong fluorescence.[61]

From this observation, the authors wondered if the isomerization and especially its hindrance could be used to establish a new sensing mechanism. By coordination of an analyte, it could be possible to restrict the conversion between *E* and *Z* isomer and increase the fluorescence emission. A coumarin derivative was the first example of a fluorescence sensor working with this signaling mechanism.

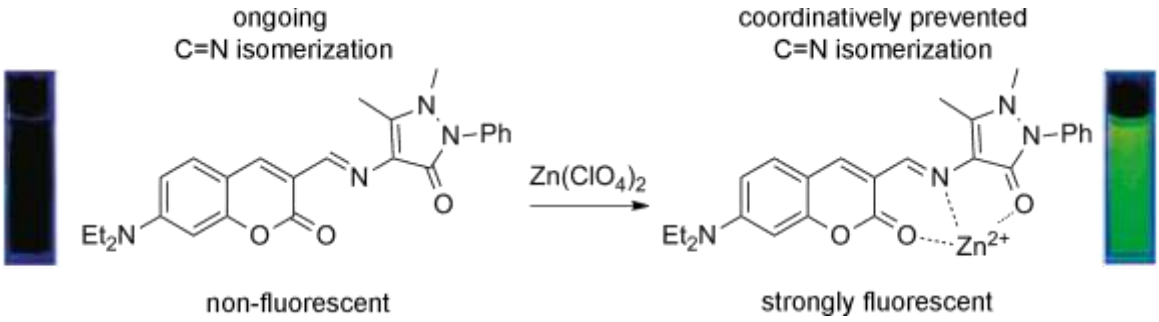

Figure 1-17: Left: No emission without zinc cations. Right: Pronounced fluorescence emission in the presence of zinc perchlorate in acetonitrile.[61]

The prepared coumarin derivative (Figure 1-17 left) is non-fluorescent, because of the ongoing C=N isomerization. Addition of zinc perchlorate results in intense fluorescence emission due to the coordination of the zinc cation by two oxygen and one nitrogen atom. Therefore, the isomerization is inhibited and the changed output is observable.[61]

This sensing mechanism was applied by several research groups to develop sensors among others for magnesium(II)[62], aluminum(III)[63], iron(III)[64], zinc(II)[65] or mercury(II)[66] cations as well as anions e.g. hydrogen sulfite[67].

1.4 Scope

The title of this thesis “anthracene based colorimetric molecular sensors” includes three main buzzwords.

One key term thereof is “colorimetric”, describing the desired color changing nature of the sensor’s response (Figure 1-18 right). The clear demarcation of sensing principles based exclusively on intensity variations (Figure 1-18 left) delivered the initial ideas for synthetic targets. Another guideline is found in the expression “anthracene based”, defining the used fluorophore. The high quantum yield of its unsubstituted parent compound[68] as well as the possibility to derivatize its scaffold are some of the provided advantages. The third guidance, “molecular sensors”, describes the aspired behavior of the examined systems to detect analytes.

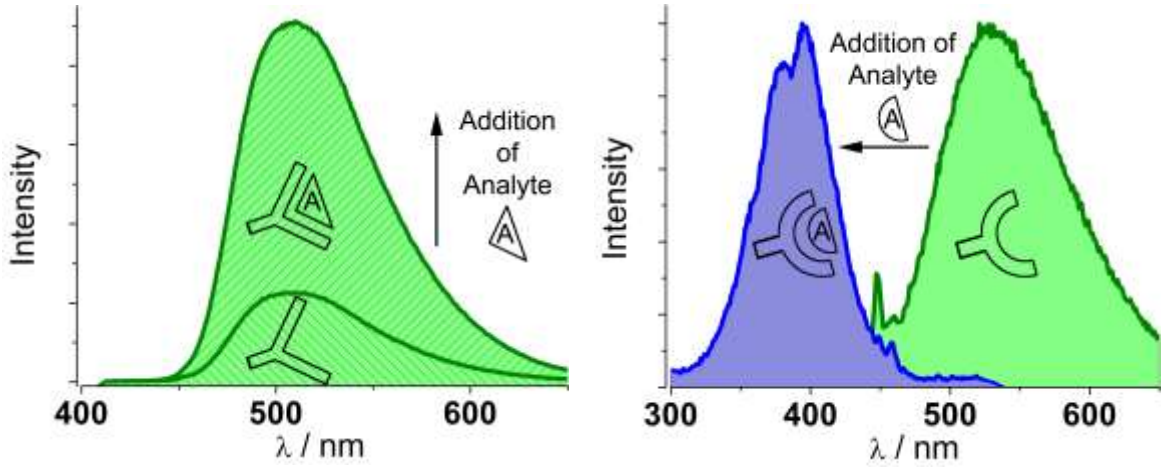

Figure 1-18: Left: Intensity variation based response after addition of an analyte. Right: Colorimetric response after addition of an analyte.

From these deliberations, the first major issue is the preparation of anthracene derivatives possessing a high potential to vary their luminescence behavior in the presence of targeted analytes colorimetrically. The comprehensive characterization of these potential sensors is crucial to ensure their structure as well as their purity. Especially NMR spectroscopy, mass spectrometry, elemental analysis and X-ray diffraction should be applied to achieve this.

The second major part during this thesis is to investigate the luminescence properties of the prepared potential sensors. A general procedure has to be established to guarantee a reliable strategy for maximum comparability of different derivatives.

The main analytical tool is obviously fluorescence spectroscopy. But UV/Vis spectroscopy should also be useful to enlighten non-radiative processes.
The detection of analytes is mainly carried out in solution, so NMR spectroscopy could help to understand ongoing luminescent changes. Nevertheless, helpful insights should be accessible from the solid state structure of potential sensors, especially in comparison with structures received from analyte-sensor aggregates. The method of choice for this is single crystal X-ray diffraction.
Furthermore, the potential sensors should be investigated in application-near solvents. Alcoholic solutions would probably be the best choice due to their capability to dissolve metal salts as well as prepared organic derivatives. Another important feature is the stability, not only of the sensor itself but also of its analyte-sensor aggregate. A reversible addressability of two stable colorimetric states in a selective fashion would be a valuable contribution to the field of luminescence sensors.

2 Results and Discussion

To achieve the formulated aim of a colorimetric response, it was necessary to work aside the PET effect. As described in chapter 1.3.1, sensors bearing the typical fluorophore-spacer-receptor build increase their intensity by coordination of suitable analytes but exhibit in general no shift of their emission wavelength.
Two fundamentally different approaches were explored during this thesis.

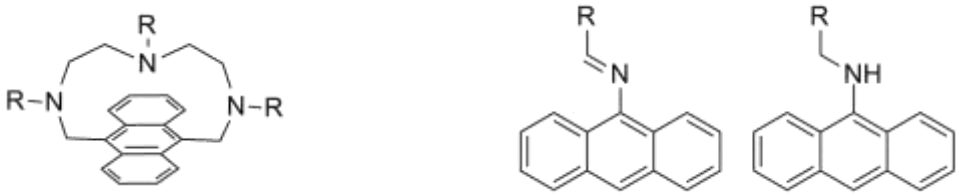

Figure 2-1: Scaffolds used for the construction of anthracene based colorimetric molecular sensors in this thesis. Left: Ansa-bridged anthracenes. Right: Anthracene derivatives without spacer.

The left structure in Figure 2-1 represents ansa-bridged anthracenes and is discussed throughout chapter 2.1. The general idea of preparing and investigating this type of molecules was to create a binding site for metal cations directly above the anthracene π-system. A bonded metal ion should affect the emission wavelength and provide a colorimetric response.
In the second main part of this thesis (chapter 2.2), anthracene derivatives without spacer between the fluorophore and receptor are examined. A subcategorization into imines and amines (Figure 2-1 right) was obvious due to their different expected signaling mechanisms. The imines contain a C=N double bond and so the isomerization or its hindrance should allow conclusions about the absence or presence of specific analytes (cf. chapter 1.3.5).
After reduction of this double bond, the formed amines have to possess a different signaling mechanism. Due to the lack of a spacer between the amine and the anthracene fluorophore, their scaffold is reminiscent of ICT sensors (cf. chapter 1.3.2).
But to evaluate these theoretical considerations, potential sensors with the mentioned structural features were synthesized and investigated by fluorescence spectroscopy.

2.1 Ansa-bridged anthracenes

The interest in bridged anthracenes, also called anthracenophanes, arose from their benzene analogs, the (para)cyclophanes. Both classes are studied intensively because of their challenging synthesis and strained steric scaffold.[69] The first synthesis of an anthracenophane with an alkyl bridge consisting of ten carbon atoms was achieved in 1974 and introduced the smallest member of this class for decades.[70]

More than 20 years later, the first azaanthracenophane was presented via a RICHMAN-ATKINS[71]-like cyclization. A Spanish research group published a series of anthracenophanes whose bridge included three to five nitrogen atoms. For synthetic reasons, the nitrogen atoms were protected by tosylate groups and unfortunately deprotection led to decomposition of the molecules.[72]

It took three additional years, before an American research group was able to synthesize the first unprotected azaanthracenophanes in 2001. They succeeded by using the SES (*β*-trimethylsilylethanesulfonyl) protection group (Scheme 2-1).[73]

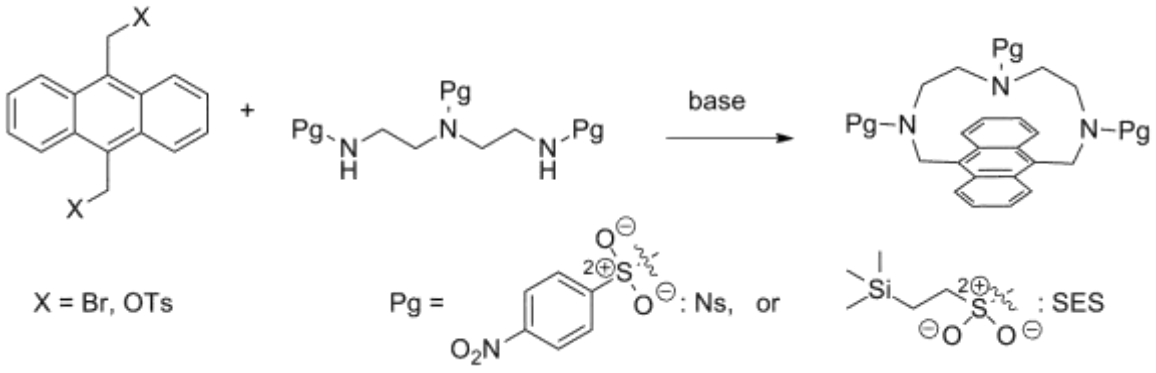

Scheme 2-1: Reaction path to protected azaanthracenophanes (Pg = Ns[74], Pg = SES[73]).

In the following year the Spanish researchers, who published the tosyl protected derivatives, were also able to present a synthetic route to unprotected azaanthracenophanes. For protection they chose the nosyl (Ns: *p*-nitrobenzenesulfonyl) group.[74]

Although the synthesis of these azabridged anthracenes has been known for more than ten years, no luminescence properties of this class are available.

Their preorganized coordination sphere of the multiple nitrogen donor sides on the one hand and the possibility of a π-coordination of the anthracene moiety on the

other hand seem to offer a great potential for metal coordination. This arrangement could favor the coordination of a special ion size dependent on the bridge length and introduce thereby a selectivity towards particular metal salts. Especially the π-coordination of a metal cation should have a strong influence on the luminescence properties. A manifold discussed example of the color changing influence caused by a metal-π-coordination is delivered for example by the research field of metallocenes.[75] Therein the metal cation boned by two cyclopentadienyl moieties determines the color of the complex.[76]

The adoption of a metal-π-interaction of azaanthracenophanes seems to be a promising starting point for luminescence sensors.

2.1.1 9,10-(Dibromomethyl)anthracene (1)

As shown in Scheme 2-1 compound **1** is needed in the synthesis of anthracenophanes, irrespective of the chosen protection group. It is obtained via the procedure of GUNNLAUGSSON and coworkers from 2005.[77]

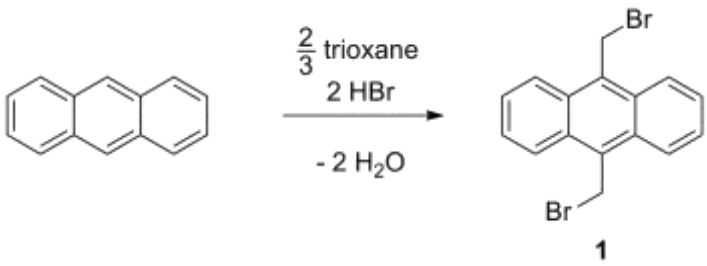

1

Scheme 2-2: Synthesis of **1** by a bromation reaction of anthracene.

The synthesis was carried out with one half of the scheduled quantity used in literature[77] and was boiled for 20 h (Scheme 2-2). The resulting mixture showed approximately 30 % conversion to the desired product and some side products.

Consequently the reaction conditions were changed for improvement. The reaction was started with anthracene and two equivalents of 1,3,5-trioxane at room temperature. After 24 h another two equivalents of 1,3,5-trioxane were added and one day later the conversion was checked by ^{1}H-NMR (roughly 35 %). Two further equivalents of 1,3,5-trioxane were added and after additional 24 h the reaction mixture showed more than 50 % conversion and just small quantities of side products.

Three days later the reaction mixture was filtered off and the precipitate was washed with distilled water and small amounts of ethanol. The crude product was purified by recrystallization from chloroform and 42 % were isolated as yellow powder.

Although this reaction protocol only leads to moderate conversion, acceptable yields can be achieved due to the low solubility of **1** in organic solvents. For this organic impurities and remaining starting material can be separated easily because of their higher solubility.

A drawback of the low solubility is limited access to NMR experiments. Even saturated solutions of **1** are too diluted to record meaningful ^{13}C- or 2D-NMR spectra. This is a disadvantage for the assignment of the peaks but due to the agreement with previously reported ^{1}H-NMR data[77] and additional confirmation via EI mass spectrometry as well as elemental analysis the preparation was verified.

This preparation offers the possibility to introduce a methylene bridge and a bromine atom in one synthesis. Thereby a reactive substituent was placed in 9- and 10-position of the anthracene framework for a subsequent step.

2.1.2 1,4,7-Tris(*p*-nitrobenzenesulfonyl)-1,4,7-triazaheptane (2)

The first attempt to generate an azaanthracenophane follows the synthetic route of GARCÍA-ESPAÑA and LUIS.[74] Their route was used because the protection group was commercially available whereas the alternative route of HOYE and coworkers takes a protection group from an additional two-step synthesis.

Therefore, the nosyl-protected amine was synthesized as the second starting material besides **1** in a RICHMAN-ATKINS-type cyclization.

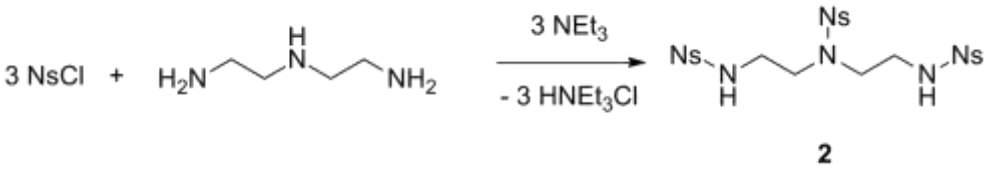

2

Scheme 2-3: Synthesis of **2** by protection of diethylenetriamine.

The reaction mixture was stirred for 48 h in DCM at room temperature. Triethylamine was used as a base to neutralize the byproduct HCl. The added amounts of the

reactants were chosen as published.[74] For purification an aqueous solution containing Na_2CO_3 was added, the precipitate was filtered off and washed with distilled water (Scheme 2-3).

These reaction conditions led to 20 % of an unexpected byproduct that was characterized qualitatively and quantitatively by ^{1}H-NMR spectroscopy and confirmed by ESI mass spectrometry as the asymmetric 4-times protected diethylenetriamine.

The two derivatives could only be separated by applying two times column chromatography. Three attempts of recrystallization from different solvents (acetone, DCM, toluene) were not successful to separate the mixture.

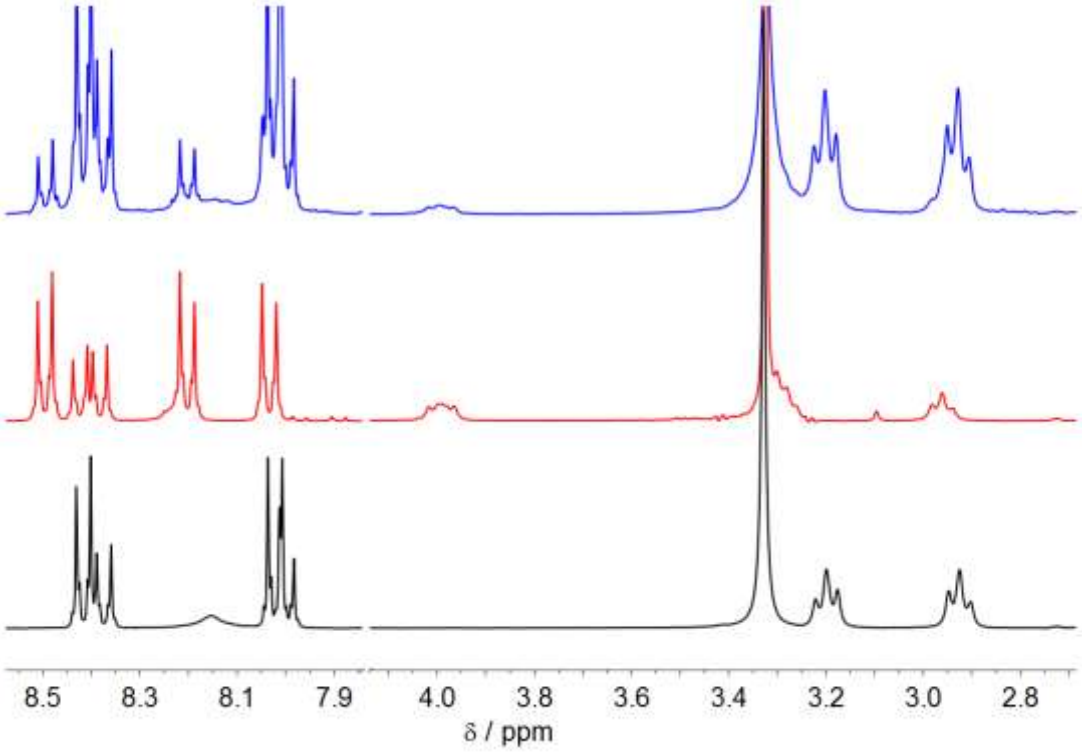

Figure 2-2: ^{1}H-NMR spectra in DMSO-d_6 of: Crude product; mixture of **2** and the asymmetric fourfold protected diethylenetriamine (top, blue). Purified asymmetric 4-times protected diethylenetriamine (middle, red) and **2** purified via two times column chromatography (bottom, black).

Figure 2-2 displays a comparison of the ^{1}H-NMR spectra containing the crude reaction product (blue line) and the two isolated species after purification, the asymmetric 4-times protected diethylenetriamine (red line) and **2** (black line). The first one can be seen in the blue spectrum at the signals of δ = 3.99 ppm, 8.20 ppm and 8.49 ppm, whereas only the one signal at 3.20 ppm of **2** is not superimposed in the blue ^{1}H-NMR spectrum. Because **2** is the main species in the crude product, the re-

maining signals of **2** at δ = 2.93 ppm, 8.01 ppm and 8.39 ppm can be assigned easily in the blue ^{1}H-NMR spectrum.

After the second column chromatography only 6 % of the desired product were isolated. So the reaction and purification conditions were varied.
The best results were achieved by using one third of the suggested scheduled quantity and a deficit of nosyl chloride (2.9 eq.). For purification the precipitate was filtered off and washed with a saturated NH_4Cl solution and water (for details see chapter 4.4.2).
By this procedure a yield of 36 % was obtained and the product contained less than two weight percent NH_4Cl and no fourfold nosylated amine. This just moderate yield is compensated by a shortened purification procedure compared to the suggested one via column chromatography. The structure of **2** was confirmed via 1D- and 2D-NMR spectroscopy, ESI mass spectrometry and elemental analysis.

2.1.3 Attempts to 2',5',8'-tris(*p*-nitrobenzenesulfonyl)-2',5',8'-triaza-[9](9,10)anthracenophane (3) and 2',5',8'-triaza[9](9,10)-anthracenophane (4)

After synthetic access to **2** the next step was to convert it with **1** into the nosylated azaanthracenophane **3**. GARCÍA-ESPAÑA and LUIS recommended a one-pot synthesis, wherein cyclization and deprotection are performed simultaneously, to the unprotected azaanthracenophane **4**. Herein they found a better yield compared to the two consecutively performed steps.[74]

So both ways, the synthesis of the nosyl protected (**3**) and the unprotected (**4**) ansa-bridged anthracenes, were tried according to Scheme 2-4.

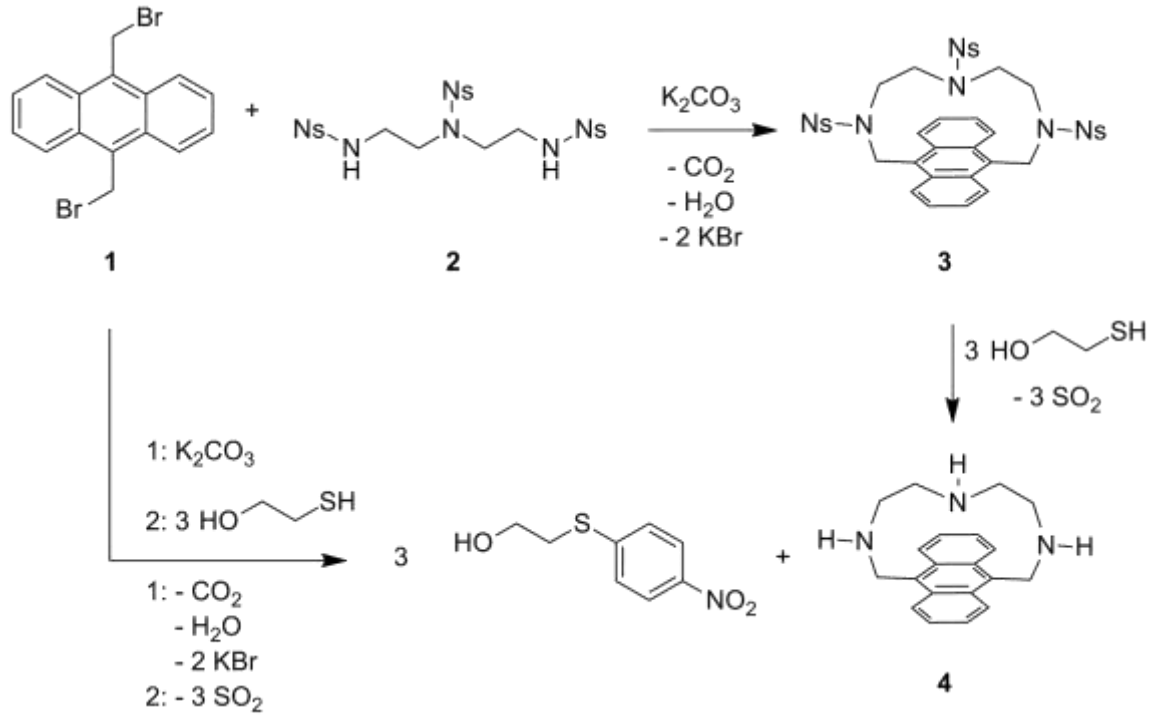

Scheme 2-4: Synthesis of **4** via **3** (top) or by a one-pot synthesis (bottom).

At first the one-pot synthesis of cyclization and deprotection was attempted. The only difference between the reported and tested procedure was the scheduled quantity (one fifth).

A solution of **1** in DMF was added in a 1:1 stoichiometric ratio to a mixture containing the protected amine **2** and an excess of potassium carbonate in DMF. The reaction mixture was stirred at 90 °C for 3 days. After cooling to room temperature an

excess of β-mercaptoethanol was added for deprotection and stirring continued at room temperature for additional 20 h.

For purification the suspension was filtered, washed with DMF and the residue as well as the filtrate was treated as described in the literature: dried, dissolved in 3 M hydrochloric acid and washed with DCM, basified, extracted with chloroform, dried and further purified via column chromatography. In none of the resulting fractions the desired product **4** was present.

A second reaction was carried out with all conditions as described before, except for the solvent, which was changed to acetonitrile and the temperature was set to its boiling temperature of 82 °C. This was done because acetonitrile is used in nucleophilic substitution reactions quite frequently.[78]

Again **4** was neither found in the residue nor in the filtrate.

Due to this throwback the synthesis was tried consecutively: at first the isolation of **3** and afterwards deprotection to **4**. Again the reaction was set up according to the published procedure of GARCÍA-ESPAÑA and LUIS but with one fifth of the scheduled quantity.

A solution of **1** in acetonitrile was added to a mixture of the protected amine **2** (stoichiometry 1:1) and an excess of potassium carbonate in acetonitrile. The reaction mixture was stirred at 82 °C for 3 days. The suspension was filtered; the filtrate was dried and purified by column chromatography. Once again the azaanthracenophane, in this case **3**, was not detected in any fraction.

After these experiences the used instructions by GARCÍA-ESPAÑA and LUIS was discarded and the one of HOYE and coworkers from 2001 was followed.

2.1.4 Sodium β-trimethylsilylethanesulfonate (5)

The synthetic route of HOYE and coworkers requires the SES-Cl (β-trimethylsilylethanesulfonyl chloride), which was synthesized according to WEINREB et al.[79] The first step to this protection group is the preparation of **5**, which is then converted into β-trimethylsilylethanesulfonyl chloride (**6**).

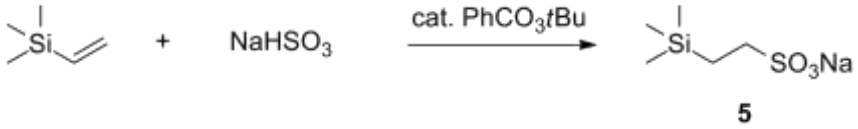

Scheme 2-5: Synthesis of **5** by a free-radical addition reaction resulting in the expected *anti*-MARKOVNIKOV product.

The reaction was carried out with 20 g vinyltrimethylsilane in methanol and catalytic amounts of tert-butylperbenzoate under inert gas atmosphere. An excess of sodium hydrogen sulfite in water was added and the reaction mixture was stirred at 50 °C for 48 h.

For purification also the described procedure of WEINREB was applied. The mixture was dried and coevaporated with methanol and **5** was isolated by extraction with methanol from the solid crude product (for details see chapter 2.1.4).

This procedure gave 67 % (27.3 g) **5**, which was confirmed by comparison with literature known ^{1}H-NMR data.[79] **5** was used without further purification in the following synthesis.

2.1.5 β-Trimethylsilylethanesulfonyl chloride (6)

After the confirmed synthesis of **5**, the next step was to follow the procedure of WEINREB et al to **6**.[79]

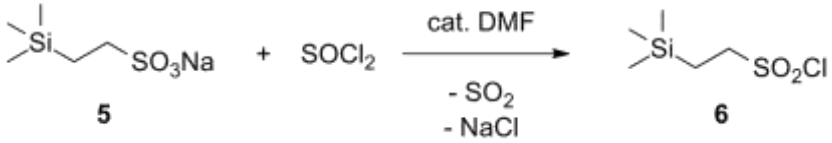

Scheme 2-6: Synthesis of **6** in thionyl chloride as solvent and reactant.

80 mL thionyl chloride were added dropwise over a period of 1 h at 0 °C to 27.3 g of crude **5** (chapter 2.1.4) under formation of SO_2. Afterwards, a catalytic amount of

DMF was added, which led to increased SO_2 generation. The reaction mixture was stirred overnight and the excess of thionyl chloride was removed by distillation. Two times 50 mL hexane were added and removed consecutively. After a third addition of 50 mL hexane, the resulting suspension was filtered off over celite and the remaining solid was washed with 75 mL hexane. The volatile components of the filtrate were removed under reduced pressure and 9 g crude product were isolated.
At this point WEINREB et al. reported with a similar scheduled quantity a crude product yield of 23 g so the reaction was obviously not working as well as described by them. Moreover, the ^{1}H-NMR spectrum shows two derivatives in the ratio of 4:1. To continue along the described procedure a vacuum distillation was performed. A low-boiling fraction (41 °C at 1.5 mbar) and a high-boiling fraction (71 °C at 0.7 mbar) were isolated in the weight ratio 2:1, which corresponded to the two sets of signals in the ^{1}H-NMR spectrum of the crude product (Figure 2-3).

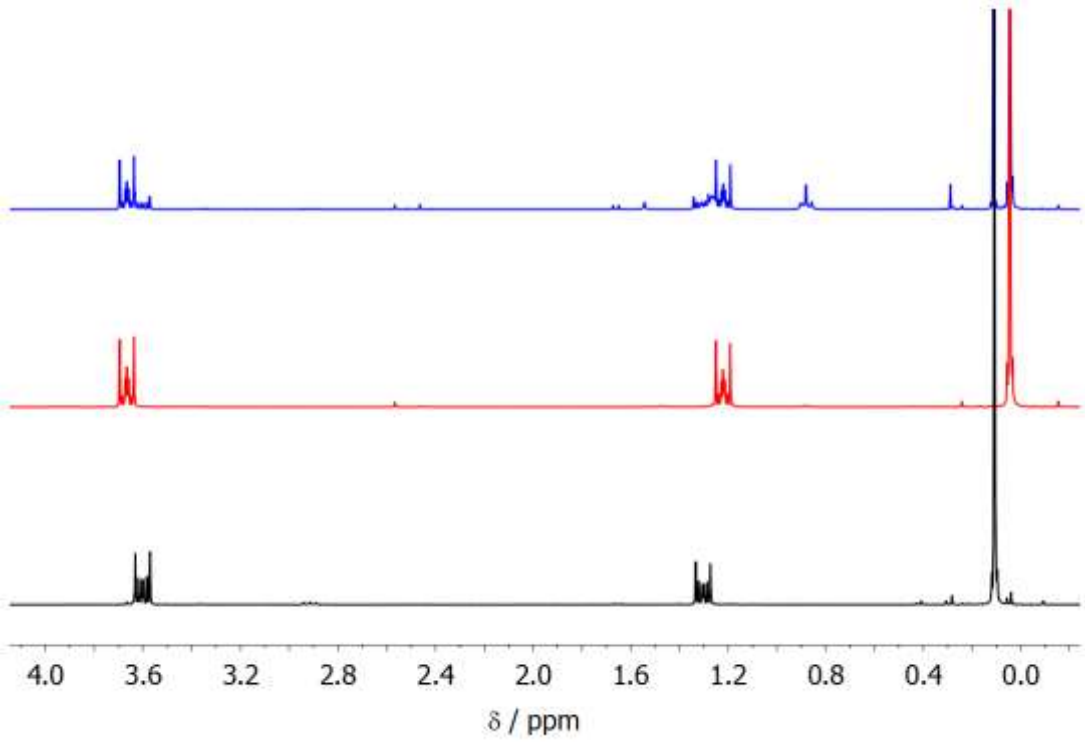

Figure 2-3: ^{1}H-NMR spectra in $CDCl_3$ of: Crude product; mixture of the high- and low-boiling point fractions (top, blue). Low-boiling fraction (middle, red) and high-boiling fraction (bottom, black) after distillation.

Figure 2-3 displays the ^{1}H-NMR spectra of the crude product (blue line) and the two species isolated via distillation, whereas the red line represents the low-boiling

point and the black line the high-boiling fraction. Both sets of signals can be seen in the blue spectrum. The first one shows its singlet at δ = 0.04 ppm and two multiplets around 1.22 ppm and 3.67 ppm and the high-boiling fraction displays a similar pattern of one singlet at δ = 0.11 ppm and two multiplets around 1.30 ppm and 3.60 ppm. Not only the chemical shift and pattern of the signals of both derivatives are similar but also their relative integrals. So the ratio between the singlet and each of the multiplets is for both compounds 9:2, indicating that both derivatives contain of a trimethylsilyl group and an ethylene bridge.

Because of these similarities it was not possible to decide which of the two fractions belongs to the desired product **6**. Even 2D-NMR correlation experiments provided no guidance for this.

EI and ESI mass spectrometry were done, but in both cases only two assignable mass to charge ratios with *m/z* = 73 and *m/z* = 93/95 were detected, which point to the fragments shown in Figure 2-4.

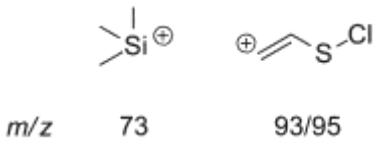

Figure 2-4: Measured *m/z* ratios with possible corresponding fragments.

In order to differentiate between the two fractions, not distinguishable by the applied analytical methods, a chemical reaction was performed of both separately in small scales. The subsequent conversion, namely the protection of diethylenetriamine (discussed in chapter 2.1.6), was chosen.

Only the high-boiling fraction gave the desired product 1,4,7-tris(β-trimethylsilylethanesulfonyl)-1,4,7-triazaheptane (**7**) so **6** was assigned to the high boiling fraction, of which 1.53 g had been isolated. The yield of 5.7 % is very small but the unexpected byproduct was removed efficiently via distillation.

Before purification, a 1:4 ratio between the desired product and the side product was estimated by ^{1}H-NMR (Figure 2-3) and so the isolation of 1.53 g from 9 g crude product points towards a suitable purification process. However, the synthesis resulted in a very low conversion of **5** to **6** but in an unexpected side product. Maybe

the temperature was not controlled properly or reactants were added too fast and caused this amount of byproducts not described by the inventors of the procedure.

2.1.6 1,4,7-Tris(β-trimethylsilylethanesulfonyl)-1,4,7-triazaheptane (7)

The next step was to generate the protected amine **7** from the isolated **6**. Its synthesis was described by HOYE and coworkers in 2001.[73]

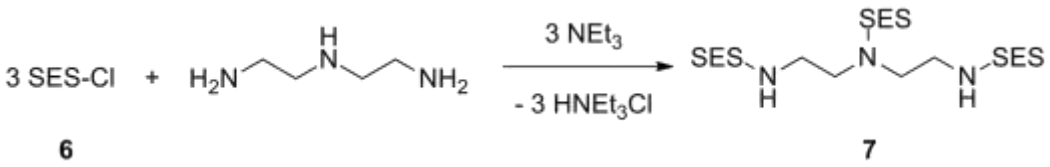

6 **7**

Scheme 2-7: Synthesis of **7** by protection of the three nitrogen atoms in diethylenetriamine.

In a smaller scale but the same stoichiometry as reported, 1 eq. diethylenetriamine and 5 eq. triethylamine were dissolved in DMF. A solution of 4 eq. **6** in DMF was added dropwise at 0 °C and the reaction mixture was stirred at 0 °C for 1.5 h. Addition of the reaction mixture to water, three times extraction with DCM and concentrating of the organic layers to dryness gave a crude product, which was purified via column chromatography.

A difficulty was the detection of the desired product in the purification process. Though **7** is non-fluorescent, detection by coloring the reaction product on DC sheets was tested. Therefore, a solution of 7-chloro-4-nitrobenzofurazan in ethanol was used as suggested for primary and secondary aliphatic amines[80] to color the aspired triamine. But even with this special procedure **7** was not monitored reliably. After testing two different ways of column chromatography, the experience suggests the following strategy: one should start with petroleum ether and ethyl acetate and increase the concentration of the polar component stepwise (e.g. 20:1 → 10:1 → 3:1) to pure ethyl acetate. The eluent of every step was concentrated to dryness, a sample of every different eluent composition was investigated by ^{1}H-NMR spectroscopy and compared to literature known ^{1}H-NMR data.

Thereby, **7** was isolated in a yield of 20 %. This is low compared to the 68 % of HOYE and coworkers and is maybe caused by the way smaller scheduled quantity (one-fiftieth).

2.1.7 2',5',8'-Tris(*β*-trimethylsilylethanesulfonyl)-2',5',8'-triaza[9]-(9,10)anthracenophane (8)

The RICHMAN-ATKINS-like cyclisation between the brominated anthracene **1** and the protected amine **7** was also performed according to HOYE and coworkers.[73]

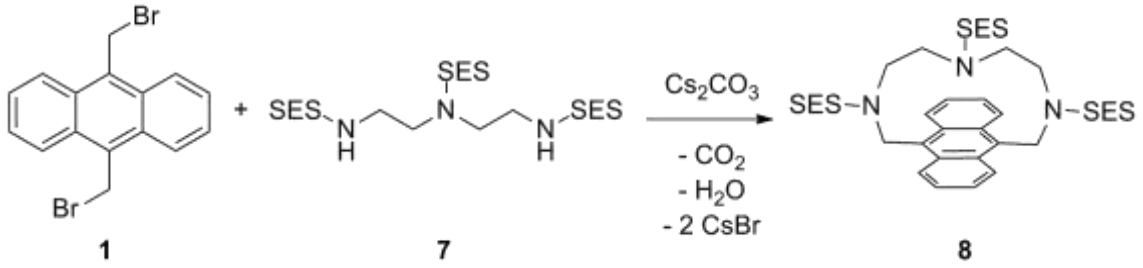

Scheme 2-8: Synthesis of **8** via a RICHMAN-ATKINS-type cyclization.

As shown in Scheme 2-8 caesium carbonate was used as a base and the stoichiometry between **1** and **7** was 1:1. The reactants were stirred at room temperature for 48 h, the volatile components were removed under reduced pressure, water was added and extracted with DCM.

The crude product was purified via column chromatography starting with a mixture of petroleum ether and ethyl acetate (5:1) and switching stepwise to pure ethyl acetate. This first purification step led to an improved quality but was not sufficient for fluorescence analysis. Therefore a second column chromatography was performed (petroleum ether and ethyl acetate 10:1 --> ethyl acetate). After this extensive purification procedure 31 mg (11 %) of **8** were isolated. So only a small amount of the target anthracenophane was obtained.

Starting with 20 g in the synthesis of the first step and isolating only 31 mg after the last is caused by the bad yields in the second (5.7 %), third (20 %) and fourth (11 %) step.

But in the end **8** was obtained in sufficient quality and because fluorescence analyses are carried out in low concentrations, the aim to characterize an azaanthracenophane by fluorescence spectroscopy was within reach.

Deprotection of the SES groups was tried only once in a µ-molar scale. By the addition of caesium fluoride in DMF the volatile compounds fluorotrimethylsilane, ethene and sulfur dioxide should be released to result in the unprotected azaanthracenophane **4**.

The comparison of obtained ^{1}H-NMR spectroscopic data with published results[73] showed that, the removal of the SES groups led to decomposition of the bridged anthracene.

Therefore the fluorescence properties of the protected derivative **8** were studied in detail to evaluate if this anthracenophane might give a proper luminescence sensor.

2.1.8 Luminescence properties of 2',5',8'-tris(β-trimethylsilylethanesulfonyl)-2',5',8'-triaza[9](9,10)anthracenophane (8)

During the fluorescence spectroscopic characterization of **8**, a general procedure was established to compare its optical properties with later on synthesized derivatives reliably.

2.1.8.1 Preliminary remarks for luminescence analysis

The first important issue was the choice of the solvent. On the one hand its polarity should be suitable to solve the synthesized organic ligands and on the other hand it had to be polar enough to dissolve metal salts and open the possibility for a screening process. It is essential to test multiple different metal cations to evaluate the sensor properties of a potential sensing system.

The solubility of metal cations is not only dependent on the solvent polarity but also on its counter anion in the metal salt. Therefore, the choice of the solvent is strongly related to the chosen anions. To enable the greatest possible comparability, every tested metal salt should have the same anion. Connected to this issue is the availability of a wide range of metal salts with this specific anion.

Apart from this a further important remark has to be considered. Polar and especially protic solvents are known to dissolve many metal salts very well by coordination of the ions. Because the concentration of the potential sensor for fluorescence applications is in the range of 10^{-4} to 10^{-6} M, a huge excess of solvent molecules is present in each measurement. Therefore, the complex forming affinity of the potential sensor has to be way higher than the binding affinity of the solvent to compensate the ligands way smaller concentration.

For applications, water would probably be the best solvent. Its availability, low costs and ecologically harmlessness are just some of the outstanding advantages. Moreover, many areas of application presuppose aqueous solutions (e.g. determining concentration of cations in blood or pollution of waters).

However, the main disadvantage can be its strong binding affinity and therefore no response of the synthesized potential sensor after addition of the tested metal salt. With these remarks in mind, the availability of metal salts containing different ani-

ons was checked and halides were found to be most spread and commercially available (especially chlorides and bromides). Bromides were preferred to the also available chlorides because of their better solubility in organic solvents (e.g. sodium and potassium bromide exhibit a higher solubility in acetone compared to the corresponding chlorides).[81]

The second step was to determine the solvent for fluorescence measurements. 0.01 M solutions of different metal bromides in several solvents were prepared and detailed tables can be found in chapter 5.1.1. Methanol turned out to solve most of the tested metal salts and was therefore chosen as the solvent for almost every fluorescence investigation throughout this thesis. It also has the advantage not to absorb light in a region where anthracene derivatives are irradiated. Methanol absorbs more than 80 % of the light with wavelengths lower than 205 nm. In comparison, the 80 % absorption of light are reached from acetone at wavelengths shorter than 335 nm and therefore the observable spectral window would have been smaller with this second solvent.[82]

Unless stated otherwise, 10^{-5} M solutions of the tested ligands were chosen, which proved to be a good magnitude in former investigations.[83] If a too low concentration is prepared, the number of excited molecules is too small and the fluorescence emission becomes feeble, whereas an immense concentration can lead to reabsorption and quenching.[84] Phenomena, concerning inappropriate concentrations, are discussed detailed in chapter 4.2.2.

In general, the solvents used for fluorescence analysis were not dried to have a simple, multiple times repeatable procedure on the one hand and to be close to aerobic conditions of applications (organic tissue) on the other hand. Only the ligand solution was stored under exclusion of air and for its preparation degased solvent was used to extend its durability. In contrast to this, the measurements were carried out under atmospheric conditions and the metal salt solutions were prepared from non-degased non-dried methanol.

As mentioned before, metal bromides were chosen for testing the response of the synthesized anthracene derivatives towards its coordination abilities of cations. For the purpose of testing, a screening process was developed to ensure maximum comparability. The procedure is displayed in Figure 2-5.

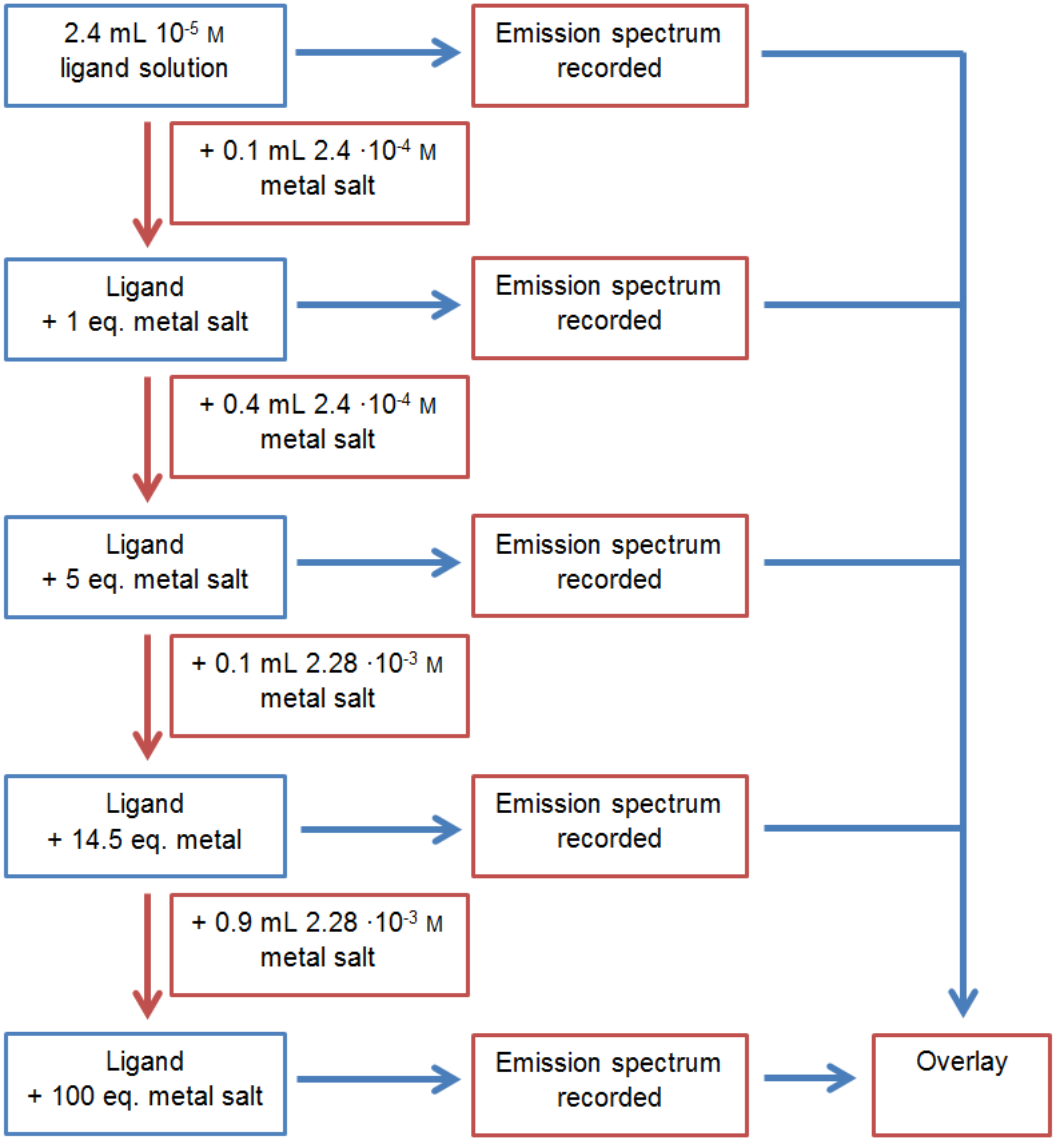

Figure 2-5: Screening procedure developed and used within this thesis.

The driving idea behind the screening procedure shown above was to develop a method that enables testing many metal bromides with feasible effort. There are more precise procedures (e.g. usage of a titrator) but the disadvantages are longer processing times and the enhanced effort of sample preparation. This screening process has the advantage to combine a relatively high throughput with a wide range of tested concentrations. From equimolar ligand to metal salt tests, up to a ratio of 1:100 one gets a good idea, which metal-ligand combinations are worth to be studied in detail.

2.1.8.2 *Excitation and emission properties of 2',5',8'-tris(β-trimethylsilyl-ethanesulfonyl)-2',5',8'-triaza[9](9,10)anthracenophane (8)*

Recording excitation and emission spectra are generally the first fluorescence spectroscopic experiments for each unexplored derivative. These spectra are necessary for comparison with further measurements and to ensure that the fluorophore is excited at a proper wavelength.

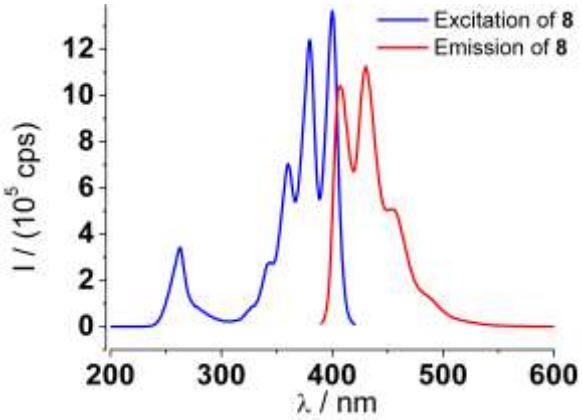

Figure 2-6: Excitaion (blue, λ_{det} = 430 nm) and emission (red, λ_{ex} = 380 nm) spectra of **8** (10^{-5} M in MeOH).

The excitation and emission properties of **8** are displayed in Figure 2-6. There is only a very small difference of 7 nm between the lowest energy band (λ = 400 nm) of the excitation spectrum and the highest energy band (λ = 407 nm) of the emission spectrum (STOKES shift). This indicates that the emitting state is also a singlet state and the radiative relaxation should be termed fluorescence, whereas a large STOKES shift would indicate phosphorescence. Life time measurements of the excited state could prove this assumption.

The excitation as well as the emission spectrum shows distinct peaks because of the resolved vibrational energy levels. Since the excitation spectrum looks like a mirror image of the emission spectrum it fulfills the mirror image rule (chapter 1.2).

The smaller band around 260 nm in the excitation spectrum of **8** is also found for its non-substituted parent compound anthracene. An analog signal is observed in the absorption spectrum of anthracene and is assigned to a π-π* transition between the electronic ground state S_0 and the third electronically excited state S_3.[85]

The emission intensity is relatively strong (approximately one million cps) compared to following investigated derivatives, which indicates the absence of a strong non-radiative process. The PET effect is such a process and seems, despite of an assembly with a spacer in between the fluorophore and the nitrogen atoms, to have no big quenching contribution. The reason therefore might be the strained steric scaffold of the ansa-bridged anthracene that disables a free rotation around the carbon-nitrogen single bonds (cf. chapter 1.3.1).

2.1.8.3 Influence of pH changes on emission properties of 2',5',8'-tris(β-trimethylsilylethanesulfonyl)-2',5',8'-triaza[9](9,10)anthracenophane (8)

After investigation of the fundamental excitation and emission properties of **8**, its response towards acid and base addition was studied. Hydrochloric acid and sodium hydroxide were chosen due to their complete dissociation in aqueous solution. As discussed for metal salt additions, a general procedure was developed to test the potential sensors at different pH values (Table 2-1).

Table 2-1: Procedure to vary the pH value of samples containing potential sensors. Performed with aqueous hydrochloric acid and sodium hydroxide solutions.

Added volume	Concentration of the additive	Concentration of H^+/OH^- in the cuvette (after addition)
0.1 mL	0.024 M	10-3 M
0.5 mL	0.024 M	5 · 10-3 M
0.1 mL	4 M	0.13 M
0.9 mL	4 M	1 M

In general, a cuvette was charged with 2.4 mL of a 10^{-5} M ligand solution in methanol. Subsequently the in Table 2-1 listed volumes (left column) with the corresponding concentrations (middle column) of aqueous hydrochloric acid or sodium hydroxide were added to result in the given concentration of acid or base in the sample (right column). This procedure allowed to monitor luminescent changes of the investigated anthracene derivatives over a wide concentration range of acid and base.

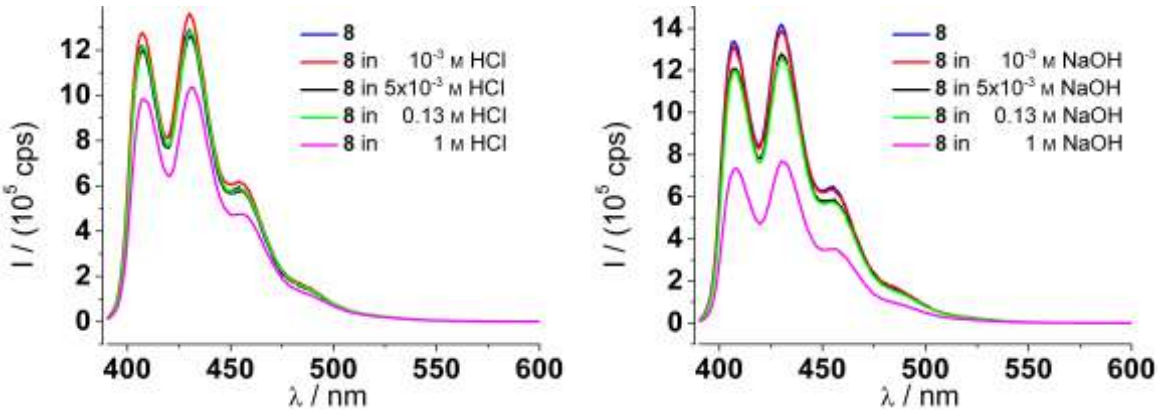

Figure 2-7: Emission spectra of **8** under acidic (left) and alkaline (right) conditions (λ_{ex} = 380 nm).

In the chosen concentration range of the anthracene derivative (10^{-5} M), its intensity is lowered by addition of a further component due to the reduced concentration of the fluorophore. So in general one has to keep in mind a dilution induced decrease of intensity when any volume is added to the cuvette bearing the potential sensor.

When sodium hydroxide is added (Figure 2-7 right), one can see the typical dilution behavior: the extend of decreasing intensity is more pronounced due to larger added volumes than to high amounts of base. This can be seen in the larger difference between the red and the black line in contrast to the smaller changes comparing the black and green line.

At the left hand side of Figure 2-7 the fluorescence behavior of **8** after addition of hydrochloric acid is displayed. When acid is added to a concentration of 10^{-3} M, the fluorescence intensity increases only marginally. The addition of acid to a concentration of $5 \cdot 10^{-3}$ M and 0.13 M showed a similar intensity compared with the starting point and finally the addition to 1 M hydrochloric acid caused a small decrease of emission intensity. The observed changes are minute but the intensity is increased and then stays at one level instead of being reduced by dilution. This hints to a small contribution of the PET effect. By coordination of protons to the nitrogen atoms of the receptor, the quenching due to the PET effect can no longer take place and therefore the intensity is increased. As supposed in section 2.1.8.2, the PET effect has only a very small quenching contribution despite of the PET typical assembly with a spacer between the fluorophore and the nitrogen receptor.

To conclude, **8** showed no pronounced pH dependency but is stable upon addition of a large excess of acid or base.

2.1.8.4 Metal screening of 2',5',8'-tris(β-trimethylsilylethanesulfonyl)-2',5',8'-triaza[9](9,10)anthracenophane (8)

The screening procedure described in section 2.1.8.1 was applied to **8** resulting in overlays that visualize fluorescence changes caused by the different tested metal bromides. The first metal salt added to a solution of **8** in methanol is shown exemplarily in Figure 2-8.

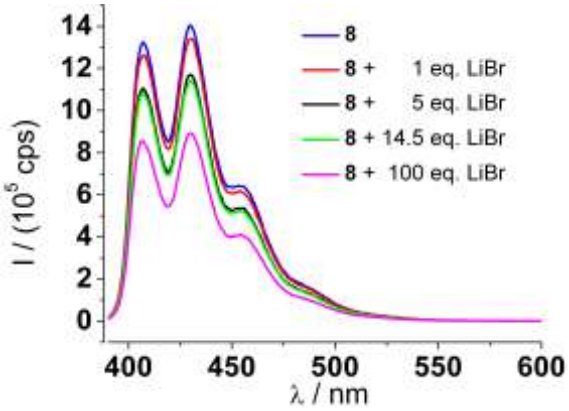

Figure 2-8: Stacked emission spectra of **8** (10^{-5} M in MeOH) before and after the addition of LiBr (λ_{ex} = 380 nm).

The addition of lithium bromide caused a decreased fluorescence intensity of **8** by diluting the sample. This can be seen especially in the difference of the red and black line compared with the difference between the black and green line. Whereas the addition of 0.4 mL and 4 equivalents resulted in a relative large change, the addition of 0.1 mL within 9.5 equivalents showed only tiny changes.

To summarize the results of further investigated metal salts in a compact way the following overview contains all fluorescence changes of **8** with cations in Figure 2-9. Only the fluorescence intensity at 430 nm is depicted in this compact illustration. This way skipped wavelength dependent information are shown detailed in chapter 5.1.2.

The first column from the left shows the behavior of **8** after adding lithium bromide (displayed in Figure 2-8). Only the emission maximum at λ = 430 nm is illustrated in the compact representation of Figure 2-9, but the trend of a decreased intensity caused by dilution, when lithium bromide was added, is also clearly visible.

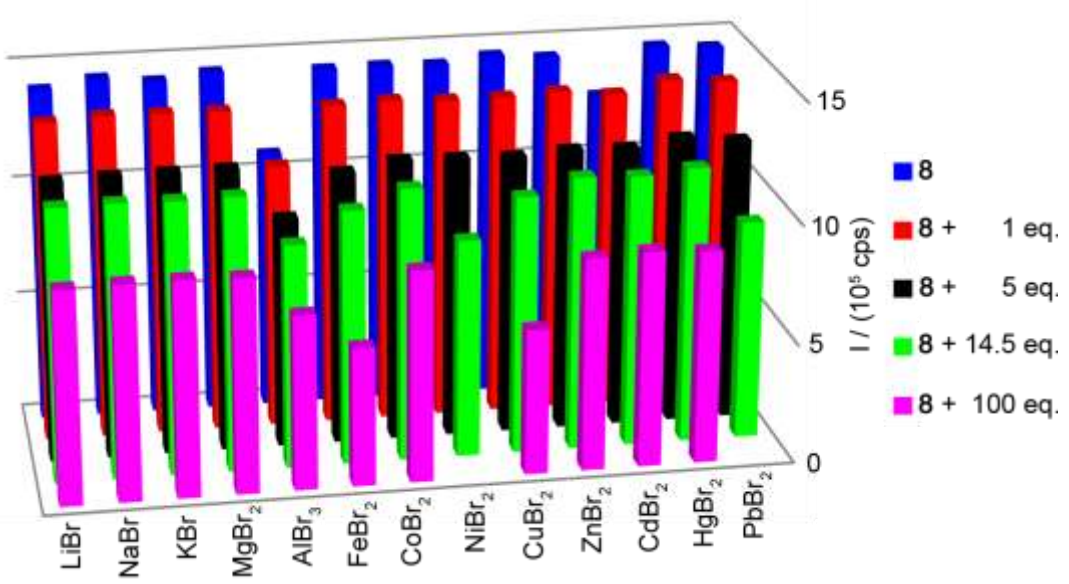

Figure 2-9: Representation of every tested combination between **8** (10^{-5} M in MeOH) and the respective metal bromide in MeOH (λ_{ex} = 380 nm, emission intensity depicted at 430 nm).

This representation enables a fast comparison between the fluorescence properties of **8** after adding different metal salts. It is obvious that the three following columns (addition of NaBr, KBr and $MgBr_2$) show a similar behavior compared to the first one. This is also true for the addition of $CoBr_2$, $ZnBr_2$ and $HgBr_2$ indicating that the addition of the listed metal bromides led only to dilution of the sample and no luminescent response of **8** towards a specific cation was observed.

Two series of measurements (addition of $AlBr_3$ and $CdBr_2$) showed smaller starting intensities of **8** before the metal salt was added. For cadmium bromide it is probably an error in this specific measurement because it was carried out at the same time the other metal salts were measured and all other spectra of $CdBr_2$ agree with the normal dilution behavior. The deviations concerning the series of measurements with aluminum bromide are much more pronounced and originate in a two months later recording date. The same solution was used and the concentration of the fluorophore **8** seemed to be lowered by time. This leads to the assumption that over the eight weeks a part of **8** decomposed by formation of an (in the explored spectroscopic region) less emitting species. This decrease in emission to 76 % is relatively low for a 10^{-5} M solution after two months and argues for the good stability of **8**.

In the cases of nickel bromide and lead bromide the data point at 100 equivalents is missing in Figure 2-9, because the general screening procedure (described in

2.1.8.1) was changed. Both mentioned metal salts were not sufficiently soluble in methanol to generate a $2.28 \cdot 10^{-3}$ M solution. Therefore, just the $2.4 \cdot 10^{-4}$ M solution was prepared and the addition was changed to: 0.1 mL corresponding to 1 equivalent, additional 0.4 mL led to 5 equivalents and the final 0.95 mL resulted in 14.5 equivalents of the particular metal salt. That is the reason why the green bars of these two salts in Figure 2-9 are smaller compared with the other cation additions due to a stronger dilution.

The last feature to mention is the pronounced quenching of the fluorescence after addition of iron bromide or copper bromide. In order to explain this behavior, UV/Vis spectra of a $2.28 \cdot 10^{-3}$ M iron bromide solution and a $2.28 \cdot 10^{-3}$ M copper bromide solution were recorded.

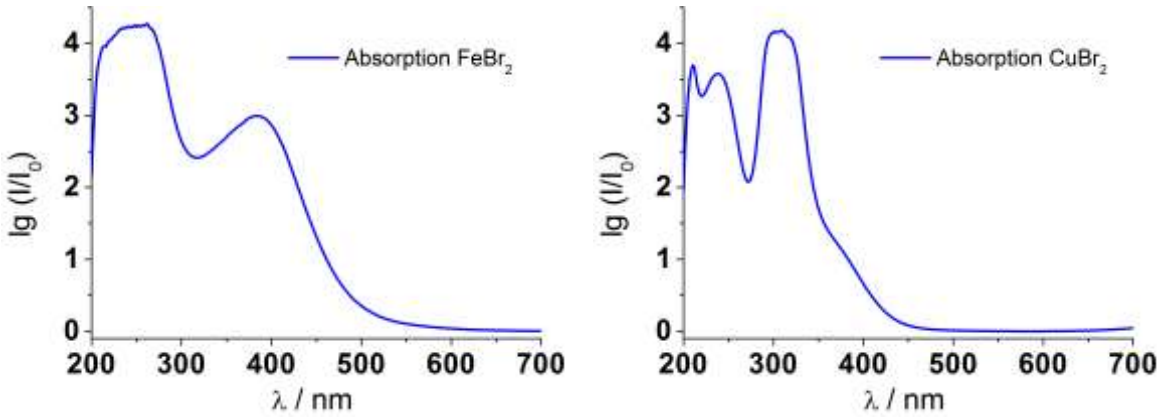

Figure 2-10: UV/Vis absorption spectra of iron bromide (left) and copper bromide (right) ($2.28 \cdot 10^{-3}$ M in MeOH).

In the left part of Figure 2-10 the absorption of an iron bromide solution is displayed that was also used for additions in the fluorescence screening process. It is important to note that the iron(II) solution was used for months, so that at the time of screening processes with different ligands the ratio of iron(II) to iron(III) was different. In the protic solvent methanol iron(II) is oxidized to iron(III) while reducing oxygen to water. This conversion is visible by a color change of the solution from light yellow to deep orange. The iron solution was not stored under inert conditions and was therefore in contact with atmospheric concentrations of oxygen. Hence, no quantitatively statement can be made about the ratio of iron(II) to iron(III) at the different screening processes. Both absorption spectra show an absorbance of more than four (iron at around 250 nm and copper at around 310 nm) were the spec-

trometer cannot illustrate the increase of the absorbance linearly. But the qualitative message that the iron and copper solutions are absorbing a fraction of the irradiating light (λ = 380 nm) at high concentrations is valid. That is the reason why fewer molecules in the sample are excited and explains the decreased fluorescence intensity after addition of large amounts iron or copper bromide.

In summary, none of the relatively small luminescence changes in Figure 2-9 seems to originate from a metal-ligand interaction between **8** and the tested metal bromides. Therefore, **8** turned out to be no proper luminescence sensor under the tested conditions of metal bromides in methanol.

There are two possible reasons for this behavior. Either **8** has a too small binding affinity towards the tested metal cations to compete with a polar protic solvent like methanol or the coordination of a metal cation by **8** does not change its luminescence properties. The bulky protection groups may hint to the first reason. They create a non-polar shell around the nitrogen atoms which should adopt the receptor role. This non-polar environment could hinder the charged metal cation from arriving the pre-coordinative center of **8**.

This assumption could be tested via deprotection of **8** but unfortunately the cleavage led to the earlier described decomposition of **8** (chapter 2.1.7).

The second reason could be evaluated by testing **8** in an aprotic less polar solvent like THF or DCM but **8** was isolated in a very small amount and even luminescence responses in the mentioned non-applicational solvents would not mean a milestone in sensor development due to their distinct differences to water.

However, the luminescence properties of **8** do not seem so justify the extensive and time consuming synthesis of bridged anthracenes like **8** and were therefore not further elaborated throughout this thesis.

2.2 Anthracene derivatives without spacer

Besides anthracenophanes, a second class of anthracene based molecules was synthesized. The idea behind this was to leave out the spacer unit between fluorophore and receptor and work aside the well-known PET effect.
The aspired synthesis is shown in Scheme 2-9.

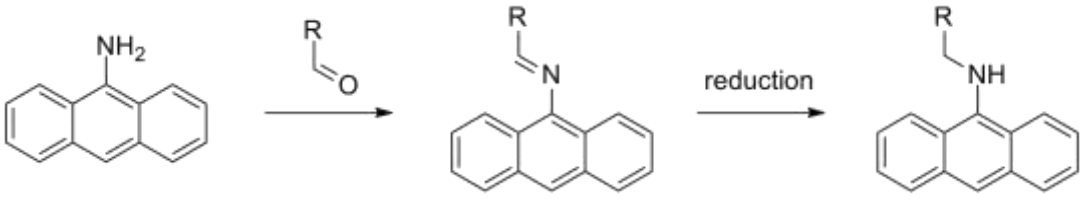

Scheme 2-9: Route to novel potential luminescence sensors in this project.

The first reaction product reflects the sensing mechanism called C=N-isomerization established by LIU and coworkers in 2007.[61] Potential colorimetric sensors build-up like the reduced product are treated from chapter 2.2.10 on. As discussed in the introduction (1.3.5), molecules with a C=N double bond show only very poor fluorescence and are therefore suitable for a luminescent "off"-state. To switch them "on" the C=N isomerization between the *E* and *Z* isomer has to be hindered. By this the non-radiative relaxation path is closed and the luminescence emission is enhanced.
At the starting point of this PhD project in 2011 the C=N-isomerization has not been transferred to the anthracene fluorophore. In 2013 a workgroup from Taiwan published the first example of a sensor working with the C=N isomerization at an anthracene fluorophore.[86]

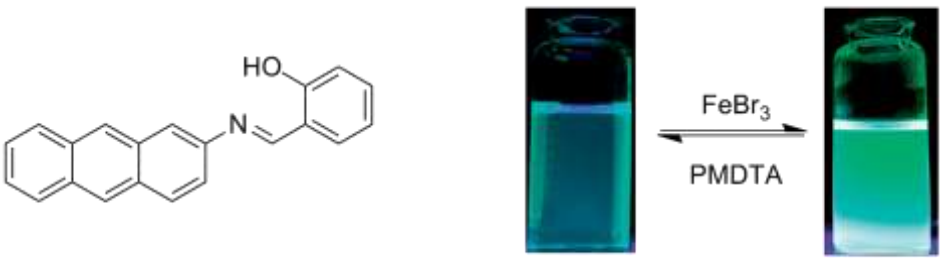

Figure 2-11: Structure (left) and fluorescence emission (right) with and without iron (III) bromide of a 2013 published fluorescence sensor.[86]

The sensor shown in Figure 2-11 was synthesized from salicylaldehyde and 2-aminoanthracene. Its fluorescence emission is greatly enhanced by the addition of iron(III) cations. Throughout their publication they show the absorption, emission and NMR spectroscopic properties. Different counter anions were tested as well as the reversibility of the iron(III) binding by adding the chelating ligand PMDTA.[86]

Without availability of this information, a similar project was initiated by derivatizing anthracene at its 9-position. The key interstage product for this route is 9-aminoanthracene, which was converted with different aldehydes to imines.
In 2009, the workgroup of GLORIUS showed the preparation of 9-aminoanthracene according to Scheme 2-10.[87]

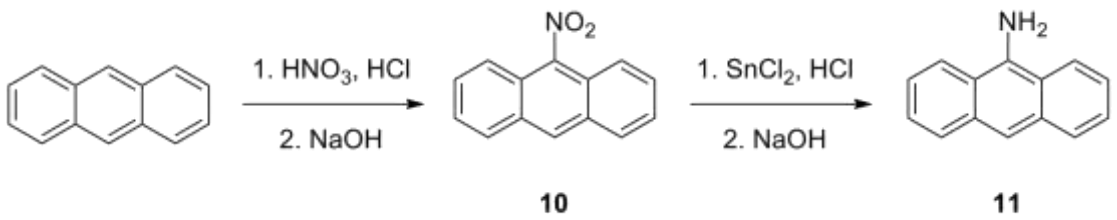

Scheme 2-10: Procedure by GLORIUS for the synthesis of **11**.[87]

So in this project, the first step towards anthracene derivatives without spacer comprises the synthesis of 9-nitroanthracene (**10**).

2.2.1 9-Nitroanthracene (10)

The route to **10** went over 9-chloro-9,10-dihydro-10-nitroanthracene (**9**), which can directly be converted to the nitro compound without purification in between. In 1951 a similar procedure was published which already described the interstage product **9**.[88]

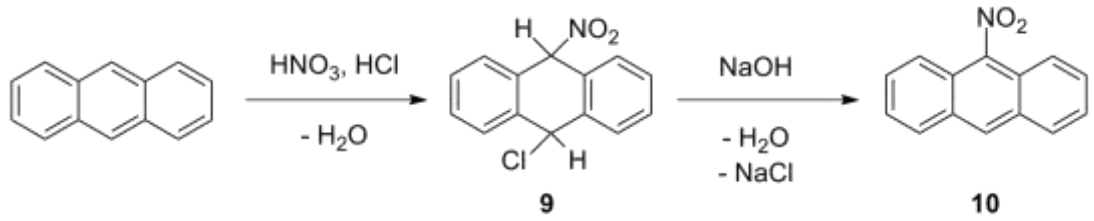

Scheme 2-11: Synthesis of **10** starting with a nitration to **9** and subsequent hydrochloric acid removal.[87]

This nitration reaction of anthracene takes place in glacial acetic acid after addition of concentrated nitric acid at room temperature (Scheme 2-11). When hydrochloric acid is added, the intermediate 9-chloro-9,10-dihydro-10-nitroanthracene (**9**) precipitates rapidly. The yellow solid **9** was filtered through a BÜCHNER funnel and washed with water extensively till the washings became neutral.

The direct conversion to **10** was achieved by pouring the solid into a warm solution of sodium hydroxide. The solution turned red, the yellow solid was filtered through a glass frit and was once again washed with water till the washings became neutral.

This reaction was carried out 4-times during this PhD thesis with a scheduled quantity around 20 g anthracene each time. Only once the quality of the resulting **10** was not satisfying without further purification. At that attempt a glass frit was used in both filtration steps to maximize the yield. A rough filtration through the larger pores of a BÜCHNER funnel seems to be necessary for the purification of **9** and thereby also the increased quality of **10**. If the quality of **10** is not sufficient, a recrystallization from glacial acetic acid can be of help. For this an inert atmosphere is required to prevent the oxidation of **10** towards anthraquinone.

This procedure described by GLORIUS proofed to be a robust synthesis that can be carried out in large scales with yields between 80 and 85 %.

The presence of **9** as an interstage product in the synthesis of **10** has been known for many decades[88] but was not investigated via X-ray diffraction in previous works. Therefore, **9** was crystallized from acetone to determine its solid state structure (Figure 2-12).

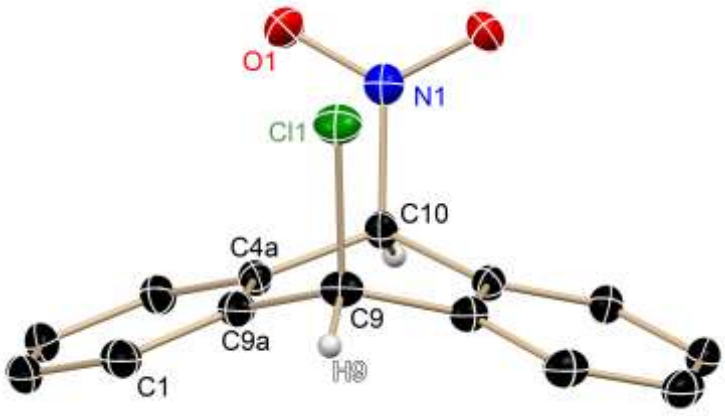

Figure 2-12: Solid state structure of **9**. Positional disorder and hydrogen atoms bond to sp^2 hybridized carbon atoms are not shown.

9-Chloro-9,10-dihydro-10-nitroanthracene crystallizes in the orthorhombic space group $Cmc2_1$ with half a molecule in the asymmetric unit. **9** is completed by a mirror plane through C9, C10, Cl1 and N1. Furthermore, there is a positional disorder between the chlorine atom and the nitro group with a side occupation factor of 7 % which is not shown in Figure 2-12 for clarity. Like all other in this thesis discussed solid state structures, the anisotropic displacement parameters of **9** are depicted at the 50 % probability level. The general treatment of hydrogen atoms is discussed in section 0.

Table 2-2 displays selected bond lengths and angles.

Table 2-2: Selected bond lengths in pm and angles in ° of **9**.

C9–Cl1	184.18(19)	Cl1–C9–C9a	108.32(9)
C10–N1	154.7(5)	O1–N1–C10	118.27(18)
N1–O1	122.6(2)	N1–C10–C4a	110.34(15)
C9–C9a	149.76(16)	C1–C9a–C9	121.44(12)
C10–C4a	150.09(14)	C4a–C9a–C9	119.14(11)
C4a–C9a	140.05(16)	C10–C4a–C9a	118.80(11)

Remarkable is the non-aromatic binding situation in the middle anthracene ring. The distances C9–C9a and C10–C4a are in a regular region of a C(sp^3)–C(sp^2) single bond (151 pm)[89] and around 10 pm longer than the distance between C4a–C9a which is similar to the bond distance in benzene (139.5 pm).[90]
Another hint towards the sp^3 hybridization of C9 and C10 is the relative small angle of 127 ° between the outer aromatic rings compared with a planar arrangement of 180 °. This angles and distances are in good agreement with the result that the carbon atoms at the 9-and 10-position of the anthracene scaffold have four binding partners each.

To conclude, the preparation of the interstage product **9** and its conversion to 9-nitroanthracene (**10**) were reliable synthesis in a multiple gram scale with good yields.

2.2.2 9-Aminoanthracene (11)

In this project, the preparation of **11** was the key step to anthracene derivatives without a spacer unit because of its important role as the central starting material for the later on synthesized imines. Thereby **11** was indirectly also crucial for the synthesis of novel amines discussed from chapter 2.2.10 on. The procedure of GLORIUS and coworkers was taken as the starting point.[87]

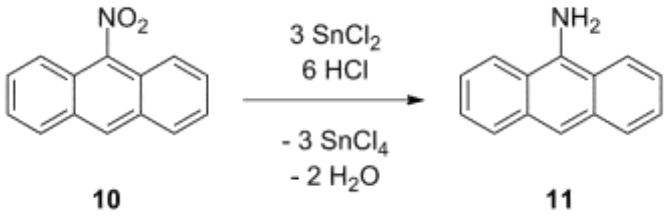

Scheme 2-12: Synthesis of **11** by reduction of the nitro to an amino group.[87]

As shown in Scheme 2-12 the reduction of the nitro group to an amino group was done with tin(II) chloride. **10** was dissolved in conc. acetic acid and tin(II) chloride was added in conc. hydrochloric acid. An excess of 5 equivalents was used at a temperature of 80 °C. Up to this point, the reaction was carried out as described by

GLORIUS. Variations were done with the chosen tin(II) chloride, the addition speed of its suspension in conc. hydrochloric acid and in the purification process.
While in the published procedure anhydrous tin(II) chloride was used, in this work the dihydrate of the reducing agent was chosen because it was suspended in aqueous hydrochloric acid anyway.
Secondly, it turned out that the mentioned suspension had not to be added via a dropping funnel over 10 minutes but could be poured through a normal funnel. No differences were visible in the resulting quantity or quality of **11**.
The most important changes were done throughout the purification process. GLORIUS and coworkers did not mention the sensitivity of **11** towards air. When 9-aminoanthracene is exposed to oxygen its color changes from orange to black. Maybe this behavior was not noticed because they directly converted it into a carbene precursor. But for the purpose of storage and long-term stability the purification of **11** had to be reworked.
After the reduction (Scheme 2-12) the reaction mixture was filtered through a glass frit under inert atmosphere and was washed many times with water till the washings became neutral. The used demineralized water was not degased but the described treatment was sufficient to avoid oxidation reactions to a large extend.
The second not mentioned problem was the formation of non-soluble tin(IV) oxide. To eliminate this problem, the organic components of the residue after filtration were dissolved through the glass frit by the addition of degased, dried chloroform. After removal of the volatile constituents the crude product was recrystallized from a mixture of hexane (degased) and chloroform (dried, degased) under inert atmosphere. With a recrystallization under inert conditions in the last purification step and therefore filtration by using a SCHLENK frit it was easily possible to store **11** in an argon glove box to guarantee its long-term stability.

By this approach a reliable procedure was established to generate the key interstage product **11** for potential luminescence sensors based on anthracene derivatives without spacer in a yield around 5.5 g and 50 % in one reaction. The quality of **11** was confirmed via NMR spectroscopy, mass spectrometry and elemental analysis.

It was also possible to determine the solid state structure of **11** via X-ray diffraction and therefore to describe its structural features in more detail than former researchers in this area.

Suitable single crystals of **11** were obtained by recrystallization from a mixture of hexane and chloroform (Figure 2-13).

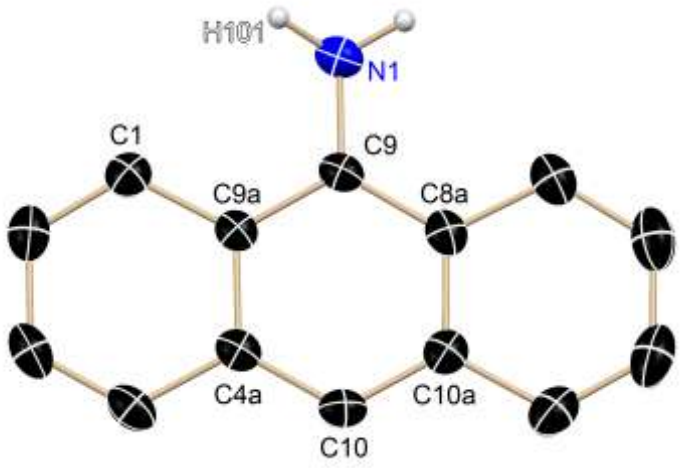

Figure 2-13: Part of the solid state structure of **11**. Hydrogen atoms bond to sp^2 hybridized carbon atoms are not shown.

9-Aminoanthracene crystallizes in the triclinic space group $P\bar{1}$ with two molecules in the asymmetric unit of which one is 2-fold disordered (described in chapter 5.2.2). The determination of hydrogen atom positions is discussed in section 0. In Table 2-3 a selection of bond lengths and angles from the completely occupied one is presented.

Table 2-3: Selected bond lengths in pm and angles in ° of **11**.

N1–C9	138.6(2)	N1–C9–C9a	118.90(16)
N1–H101	89(2)	C8a–C9–C9a	120.43(16)
C9–C9a	141.7(2)	C9–N1–H101a	116.2(14)
C1–C9a	142.2(3)	C1–C9a–C9	122.48(16)
C10–C4a	139.7(3)	C4a–C9a–C9	118.98(16)
C4a–C9a	143.0(2)	C4a–C10–C10a	120.69(17)

The displayed carbon–carbon distances of the middle anthracene ring are in the range between C(sp^2)–C(sp^2) single (147 pm) and C(sp^2)–C(sp^2) double bonds (134 pm) as expected for an aromatic hydrocarbon. Whereas the nitrogen-carbon distance is a bit shortened compared with a regular N(sp^3)–C(sp^2) single bond of 143 pm and even a N(sp^2)–C(sp^2) single bond of 140 pm.[89] Together with the relatively large carbon-nitrogen-hydrogen angle of 116.2(14) (compared with the ideal tetrahedral angle of 109.45 °) one may assume a partly delocalized nitrogen lone pair through the aromatic scaffold.

To conclude this section, the procedure of GLORIUS and coworkers to **11** had been optimized by a rework of its purification and a long-term storage option was approved. Furthermore, the solid state structure of **11** was investigated by single crystal X-ray diffraction for the first time.

2.2.3 Luminescence properties of 9-aminoanthracene (11)

During studying the synthesized potential sensors of this project, 9-aminoanthracene turned out to be a useful reference compound towards imines and amines synthesized later on.

Therefore, its absorption and emission properties were investigated as well as changes in the fluorescence emission after varying the pH value in the acidic range.

2.2.3.1 UV/Vis absorption and fluorescence emission of 9-amino-anthracene (11)

To determine a proper excitation wavelength for the following fluorescence investigations, the absorption of a 10^{-5} M solution of **11** in methanol was measured.

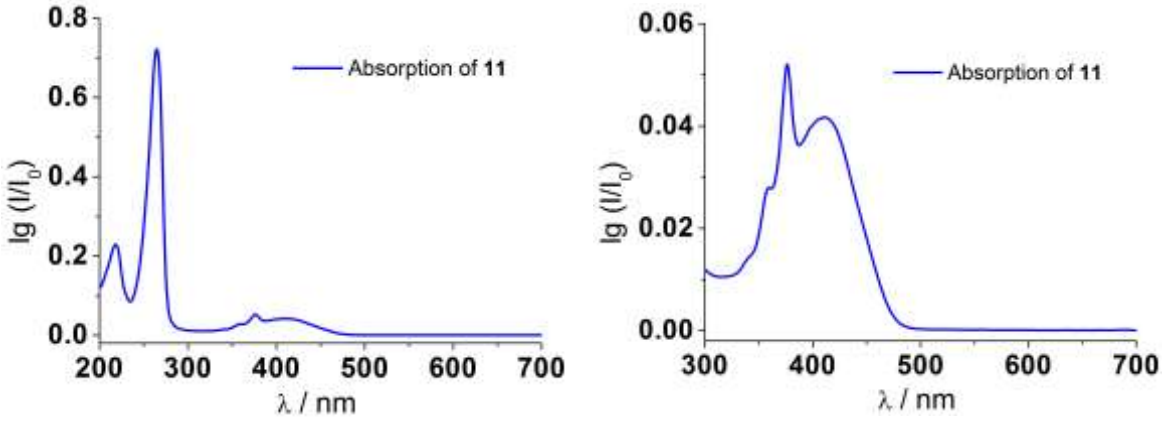

Figure 2-14: UV/Vis absorption spectra of **11**. Left: full spectrum; right: enlargement of the spectral region around 400 nm (10^{-5} M in MeOH).

In Figure 2-14 one can see the absorption features of 9-aminoanthracene. In the left spectrum three signals are visible. Two rather narrow ones at $\lambda = 218$ nm and $\lambda = 265$ nm and a broader signal around $\lambda = 400$ nm. The displayed absorption spectra are corrected by subtraction of a reference spectrum containing just methanol. Nevertheless, the energetically highest peak with $A_{218} = 0.22$ is less meaningful because methanol absorbs there quite strongly and the subtraction in that spectral region is less accurate.

Both other signals show the absorption of **11** and therefore excitation at these wavelengths should result in fluorescence emission if they belong to a radiative transition.

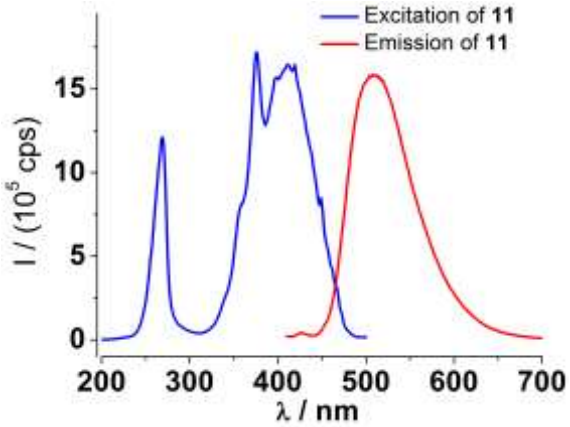

Figure 2-15: Excitation (red, λ_{det} = 510 nm) and emission (blue, λ_{ex} = 400 nm) spectra of **11** (10^{-5} M in MeOH).

Figure 2-15 displays the excitation and emission properties of **11**. Often the excitation spectrum of a compound looks like its UV/Vis absorption spectrum and this is also valid for **11** (Figure 2-14). Both show a sharp signal around 265 nm and a broader one around 400 nm whereas the broader signal exhibits in both cases an additional sharp peak around 370 nm.

The intensity ratio between these peaks is not equal in the absorption and the excitation spectrum. This indicates, that not every at 265 nm absorbed photon causes fluorescence but a larger part of the excited molecules relaxes non-radiatively compared to an excitation around 400 nm.

The emission spectrum of **11** looks like a mirror image of its absorption spectrum except of the sharp peak around 370 nm. This can be interpreted analog the case of quinine were a higher energetic shoulder is visible in the absorption but not in its emission spectrum.[24] While the transition between the ground state (S_0) and the second electronically excited state (S_2) appears in the absorption spectrum, the lifetime of this excited state is long enough for the molecules to relax to the S_1 state thermally. Therefore, the emission is not the mirror image of the whole absorption spectrum but of the $S_0 \rightarrow S_1$ transition.

A similar behavior is valid for the transition between the S_0 and S_3 state. It is observable in the absorption as well as in the excitation spectrum (at 265 nm) but a direct radiative relaxation to the ground state is not recorded for **11** in the corresponding emission spectrum. In the case of anthracene the non-radiative relaxation constant for the internal conversion $S_3 \rightarrow S_1$ was estimated to $2 \cdot 10^{13}$ s^{-1} and is the

reason anthracene emits fluorescence exclusively from the first electronically excited state (S_1).[91]

The STOKES shift of 98 nm between the maxima of absorption (λ = 411 nm) and emission (λ = 509 nm) is relatively large compared to 7 nm of **8** and could be a hint to phosphorescence. However, this large difference is partly caused by the absence of a vibrational structure in absorption and emission of **11**. Therefore, the difference between absorption and emission could not been extracted from the energetically lowest vibrational absorption peak and the highest energetically vibrational state of the emission but from the maxima of the broad signals.

In order to explore if the large STOKES shift accompanies with an occupied excited triplet state and therefore phosphorescence, the lifetime of the excited state was measured during a workshop and exhibition of the company HORIBA SCIENTIFIC in Essen 2014. The received figure is displayed in chapter 5.1.4 and reveals a single exponential decay with a lifetime of 7.9 ns for **11**.

This nanosecond lifetime is typical of a fluorescence process and therefore the population of a triplet state can be excluded. Only the lifetime of this derivative was explored but because of the similar, non-heavy atom containing scaffolds prepared and investigated during this project with comparable STOKES shifts, the ongoing radiative processes may all be termed fluorescence. However, emission changes caused by the addition of metal salts were termed luminescence because of the potentially heavy atom containing aggregates.

2.2.3.2 Addition of acids to 9-aminoanthracene

For comparability, the luminescence properties of **11** after addition of acids were tested. Therefore, hydrochloric acid was chosen because of its complete dissociation in water and aluminum bromide to evaluate the presence of a LEWIS acidic metal cation[92].

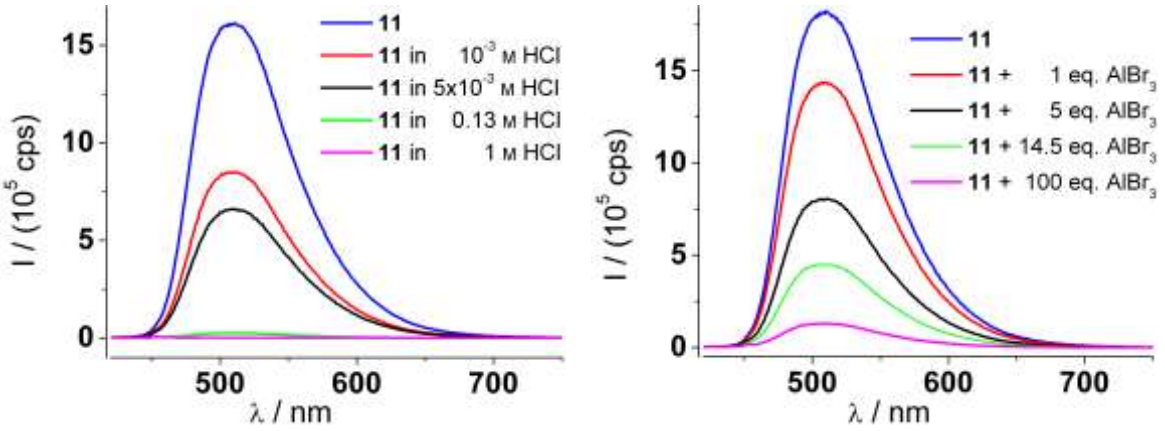

Figure 2-16: Stacked emission spectra of **11** (10^{-5} M in MeOH) before and after the addition of: aqueous HCl (left), $AlBr_3$ in MeOH (right) (λ_{ex} = 400 nm).

In the left part of Figure 2-16 the emission spectra upon addition of hydrochloric acid are displayed. When acid was added to a concentration of 10^{-3} M the intensity decreased to about half of its starting value. The addition of larger amounts led to a further decrease until at a 1 M concentration no emission of **11** was left. A similar behavior can be seen in the case of aluminum bromide (Figure 2-16 right). The more metal salt was added the less radiation reached the detector. The decrease is less pronounced than in the case of hydrochloric acid because substantially lower concentrations were added.

Both overlays show no wavelength changes and in both samples a non-luminescent derivative was forming.

2.2.4 9-Anthracenesalicylimine (12)

The condensation reaction between a primary amine and an aldehyde is known for more than one century and the reaction products belong to the substance class of SCHIFF bases named after the German chemist HUGO SCHIFF.[93]

With the synthesis of **12** the C=N isomerization should be transferred to the anthracene fluorophore. The synthesis of 9-aminoanthracene (**11**) was achieved, improved and the first aldehyde to combine with was salicylaldehyde.

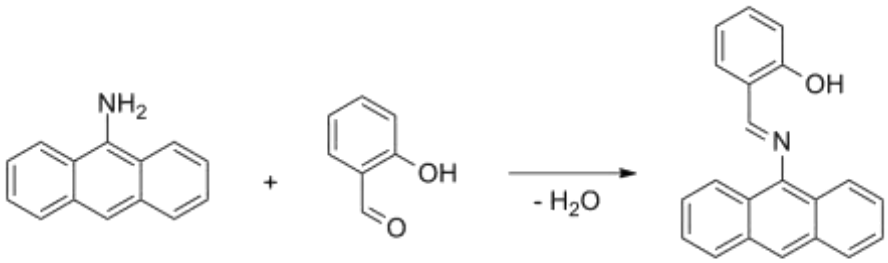

11 **12**

Scheme 2-13: Synthesis of **12** by combination of **11** with salicylaldehyde.

The reaction shown in Scheme 2-13 was carried out several times but the best results were achieved with the following conditions. Ethanol (degased) was chosen as solvent and inert conditions were applied. An excess of salicylaldehyde (1.5 eq.) was added and the reaction mixture was heated to the boiling point of the solvent. Meanwhile, a yellow precipitate was forming and after 1.5 h the conversion was tested via ^{1}H-NMR spectroscopy. The resulting spectrum is displayed in Figure 2-17. The aromatic region of the blue spectrum, belonging to the reaction mixture after boiling for 1.5 h, looks complex but the signals can be assigned easily by comparison to the below spectra. Herein the starting materials **11** (red) and salicylaldehyde (black) as well as the desired reaction product **12** (green) are displayed. Due to only little overlap of the chemical shifts belonging to the three species, every compound can be assigned and by this a ratio between the present components can be determined.

Especially the signals of **11** at 6.61 ppm and **12** at 8.95 ppm can be used to identify the conversion of the reaction at different times to monitor the progress of the reaction because they are distinctively separated from further peaks.

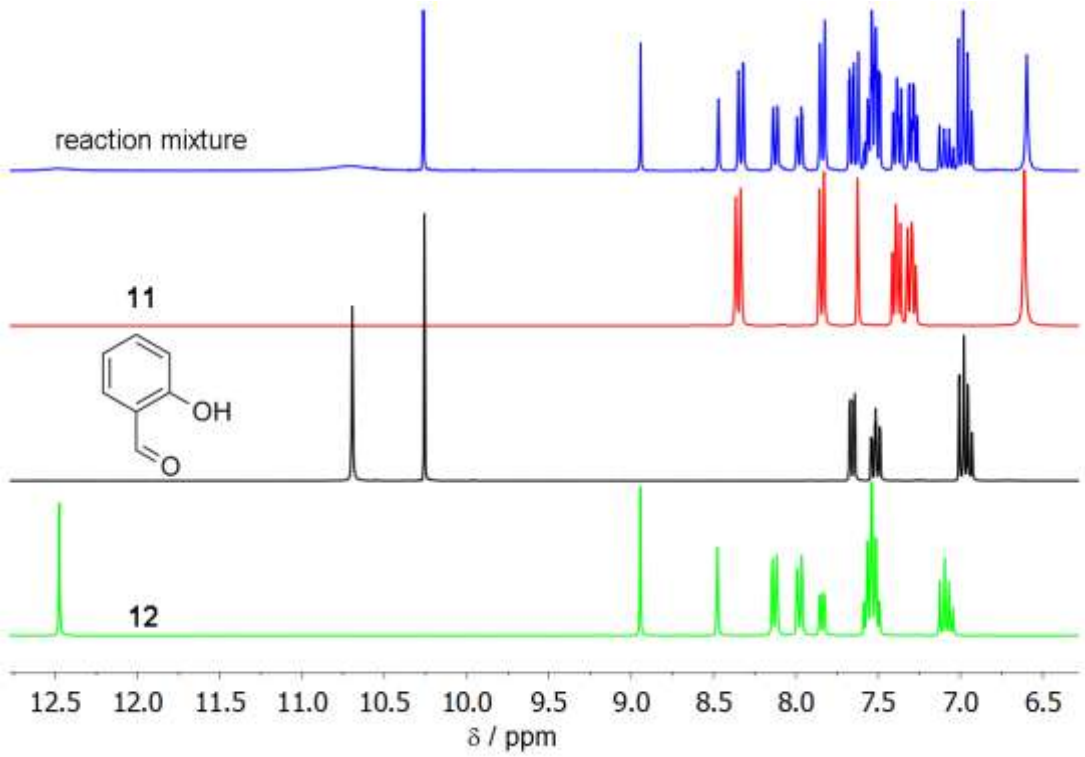

Figure 2-17: ^{1}H-NMR spectra in DMSO-d_6 of: reaction mixture (top, blue), the starting materials **11** (red, second) and salicylaldehyde (black, third) and the reaction product **12** (bottom, green).

Despite of this seemingly good initial position from the spectroscopic point of view, the ratio could not be determined exactly because of the precipitating reaction product. So a taken sample of the reaction mixture is only a hint to the real conversion. From the blue spectrum, a ratio of 1.5:1 between **11** and **12** was determined. Therefore the reaction mixture was heated for additional 2 h resulting in a ratio of 0.46:1 and thereby an ongoing reaction. After further 2.5 h of heating the reaction mixture was stirred at room temperature overnight.

For purification, the formed precipitate was filtered through a glass frit at inert atmosphere and was washed with ethanol. The solid was stored in a glove box and turned out to be very pure in a yield of 93 %. The quality is visible in the ^{1}H-NMR spectrum displayed in the green line of Figure 2-17 and in the excellent agreement of the measured elemental analysis with the calculated mass fractions (chapter 4.4.9).

Furthermore, the solid state structure of **12** was determined via X-ray diffraction (Figure 2-18) after obtaining single crystals by slowly evaporating its solvent chloroform.

9-Anthracenesalicylimine crystallizes in the triclinic space group $P\bar{1}$ with one molecule in the asymmetric unit.

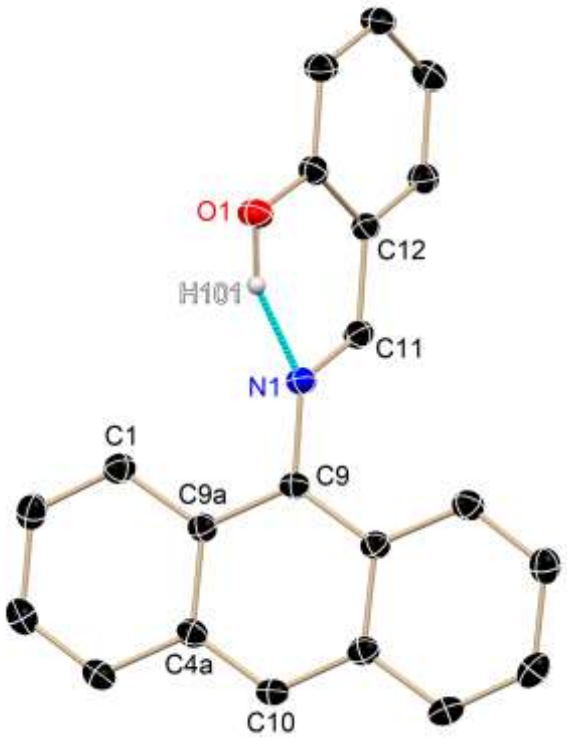

Figure 2-18: Solid state structure of **12**. Hydrogen atoms bond to sp^2 hybridized carbon atoms are not shown.

The largest deviation one carbon atom exhibits to a plain through all anthracene carbon atoms is with 3.0 pm very small, indicating that the anthracene moiety is nearly planar. A plane through the phenyl ring is twisted to the first mentioned one by 70.056(42) ° and therefore a delocalized π-system along the whole molecule seems to be unlikely.

Table 2-4: Selected distances in pm and angles in ° of **12**.

C9–N1	141.94(13)	N1–C9–C9a	117.61(9)
C11–N1	128.51(14)	N1–C11–C12	121.34(10)
C11–C12	145.65(14)	C9–N1–C11	120.84(9)
O1–H101	98.8(19)	C1–C9a–C9	122.36(9)
O1–N1	259.03(14)	C9a–C4a–C10	119.55(9)
N1···H101	168.9(19)	O1–H101···N1	149.7(16)

Some selected bond lengths and angles as well as information about the hydrogen bond in **12** are displayed in Table 2-4.

The bond distance between the nitrogen atom N1 and the carbon atom C11 corresponds to a regular N(sp^2)–C(sp^2) double bond of 129 pm and suggests also a localized double bond. Furthermore, the distance between C9 and N1 fits a normal N(sp^2)–C(sp^2) single bond with 140 pm.[89]

Also noticeable is the intramolecular hydrogen bond between the hydroxyl group as donor and the imine function as acceptor. Following a classification by JEFFERY the observed geometry points towards a moderate strength. In this category the hydrogen–acceptor distance is found between 1.5 and 2.2 Å, the angle of the three involved atoms is larger than 130 ° and the distance found between the acceptor and the donor lies in the range of 2.5 to 3.2 Å.[94] The geometric results of the solid state investigations are at the shorter side of the categorized values. Therefore, the intramolecular hydrogen bond strength in **12** can be termed moderate, nearly strong.

In conclusion, **12** was synthesized for the first time and by this an anthracene derivative with a C=N double bond directly linked to the fluorophore was prepared. A very high yield of 93 % was achieved and **12** was fully characterized (NMR spectroscopy, mass spectrometry, elemental analysis and X-ray diffraction).

2.2.5 Detailed analytical investigations on 9-anthracenesalicylimine (12)

Being the first potential sensor without a spacer unit between the fluorophore and the receptor unit in this project, **12** was examined carefully. After the successful synthesis extensive spectroscopic studies were carried out on this molecule.

2.2.5.1 UV/Vis absorption and fluorescence emission of 9-anthracenesalicylimine (12)

The first investigations were done by UV/Vis spectroscopy to evaluate the absorption properties of **12**. This allowed the identification of a suitable excitation wavelength for following emission studies.

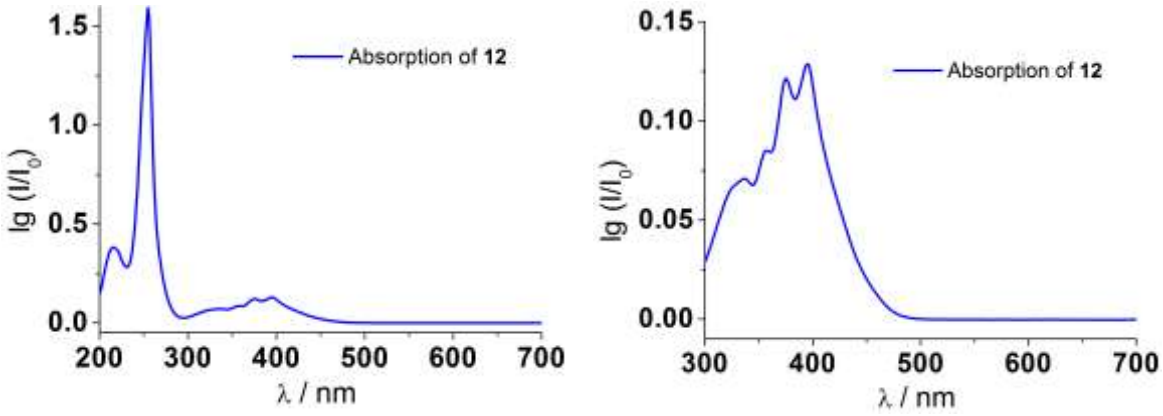

Figure 2-19: UV/Vis absorption spectra of **12**. Left: full spectrum; right: enlargement of the spectral region around 400 nm (10^{-5} M in MeOH).

The absorption spectrum shown in Figure 2-19 is similar to that of 9-aminoanthracene (Figure 2-14). The most intense signal at λ = 255 nm is shifted by 10 nm compared to **11** and the broader signal of **11** around 400 nm is more structured in the case of **12** with maxima at 337 nm, 357 nm, 375 nm and 395 nm. This pattern is observable due to resolved vibrational energy levels. The absorption of **12** is with A_{255} = 1.59 stronger than **11** with a maximum of A_{265} = 0.72.

To compare these two species in more detail, the excitation and emission of **12** is displayed in Figure 2-20.

The luminescence emission shown by the red line is weak compared to the two derivatives **8** and **11** investigated before. Just a few thousand cps are emitted here

whereas **8** and **11** had intensities in the range of one million cps. This is also visible in the low signal to noise ratio. The small intensity exposes also the RAMAN peaks of the solvent methanol. This phenomenon is discussed in chapter 4.2.2.

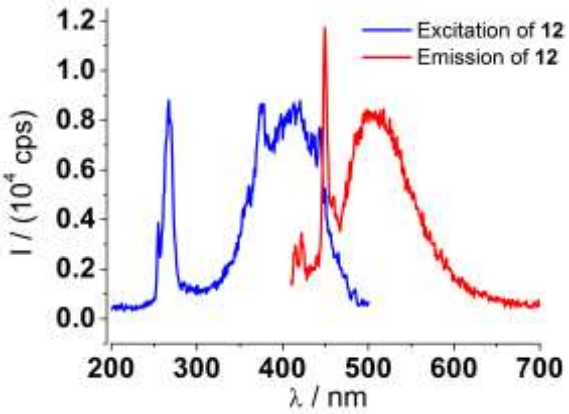

Figure 2-20: Excitation (blue, λ_{det} = 510 nm) and emission (red, λ_{ex} = 397 nm) spectra of **12** (10^{-5} M in MeOH).

The in general relatively weak emission of **12** is a hint towards a working C=N isomerization. Despite of the even stronger absorption of **12** compared to **11** its emission intensity is way lower.

In fact, the weak emission seen in the red curve of Figure 2-20 is not caused by **12**. This statement is confirmed by comparing the UV/Vis absorption with the excitation spectrum of **12**. As mentioned in section 2.2.3.1, the UV/Vis absorption spectrum often looks like the excitation spectrum. This is not the case for **12**. While the first one exhibits a vibrational structured band, the second has a broad maximum around λ = 400 nm with a shoulder at 370 nm. This shoulder is also present in the absorption and excitation spectra of **11** and gives a first hint that the already low emission in Figure 2-20 originates from **11** instead of **12**.

Two additional arguments for this are exhibited in Figure 2-21.

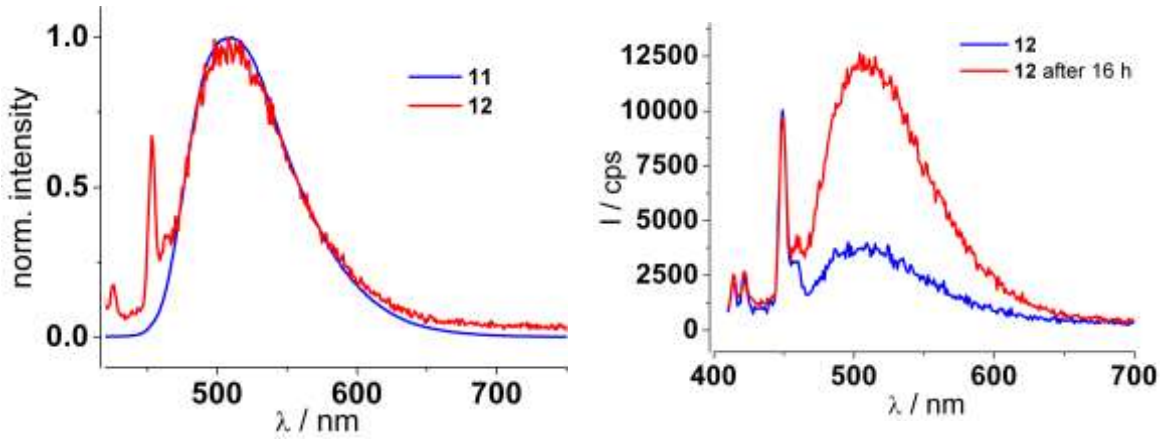

Figure 2-21: Left: compared emission of **11** and **12**. Right: stability of **12** after 16 h.

At the left side the emission spectra of **11** and **12** are compared. The curves are very similar except for their intensity. The signals are normalized but one can still see the larger noise in the red curve of **12** and the resolved RAMAN peaks of methanol (cf. chapter 4.2.2) whereas neither is visible in the blue spectrum.

A further sign for fluorescence of **11** instead from **12** is the increased emission intensity shown in the right part of Figure 2-21. After a period of 16 hours the emission around $\lambda = 510$ nm increased by a factor of approximately three. This could mean a raised concentration of the emitting species and is possible by formation of this derivative over time from the non-radiative species **12**.

The back reaction to the starting material of **12** seems plausible in the protic solvent methanol, containing traces of water.

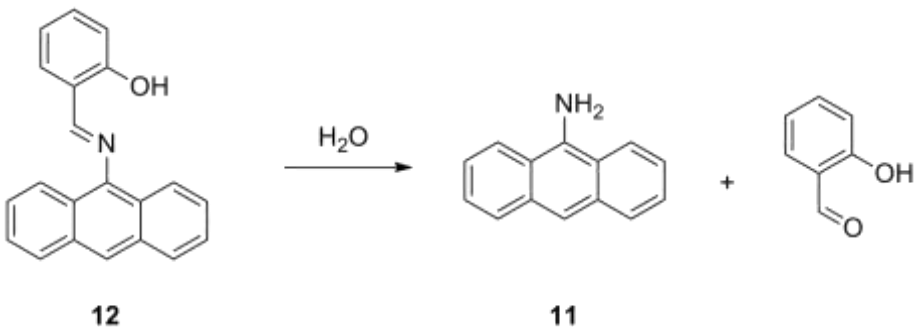

Scheme 2-14: Back reaction of **12** to its starting materials.

The extent of this back reaction, shown in Scheme 2-14, can be estimated by the fluorescence intensity at $\lambda = 510$ nm of **11**. If the imine is 100 % decayed to 9-

aminoanthracene, the fluorescence emission should reach an intensity of about 1.5 million cps for a 10^{-5} M solution as observed before (Figure 2-15). This is only true if no further conversion of **11** occurs and only possible if enough water is present in the used methanol. With this in mind, the increased emission in the right part of Figure 2-21, combined with the low intensity ($<1.5 \cdot 10^4$ cps), suggests a back reaction of less than 1 % after 16 h .This hints to an imine more stable than envisaged at first glance.

Two further arguments that support the hypothesis of a proceeding back reaction and emission that is exclusively caused by 9-aminoanthracene become obvious through the analysis of fluorescence and ^{1}H-NMR spectroscopic experiments after the addition of acids to **12** in the next sections.

2.2.5.2 Fluorescence analysis after the addition of acids and bases to 9-anthracenesalicylimine (12)

The first approaches to evaluate the fluorescence sensor capability of the synthesized imine **12** were to vary the pH value by adding acids or bases respectively. A procedure analog to the investigation of **8** was applied and the conditions are listed in Table 2-1.

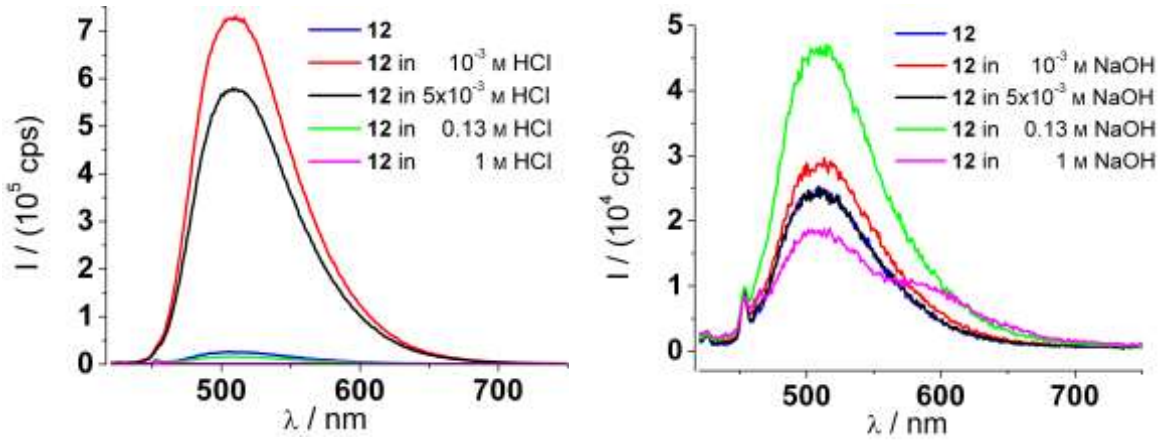

Figure 2-22: Emission spectra of **12** under acidic (left) and alkaline (right) conditions (λ_{ex} = 400 nm).

In the left part of Figure 2-22 one can see the very strong response of **12** towards protons. When hydrochloric acid is added till a concentration of 10^{-3} M is reached, the luminescence intensity is enhanced to more than $7 \cdot 10^5$ cps (30-times amplified). But the addition of more acid led to a decrease of emission; especially a very

large excess to a concentration of 0.13 M resulted in a lower radiation than in the beginning of the experiment. Adding even more hydrochloric acid up to a 1 M solution caused the complete quenching.

In contrast, the changes after addition of sodium hydroxide solution were moderate and lacking a clear tendency. The addition to a concentration of 10^{-3} M yielded a small increase, after the next addition the emission decreased and a 0.13 M solution resulted in a stronger enhancement of luminescence. The last addition caused once again a decrease to a less intense emission than the starting point not explainable by dilution exclusively. At a very high concentration of sodium hydroxide a second band around 600 nm appears but is low in intensity. However, concerning the large excess that was added to **12** the changes are moderate and **12** seems to be stable to huge amounts of strong bases.

It is obvious that **12** is not stable in the presence of acids. The increase in intensity described above is once again a sign of the back reaction towards **11** and in fact the subsequent quenching was also observed in the case of 9-aminoanthracene after the addition of hydrochloric acid (Figure 2-16 left). If no second process would take place lowering the concentration of **11**, an emission of around 1.5 million cps would be expected. The only half intense luminescence in the left part of Figure 2-22 is an additional hint for the further conversion of the formed 9-aminoanthracene to non-fluorescent derivatives.

Because no stoichiometric contribution of protons is needed (cf. Scheme 2-14) in the back reaction of **12**, they seem to adopt a catalytic role. **12** reacts very slowly in the absence of protons as seen in the right part of Figure 2-21. So protons accelerate the cleavage of the imine whereas their addition also enlarged the concentration of water and thereby of a reactant. It is important to mention, that the enhanced concentration of water cannot be the main reason for the back reaction of **12** towards **11**, because the same amount of water has been added in the case of sodium hydroxide (Figure 2-22 right).

Another argument for the catalytic role of protons in the imine cleavage can be found evaluating the NMR spectroscopic experiments in the following section.

In summary, there are two ongoing processes when protons are added to **12**. The first one is the back reaction to **11** and the second one is a further conversion of **11** to non-fluorescent products.

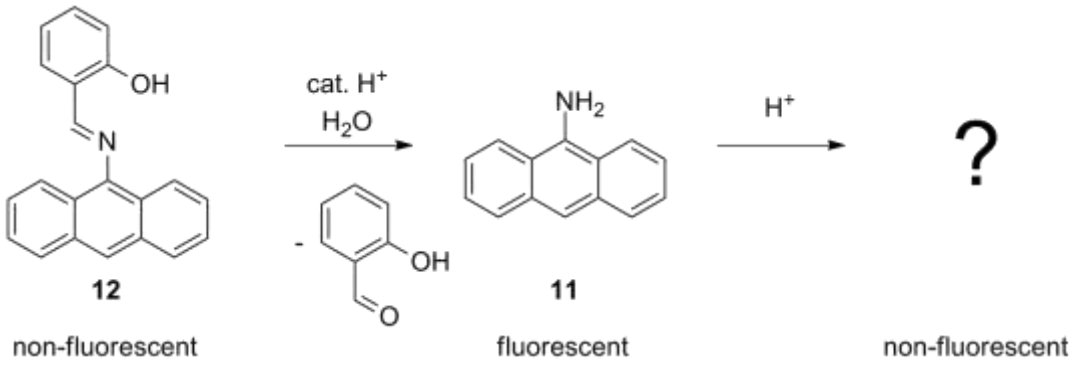

Scheme 2-15: Back reaction of the non-fluorescent **12** to its fluorescent starting material **11** and further conversion to non-fluorescent products.

Assuming an imine cleavage catalyzed by protons, the amount of the added acid should accelerate the reaction but not determine the extent of conversion.
Therefore time resolved emission spectra of **12** after the addition of hydrochloric acid were recorded.

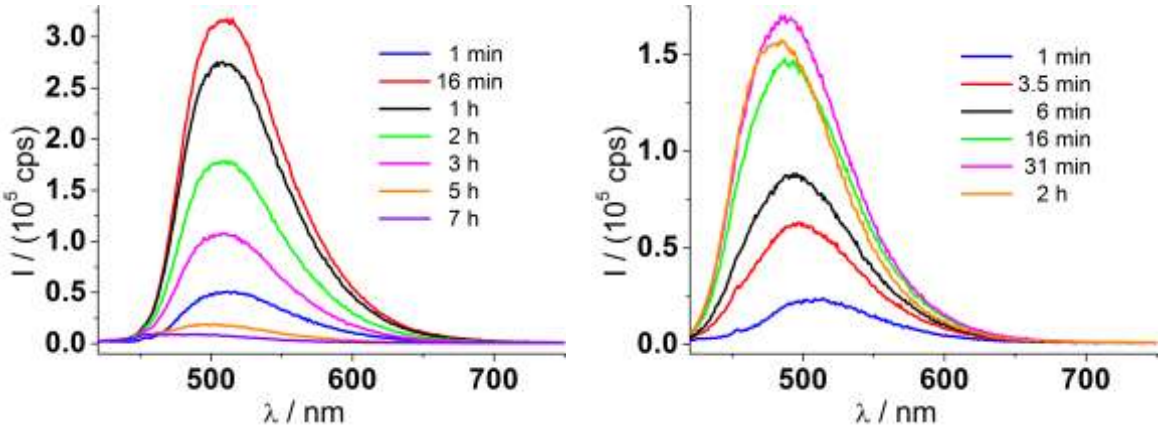

Figure 2-23: Emission spectra of a 10^{-5} M solution of **12** in MeOH after addition of 10 eq. HCl (left) and 100 eq. $AlBr_3$ (right) (λ_{ex} = 400 nm).

In the left part of Figure 2-23 the time dependent emission of **12** after addition of 10 eq. hydrochloric acid is displayed. Every 15 minutes a spectrum was recorded and a selection is shown here. After one minute the intensity rose to around $5 \cdot 10^4$ cps at 510 nm indicating the formation of **11**. The fluorescence maximum is reached after 16 minutes and followed by a slower decrease that can be monitored

in an hour time scale. So in the beginning the formation of **11** is faster than its further conversion into non-fluorescent products and the intensity rises but after 16 minutes the opposite is true. Here, the second reaction becomes faster than the first one and the intensity decreases because of lacking starting material **12** and the accompanied increased concentration of **11**.

However, the intensity after 16 minutes of around $3 \cdot 10^5$ cps is not only less intense than the emission of a 10^{-5} M solution of **11** but also just half-way in respect to the maximum intensity of **12** after addition to 10^{-3} M hydrochloric acid (Figure 2-22 left). By this observation, one can conclude that a smaller amount of added acid results in a later reached and less intense maximum emission.

The same trend, at first increase and afterwards decrease of fluorescence emission, can be seen in the right part of Figure 2-23. One minute after addition of 100 eq. aluminum bromide the emission rose to around $2 \cdot 10^4$ cps and increased till 31 minutes to about $1.5 \cdot 10^5$ cps. Afterwards the intensity slowly decreased (orange line after 2 h). Here, instead of aqueous hydrochloric acid a solution of aluminum bromide in methanol was added to the ligand solution in methanol. Because of the much smaller amount of water content a quantitative comparison is not possible, but qualitatively one can realize the same tendency in both experimental setups.

This is once again a sign that a large excess of water is not needed for the acid catalyzed imine cleavage of **12** to **11** neither for the following conversion of **11** to non-fluorescent products.

To conclude, the prepared imine **12** reacts acid catalyzed to 9-aminoanthracene which is further converted to non-fluorescent products according to Scheme 2-15.

2.2.5.3 NMR spectroscopic analysis on 9-anthracenesalicylimine (12)

A structural confirmation of the proposed decomposition of **12** can be found through ^{1}H-NMR spectroscopic investigations. Therefore, **11** and **12** were again treated with hydrochloric acid and NMR spectra were recorded. In the first part acid was added to **11** to understand its decomposition and in a second part the decay of **12** to **11** is discussed.

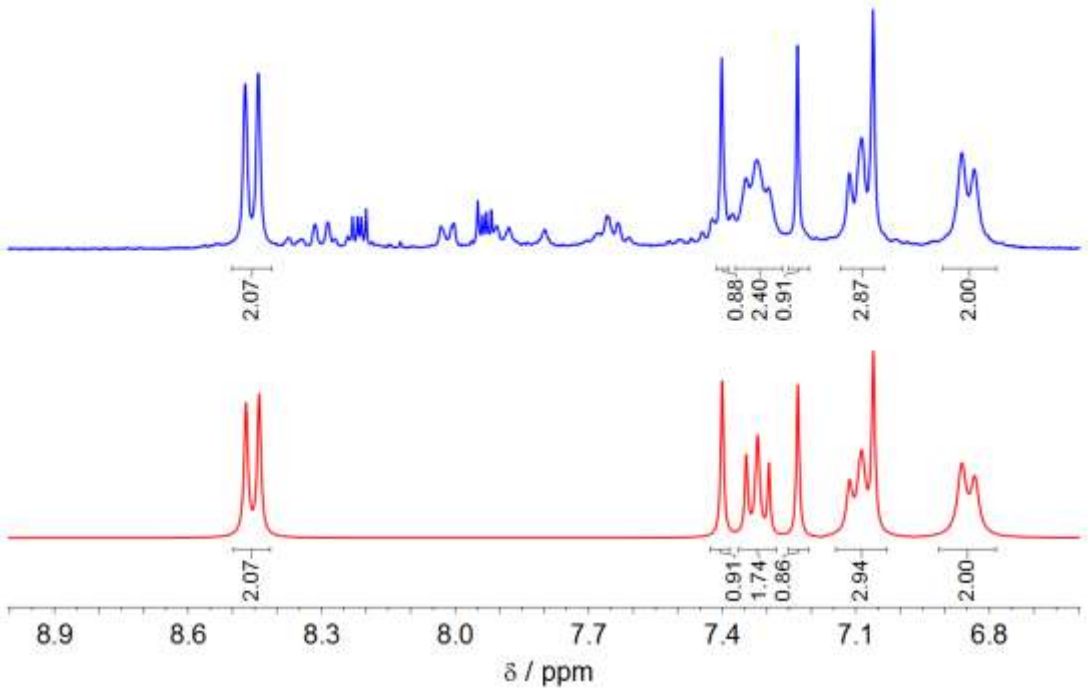

Figure 2-24: Measured ^{1}H-NMR spectrum of **11** in DMSO-d_6 after addition of HCl (top) and ^{1}H-NMR spectrum derived via deconvolution of the first one to illustrate its main species (bottom).

It has to be taken into account that luminescence studies are carried out in a concentration range of 10^{-5} M whereas NMR investigations require 1000-fold higher concentrations of around 10^{-2} M. So it is not possible to work under exactly the same conditions but one can transfer ideas from one spectroscopic technique towards the other.

To receive the upper ^{1}H-NMR spectrum (blue) of Figure 2-24 **11** was dissolved in DMSO-d_6, 10 eq. aqueous hydrochloric acid were added and the mixture was stored overnight exposed to air. After one day the displayed NMR spectrum was recorded. Within the depicted aromatic region of the spectrum several species are visible and one of them is highlighted via deconvolution in the lower part of Figure 2-29.

This red spectrum exhibits two doublets at δ = 6.85 ppm and 8.46 ppm. The signal around 7.09 ppm consists of one triplet and one sharp peak at its low field side and a second triplet is found at 7.32 ppm. These four signals (the two doublets and the two triplets) are similar in intensity and typical for a 1,2-substituted aromatic system. The three sharp peaks at 7.06 ppm, 7.23 ppm and 7.40 ppm are by themselves also similar in intensity and show a spacing of 51.0 Hz.

This points towards a ^{14}N-^{1}H coupling that can also be found in ammonium with 52.8 Hz.[95] ^{14}N is with a natural abundance of 99.6 % mainly present in non-isotopic enriched samples and has a nuclear spin of 1.[96] Therefore, a $^{1}J_{14N\text{-}1H}$ coupling results in a triplet with intensities of 1:1:1 and is resolved only in very symmetric systems.

Added up, these three sharp peaks bear an integral between two and three (compared to the other aromatic signals in the red spectrum with an intensity of two) but part of their intensity may be caused by underlying further signals of unresolved aromatic derivatives. Therefore the corresponding number of protons should be two.

So the main product shown in the spectra of Figure 2-24 should consist of two 1,2-substituted aromatic substituents and one symmetric NH_2 group. The discussed spectroscopic features fit to the oxidized derivative shown in Scheme 2-16.

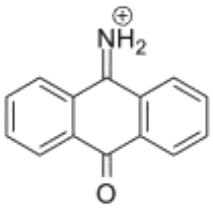

Scheme 2-16: Oxidation product of **11** after addition of HCl. The chloride anion is not depicted.

A similar observation without the presence of protons was made in 1956. An American research group discussed the oxidation of **11** based on melting point and color changes after stirring a solution of 9-aminoanthracene in benzene or ethanol for two or three days.[97] Following their description, **11** showed a melting point of around 147 °C and the - in their publication called - anthraquinone monoimine melted around 224 °C. They obtained it in a yield between 13 and 19 % and confirmed its composition via elemental analysis.

In combination with their observations it seems plausible that one of the decomposition products of **11** in acetic media is the protonated anthraquinone monoimine shown in Scheme 2-16.

The second process observed by ^{1}H-NMR was the acid catalyzed reaction of **12** towards **11**. Two different concentrations of hydrochloric acid were added to a NMR tube containing **12** in DMSO-d_6. In the first case 0.1 eq. HCl in 0.1 mL water was added. After mixing of the reagents, shimming and locking the NMR tube in the spectrometer (lasted altogether approximately 2 minutes) 60 spectra were recorded with a 60 second interval between each measurement to monitor this cleavage reaction time dependently.

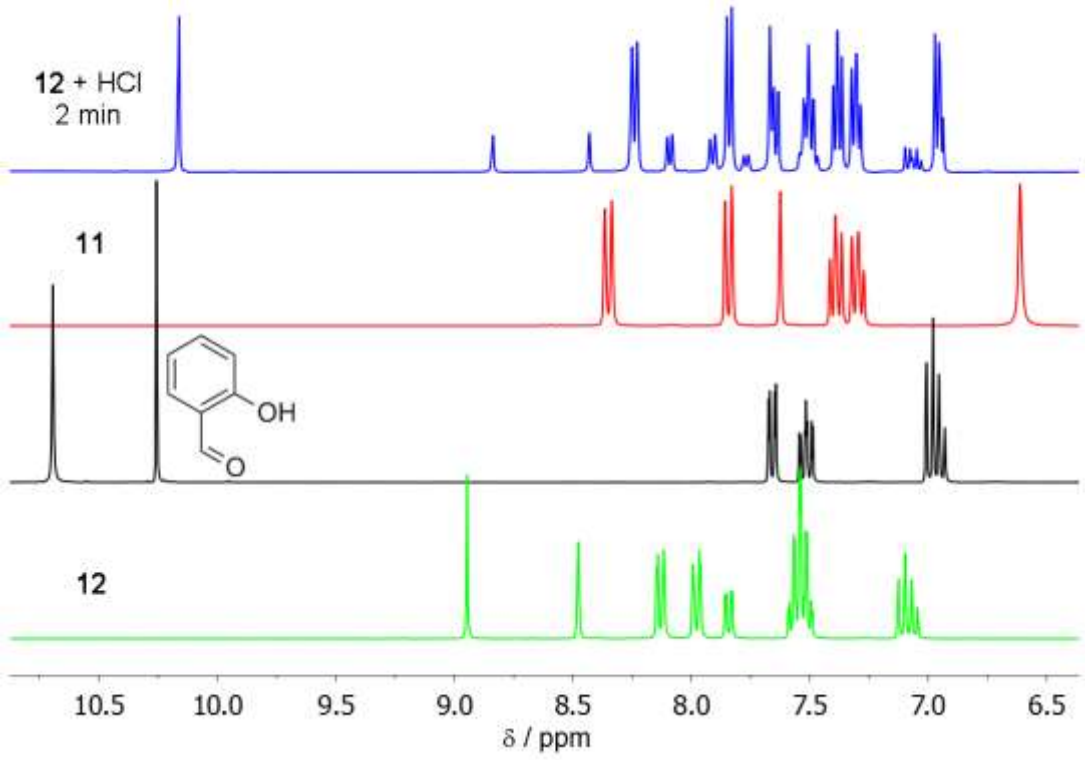

Figure 2-25: ^{1}H-NMR spectra in DMSO-d_6 of: **12** reacted with HCl (top, blue), **11** (red, second), salicylaldehyde (black, third) and **12** (bottom, green).

The blue line in Figure 2-25 shows the first spectrum of this series approximately two minutes after the addition of aqueous hydrochloric acid to **12**. Three species are present there and are displayed below for comparison. One is the original substance **12** (green line) and the other two are **11** (red) and salicylaldehyde (black). Minor

deviations in chemical shifts between the first measured spectrum and the three following ones are caused by the addition of water and the resulting change of the susceptibility of the solvent mixture.

This is, besides luminescence spectroscopy, a second strong indication that **12** reacts acid catalyzed to its starting materials **11** and salicylaldehyde. Only 0.1 equivalents acid converted the majority **12** in 2 minutes.

In a further experiment 0.01 eq. hydrochloric acid were used and observed for 15.5 hours in a NMR tube. The changes between two consecutive spectra were tiny so Table 2-5 displays a selection of measured ratios between **11** and **12** at different points in time.

Table 2-5: Ratio between **11** and **12** at different times.

	0.1 eq. HCl	0.01 eq. HCl
2 min	4 : 1	2 : 1
62 min	5 : 1	-
15.5 h	-	7 : 1

For this comparison the integrals of the signals at δ = 8.09 ppm for **12** and 8.24 ppm for **11** were used. The addition of hydrochloric acid in water led to the precipitation within the NMR tube. This precipitate was investigated and turned out to consist mainly of **12**. This leads to an overestimated conversion of **12** to **11**. But despite of this difficulty, Table 2-5 displays a clear tendency.

Again, already after 2 minutes a large part of **12** reacted acid catalyzed to **11** and longer reaction times increased its conversion. Sub-stoichiometric amounts of acid led to a major turnover of **12** but no further conversion of **11** or formation of side products was observed.

2.2.5.4 Solid state structural investigations on non-fluorescent decomposition products of 9-aminoanthracene (11)

Fluorescence and NMR spectroscopic experiments carried out in the previous sections established the acid catalyzed conversion of **12** to **11** and the further reaction of **11** to some non-fluorescent derivatives.

While the first conversion resulted in a single product (**11**) the subsequent reaction showed a mixture of derivatives in the NMR spectrum of which only one could be assigned. To receive additional information, crystallization approaches on decomposition products of **11** were carried out.

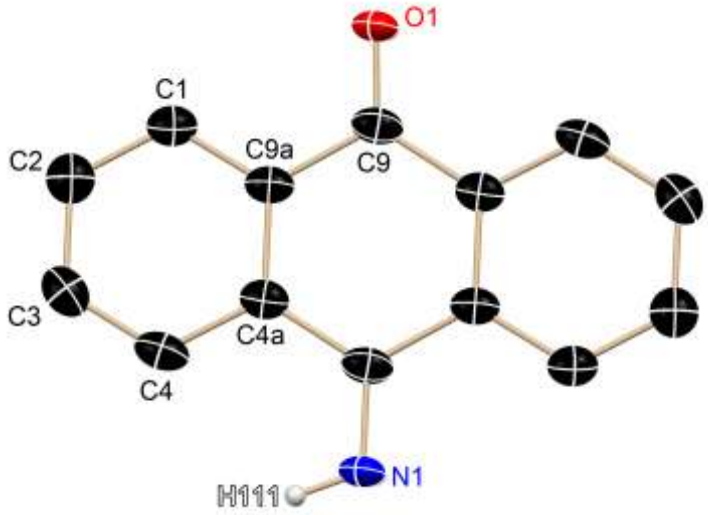

Figure 2-26: Solid state structure of anthraquinone monoimine. Positional disorder and hydrogen atoms bond to sp^2 hybridized carbon atoms are not shown.

The first investigated single crystal turned out to consist of two co-crystallized derivatives. One of them was anthraquinone monoimine whose presence was discussed in the previous chapter. Its protonated form was the only NMR-assignable decomposition product of **11** after addition of hydrochloric acid. The crystallization was carried out in the absence of hydrochloric acid so the non-protonated form is found in the solid state.

Only half of the anthraquinone monoimine shown in Figure 2-26 is present in the asymmetric unit and the molecule is completed by a center of inversion. Therefore, a disorder between O1 and N1 bearing H111 with a side occupation factor of 0.5 is

present. The hydrogen atom positions were determined throughout this thesis as discussed in section 0

Table 2-6: Selected bond lengths in pm and angles in ° of anthraquinone monoimine.

C9–O1	120(3)	O1–C9–C9a	118.0(19)
C9–N1	130(4)	N1–C9–C9a	121(2)
N1–H111	87(7)	C9–N1–H111	113(6)
C9–C9a	148.6(3)	C4a–C9a–C9	121.05(17)
C4a–C9a	140.4(2)	C9a–C4a–C4	119.40(17)

In Table 2-6 a selection of bond lengths and angles of anthraquinone monoimine are displayed. The middle ring of the anthracene framework is no longer aromatic but shows alternating bond distances. For example the bond between C9 and C9a is a bit longer than a regular C(sp^2)–C(sp^2) single bond with a reported typical bond length of 147 pm.[89] On the other hand the distance between C4a and C9a is similar to the bond length in benzene with 139.5 pm[90] and points towards aromatic outer rings. The connection of the oxygen and nitrogen atoms to the carbon scaffold via double bonds is also visible in their distances. The distance between C9 and O1 is similar to a C(sp^2)–O double bond with a reported typical length of 121 pm. An analog situation is found between C9 and N1 with a standard C(sp^2)–N(sp^2) double bond of 129 pm.[89]

The second derivative that co-crystallized with anthraquinone monoimine was termed in 1969 by CHAPMAN and LEE "photodimer of 9-aminoanthracene".[98] Their nomenclature was used during this project because of the otherwise less intuitive denomination. These two researchers were the first and till today only scientists who published structural information about this dimer.

Besides half of the anthraquinone monoimine molecule, the asymmetric unit includes also one half of the photodimer of 9-aminoanthracene (Figure 2-27) and the other half is given by a center of inversion. A positional disorder is present, too, where a nitrogen atom is bond to C30 instead of C29 with a side occupation factor of 0.05.

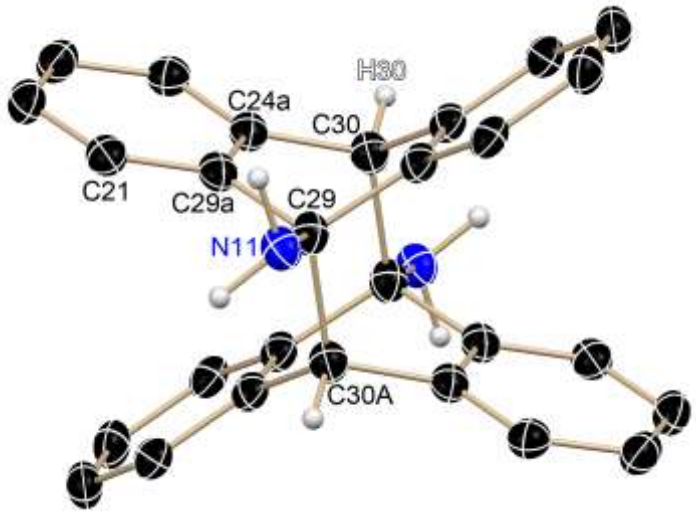

Figure 2-27: Solid state structure of the photodimer of 9-aminoanthracene. Positional disorder and hydrogen atoms bond to sp^2 hybridized carbon atoms are not shown.

Detailed crystallographic information about the two co-crystallized derivatives are shown in chapter 5.2.4. Table 2-7 displays bond distances and angles of the photodimer of 9-aminoanthracene.

Table 2-7: Selected bond lengths in pm and angles in ° of the photodimer of 9-aminoanthracene.

N11–C29	146.8(2)	N11–C29–C29a	114.45(14)
C29–C29a	153.4(2)	C29–C29a–C24a	117.60(15)
C29a–C24a	140.2(2)	C29a–C24a–C30	117.71(16)
C24a–C30	151.6(2)	C24a–C30–H30	106.6(13)
C21–C29a	139.4(2)	C21–C29a–C29	123.51(16)

Reminiscent of the last discussed derivative, the middle ring is also not aromatic and the bond lengths C29–C29a and C24a–C30 are in the range or slightly longer than a typical C(sp^2)–C(sp^3) single bond with 151 pm. In this case, the nitrogen carbon distance N11–C29 is similar to a standard N(sp^3)–C(sp^3) bond of 147 pm and points towards a sp^3 hybridized nitrogen atom.[89] The distance between C29 and the symmetry derived C30A is with 162 pm way larger that a regular C(sp^3)–C(sp^3) single bond of 154 pm. This is caused by the repulsion of the two close anthracene units.

In summary, both discussed structures have been proposed by former researchers, yet these are the first determinations of their solid state structure via X-ray diffraction.

Furthermore, a second single crystal with another unreported solid state structure was isolated. This crystal was also obtained after decomposition of **11** and consisted of 9,9'-dihydro-10,10'-diiminio-9,9'-bianthracene.

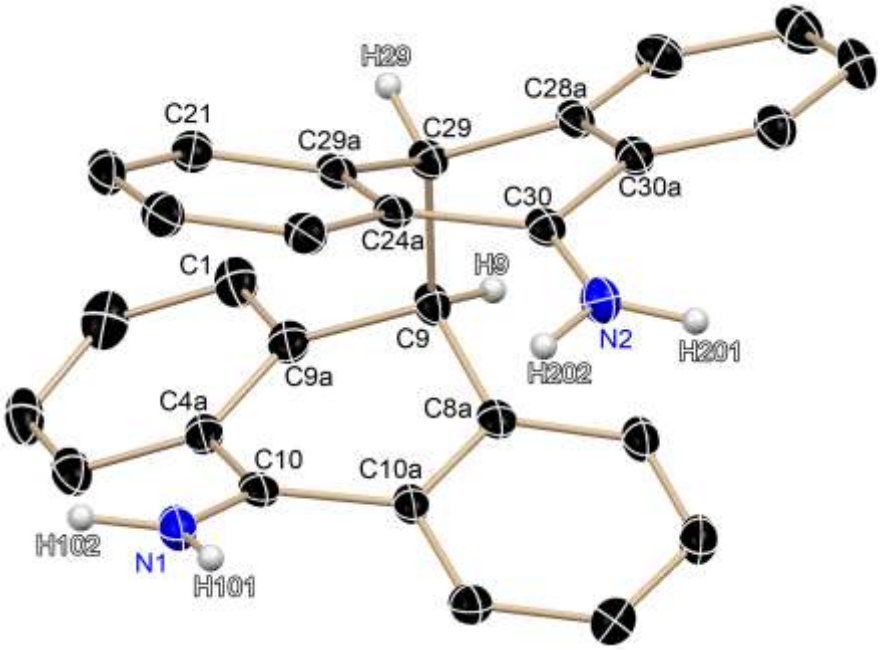

Figure 2-28: Solid state structure of 9,9'-dihydro-10,10'-diiminio-9,9'-bianthracene. Hydrogen atoms bond to sp^2 hybridized carbon atoms are not shown. Counter ions and water molecules are omitted for clarity.

9,9'-Dihydro-10,10'-diiminio-9,9'-bianthracene crystallizes in the orthorhombic space group $Pna2_1$. The asymmetric unit includes one molecule shown in Figure 2-28, four water molecules and two chloride anions.

This investigated derivative can be seen as a combination of both previously discussed decomposition products of **11**. It is also a dimeric structure like the photodimer of 9-aminoanthracene but only connected via the C9 position and not linked by the C10 position, too. A similarity to anthraquinone monoimine is the imine at the C10 position that bears an additional proton in 9,9'-dihydro-10,10'-diiminio-9,9'-bianthracene. The protons at the imine nitrogen atoms and cocrystallized chloride ions are obviously introduced by hydrochloric acid during crystallization.

The displayed bond lengths and angles of Table 2-8 point once again to a non-aromatic inner anthracene ring. The experimentally found distances are matching quite well typical localized double and single bond lengths. For example, the two nitrogen–carbon distances are close to a standard $C(sp^2)$–$N(sp^2)$ double bond (129 pm). The spacing between C10 and C4a as well as the one between C24a and C30 correspond to $C(sp^2)$–$C(sp^2)$ single bonds of typically 147 pm.

Table 2-8: Selected bond lengths in pm and angles in ° of 9,9'-dihydro-10,10'-diiminio-9,9'-bianthracene.

N1–C10	129.0(3)	N1–C10–C4a	121.8(2)
C10–C4a	146.2(3)	C4a–C9a–C9	120.4(2)
C9a–C9	150.7(3)	C9a–C9–C8a	112.21(19)
C9–C29	161.0(3)	C9a–C9–C29	110.58(18)
C24a–C30	146.9(3)	C9a–C9–H9	107.6
N2–C30	129.9(2)	N2–C30–C24a	121.00(19)

It is noteworthy, that the distance between C9 and C29 is much larger than a common $C(sp^3)$–$C(sp^3)$ single bond with 154 pm.[89] This is caused by the sterical strain of the two densely arranged anthracene moieties. While the angles C9a–C9–C8a and C9a–C9–C29 are slightly larger than the ideal tetrahedral case of 109.5 °,[99] angles that involve H9 are on the other hand smaller.

In summary, the decomposition of **11** was investigated via X-ray diffraction and three species were characterized by this method for the first time. These solid state structures give an idea about the ongoing process when **11** is exposed to air and especially when acids are added that accelerate the conversion of **11** to non-fluorescent products.

2.2.5.5 Fluorescence analysis after the addition of metal salts to 9-anthracenesalicylimine (12)

To investigate the luminescence behavior of **12** towards various metal salts in different concentrations, the developed screening procedure introduced in section 2.1.8.1 was applied. To a 10^{-5} M solution of **12** in methanol the chosen metal bromides were added and the luminescence emission was detected.

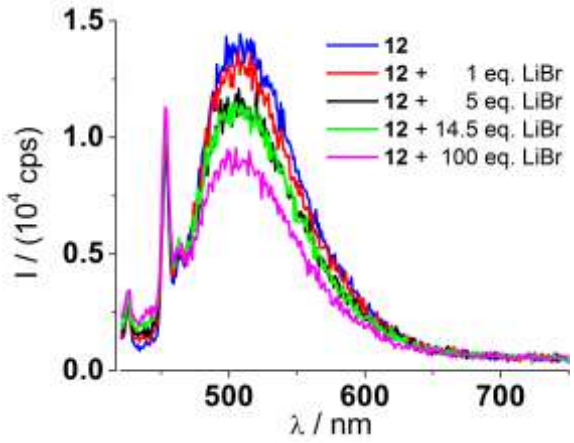

Figure 2-29: Stacked emission spectra of **12** before and after the addition of LiBr (10^{-5} M in MeOH, λ_{ex} = 400 nm).

The first selected example is displayed in Figure 2-29 and shows the emission before and after addition of lithium bromide. In general the spectra exhibit a poor signal to noise ratio because of the relatively weak fluorescence. And even this weak fluorescence is not caused by **12** but by its decomposition product **11** as discussed detailed in the previous sections.

Accordingly, no emission of **12** is visible in the emission spectra as aspired for a system including a very efficient quenching mechanism like the present C=N isomerization.

Adding lithium cations, **12** does obviously not change its luminescence properties. 1 eq. lithium bromide only lowers the emission by dilution and the same is true for the further additions, since larger added volumes resulted in more pronounced decreases of emission than higher amounts in less solvent. For example, the gap between the curves belonging to the addition of 1 eq. LiBr (red) and 5 eq. LiBr (black) is larger than the difference between 5 eq. LiBr and 14.5 eq. LiBr (green).

Similar to the previous discussed example of lithium bromide the addition of different metal bromides was investigated and the luminescence response is summarized in Figure 2-30.

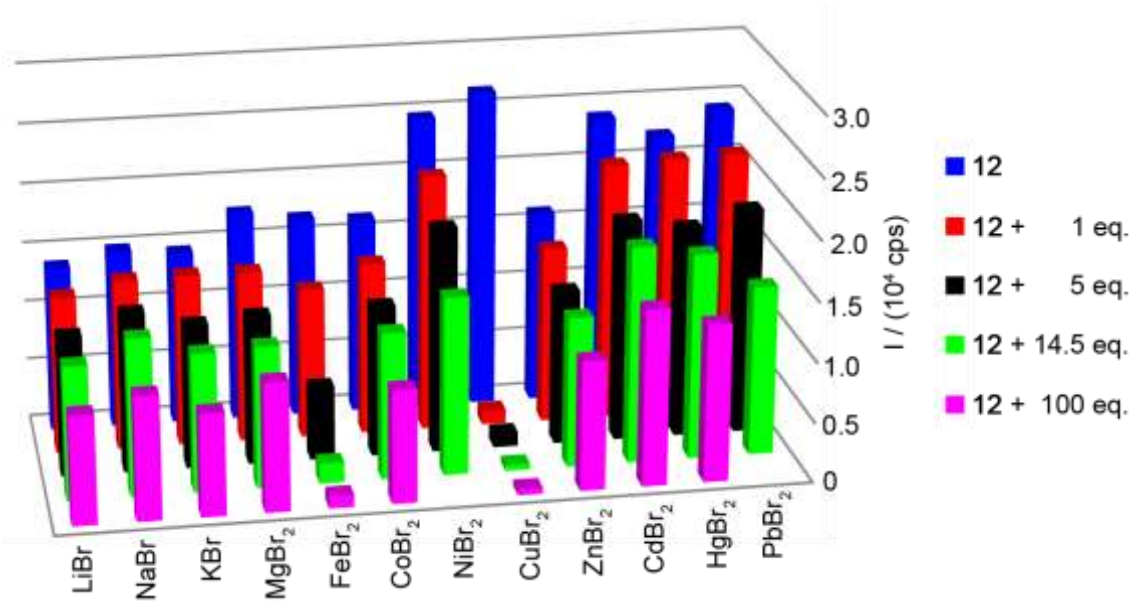

Figure 2-30: Representation of every tested combination between **12** and the respective metal bromide in MeOH (10^{-5} M, λ_{ex} = 400 nm, emission depicted at 510 nm).

The first column from the left gives a compact overview of the results shown in Figure 2-29. As explained, the luminescence intensity is lowered by dilution of the added lithium bromide in methanol. In this condensed picture only the emission at 510 nm is displayed but the full wavelength dependent information can be found in chapter 5.1.5.

It is obvious at the first glance that no addition of a tested metal salt increased the luminescence emission of **12** significantly. In most cases (LiBr, NaBr, KBr, $MgBr_2$, $CoBr_2$, $NiBr_2$, $ZnBr_2$, $CdBr_2$, $HgBr_2$ and $PbBr_2$) the intensity is even decreased by dilution. For copper and iron bromide the intensity is decreased because of the absorption by iron and copper cations explained in section 2.1.8.4 and visualized in Figure 2-10. The data points for 100 eq. nickel and led bromide are missing because their solubility is too low to prepare the $2.28 \cdot 10^{-3}$ M solution in methanol needed in the screening process for their large excess.

Noticeable is the varying intensity of the prepared starting sample before metal cations were added. There is a rough trend of increasing emission without the addition

of metal bromides (blue bars) from left to right and it gets clearer when the measurement order is considered. On the first day of this experimental series the metal salts LiBr, NaBr, KBr, $MgBr_2$, $FeBr_2$, $CoBr_2$ and $ZnBr_2$ were tested. One day later the remaining bromides were tested. The intensity of the stock solution increased by the formation of **11** overnight as shown in the right part of Figure 2-21. Therefore, this experimental series confirms once again the slowly ongoing conversion of **12** to **11**.
The response of **12** to metal bromides, acids and bases can be summarized strikingly by a picture of solutions containing **12** in a 10^{-5} M concentration in methanol and 10 eq. of one metal salt, acid or base, respectively, under exposure to UV light.

Figure 2-31: Behavior of **12** with respectively 10 eq. of acid, base or metal bromide in MeOH.

Luminescence changes of **12** can be seen in Figure 2-31 at first glance. Added protons or aluminum bromide increase the emission and, as discussed in the previous sections, the formation of **11** is responsible for this.

The absence of a clear increase of luminescence (apart from the addition of protons) was a drawback during this project. After the not visible emission of **12** and by this its suitable "off" state behavior it had been expected that coordinated metal salts to the nitrogen and oxygen donor atoms would have prevented the ongoing E/Z-isomerization. Their addition should have depressed this non-radiative relaxation pathway and, thereby, enable luminescence.
As discussed for **8** there are two possibilities that could cause the observed behavior of **12**. Either the coordination of cations does not omit the non-radiative relaxation process, namely the C=N isomerization, or none of the tested cations was complexed by the chelate ligand **12**.
A reason for the second explanation may be the large excess of the polar protic solvent methanol. Maybe the binding affinity of the prepared imine is too low to compete with the many times higher concentrated solvent.

A series of experiments was set up to check this second assumption and overcome the unspectacular behavior of **12** towards metal cations. The idea behind this was to add a base and deprotonate the hydroxyl group and thereby enhance the complex building affinity of the chelating ligand before the metal salts were added (pK_A of phenolic compounds ~10)[100].

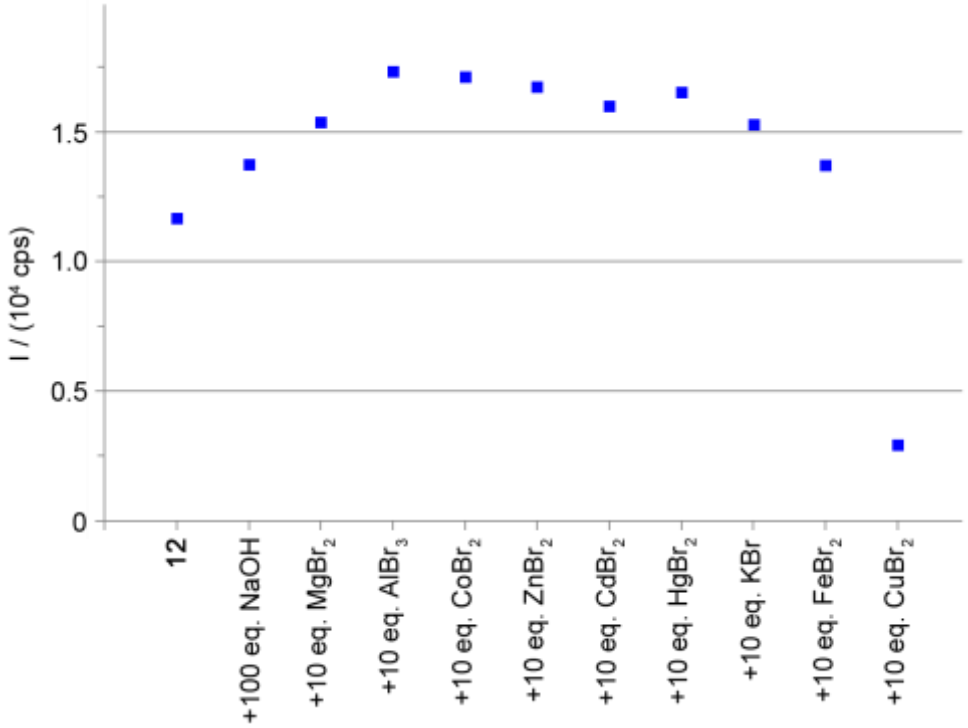

Figure 2-32: Overview about the emission of a solution including **12** in MeOH to which 100 eq. NaOH and successively 10 eq. of different metal bromides were added (10^{-5} M, λ_{ex} = 397 nm, emission depicted at 510 nm).

Figure 2-32 is showing the results of at first addition of 100 eq. sodium hydroxide and then successively 10 eq. of different metal salts. The experiment was carried out in the same cuvette and one emission spectrum was recording after every addition. Only the emission at 510 nm is depicted to monitor the intensity changes clearly. For the wavelength dependent information see Figure 5-15.

In the beginning the fluorescence intensity is increased by the additions of NaOH and $MgBr_2$ till to a maximum after adding $AlBr_3$ was reached and then a trend of slow decreases was observed whereas $CuBr_2$ led to a much stronger drop of intensity. This behavior may be explained by at first forming **11** despite of the alkaline excess, which is also visible in the right part of Figure 2-22. The second observation of

a slowly decreasing emission seems mainly caused by dilution and the third one, namely the quenching by copper bromide, was also observed without addition of NaOH and is based on absorption (cf. Figure 2-10 right).

In a second experiment a higher amount of base was added to vary the pH.

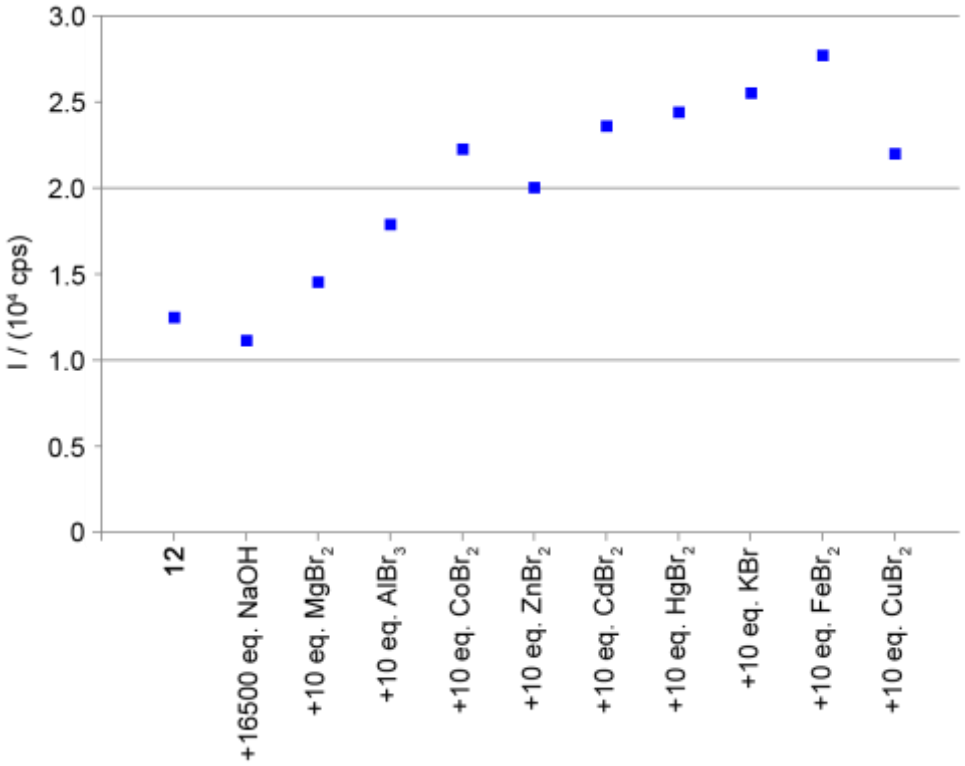

Figure 2-33: Overview about the emission of a solution including **12** in MeOH to which 16500 eq. NaOH and successively 10 eq. of different metal bromides were added (10^{-5} M, λ_{ex} = 397 nm, emission depicted at 510 nm).

The overview shown in Figure 2-33 was generated in an analog way to the previous one bearing the only difference with 16500 eq. sodium hydroxide and an even more alkaline medium.

Here, a stronger increase in intensity is visible but when taking into account the detailed presentation of Figure 5-16 one recognizes that this is mainly caused by an raising of the whole spectral range. Maybe some hardly soluble metal hydroxides were forming that scattered the incoming beam. This effect is most pronounced near the irradiation wavelength. Also noticeable is the weaker quenching after addition of copper bromide that may also be caused by the formation of even in water hardly soluble copper hydroxide or copper oxide.[101]

But the most important insight of both measured series is the absence of a new luminescent species. The addition of sodium hydroxide did not generate the aspired effect of strongly increased intensity that would indicate a restricted C=N isomerization.

To conclude this detailed analytic section of **12**, despite of absorption **12** showed no luminescence emission. This indicates the well ongoing non-radiative C=N isomerization.
Acids catalyze its decomposition to **11** and accelerate a further conversion to a series of non-fluorescent products (observed via fluorescence and NMR spectroscopy and structure determination via X-ray diffraction).
Neither in neutral nor in alkaline media a new luminescent species was forming after addition of metal bromides and therefore **12** proved not to be a proper luminescent sensor under the tested conditions.

For the next step a similar molecular arrangement was realized to compare its structural and luminescent spectroscopic properties with **12** and to extend the synthetic range of the imine synthesis based on 9-aminoanthracene.

2.2.6 9-Anthracenepicolylimine (13)

The second synthesized imine was 9-anthracenepicolylimine (**13**) bearing a C=N double bond like **12**. Therefore, **13** should also be hardly luminescent and once again hindrance of its C=N isomerization should cause an increased luminescence intensity.

2-Pyridinecarboxaldehyde was combined with **11** in ethanol to obtain **13** (Scheme 2-17). By using an excess of 1.5 eq. aldehyde a complete conversion was observed via ^{1}H-NMR spectroscopy after stirring the reaction mixture at 78 °C for 2.5 h.

In contrast to **12** which precipitated during the reaction, **13** was soluble in ethanol. That is why another procedure for the isolation of **13** had to be developed. Different mixtures of solvents were tried to recrystallize the crude product and the best purification process turned out to include a recrystallization from pure degased hexane.

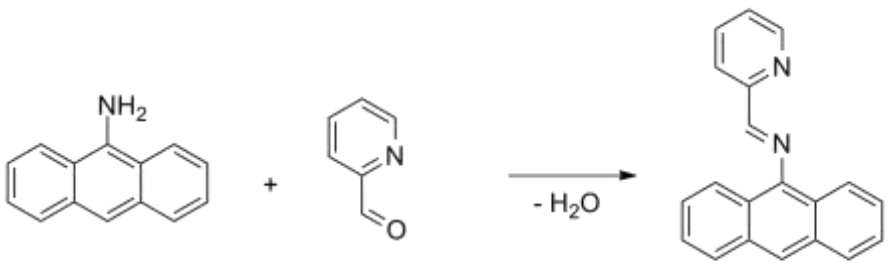

11 **13**

Scheme 2-17: Synthesis of **13** out of **11** and 2-pyridinecarboxaldehyde.

The absence of oxygen was crucial for an exclusion of oxidation reactions. By this, **13** was obtained in a reliable reaction with very good yields (90 %) and high purity.

It was also possible to prepare suitable single crystals for X-ray diffraction of **13** by solvation in hexane and afterwards slow evaporation of the solvent (Figure 2-34).

The monoclinic space group $P2_1/c$ was found for **13** and one molecule shown in Figure 2-34 is present in the asymmetric unit. C9 deviates most out of a plane through all anthracene carbon atoms by 10 pm and indicates thereby a planar anthracene scaffold. Even more planar is the pyridine ring where the largest deviation to a plane containing the five carbon and the nitrogen atom is 0.5 pm. These two aromatic systems are twisted by 61.739(47) °, which is around 8.3 ° less distorted

than in the case of **12**, but this geometry should still not allow any noticeable conjugation.

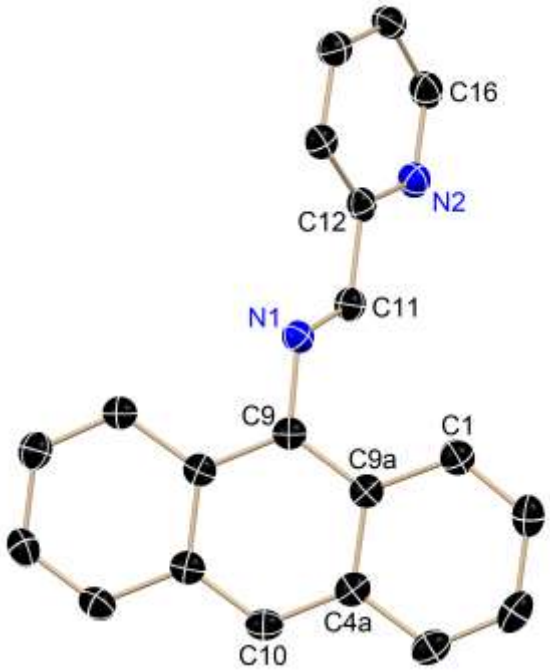

Figure 2-34: Solid state structure of **13**. Hydrogen atoms bond to sp^2 hybridized carbon atoms are not shown.

A selection of distances and angles of 13 is shown in Table 2-9. As observed for **12**, **13** shows also located double and single bonds around the imine group. For example the distance between C9 and N1 is even a bit elongated compared to a regular C(sp^2)–N(sp^2) single bond with 140 pm and the spacing N1–C11 is actually shorter than the standard C(sp^2)–N(sp^2) double bond of 129 pm.[89] This is the opposite one expects for a delocalization where the distances should converge.

Table 2-9: Selected bond lengths in pm and angles in ° of **13**.

N1–C9	141.64(19)	N1–C11–C12	121.87(14)
N1–C11	127.42(19)	C11–N1–C9	118.78(13)
C11–C12	147.5(2)	N1–C9–C9a	122.12(13)
N2–C12	134.82(19)	N2–C12–C11	115.18(13)
N2–C16	134.2(2)	C9–C9a–C4a	118.57(14)
C10–C4a	139.5(2)	C9a–C4a–C10	119.80(14)
C9–C9a	141.5(2)		

The carbon–carbon distances in the anthracene moiety are similar to the bond length found in benzene of 139.5 pm[90] and the bond angles displayed in Table 2-9 are all around 120 ° confirming that every atom shown in Figure 2-34 is sp^2 hybridized.

The synthesis of **13** turned out to work very well like the one of **12** although another purification procedure had to be developed. So their spectroscopic properties are open for comparison.

2.2.7 Luminescence properties of 9-anthracenepicolylimine (13)

Especially the similarities and differences between **12** and **13** should be evaluated during this chapter. Therefore, the same procedure was used as for **12** of at first determining the absorption properties of **13** followed by an investigation of its emission behavior and afterwards testing its sensor capability towards pH value changes and metal salts.

2.2.7.1 UV/Vis absorption and fluorescence emission of 9-anthracenepicolylimine (13)

Once again the first experiment was to determine a suitable excitation wavelength by monitoring the absorption of **13** between 200 and 700 nm.

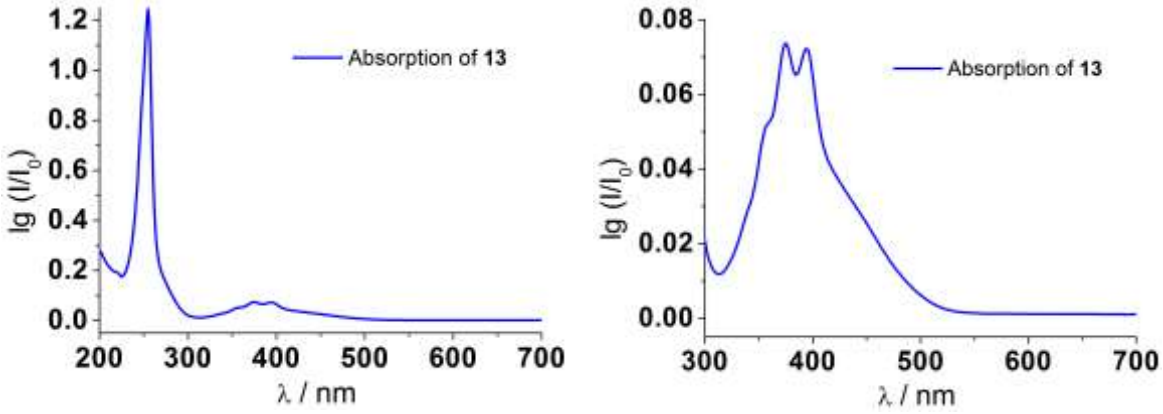

Figure 2-35: UV/Vis absorption spectra of **13**. Left: full spectrum; right: enlargement of the spectral region around 400 nm (10^{-5} M in MeOH).

As displayed in Figure 2-35, **13** shows similar absorption features like **12**. There is also a sharp maximum at λ = 255 nm as well as a broader one around 400 nm that shows a vibrational structure. Despite of their similarities, a difference between the two imines can be found in extend of the absorption wherein **13** shows a weaker response to the incoming light.

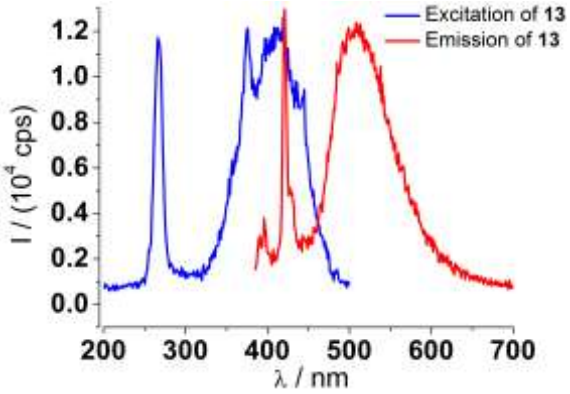

Figure 2-36: Excitation (blue, λ_{det} = 510 nm) and emission (red, λ_{ex} = 375 nm) spectra of **13** (10^{-5} M in MeOH).

The in Figure 2-36 depicted excitation and emission spectra point once again to the presence of **11**. As discussed in section 2.2.5.1 based on the example of **12**, the excitation spectrum of **13** shows differences to its absorption spectrum that are unlikely for the same optical observed species. While the right part of Figure 2-35 exhibits a vibrational structured band, the blue curve of Figure 2-36 looks more like the excitation spectrum of **11** (blue curve in Figure 2-20). Finally, its emission with a broad band around 510 nm displayed by the red curve fits the radiation of excited **11** quite well, too.

Despite of absorption, **13** shows no emission. The only emitting species in the red curve of Figure 2-36 turned out to be **11**. Therefore, the C=N isomerization seems to be also present and opens a non-radiative deactivation pathway for excited molecules of **13**.

2.2.7.2 Fluorescence analysis after the addition of acids and bases to 9-anthracenepicolylimine (13)

The assumption that **13** also decomposes towards **11** is confirmed by addition of acids to **13**. Again aqueous solutions of hydrochloric acid and sodium hydroxide were chosen to vary the pH value of the investigated sample.

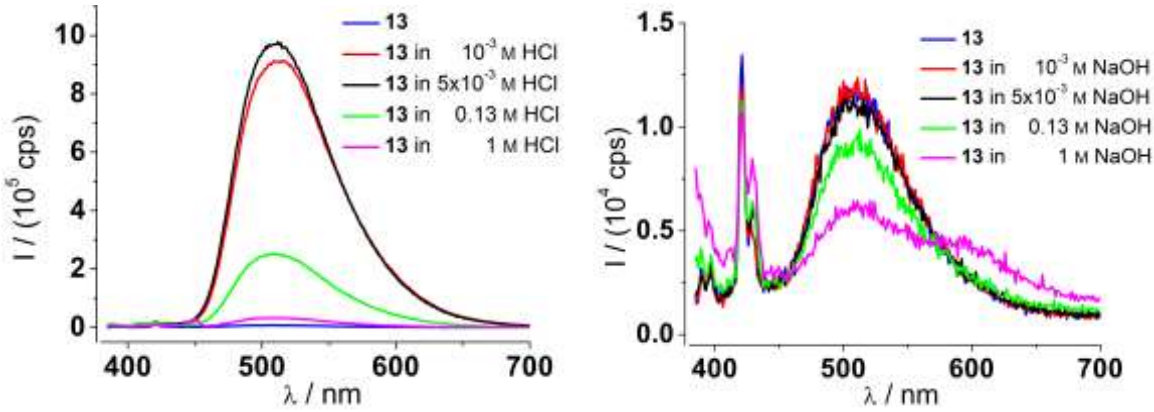

Figure 2-37: Emission spectra of **13** under acidic (left) and alkaline (right) conditions (λ_{ex} = 375 nm).

In the left part of Figure 2-37 the emission changes are presented after addition of hydrochloric acid. At first one can see a very strong increase in intensity up to a concentration of HCl about $5 \cdot 10^{-3}$ M but higher amounts of acid clearly decreased the fluorescence emission.

In contrast, the addition of sodium hydroxide revealed only small changes. Additions up to a sample concentration of 0.13 M NaOH caused only dilution and a further amount of the base to a concentration of 1 M led to a small increase of intensity below 400 nm that may be caused by scattered light of the incoming beam. Additionally, a signal around 600 nm appears but is only weak in intensity. So **13** seems to be stable even in concentrated bases, too.

Acids, however, lead to an increase at first and higher concentrations to a decrease of fluorescence intensity. Exactly the same behavior was observed for **12** and so the proposed description of at first formation of a fluorescent species out of a non-fluorescent one and a further conversion towards some non-emitting derivatives can be generalized.

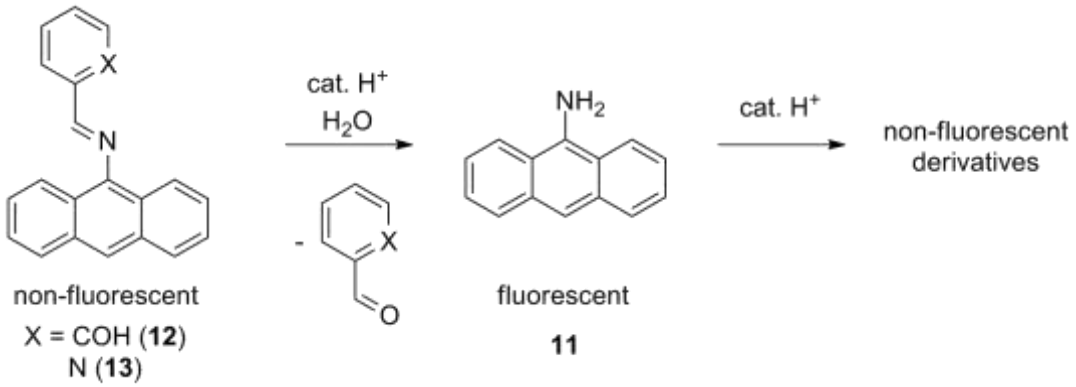

Scheme 2-18: Back reaction of the non-fluorescent **12** and **13** to their fluorescent starting material **11** and further conversion to non-fluorescent products.

Not only the shown behavior of **13** towards hydrochloric acid but also other measurements like time dependent observations of the fluorescence emission after addition of different acids suggested the proposed sequence shown in Scheme 2-18. Like already discussed for **12** in Figure 2-23, **13** also displays similar changes with aqueous HCl as well as in methanol with aluminum bromide (Figure 5-17).

2.2.7.3 Fluorescence analysis after the addition of metal salts to 9-anthracenepicolylimine (13)

The screening procedure introduced in Figure 2-5 was also applied to **13**. Thereby, various metal bromides were added to the investigated derivative in several concentrations. The solvent methanol was maintained as well as the 10^{-5} M solution to ensure comparability**.**

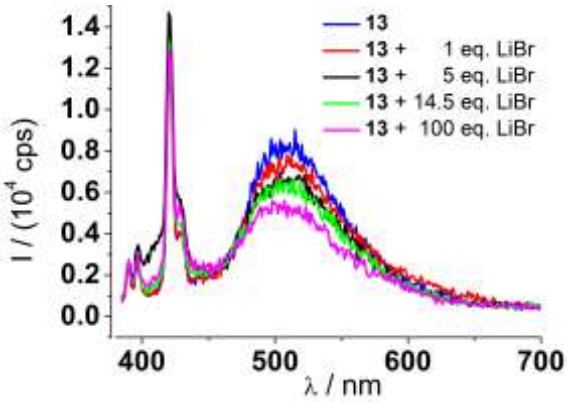

Figure 2-38: Stacked emission spectra of **13** before and after the addition of LiBr (10^{-5} M in MeOH, λ_{ex} = 375 nm).

In the case of lithium bromide displayed in Figure 2-38 one can see once more mainly dilution. The amount of added solvent influenced the intensity stronger than the increasing concentration of lithium bromide. The difference between the red line representing 1 eq. of LiBr and the black curve with 5 eq. was more pronounced than the changes after addition of further 9.5 eq. in the corresponding green line.
Noticeable is the increased intensity in the low wavelength region around 400 nm after the addition of 5 eq. lithium bromide. But due to its absence at higher concentrations of the metal salt and in respect of its low intensity it may be caused by an inaccuracy of the measurement.

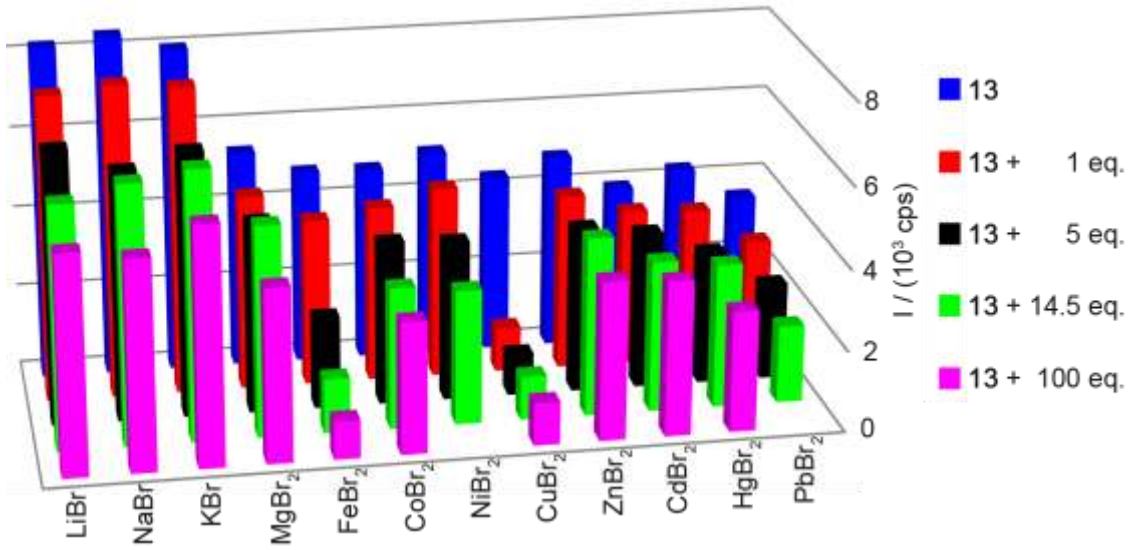

Figure 2-39: Representation of every tested combination between **13** and the respective metal bromide in MeOH (10^{-5} M, λ_{ex} = 375 nm, emission depicted at 510 nm).

Comparing the different tested metal bromides (Figure 2-39) the trend shown in the example of lithium bromide is visible to a high extend. The increase of added metal salt in methanol is followed by a decrease of emission that is mainly caused by dilution. Iron and copper bromide led to an even lower radiation originating in their absorptive behavior regarding to the incoming beam (Figure 2-10).
The main trend of growing emission by time observed for **12** in chapter 2.2.5.5 is reversed in this case. After the first three series of measurements with lithium, sodium and potassium bromide a clear decrease in intensity can be seen in the further experiments carried out one day later. So for this performed screening procedure the concentration of **11** in the stock solution used in the present investigation was

lowering over time. This indicates that the formation of **11** was slower than its decomposition to non-fluorescent derivatives described in Scheme 2-18.

One main disadvantage of the presentation type used is the compression of every recorded emission spectra to only one value namely the intensity at λ = 510 nm. By this, changes in other spectral regions are not presented. New signals could be missed especially because the emission of **13** is not visible and only the fluorescence signal of **11** is monitored at a wavelength of 510 nm. This was not crucial for the discussion of **12** because no new signals appeared after addition of metal bromides. In the case of **13** mainly potassium and cadmium bromide caused such changes. All other wavelength dependent information can be found in chapter 5.1.6.

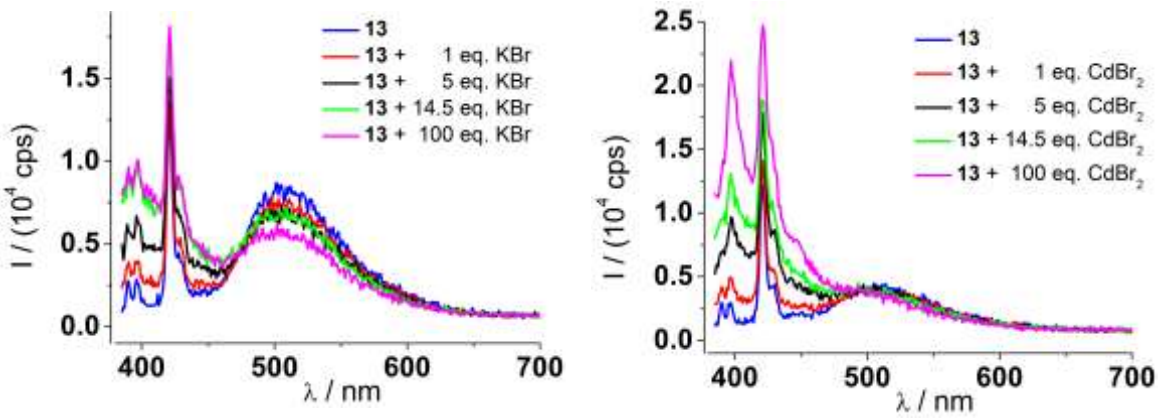

Figure 2-40: Emission properties of **13** after addition of potassium bromide (left) and cadmium bromide (right) (10^{-5} M in MeOH, λ_{ex} = 375 nm).

Emission changes of **13** after addition of potassium bromide are displayed in the left part of Figure 2-40. An increase of metal salt caused a luminescent response around 400 nm. The relatively broad signal is superimposed by the RAMAN signals of methanol but can be noticed easily. In the right part of Figure 2-40 a similar behavior is evident after the addition of cadmium bromide. The luminescence emission is also increasing by the rising amount of metal salt but the intensity is higher and the signal shows a structured appearance in contrast to the spectra of potassium bromide addition. Whereas one equivalent only caused a small increase in intensity larger additions resulted in more pronounced changes.

This are the first indications that an imine of 9-aminoanthracene could complex a metal and reports its presence by a luminescent output. To explore the best excita-

tion wavelength for this luminescent arrangement, excitation and emission spectra were recorded of a sample including **13** and 100 eq. cadmium bromide.

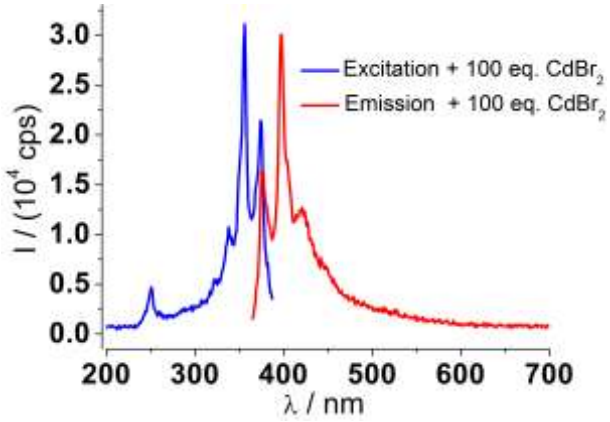

Figure 2-41: Excitation (blue, λ_{det} = 397 nm) and emission (red, λ_{ex} = 356 nm) spectra of **13** + 100 eq. cadmium bromide (10^{-5} M in MeOH).

The formed species turned out to emit best when irradiated at 356 nm and showed a maximum emission of around 30000 cps at 397 nm (Figure 2-41). Compared to molecules without distinct non-radiative relaxation pathways like **8** and **11**, this emission is low but in contrast to its non-emitting parent compound **13** whose emission was not observed at all it is a clear enhancement.

To what extent not only a change in intensity but even a shift of the emitting wavelength is present cannot be estimated because **13** is non-fluorescent. Only the absorption spectrum in Figure 2-35 gives a hint. Its sharp maxima at 375 nm and 394 nm are quiet shifted from the also sharp maximum of **13** + 100 eq. cadmium bromide with 356 nm in the corresponding excitation spectrum. This change is most likely influencing the emission wavelength, too and suggests a blue shift of the emission when cadmium bromide is added.

Despite of the findings concerning cadmium and potassium bromide, supporting the assumption that imines such as **12** and **13** could detect metal cations even in polar protic solvents like methanol, their lability towards protons stays a drawback.

To overcome this drawback, synthetic efforts were done to derivatize the imines. The idea was to use ketones instead of aldehydes in the condensation reaction with the primary amine **11**. In general, ketones are less reactive than aldehydes and the desired effect was to stabilize also the anthracene imines.

2.2.8 9-Anthracene-(α-methylpicolyl)imine (14)

The chosen ketone was 2-acetylpyridine to generate an imine comparable to **13**. Once again, 9-aminoanthracene was the starting material for this synthesis and its connection to 2-acetylpyridine is accompanied by the elimination of water.

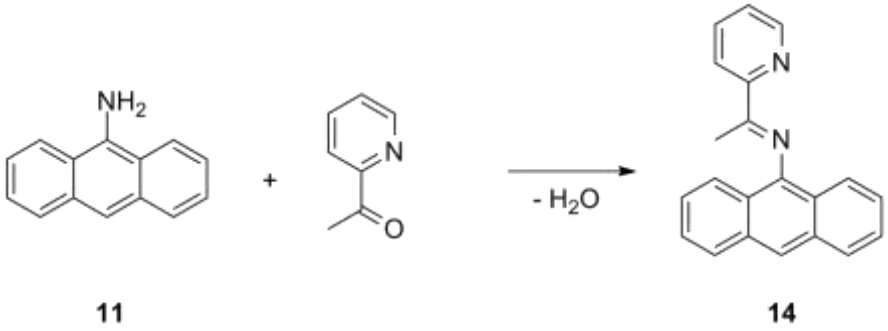

11 **14**

Scheme 2-19: Synthesis of **14** between **11** and 2-acetylpyridine.

The first attempt was similar to the established synthetic procedure of **13**. 0.5 g **11** was suspended in degased ethanol and 1.1 eq. 2-acetylpyridine were added under inert conditions. The reaction mixture was stirred at the boiling point of ethanol for four hours and the stirring was afterwards continued at room temperature overnight.

Three approaches of recrystallization were done after removal of the volatile components under reduced pressure (MeOH, hexane + chloroform, hexane) and resulted in quite pure **11**. Therefore, the reaction conditions were varied and are summarized in Table 2-10.

Table 2-10: Performed synthetic attempts to **14**. All reactions were carried out under inert atmosphere. Number behind the approach letter: this reaction was monitored at different times (v. s.: see conditions above). The yields were estimated via integrals of ^{1}H-NMR spectra and were not isolated.

Approach no.	Amount of **11**	Equivalents of 2-acetylpyridine	Solvent	Reaction time (temperature)	Additives or used equipment	Received anthracene derivative (yield)
A	0.51 g	1.1	10 mL EtOH	4 h (78 °C) + 16 h (r.t.)	-	**11**
B1	0.25 g	1.1	5 mL EtOH	16 h (78 °C)	10 eq. NEt_3	**11**
B2	v. s.	+ 5.0	v. s.	+ 16 h (78 °C)	v. s.	**11**
C	0.25 g	34.5	-	4 d (188 °C)	-	several
D1	0.51 g	16.9	-	18 h (r.t.)	-	**11** + **14** (4 %)
D2	v. s.	v. s.	-	+ 22 h (85 °C)	-	**11** + **14** (67 %)
D3	v. s.	v. s.	-	+ 5 h (85 °C)	-	**11** + **14** (80 %)
D4	v. s.	v. s.	-	+ 17 h (85 °C)	-	**11** + **14** (91 %)
D5	v. s.	v. s.	-	+ 27 h (85 °C)	-	**11** + **14** (92 %)
E1	0.37 g	1.1	8 mL EtOH	16 h (r.t.)	3 Å molecular sieve	**11**
E2	v. s.	v. s.	v. s.	+ 6 h (78 °C)	v. s.	**11** + **14** (3 %)
E3	v. s.	v. s.	v. s.	+ 22 h (78 °C)	v. s.	**11** + **14** (13 %)
E4	v. s.	v. s.	v. s.	+ 3 d (78 °C)	v. s.	**11** + **14** (33 %)
F1	0.38 g	1.1	8 mL THF	15 h (66 °C)	-	**11**
F2	v. s.	v. s.	v. s.	+ 24 h (66 °C)	+ 3 Å molecular sieve	**11** + **14** (2 %)
F3	v. s.	v. s.	+ 40 mL THF	+ 16 h (66 °C)	v. s.	**11** + **14** (3 %)
G	0.38 g	1.1	8 mL EtOH	3 d (78 °C)	3 Å molecular sieve	**11** + **14** (26 %)
H1	0.25 g	1.1	5 mL EtOH	23 h (78 °C)	dried EtOH	**11** + **14** (22 %)
H2	v. s.	v. s.	v. s.	+ 5 d (r.t.)	v. s.	**11** + **14** (29 %)
H3	v. s.	v. s.	v. s.	+ 22 h (78 °C)	+ 3 Å molecular sieve	**11** + **14** (32 %)
H4	v. s.	v. s.	v. s.	+ 6 d (78 °C)	v. s.	**11** + **14** (44 %)
I1	0.51 g	1.1	20 mL toluene	5 h (111 °C)	water separator	**11** + **14** (5 %)
I2	v. s.	v. s.	+ 5 mL EtOH	+ 6 h (78 °C)	v. s.	**11** + **14** (6 %)
J1	0.50 g	3.0	10 mL EtOH	16 h (78 °C)	dried EtOH	**11** + **14** (24 %)

J2	v. s.	v. s.	v. s.	+ 3 d (78 °C)	v. s.	**11** + **14** (71 %)
J3	v. s.	v. s.	v. s.	+ 3 d (78 °C)	v. s.	**11** + **14** (72 %)
J4	v. s.	v. s.	v. s.	+ 4 d (78 °C)	v. s.	**11** + **14** (71 %)
K1	0.59 g	8.8 eq.	-	16 h (85 °C)	-	**11** + **14** (38 %)
K2	v. s.	v. s.	-	+ 28 h (85 °C)	-	**11** + **14** (72%)
K3	v. s.	v. s.	-	+ 20 h (85 °C)	-	**11** + **14** (82%)
K4	v. s.	v. s.	-	+ 29 h (85 °C)	-	**11** + **14** (88%)
K5	v. s.	v. s.	-	+ 3 d (85 °C)	-	**11** + **14** (92%)

Overall, eleven attempts were carried out; most of them with several different extraction times. Each extracted sample was investigated by ^{1}H-NMR spectroscopy to determine the conversion. The yields given in Table 2-10 were not isolated by purification but estimated via the integrals of the corresponding ^{1}H NMR spectra. For **11** the signal at δ = 6.61 ppm of the amino group was chosen and for **14** the high field singlet at δ = 2.06 ppm was selected. Both peaks separated from the aromatic region where the starting materials **11** and 2-acetylpyridine as well as the desired product **14** show most of their partly overlapping signals.

Except from approach **C** the formation of undesired byproducts was observed only in small quantities. The long reaction time combined with a too high temperature may have caused this decomposition.

From this list of attempts it is obvious that the synthesis of imines based on ketones is challenging compared to imines out of aldehydes. For example, it was not possible by the use of nearly equimolar amounts of 2-acetylpyridine to achieve a sufficient conversion in an acceptable times. Attempt **H** shows the best results of the listed ones under these equimolar additions, where the solvent ethanol was dried with molecular sieve before the reaction.

The application purpose of molecular sieve was not only to dry the solvent before the reaction but also to trap the arising water during the condensation reaction. It turned out that the achieved yields were higher (comparing **E1**-**E4** to **A** or **B**) but even very long reaction times of several days resulted only in conversions between 26 % (**G**) and 44 % (**H4**). A further try with a water separator was also not successful in toluene and the addition of ethanol did not improve conversion.

The best results were achieved in the series **D1**-**D5** and **K1**-**K5** where 2-acetylpyridine was used as solvent. The high concentrations seem to pay off and alt-

hough long reaction times of several days are still necessary, conversions of more than 90 % can be reached. The series **K1**-**K5** took longer but required less 2-acetylpyridine.

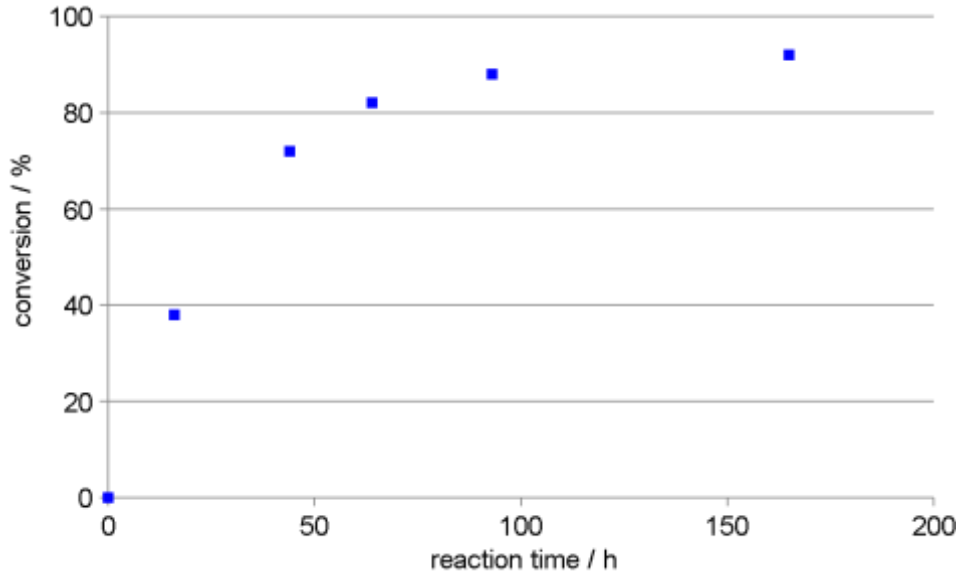

Figure 2-42: Conversion of **14** in the attempts **K1**-**K5** at the related moment of extraction.

Figure 2-42 displays graphically the in Table 2-10 listed conversion of **14** at the corresponding extraction times of the approach **K1**-**K5**. So 50 till 100 hours are recommended for conversions above 80 %. But also reaction times over 150 h still increase the yield although to a minor degree.

After these various attempts to achieve a good conversion of **11** to **14** the purification of the crude product turned out to be challenging, too. Eight recrystallizations and three times column chromatography led to the estimation that these two strategies were not suitable to purify **14**.

The solution of the problem was drying the reaction mixture, dissolve the crude product in acetonitrile and extract it many times with hexane. The detailed description can be found in chapter 4.4.11.

By this procedure **14** was isolated in a yield of 36 % with less than two percent anthraquinone. Although the yield is much lower than in the case of imines from aldehydes (around 90 %), it was possible to establish a synthesis and purification process for **14** with very small amounts of impurities.

2.2.9 Luminescence properties of 9-anthracene-(α-methylpicolyl)-imine (14)

After its accomplished synthesis the properties of **14** should be evaluated. Especially the stability towards protons was a major interest and reason for this derivatization. But also the sensoric properties of **14** were explored and compared to its aldehyde based analog **13**.

2.2.9.1 UV/Vis absorption and fluorescence emission of 9-anthracene-(α-methylpicolyl)imine (14)

The approved procedure including at first determination of a suitable excitation wavelength for the tested anthracene derivative was also applied to **14**.

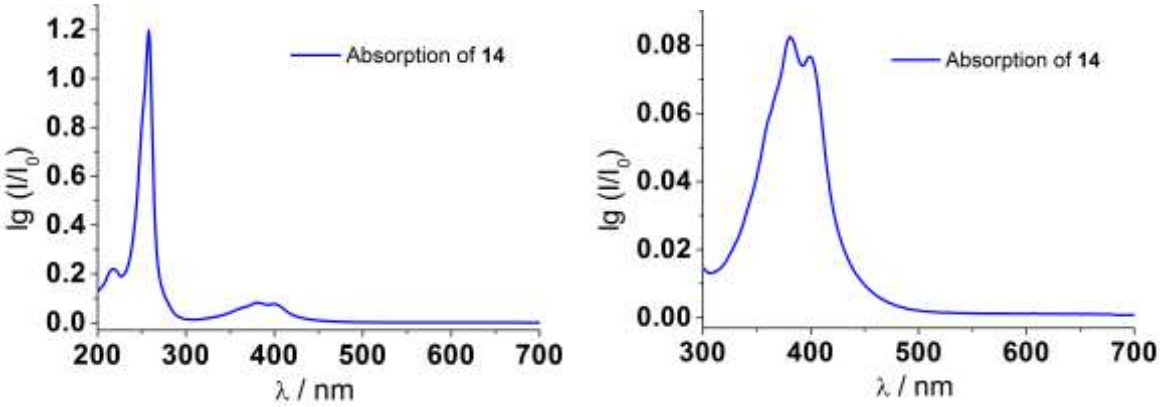

Figure 2-43: UV/Vis absorption spectra of **14**. Left: full spectrum; right: enlargement of the spectral region around 400 nm (10^{-5} M in MeOH).

Once again, the absorptive properties of **14** shown in Figure 2-43 are similar to those of **12** and especially to the displayed curve form of **13** in Figure 2-35. But not only the shape is comparable as in the case of **12** but also the numerical values of absorption are nearly equal.

The related excitation and emission spectra are displayed in Figure 2-44.

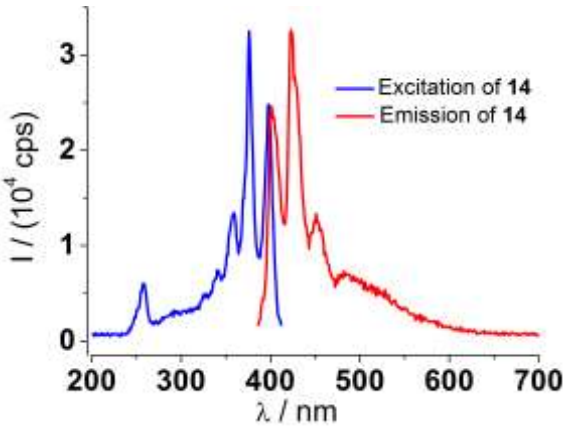

Figure 2-44: Excitation (blue, λ_{det} = 422 nm) and emission (red, λ_{ex} = 376 nm) spectra of **14** (10^{-5} M in MeOH).

Noticeable is the visible luminescence in the emission spectrum recorded of a solution of **14** in methanol. **11** does not seem to be present because the dominance of the broad band around 510 nm is missing. Therein, obvious differences to **12** and **13** are found and maybe the derivatization caused the aspired stability.

The excitation spectrum shows similarities and differences regarding the absorption spectrum of **14**. On the one hand the positions of the peaks differ less than 5 nm (assuming a poorly resolved shoulder in the excitation spectrum around 360 nm) that points to observation of the same species by both techniques. On the other hand these bands are much more structured in the excitation spectrum than in the corresponding absorption spectrum. The peaks are sharp in the blue line of Figure 2-44, whereas the UV/Vis spectrum shows only two not clearly separated signals with an additional shoulder on the low wavelength side of the band.

Either the C=N isomerization in **14** is much weaker than in **12** and **13** and allows the observation of luminescence or the emission is once again not originating in the imine but in the presence of an impurity.

A first guess would be the contamination with anthraquinone of which around 1.5 % was left after purification but anthraquinone is also poorly fluorescent and its presence in an about $1.5 \cdot 10^{-7}$ M concentration should not be observable. Nevertheless, emission and excitation spectra of anthraquinone were recorded and are displayed in the supplement (Figure 5-1). Hence, the maxima of emission and absorption differ by around 25 nm, the signals in the spectra of **14** cannot be assigned to anthraquinone.

A hint that they do not belong to **14** either can be found in experiments after addition of acids in the following section.

2.2.9.2 Fluorescence analysis after the addition of acids and bases to 9-anthracene-(α-methylpicolyl)imine (14)

Especially the stability of **14** towards acids had to be investigated because the imines prepared from aldehydes showed an extensively discussed lability towards protons (chapter 2.2.5).

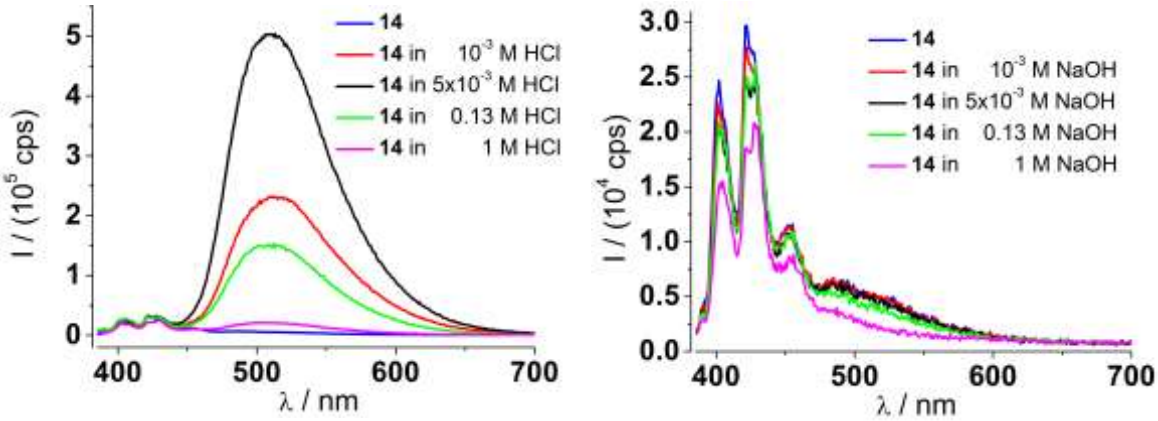

Figure 2-45: Emission spectra of **14** under acidic (left) and alkaline (right) conditions (λ_{ex} = 375 nm).

The addition of hydrochloric acid to **14** resulted in changes similar to those of **12** and **13**. A broad band around 510 nm arises indicating the formation of **11**. At an acid concentration of 10^{-3} M, the fluorescence emission increased to more than 200000 cps and rose when the fivefold amount of hydrochloric acid was reached. Further acid caused the opposite trend of a decreasing intensity (left part of Figure 2-45).

In contrast, adding sodium hydroxide in equal amounts only resulted in dilution by lowering the concentration of the emitting species. Once again, **14** seems to be stable to bases and labile to acids. From this experiment, one should conclude that the stability cannot be improved by using ketones instead of aldehydes in the synthesis of imines from 9-aminoanthracene.

Noticeable is the nearly constant intensity around 425 nm. One would expect that **14** is cleaved to **11** and the corresponding ketone or aldehyde followed by a conversion of **11** to non-fluorescent species like **12** and **13** do (Scheme 2-18). So if the signal

observed in the red line of Figure 2-44 would belong to **14**, it should decrease with increasing amounts of **11** indicated by the rising band around 510 nm.

Therefore, an additional experiment was carried out where a large excess of hydrochloric acid was added to a 10^{-5} M solution of **14** and was allowed to react for 24 h (Figure 5-23 left). Even after this reaction time the intensity at λ = 425 nm had not decreased. This leads to the estimation that **14** is also non-fluorescent and the emission observed in Figure 2-44 is caused by an impurity that is present in a very small amount that is not visible in the recorded mass and NMR spectra.

The time dependent behavior of **14** towards aluminum bromide and hydrochloric acid was investigated too and is displayed in chapter 5.1.7. An analogous behavior to the previous discussed imines was found.

2.2.9.3 Fluorescence analysis after the addition of metal salts to 9-anthracene-(α-methylpicolyl)imine (14)

Despite of the unchanged behavior of **14** concerning acids, its response to metal bromides was tested via the in section 2.1.8.1 established screening procedure.

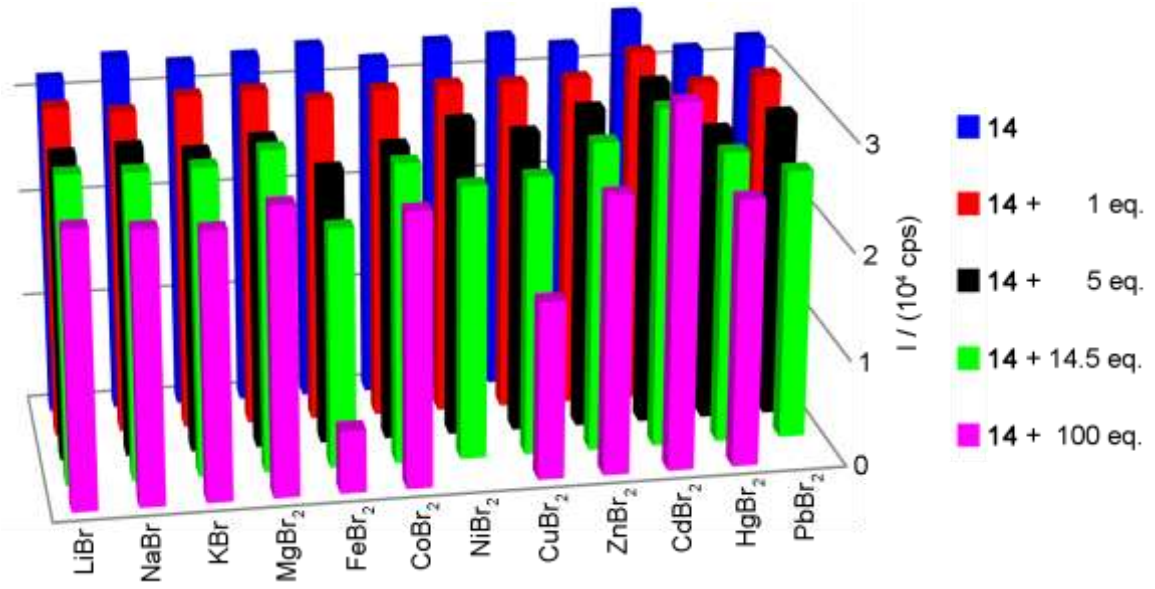

Figure 2-46: Representation of every tested combination between **14** and the respective metal bromide in MeOH (10^{-5} M, λ_{ex} = 376 nm, emission depicted at 423 nm).

The compact overview of Figure 2-46 allows again to display only the emission at one specific wavelength. This time not the most pronounced radiating transition of

11 with 510 nm was chosen but the maximum of Figure 2-44 at 423 nm. The wavelength dependent information are shown in the supplement (chapter 5.1.7). The measurement with lithium bromide is once again typical of many metal salt additions. The quantity of added volume had a larger influence on the decrease of emission than the amount of metal bromide. This is true for lithium, sodium, potassium, magnesium, nickel, cobalt, zinc, mercury and lead bromide. The presence of huge amounts of iron and copper bromide caused a more pronounced decrease of intensity due to their absorptive behavior (Figure 2-10). Changes originating from by aluminum bromide are displayed in the right part of Figure 5-24 and are not included in Figure 2-46 due to their strong response caused by protonation instead of a coordinative interaction of the metal salt.

Of greater interest are two observations. The first one concerns the response to cadmium bromide. The addition of cadmium bromide is the only one which caused an increase of emission at the displayed wavelength. A similar behavior was discussed for **13** where also the presence of cadmium resulted in the largest changes. The analogous structure of **13** and **14** implies also related binding properties towards metal cations and an experimental verification can be found in the response of both derivatives to cadmium bromide.

The second observation was the constant starting intensity in this series of measurements. No trend of increased or decreased intensity of the blue column over time can be noticed. In both further investigated imines **12** and **13** such a trend was obvious but the absence of a variation concerning the starting intensity points towards an enhanced stability of **14** to air and moisture. A long term measurement over three days was carried out and supports this suggestion of a high durability of **14** (Figure 5-23 right).

To conclude the synthesis and investigated properties of **14**, the reaction and purification of **14** was more challenging and time consuming compared to the other prepared imines. Its stability towards air and moisture is increased but still the major drawback of lability towards acids remained unchanged. Of all tested metal bromides only the addition of cadmium bromide led to small luminescence changes that may originate in a metal-ligand interaction.

After the extensive investigation of three novel imines (**12**, **13** and **14**), this subclass of substances showed interesting features. For example their low emission despite of absorption (C=N isomerization) or the high selectively response of **13** and **14** to cadmium compared to other bromides. But the disadvantages of acid lability and relatively low emission of the formed imine-cadmium species were also noticed.

These results led to the estimation, that the imines with two donor atoms (nitrogen or oxygen) from aldehydes or ketones are no promising class of potential luminescent sensors.

Therefore, a fundamentally structural change for further synthesized and investigated anthracene derivatives was made while maintaining the advantage of the approved synthetic access to imines from aldehydes in high yields and very good purity.

2.2.10 9-Anthracenesalicylamine (15)

The idea was to derivatize the synthesized imine **12** by reducing its C=N double bond. This should effect the stability towards protons as well as the underlying signaling mechanism. Without the C=N double bond the C=N isomerization does no longer exist and therefore, the strong non-radiative relaxation process should vanish. Of course another signaling mechanism has to be present in the resulting secondary amine to not only coordinate a metal cation but also report its presence via a luminescent output. The ICT mechanism could provide such a mechanism due to the absence of a spacer between fluorophore and receptor. This signaling mechanism is discussed in chapter 1.3.2.

Scheme 2-20 represents on the first glance a simple reduction of the imine **12** to its amine **15**. Many attempts were carried out to identify suitable reaction conditions. The reducing agent $NaBH_4$ turned out to give the best results in comparison to $Li[AlBH_4]$ and two alkyl-containing reducing agents $K[BEt_3H]$ and $Na[BEt_3H]$. These two last-mentioned were soluble in organic solvents and were applied in solution. The potassium salt was used as a 1 M solution in THF and the sodium one as a 1 M or 2 M solution in toluene. This application in solution turned out to be advantageous in the reduction of other imines later on.

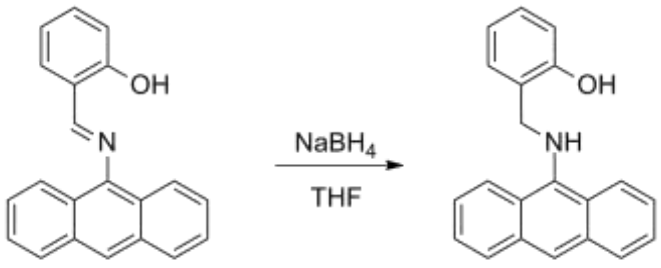

12 15

Scheme 2-20: Synthesis of **15** by reduction of the C=N double bond.

But the reaction of **15** was optimized to solvation of **12** in THF and addition to 5 eq. $NaBH_4$ in THF. Its purification was also tried along several paths. For example, purification by protonation was one of the used ways. Therefore, the volatile components of the reaction mixture were removed under reduced pressure and the crude product was dissolved in ethylacetate and water. The organic layer was separated

and treated with aqueous hydrochloric acid to cause a light yellow precipitate namely the protonated amine **15**. This formed solid was washed with ethylacetate and redissolved by addition of aqueous sodium carbonate solution. The described purification process was suitable to remove side products but gave varying yields between 18 and 50 %.

The best clean up procedure was removal of the volatile components under reduced pressure, dissolving the residue in chloroform and water and recrystallize the crude reaction product, obtained from the organic layers, from hexane and chloroform. By this, **15** was isolated purely in a yield of 74 %.

Besides this, single crystals of a further recrystallization from hexane and ethylacetate were suitable to determine the solid state structure of **15** via X-ray diffraction.

The amine **15** crystallizes in the orthorhombic space group *Fdd*2 where the asymmetric unit contains two of the molecules shown in Figure 2-47. Whereas the displayed one is the (*S*) isomer, the other molecule exhibits (*R*) arrangement of the substituents around the nitrogen atom following the CIP nomenclature.[102]

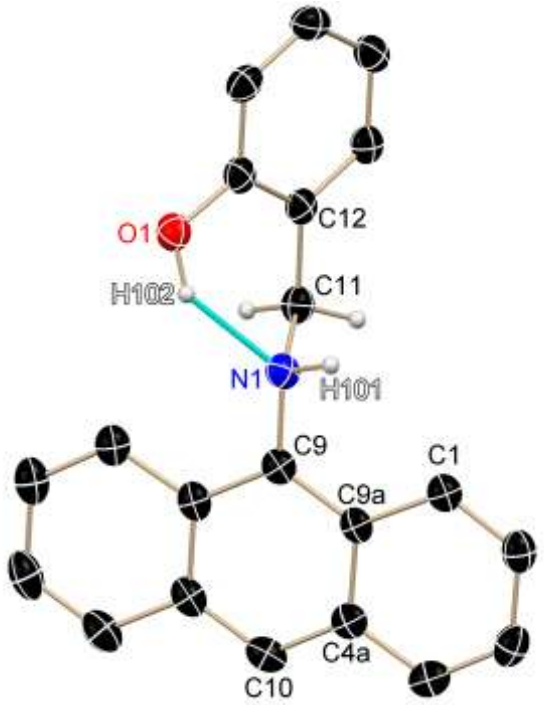

Figure 2-47: Solid state structure of **15**. Hydrogen atoms bond to sp^2 hybridized carbon atoms are not shown.

For this present chiral space group the FLACK parameter[103] was determined to x = -0.09(15) and indicates the right assignment of the stereogenic center. The crystallized **15** showed a racemic mixture but the molecules should not maintain their configuration in solution due to the in general low inversion barrier of tertiary amines.[104]

Table 2-11: Selected distances in pm and angles in ° of **15**.

N1–C9	142.5(4)	N1–C11–C12	110.2(2)
N1–C11	148.9(4)	C11–N1–C9	114.6(2)
C11–C12	151.0(4)	N1–C9–C9a	121.0(3)
O1–H102	136.7(4)	O1–H102···N1	136(3)
N1···H102	198(4)	C9–C9a–C4a	119.2(3)
C9–C9a	140.8(5)	C9a–C4a–C10	119.8(3)

In Table 2-11 chosen bond lengths and angles as well as information about an intramolecular hydrogen bond of **15** are listed. The reduction of the carbon–nitrogen double bond to a single bond is also reflected in the spacing between C11 and N1 that is now even a bit longer than a standard C(sp^3)–N(sp^3) single bond of 147 pm[89] and therefore elongated by around 20 pm compared to **12**. The angle around C11 (N1–C11–C12) is close to the ideal tetrahedral angle of 109.5 ° and proves – together with the four bonding partners as well as its typical single bond lengths to C12 and N1 – its sp^3 hybridization.

Also noticeable is the intramolecular hydrogen bonding where O1 is the donor bearing H102 and N1 acts as acceptor. This hydrogen bonding is weaker than in the case of **12** judged by the related geometrical data. The nitrogen–hydrogen distance is about 30 pm longer and the angle O–H–N is more than 10 ° further away from a linear arrangement of 180 °. Interestingly, the geometrical situation of the second molecule in the asymmetric unit points to a stronger hydrogen bonding than the displayed (*S*) derivative. A distance between the acceptor N21 and H122 of 180(5) pm and a corresponding O–H–N angle of 150(5) ° are closer to the hydrogen bond in **12** than its enantiomer of **15**. This deviation between the isomers is most likely caused by their varied packing and would not be present in solution.

Nevertheless, the strength of all three hydrogen bonding situations would be assigned as moderate according to JEFFERY because their acceptor–hydrogen distances are in the range between 1.5 and 2.2 Å and their donor–hydrogen–acceptor angles are larger than 130 °.[94]

2.2.11 Luminescence properties of 9-anthracenesalicylamine (15)

In contrast to the last three investigated potential luminescence sensors, **15** includes an amine group directly linked to the anthracene instead of an imine like in the cases of **12**, **13** and **14**. Therefore, the expectations concerning the luminescent behavior were different. For example, **15** itself should not provide such a good "off" state like the imines due to the absence of the structural requirements for an efficient non-radiative relaxation pathway (C=N double bond). Instead the coordination of the nitrogen lone pair could result in a shift of the emission wavelength due to its no longer delocalization to the anthracene π-system.

2.2.11.1 UV/Vis absorption and luminescence emission of 9-anthracenesalicylamine (15)

The approved procedure of at first determining a suitable excitation wavelength by recording an absorption spectrum was also performed for **15**.

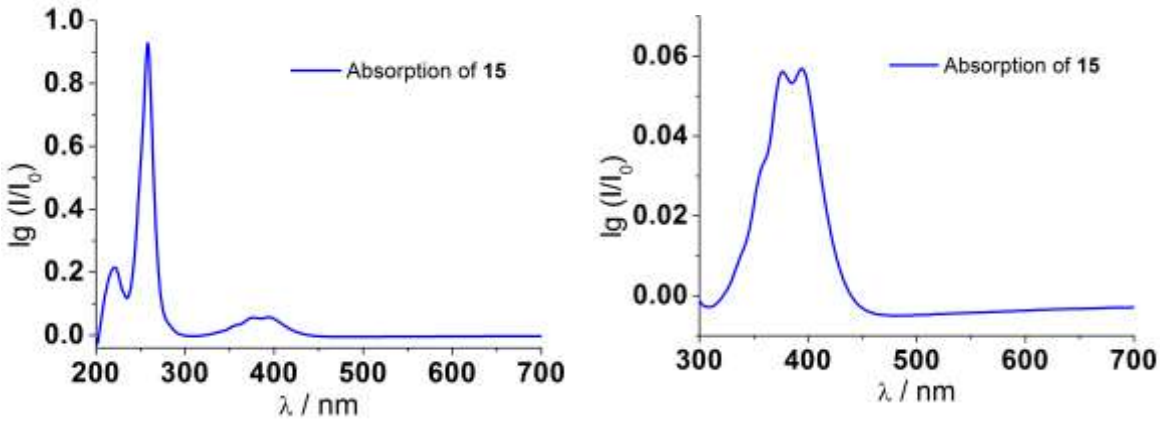

Figure 2-48: UV/Vis absorption spectra of **15**. Left: full spectrum; right: enlargement of the spectral region around 400 nm (10^{-5} M in MeOH).

As displayed in Figure 2-48, **15** shows two bands whereof the larger one at λ = 258 nm shows a sharp peak. The other one around 380 nm exhibits two maxima

at 376 nm and 394 nm as well as a shoulder at about 357 nm. This absorptive behavior is similar to its starting material **12** but a bit less intense and the maxima of the imine were more pronounced that enabled the identification of four bands instead of two and one shoulder.

The excitation and emission properties of **15** are presented in Figure 2-49.

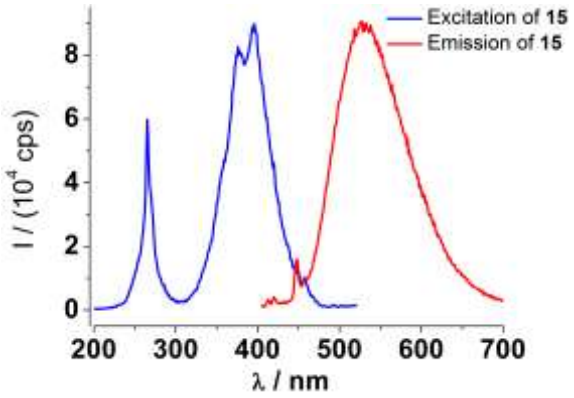

Figure 2-49: Excitation (blue, λ_{det} = 530 nm) and emission (red, λ_{ex} = 396 nm) spectra of **15** (10^{-5} M in MeOH).

In the case of **15** the excitation spectrum fits the absorption spectrum very well indicating that the same species was observed by both spectroscopic methods. Only the lowest wavelength peak differs by 7 nm but the others are almost equal. The luminescent emission shows a large STOKES shift of around 130 nm that could be a hint towards a long lifetime of the excited molecules. This spacing between the energetically lowest band of the excitation spectrum and lowest wavelength signal of the emission spectrum is by over 30 nm more pronounced than in **11** where also a relatively high STOKES shift was observed. But lifetime measurements revealed a regular fluorescent lifetime of 7.9 ns for **11**. Besides this even larger STOKES shift, the less intense emission could be a second hint that **15** may have a longer occupied excited state and its radiative relaxation should rather be termed phosphorescence. Lifetime measurements could reveal this property of **15**.

As mentioned, the luminescent emission is less intense than in the case of **11** or **8** but is clearly detectable in contrast to the investigated imines. Therefore, it was possible to follow spectroscopic changes of **15** precisely due to its distinct emission.

2.2.11.2 Luminescence analysis after the addition of acids and bases to 9-anthracenesalicylamine (15)

Due to the absence of the C=N double bond **15** should not decompose to **11** because the addition of water should not cleave a regular carbon–nitrogen single bond. So protons cannot accelerate this reaction like they did in the case of the synthesized imines after addition of acid.

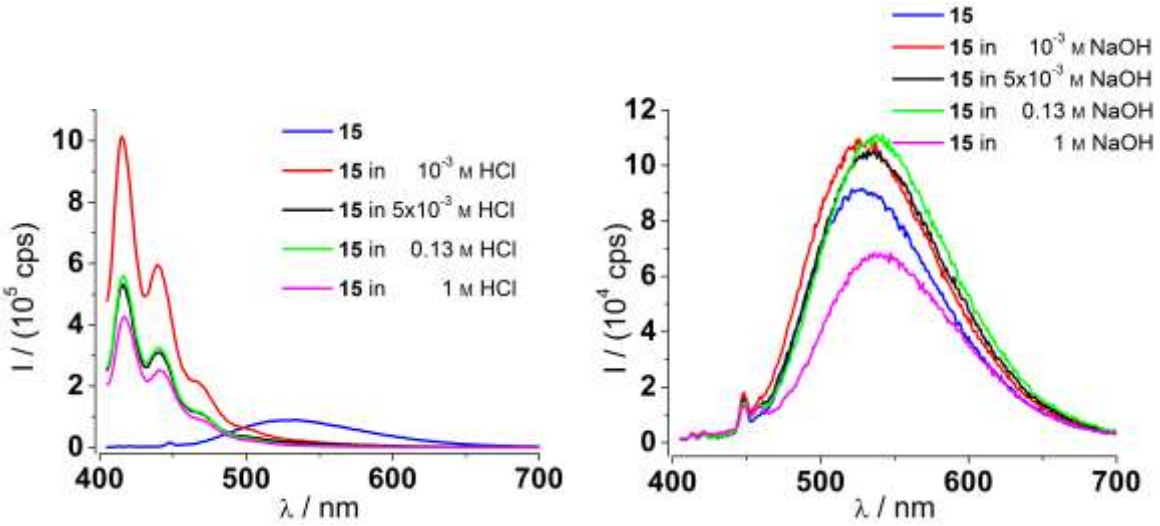

Figure 2-50: Emission spectra of **15** under acidic (left) and alkaline (right) conditions (λ_{ex} = 396 nm).

The luminescence changes after addition of hydrochloric acid displayed in the left part of Figure 2-50 are immense. After adding hydrochloric acid till a concentration of 10^{-3} M was reached, the emission increased to around one million cps and is obviously shifted hypsochromic (to higher energy). A larger amount of added acid caused a decrease of intensity that cannot be explained just by dilution but both the high intensity and the new structured band maintained.

The increase in intensity around a factor of ten is remarkable by its own, but the change of the emission wavelength by more than 100 nm is even more important because a clear change in the emitting wavelength is easily detectable even without a fluorescence spectrometer. The combination of both, increase in intensity and a marked shift in wavelength is exactly the desired response of a luminescence sensor system.

On the other hand the presence of a base caused only very little changes. Small amounts increased the emission and a very large excess up to a 1 M solution led to a

decrease of intensity. Compared to acid, these tiny changes indicate the stability of **15** towards bases.

After this striking result further experiments with addition of hydrochloric acid were carried out.

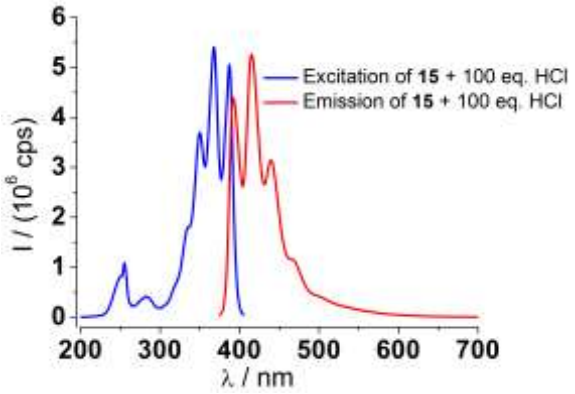

Figure 2-51: Excitation (blue, λ_{det} = 415 nm) and emission (red, λ_{ex} = 368 nm) spectra of **15** in methanol + 100 eq. aqueous hydrochloric acid.

Figure 2-51 displays the excitation and emission of the new formed species after addition of 100 eq. hydrochloric acid to **15**. Comparing this illustration with the excitation and emission spectra in Figure 2-49 of the non-protonated **15**, several differences are visible.

At first the curve form differs notably. Whereas **15** showed a broad band in its emission spectrum and hardly distinguishable maxima in the corresponding excitation spectrum, the protonated derivative exhibits more structured signals. The maxima of the excitation spectrum are with λ = 255 nm, 282 nm, 350 nm, 368 nm and 387 nm blue-shifted by 7 or 8 nm compared with **15** and this causes also a different suitable excitation wavelength for both derivatives. This is the main reason why the intensity in Figure 2-51 is with more than five million cps five-fold enlarged compared to the red line in the left spectrum of Figure 2-50. The excitation wavelength of λ_{ex} = 396 nm is ideal for **15** but not for its protonated counterpart and by optimization of the excitation wavelength to λ_{ex} = 368 nm this difference in intensity arose. The used spectrofluorometer can report intensities up to two million cps reliably so this high observed intensity may contain an error in its absolute number but the trend to such a large emission stays unchanged.

Moreover, the STOKES shift decreased dramatically to 5 nm and could indicate together with the discussed intensity a shorter lifetime of the excited state.

The next study was carried out on the reversibility of the proton detection process. Therefore, 100 eq. of hydrochloric acid and sodium hydroxide were alternately added and after each addition an emission spectrum was recorded.

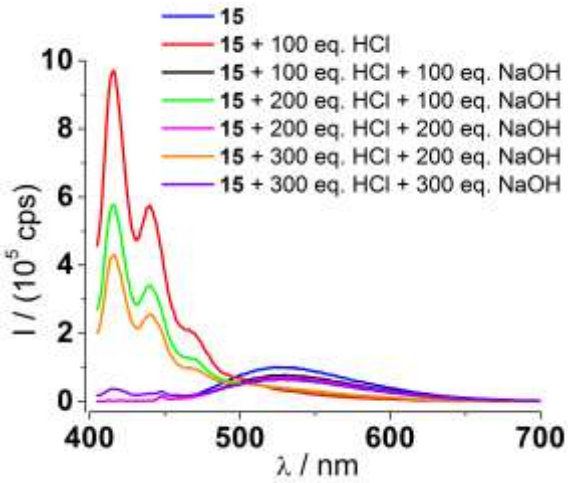

Figure 2-52: Emission of **15** in methanol before and after alternately added 100 eq. aqueous hydrochloric acid and 100 eq. aqueous sodium hydroxide (λ_{ex} = 396 nm).

The changes between the blue and the red spectrum of Figure 2-52 are similar to the protonation behavior shown in the left part of Figure 2-50. Additional insights can be gained by comparing the red with the black line. By addition of 100 eq. sodium hydroxide, the previous spectral changes were reversed and the typical band of **15** formed. These changes were achieved two further times by the same procedure of at first acid and secondly base addition to the same sample.

Although the intensity decreased during each protonation-deprotonation cycle, the reversibility is clearly evident. At last the protonated species of **15** turned out to be stable over the observed time of several minutes and a summary of this experiment can be found in the right part of Figure 5-31.

The pronounced hypochromic shift upon protonation is also observed in sensor systems working based on the ICT mechanism (discussed in chapter 1.3.2). The response combined with the fulfilled geometric criterion, the absence of a spacer between fluorophore and receptor, leads to the estimation that **15** detects protons based on the ICT mechanism.

2.2.11.3 Luminescence analysis after the addition of metal salts to 9-anthracenesalicylamine (15)

Besides varying the pH value by addition of acids and bases, the luminescent response of **15** towards different metal bromides was tested via the established procedure described in section 2.1.8.1. A summary of all tested metal salts is given in Figure 2-53 and the corresponding wavelength dependent information are displayed in chapter 5.1.8.

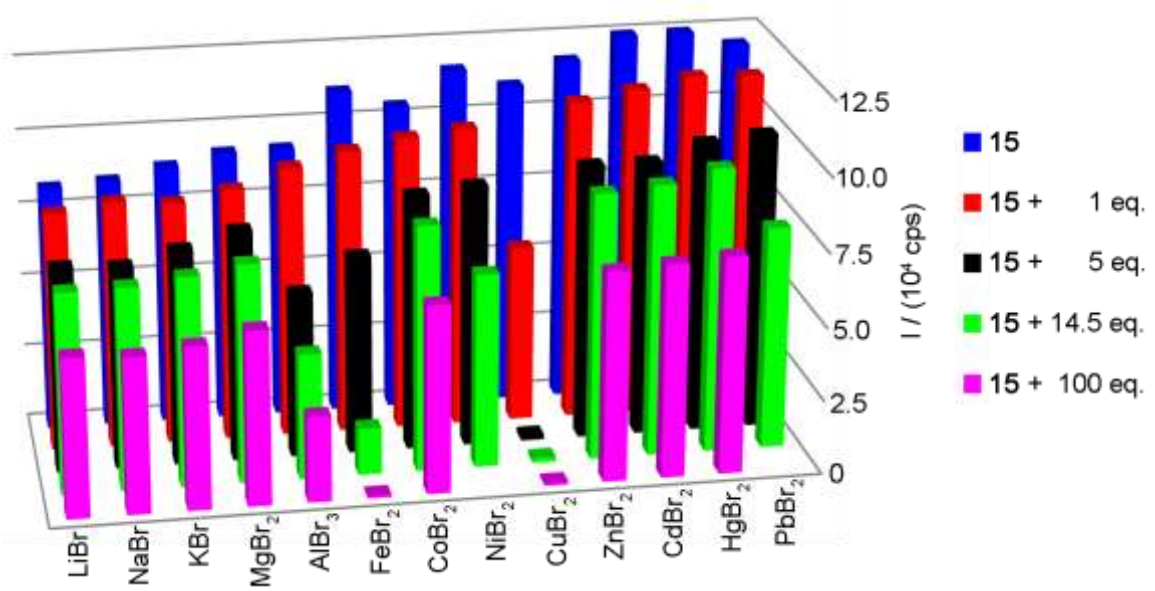

Figure 2-53: Representation of every tested combination between **15** and the respective metal bromide in MeOH (10^{-5} M, λ_{ex} = 396 nm, emission depicted at 530 nm).

Many of the illustrated metal bromides caused the same luminescent behavior of a small decreasing intensity between the blue and the red bar, a more pronounced one between the red and the black one, the smallest change between the black and the green column and the largest decrease of intensity between the green and the magenta one. This is true for lithium, sodium, potassium, magnesium, cobalt, zinc, cadmium and mercury bromide, indicating that in these cases the added volume had a stronger influence on the detected cps than the amount of metal salt. An analogous behavior is visible for nickel and lead bromide, just with the most pronounced change between the black and the green bar because of the biggest added volume in this step. All mentioned metal salts do not seem to change the intensity by their presence but just by dilution due to their solvent methanol.

Noticeable is the increasing intensity following the blue columns from the left to the right. The summarized measurements were carried out during one day and the composition of the stock solution changes over these hours by developing a stronger emitting species at the depicted wavelength of 530 nm. This trend was investigated by monitoring the stability of **15** after 5 days and is summarized in the left part of Figure 5-31. There, not only a strong increase of intensity is visible but also a shift in wavelength to a maximum of 510 nm. This indicates the unexpected formation of **11** out of **15** over time.

Stronger quenching effects can be observed in the presence of aluminum, iron and copper bromide whereas the last one is caused by absorption of the copper ions (Figure 2-10 right). For the other two experiments the wavelength dependent information are given in Figure 2-54.

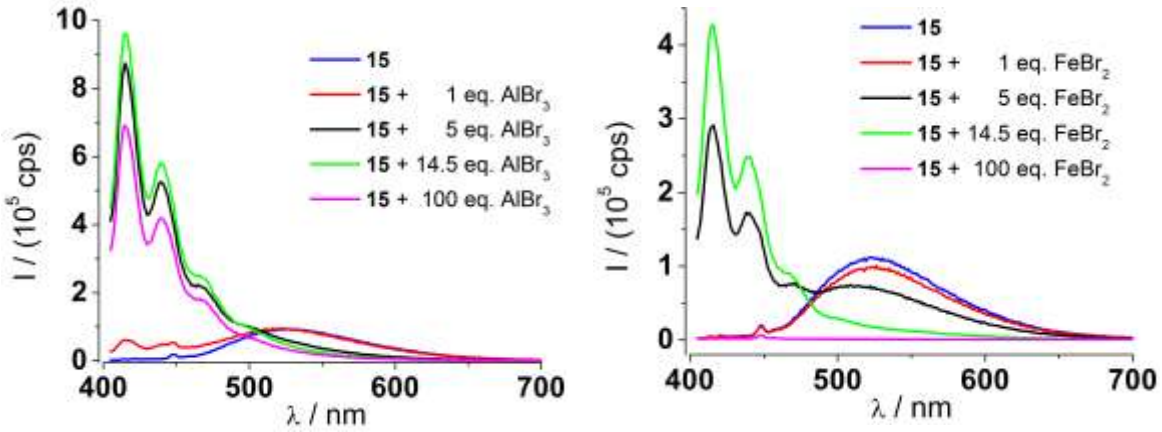

Figure 2-54: Emission properties of **15** after addition of aluminum bromide (left) and iron bromide (right) (10^{-5} M in MeOH, λ_{ex} = 396 nm).

Similarities and differences are visible comparing the response of **15** towards aluminum and iron bromide. On the one hand the addition of 1 eq. resulted in both cases only very tiny changes although the presence of 1 eq. aluminum points to the subsequent course by a small increase of intensity at 415 nm. Larger amounts of both salts, namely 5 eq. and 14.5 eq., populate the same luminescent species that is known from the protonation experiments with hydrochloric acid and should in this case also be the protonated amine **15**. As discussed in section 2.1.8.4 not only iron(II) is present but also iron(III) by oxidation over time of the metal bromide so-

lution by present oxygen. So both metal(III) cations are LEWIS acidic and release protons out of methanol or traces of water.
On the other hand a clear difference is observed after addition of 100 eq. metal salt. Whereas aluminum bromide reduced the intensity only by a small amount due to dilution, the iron salt quenched the detected radiation completely. This is as discussed before caused by absorption of the iron solution (Figure 2-10 left). The maximal reached intensity is also different among these two experiments and the reason is again the absorptive behavior of the iron cations.
So **15** does not show a noteworthy response towards the tested metal cations apart from the side reaction of protonation.

To conclude, **15** showed a tremendous reversible luminescent response towards protons and is characterized by a very strong increase of intensity and more important a distinct change of its emission wavelength by more than 100 nm. This protonated species is stable during the experiments.
Disadvantages are the lability of **15** in the solution of methanol and its poor response towards the tested metal salts in methanol.
The addressability of this luminescent completely different protonated state and the switchability between it and **15** arouses interest of similar constructed derivatives working based on the ICT mechanism.

2.2.12 9-Anthracenepicolylamine (16)

The next step was obviously the synthesis and investigation of the amine derived by reduction of **13**. Therefore, a suitable procedure for the preparation as well as its purification had to be developed.

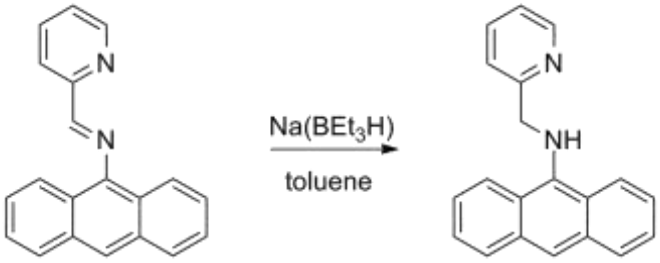

13 **16**

Scheme 2-21: Synthesis of **16** by reduction of the C=N double bond in **13**.

Different reducing agents were also tested in the synthesis of **16**. The usage of hardly soluble reagents like $NaBH_4$ or $LiAlH_4$ only caused moderate conversion after long reaction times. In contrast the two hydrides $Na(BEt_3H)$ and $K(BEt_3H)$, which were provided in the organic solvents toluene or THF as 1 M solutions resulted in almost complete conversion. A reason for this may be the different polarity of the used imines. **12** is more polar and its interaction with the hardy soluble reagents could be enhanced. On the other hand **13** is less polar and prefers reduction via reducing agents which are better soluble in organic solvents. Both alkyl containing hydrides $Na(BEt_3H)$ and $K(BEt_3H)$ showed similar results despite of the different solvents they introduced for the reaction.

Although the conversion was almost quantitatively, some byproducts formed in small amounts and the purification turned out to be time-consuming. The best results in quality and quantity were achieved by at first removal of the volatile components under reduced pressure, dissolving the residue in ethylacetate and water and extraction of the aqueous layer with ethylacetate. The crude product was purified by column chromatography (pentane/ethaylacetate, 20:1 → 2:1) and subsequent recrystallization from hexane and ethylacetate.

Both alkyl containing reducing agents resulted in the same isolated yield of 23 % after passing this purification process. Even though in the case of $K(BEt_3H)$ in THF

partly other solvents were used. This yield is only moderate compared with 74 % achieved in the reduction of **12** to **15** but is sufficient to investigate **16** and compare its properties to **15**.

After recrystallization from hexane and ethylacetate suitable single crystals for solid state structure determination via X-ray diffraction were obtained.

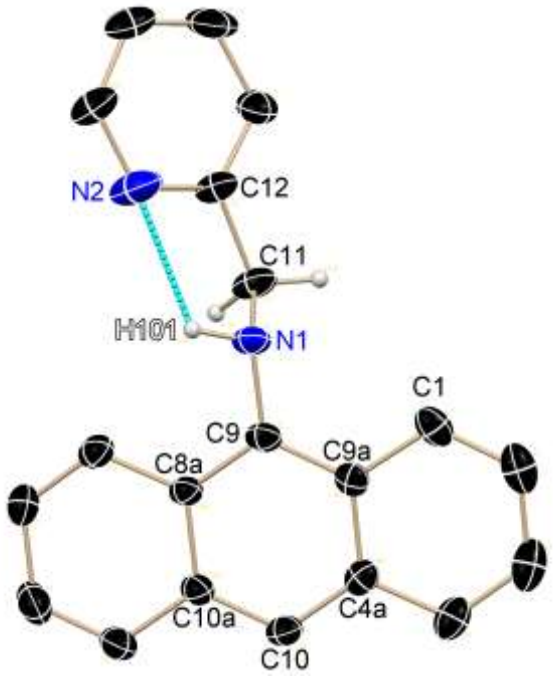

Figure 2-55: Solid state structure of **16**. Hydrogen atoms bond to sp^2 hybridized carbon atoms and positional disorder are not shown.

16, shown in Figure 2-55, crystallizes in the monoclinic space group *C*2 with one molecule in the asymmetric unit. Following the CIP nomenclature for stereogenic center the displayed enantiomer is the (*R*) isomer but it is positionally disordered with the (*S*) isomer and exhibits a side occupation factor of 0.51(3). In this alternative configuration only the position of the hydrogen atom H101 differs in the solid state. The hydrogen atom switches its position with the nitrogen lone pair in the mentioned (*S*) isomer.

Moreover, an intramolecular hydrogen bond exists between N1 as the donor atom, H101 and N2 as acceptor. Despite of this structurally stabilizing element the side occupation factor shows no significant preference for the displayed (*R*) enantiomer although this intramolecular hydrogen bond is not present in the (*S*) enantiomer. On the other hand the (*S*) isomer is stabilized by an intermolecular hydrogen bond be-

tween N1, H101 and the N1 atom of the next molecule. Both interactions seem to stabilize the packing similarly because both isomers are equally present and **16** crystallizes in a racemic mixture.

A second positional disorder exists in the solid state structure of **16**. C11 is shifted with its borne hydrogen atoms by 40 pm and the illustrated derivative shows a side occupation factor of 63(2) %.

Table 2-12: Selected distances in pm and angles in ° of **16**.

N1–C9	141.9(2)	N1–C11–C12	107.7(5)
N1–C11	150.0(7)	C11–N1–C9	112.7(3)
C11–C12	152.0(6)	N1–C9–C9a	120.61(15)
N1–H101	92(3)	N1–H101···N2	114(3)
N2···H101	226(3)	C9–C9a–C4a	119.55(14)
C9–C9a	140.7(2)	C9a–C4a–C10	119.83(15)

Table 2-12 contains bond lengths and angles as well as information about the intramolecular hydrogen bonding situation of **16**. The present hydrogen bond would be classified as weak following JEFFERY.[94] Its hydrogen–acceptor distance is longer than 2.2 Å and the nitrogen–hydrogen–nitrogen angle is smaller than 130 °. Furthermore, it is also the weakest one observed during this project in comparison with the hydrogen bonds in **12** or **15** judged by the mentioned geometrical values.

The bond distances containing C11 should be considered with caution and their slight variation from standard $C(sp^3)$–$C(sp^2)$ or $C(sp^3)$–$N(sp^3)$ single bond distances may be caused by the disorder of this atom. The bond distances and angles inside the anthracene moiety are typical for an aromatic bonding situation. The largest deviation of one carbon atom to the anthracene plane by 10 pm confirms an aromatic conjugated system including all three annulated six-membered rings.

Although **16** was isolated only in a moderate yield, its synthesis is reported herein for the first time and additionally **16** was characterized fully by one and two dimensional NMR spectroscopy, EI mass spectrometry, elemental analysis and X-ray diffraction.

The next step was to explore the luminescent properties of **16** and compare them especially to the previously prepared amine **15**.

2.2.13 Luminescence properties of 9-anthracenepicolylamine (16)

This chapter deals with the question if the response of **16** towards protons is similar to that of **15** or if the change from a 2-hydroxyphenyl to a 2-pyridyl substituent effected this behavior. Also the stability of **16** was of major interest because this was a drawback of the amine **15**.

2.2.13.1 UV/Vis absorption and luminescence emission of 9-anthracenepicolylamine (16)

Like before, the basic optical spectroscopic experiment was to the recording of an absorption spectrum of **16**. This allows the excitation at a proper wavelength and as mentioned above, a comparison of the absorption with the excitation spectrum of one molecule results in an estimation of potentially ongoing non-radiative processes.

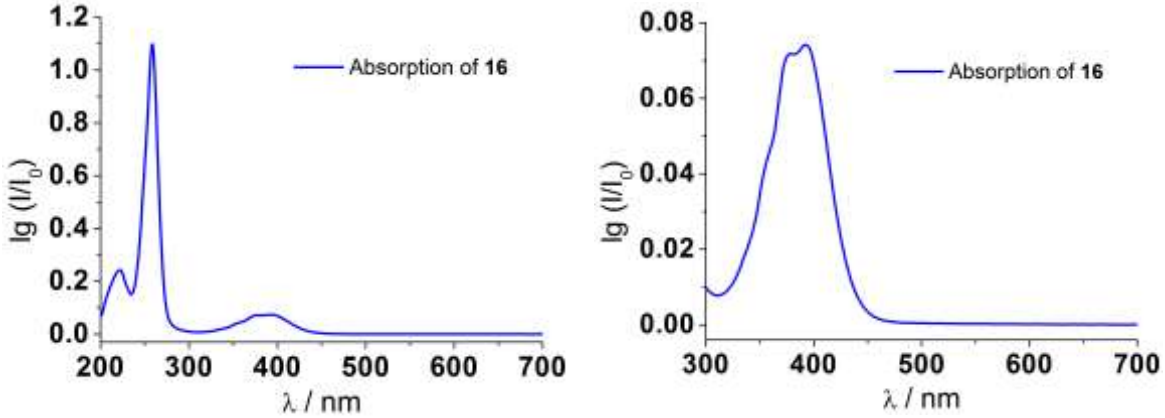

Figure 2-56: UV/Vis absorption spectra of **16**. Left: full spectrum; right: enlargement of the spectral region around 400 nm (10^{-5} M in MeOH).

The absorption of **16** displayed in Figure 2-56 is very similar to that of **15** shown in Figure 2-48. The peak positions are almost identical and the curve shape is hardly changed. Only the intensity is a bit enhanced in the absorption spectrum of **16**. This points towards a similar absorptive behavior of both synthesized amines.
The corresponding excitation and emission spectra show further similarities.

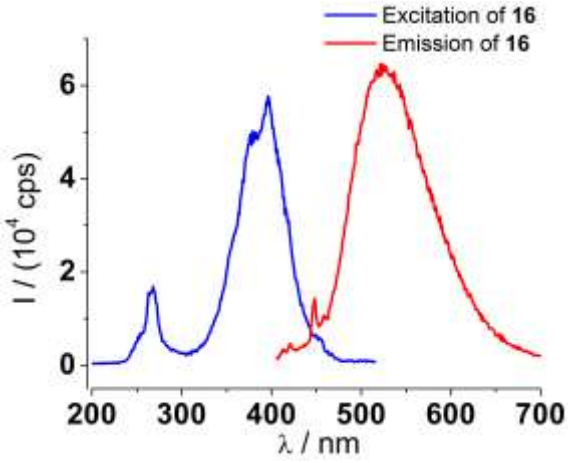

Figure 2-57: Excitation (blue, λ_{det} = 525 nm) and emission (red, λ_{ex} = 396 nm) spectra of **16** (10^{-5} M in MeOH).

Comparing the blue line of Figure 2-57 with the absorption spectrum presented before, a resembling curve shape as well as just by a few nm varying peak positions can be found.

Moreover, the similarities between the emissive properties of **15** and **16** are obvious. The in both cases relatively broad, not by vibration structured band is just shifted by around 5 nm to larger energy. **16** shows also a distinct STOKES shift of nearly 130 nm and a similar luminescence intensity. So the same annotations concerning the assumed relatively long lifetime as well as the proposed umbrella term luminescence for the radiative relaxation can be transferred from **15** to **16** (section 2.2.11.1).

2.2.13.2 Luminescence analysis after the addition of acids and bases to 9-anthracenepicolylamine (16)

Topic of this section was to investigate the impact of pH changes towards the luminescent properties of **16**. Therefore, the approved additives hydrochloric acid and sodium hydroxide were used (cf. Table 2-1).

In the left part of Figure 2-58 the addition of acid to **16** is displayed. A concentration of 10^{-3} M resulted in a decreasing intensity around 525 nm but formation of a new luminescent species at λ = 416 nm. This maximum of the new band deviates only by 1 nm from the most intense peak of the protonated **15** and indicates a similar stage of **16** after addition of hydrochloric acid.

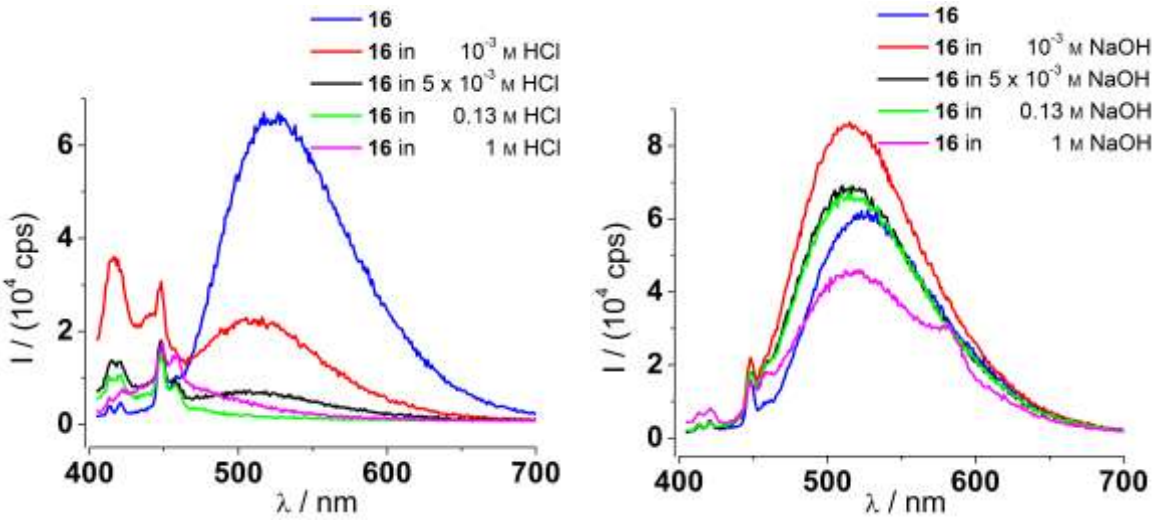

Figure 2-58: Emission spectra of **16** under acidic (left) and alkaline (right) conditions (λ_{ex} = 396 nm).

But in contrast to **15** this protonated species is not stable and decays to a non-luminescent one with enlarged concentration of acid. Even the red line in the left part of Figure 2-58 shows a very small intensity compared to the protonated **15** (Figure 2-50 left) so the decomposition process seems to be relatively fast.

On the other hand **16** looks stable towards a large excess of base. When aqueous sodium hydroxide was added to a concentration of 10^{-3} M the intensity increased but higher amounts led to a decrease of detected emission that is only moderately even after a 1 M concentration of NaOH was reached.

So this labile protonated state proves that **16** is no suitable switchable luminescent pH sensor despite of its similar structure compared to **15**.

2.2.13.3 Luminescence analysis after the addition of metal salts to 9-anthracenepicolylamine (16)

After discovery of this quiet different behavior of **15** and **16** towards protons, the response of **16** to metal bromides was investigated throughout this section. Therefore, the established screening procedure discussed in section 2.1.8.1 was applied to a 10^{-5} M solution of **16** in methanol. The full wavelength dependent information of every metal bromide addition, not displayed during this section, can be received in chapter 5.1.9.

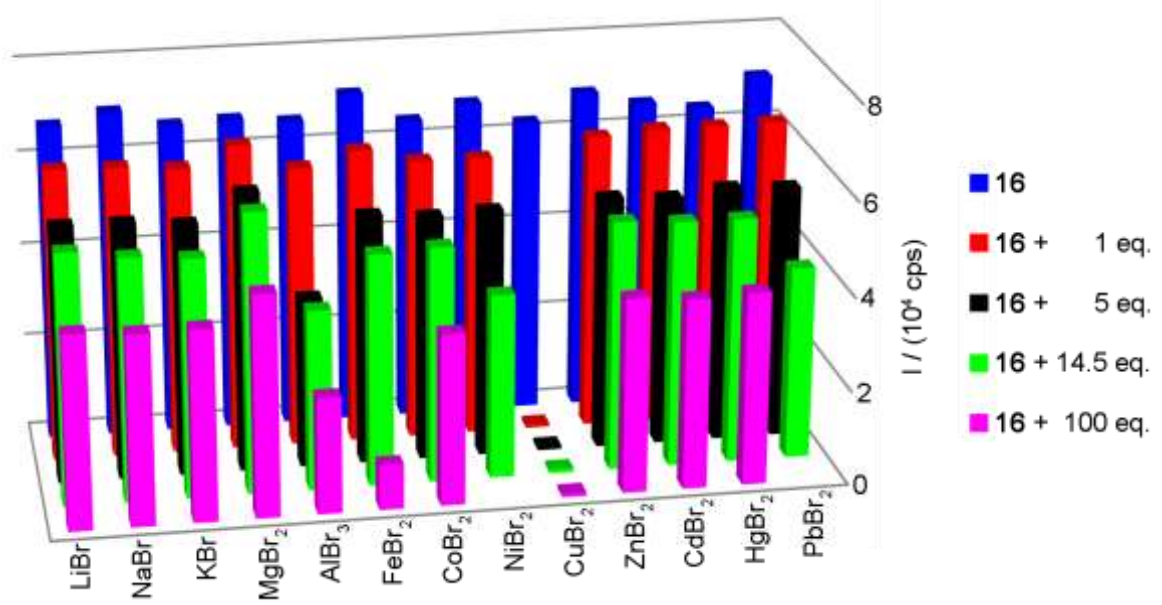

Figure 2-59: Representation of every tested combination between **16** and the respective metal bromide in MeOH (10^{-5} M, λ_{ex} = 396 nm, emission depicted at 525 nm).

Figure 2-59 evinces similarities and differences in the luminescence response of **16** towards the amine **15** investigated earlier (Figure 2-53). On the one hand the major part of metal salt additions also resulted in a decrease of intensity caused by dilution, valid for lithium, sodium, potassium, cobalt, nickel, zinc, cadmium, mercury and lead bromide. This is indicated by the more pronounced gap between their red and the black columns than the difference between the black and the green bars, although, the second mentioned addition contained a larger amount of metal salt but less volume of solvent. Magnesium bromide shows a less pronounced decrease in intensity with increasing concentration and this is caused by enhancement at the low wavelength side of the signal (Figure 5-39 right).

Noticeable is the unchanged starting intensity of the stock solution of **16**. Even though this series of measurements was carried out over three days no trend of increasing or decreasing starting intensity was observed. In reverse this proves the stability of **16**. So this enhanced durability whose absence was a major drawback of **15** is a welcomed change in the properties of **16**.

Another similarity is the quenching along with enhanced concentration of iron and copper bromide. But in the extent of quenching, some differences are found. Also aluminum bromide causes different responses in **15** and **16.**

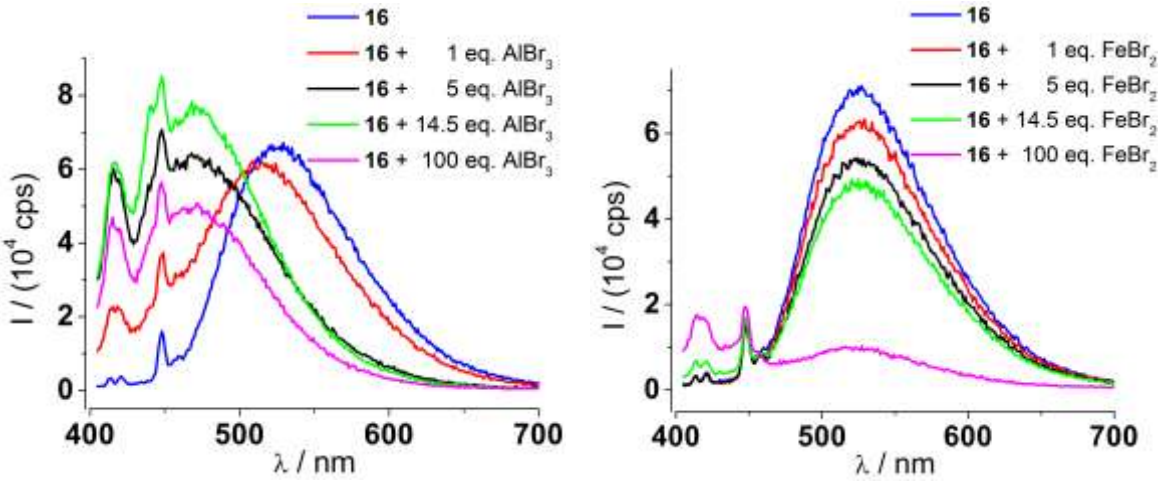

Figure 2-60: Emission properties of **16** after addition of aluminum bromide (left) and iron bromide (right) (10^{-5} M in MeOH, λ_{ex} = 396 nm).

The addition of iron bromide (Figure 2-60 right) caused only at 100 eq. changes distinguishable from dilution. Around 415 nm the typical protonation signal is visible whereas in general the intensity is decreased by the absorptive behavior of the colored iron solution.

Aluminum ions resulted in different changes than protonation this time (Figure 2-60 left). Whereas the addition of acid quenches the luminescence almost completely, aluminum cations led to the formation of a new relatively broad band around 470 nm indicating a coordination of aluminum cations by **16**. But maybe the left smaller signal at 415 nm is also a sign of partial protonation because its maximum is comparable to the protonated species. To investigate this in more detail, time dependent measurements were carried out as well as the addition of aluminum bromide in the aprotic solvent DMF.

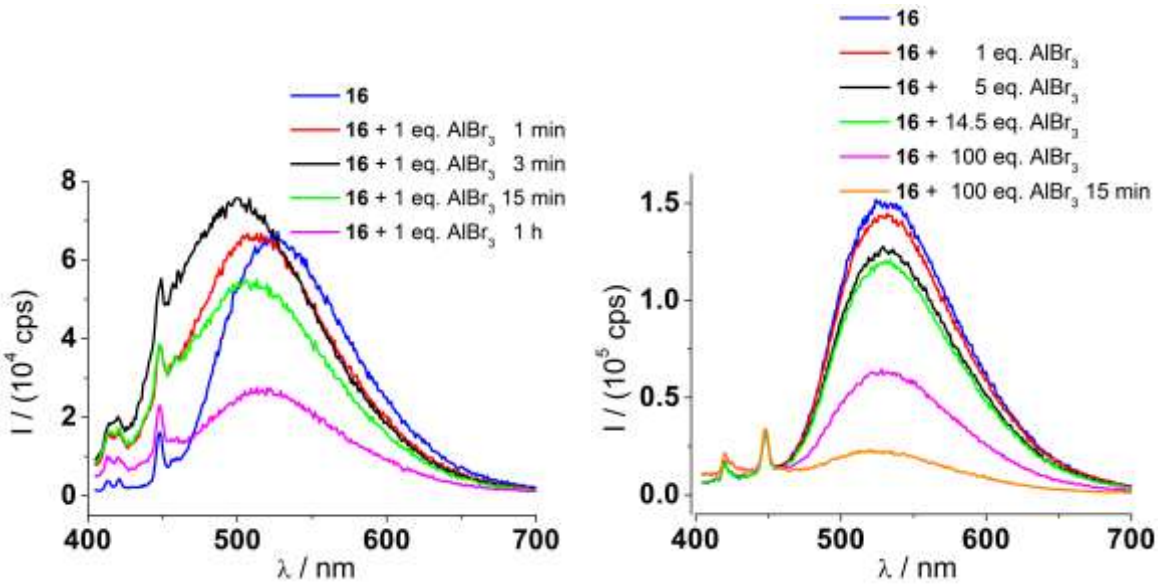

Figure 2-61: Emission spectra before and after addition of aluminum bromide to **16**. Time dependent in methanol (left) and in the aprotic solvent DMF (right) (10^{-5} M, λ_{ex} = 396 nm).

The addition of 1 eq. aluminum bromide in methanol to **16**, shown in the left part of Figure 2-61, caused a changing behavior over time. After one minute a slight hypochromic shift although no changes in intensity were observed. But already after three minutes the maximal intensity and shift was reached and longer periods of time resulted in a decrease of intensity and shift backwards. This could be a hint to an also unstable luminescent species that is converted to non-luminescent products like in the case of protonation.

In the right part of Figure 2-61 a 10^{-5} M solution of **16** in DMF was treated with aluminum bromide dissolved in DMF, too. In the absence of a protic solvent no shift in wavelength was observed but a decrease of intensity that became more pronounced after a period of 15 minutes.

So even if **16** shows a luminescent response to aluminum cations that is different from protonation this state is not stable and therefore, this is no example of a proper sensor capability.

Remarkable is the very strong quenching of copper ions in Figure 2-60. Even 1 eq. led to a complete vanished emission. This was investigated in detail to understand the underlying process.

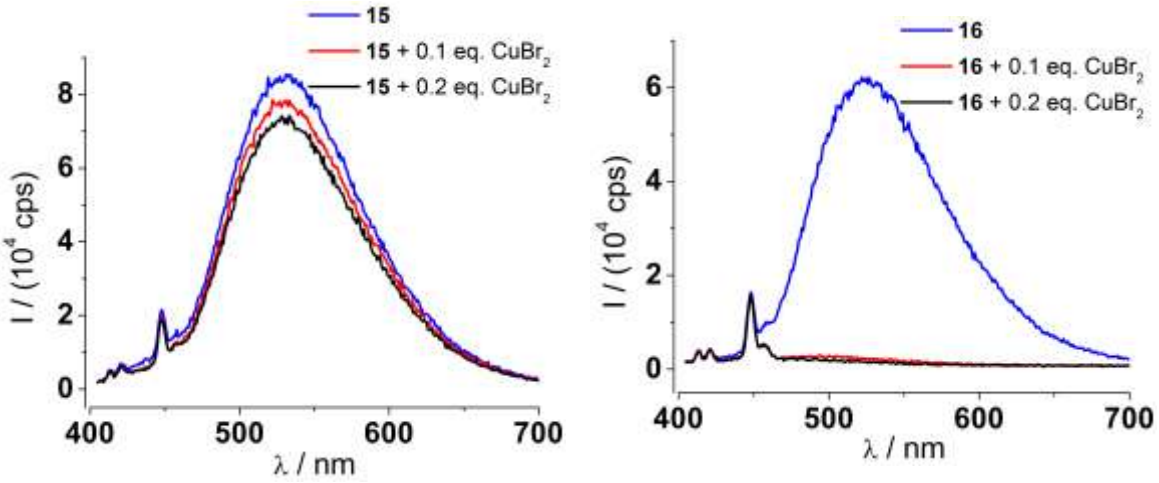

Figure 2-62: Emission spectra before and after addition of copper bromide to **15** and **16** (right) (10^{-5} M in MeOH, λ_{ex} = 396 nm).

The different luminescent responses of **15** and **16** towards copper ions are compared in Figure 2-62. Whereas only slight changes after addition of 0.1 and 0.2 eq. copper bromide to **15**, most likely caused by dilution, are visible in the left part, another behavior of **16** is visible towards this sub-stoichiometric amount of copper. The emission of **16** is completely quenched even after 0.1 eq. indicating a strong interaction between the amine and the metal cation.

Such a sub-stoichiometric addition is uncommon to cause the observed quenching by coordination and so one possibility is the catalytic decomposition of **16** by copper cations to a non-luminescent species.

To check this, different concentrations of ethylenediamine were added to a copper containing solution of **16** in methanol because of the known strong affinity of ethylenediamine towards copper(II) cations.[105] An increase of intensity with rising concentration of ethylenedimaine would suggest the reversible coordination between copper cations and **16**.

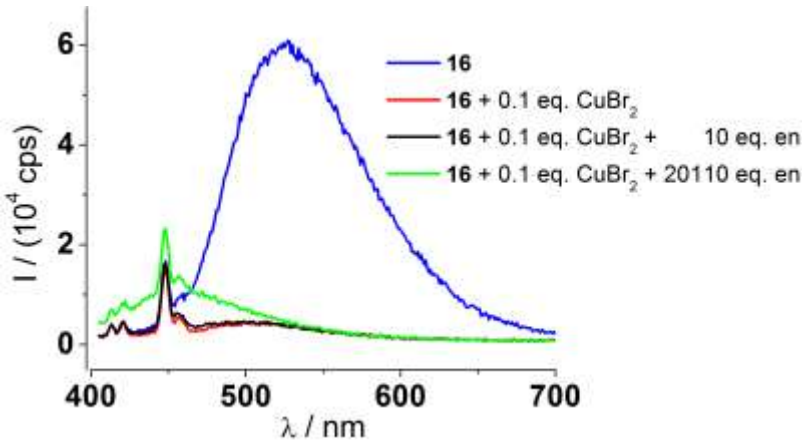

Figure 2-63: Emission spectra of **16** before and after addition of copper bromide and ethylenediamine (en) (10^{-5} M in MeOH, λ_{ex} = 396 nm).

As observed before, 0.1 eq. of copper bromide quenched the emission of **16** completely. Even the 100-fold excess of ethylenediamine over copper is unable to restore the emission of **16**. A larger excess of 20110 eq. ethylenediamine resulted in some intensity around 455 nm but this is more likely an impurity of the added diamine than a recovered emission of **16** due to the different curve shape.
So this experiment is a further hint that copper(II) ions led to decomposition of the synthesized anthracene derivative to non-luminescent products instead of a coordination between **16** and copper. Still **16** is able to signal the presence of very low copper concentrations but in an undesired and irreversible way.

To conclude the optical properties of the synthesized amines **15** and **16**: Despite of the similar build-up, different luminescence properties were discovered. The absorption and emission spectra were almost equal in intensity as well as curve shape and peak positions. But the stability of both investigated amines in their solvent methanol varied considerably. **15** turned out to decay to **11** whereas **16** was stable in a 10^{-5} M solution over days. In return, the response of **15** towards protons was strikingly. Additionally, the formation of a reversible in terms of luminescence completely different protonated state was a sign that this prepared class of molecules could give rise to promising colorimetric sensors.
Especially the impact on the luminescent properties of this relatively small structural variation between **15** and **16** inspired the preparation of a further new derivative with a similar architecture.

2.2.14 *o*-(*β*-Hydroxyethoxy)benzaldehyde (17)

To access the new derivative, the established synthetic route of condensation reaction between an aldehyde and **11** at first, followed by a subsequent reduction of the C=N doube bond was the aspired reaction path.

Therein, an aldehyde contributing an additional donor center to the anthracene based potential sensor while maintaining the phenyl body was chosen: *o*-(*β*-hydroxyethoxy)benzaldehyde (**17**). This aldehyde was prepared according to a synthesis published in 2006 by a workgroup interested in carbene catalyzed nucleophilic substitution reactions.[106]

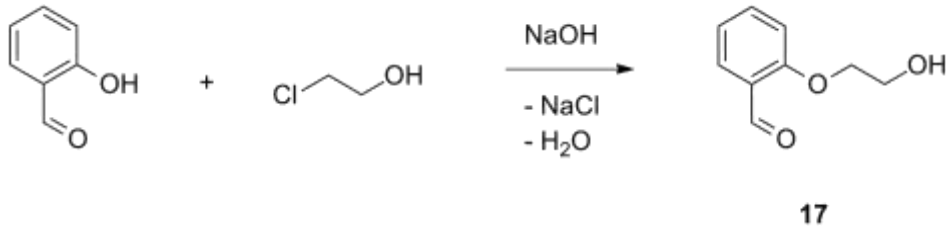

17

Scheme 2-22: Synthesis of **17** by a nucleophilic substitution reaction.

The reaction presented in Scheme 2-22 was carried out under exclusion of oxygen in degased water with sodium hydroxide as base. Its role to deprotonate the phenol proton of salicylaldehyde allows the nucleophilic substitution reaction between the alcoholate and the electrophilic carbon bearing a chlorine in 2-chloroethanol.

A slightly larger scale was scheduled compared to the published procedure but the reaction conditions like temperature or reaction time were adopted with heating the reaction mixture for 16 h to the boiling point of water. A phase separation was observed but extracted samples, later investigated via ^{1}H-NMR spectroscopy, showed that both layers contained impurities and the desired product. The organic layer exhibited a higher quantity of crude **17**.

The pH value was increased to about 10 by addition of sodium hydroxide solution and the aqueous layer was extracted with DCM four times.

The crude product was purified via column chromatography with petroleum ether and ethylacetate (10:1 → 1:1) and **17** was isolated in a yield of 42 % in good purity. This is not as good as reported (76 %), but sufficient due to the cheap starting materials. With **17** in hand the imine formation was the subsequent step.

2.2.15 9-Anthracene(*o*-(*β*-hydroxyethoxy)benzyl)imine (18)

By reaction of **17** with **11** a new imine was formed that includes three heteroatoms and, therefore, offers the possibility of a threefold metal coordination. This additional donor center is connected by an ethylene linker, which should allow a flexible usage of the hydroxyl group from a geometrical point of view.

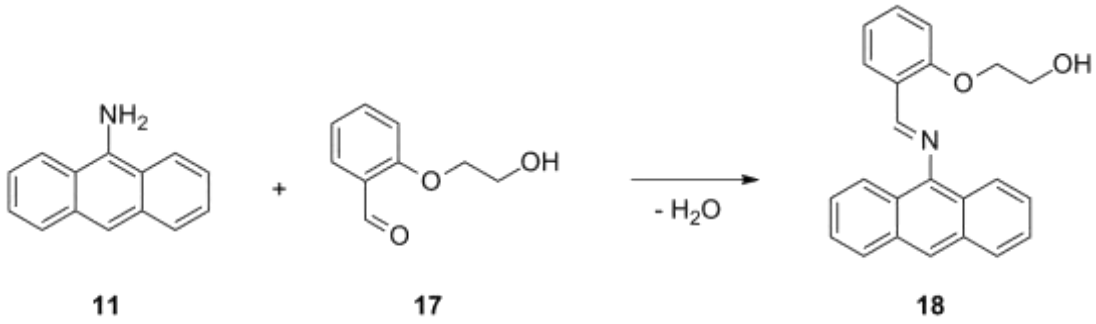

Scheme 2-23: Synthesis of **18** by condensation reaction between **11** and **17**.

Scheme 2-23 shows the reaction to **18**, which is analog to the preparation of **12** and **13**. But this time some circumstances enhanced the difficulty of isolating **18**. For instance, the conversion was lower and reached not more than 90 %, even with a 2.5-fold excess of aldehyde. Therefore, the purification was time-consuming because the remaining **11** had to be separated as well as the over-stoichiometric amount of aldehyde.

A good starting point was the crystallization of **18** from the reaction mixture, but due to its less clearly defined solubility in the used solvent than the solubility of its analogs **12** and **13**, the amount of ethanol had to be adjusted. **12** was almost insoluble in ethanol, so it was purified just by filtration, whereas **13** was well soluble in ethanol and the solvent had to be removed completely to avoid small yields after recrystallization. The solubility of **18** in ethanol was between those two extremes. So the amount of solvent was crucial to purify **18**. 10 mL turned out to solve the 3 g of starting material and ensured sufficient crystallization of **18** from the reaction mixture at -33 °C.

The next feature was the cocrystallization of ethanol with **18** from the reaction mixture. On the one hand suitable single crystals for the solid structure determination via X-ray diffraction were accessible, but on the other hand this extended the purifi-

cation process, because the cocrystallized solvent could not be separated by application of reduced pressure.

So the crystals were dissolved in ethylacetate, the volatile components were removed under reduced pressure to avoid a second cocrystallization of ethanol and the resulting solid was recrystallized from hexane and ethylacetate.

This procedure of two successive crystallizations allowed to isolate **18** in a yield of 61 % with around 2 % aldehyde left. The yield is lower than in the case of **12** and **13** where 93 and 90 % were isolated but is still good. Additionally, **18** was fully characterized by NMR spectroscopy, mass spectrometry, elemental analysis as well as solid state structure determination via X-ray diffraction.

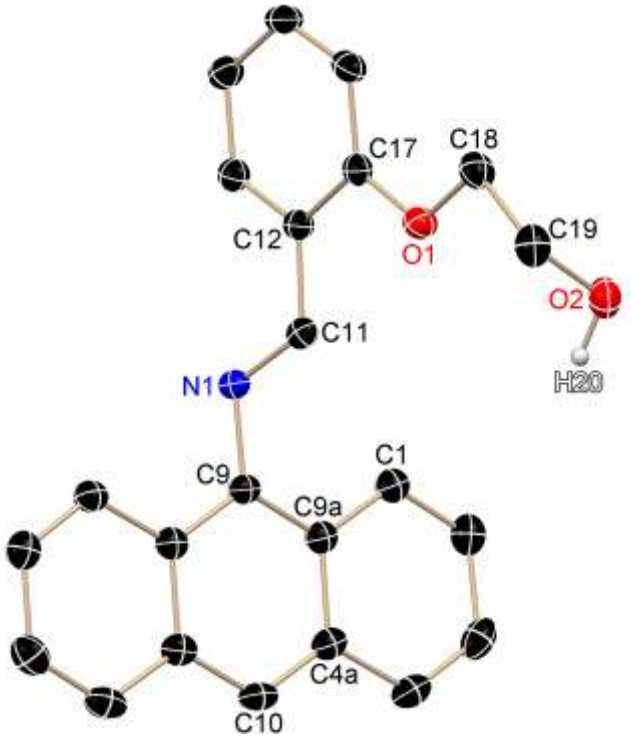

Figure 2-64: Solid state structure of **18**. Hydrogen atoms bond to carbon atoms and a cocrystallized disordered ethanol molecule are not shown.

One molecule of **18**, shown in Figure 2-64, was present in the asymmetric unit of the crystal, which belonged to the monoclinic space group $P2_1/c$. Additionally, the solvent molecule ethanol is cocrystallized in a 1:1 ratio and together they formed chains held together by hydrogen bonds. O2, bearing H20, acts as a donor and at the same time as acceptor for another ethanol molecule.

Neither N1 nor O1 are involved in any distinct hydrogen bonding, although they could also work as hydrogen bond acceptors.

Some selected bond lengths and angles of **18** are displayed in Table 2-13.

Table 2-13: Selected distances in pm and angles in ° of **18**.

N1–C9	141.68(16)	N1–C11–C12	121.21(11)
N1–C11	127.60(16)	C11–N1–C9	117.92(10)
C11–C12	146.50(17)	N1–C9–C9a	121.15(11)
C17–O1	136.68(15)	C12–C17–O1	115.85(11)
C18–O1	143.42(15)	C17–O1–C18	118.05(10)
C9–C9a	140.95(18)	C9a–C4a–C10	119.87(11)

Like for the other two stolid state investigated imines **12** and **13**, **18** shows a relatively short carbon–nitrogen distance compared to a regular C(sp^2)–N(sp^2) double bond of 129 pm. The angles and bond distances within the anthracene moiety confirm the conjugated aromatic system of the three annulated six-membered rings. And also the bond lengths around the oxygen atoms are in a normal range of C(sp^2)–O or C(sp^3)–O single bonds with 135 pm and 143 pm respectively.[89]

After the successful synthesis and complete characterization of **18**, its optical properties were investigated and are described in the following chapter.

2.2.16 Luminescence properties of 9-anthracene(*o*-(*β*-hydroxyethoxy)benzyl)imine (18)

The main point of interest during this chapter was the influence of the further oxygen donor atom introduced during the synthesis by usage of the aldehyde **17**. The performed series of measurements targeted the luminescent response of **18** to protons or metal salts. Furthermore, the comparison of these properties with its analog derivative **12** (lacking of this third donor atom) was discussed.

2.2.16.1 UV/Vis absorption and luminescence emission of 9-anthracene(o-(β-hydroxyethoxy)benzyl)imine (18)

To select a suitable excitation wavelength the approved procedure of at first recording an absorption spectrum of the investigated potential sensor was also carried out in the case of **18**.

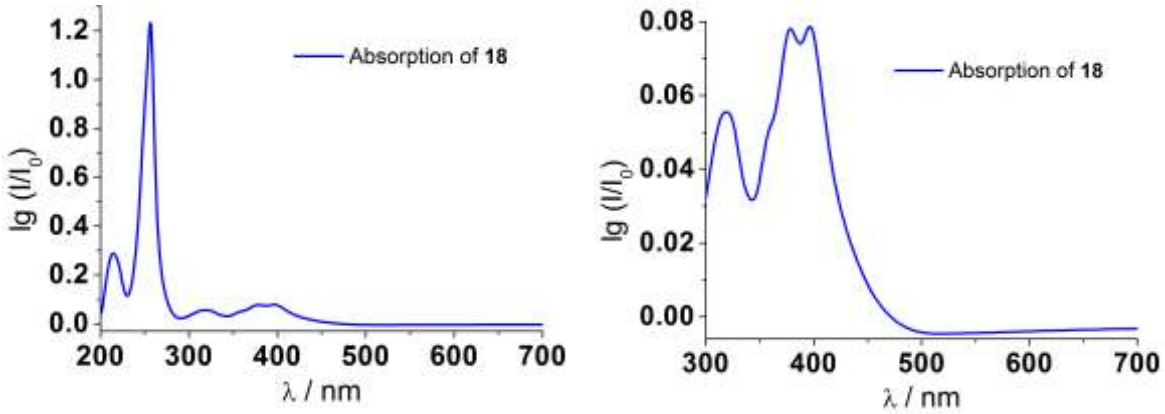

Figure 2-65: UV/Vis absorption spectra of **18**. Left: full spectrum; right: enlargement of the spectral region around 400 nm (10^{-5} M in MeOH).

In Figure 2-65 the absorption of **18** is displayed. The overall picture looks similar to the previous discussed anthracene derivatives with a very intense and sharp peak at λ = 256 nm and a more structured band around 400 nm with maxima at 396 nm and 378 nm as well as a shoulder around 358 nm. But this time an additional signal at 318 nm was observed.

Therefore, besides the regular recorded emission spectrum, where the sample was irradiated at one of the maxima in the absorption spectrum, an additional series of measurements was carried out and is summarized in Figure 2-66. Therein, superim-

posed emission spectra received at different excitation wavelengths, namely at the other local absorption maxima, are shown.

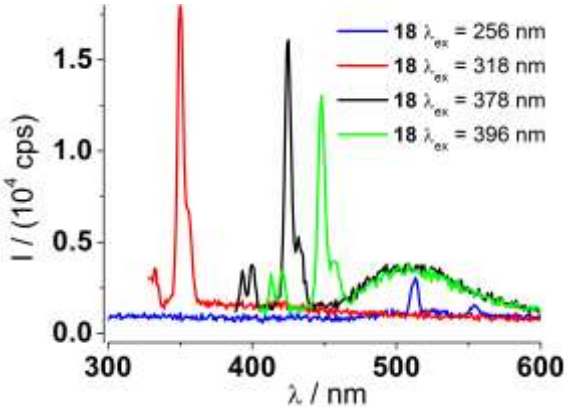

Figure 2-66: Stacked emission spectra of **18** at different excitation wavelengths (10^{-5} M in MeOH).

Noticeable is the overall weak intensity irrespective of the chosen excitation wavelength. Nearly exclusively, only the RAMAN signals of the solvent methanol are visible that are shifted due to the changed excitation wavelength (see also chapter 4.2.2). The only observable luminescent species is **11** with its broad band at λ = 510 nm in the black and green line of Figure 2-66. The present traces of **11** are not viewable in the red line, because the amine does not absorb at that spectral region.

The absence of another luminescent species despite of absorption is a clear hint to a strong ongoing non-radiative process. On the background of the determined structure of **18**, it is most likely the C=N isomerization. Indirectly also the signal at λ = 318 nm in the absorption spectrum can be assigned to **18** because of the low probability that it belongs to another strong absorbing but not emitting species.

2.2.16.2 Luminescence analysis after the addition of acids and bases to 9-anthracene(o-(β-hydroxyethoxy)benzyl)imine (18)

Of course **18** was tested in respect to the addition of acid and base. It was expected to observe a similar behavior like the other investigated imines exhibited, namely a formation of **11** with decreasing pH value, but relatively small changes upon addition of hydroxide ions. This time hydrochloric acid and sodium hydroxide were chosen as strong representatives of the pH varying additives, too (cf. Table 2-1).

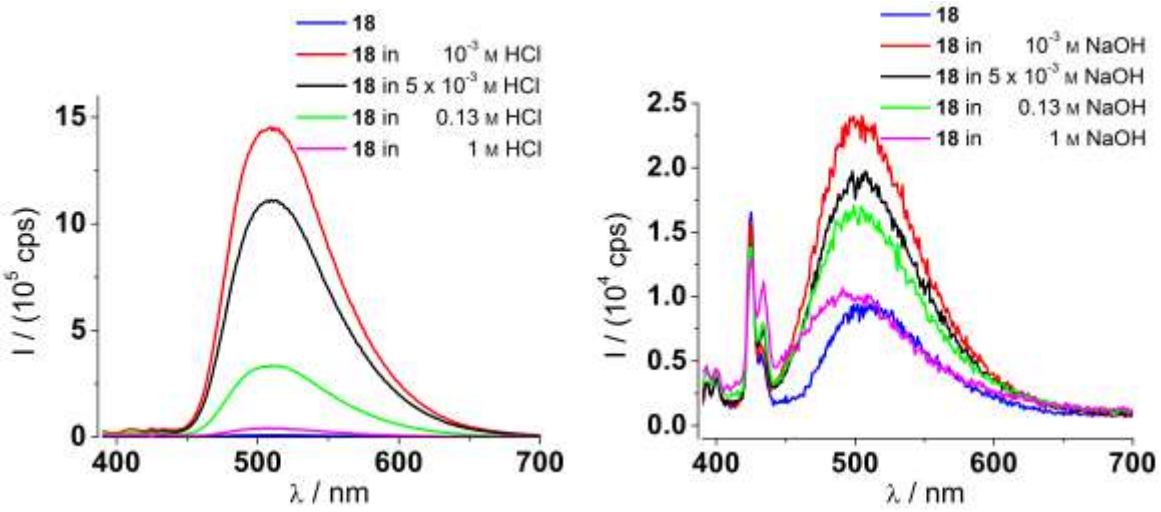

Figure 2-67: Emission spectra of **18** under acidic (left) and alkaline (right) conditions (λ_{ex} = 378 nm).

The in Figure 2-67 presented luminescent changes upon addition of acid and base to **18** fulfill the fundamental expectation obtained by spectroscopic studies of further prepared imines precisely. Protons accelerate at first the formation and afterwards the decomposition of **11**, traceable by the broad band around 510 nm, most likely in a catalytic way as discussed in chapter 2.2.5, exemplified at **12**.

On the other hand sodium hydroxide caused only moderate changes even though a slightly enhanced increase of intensity compared to **12** is detectable when a concentration of 10^{-3} M of NaOH was reached.

2.2.16.3 Luminescence analysis after the addition of metal salts to 9-anthracene(o-(β-hydroxyethoxy)benzyl)imine (18)

The fourth prepared imine **18** was also investigated regarding its response towards metal cations. Therefore, the screening procedure discussed in section 2.1.8.1 was applied to point out which metal bromide causes significant luminescent changes when added to **18**. As mentioned before, the examined imine exhibits no emission on its own and therefore, again the intensity of **11** at 510 nm was chosen to illustrate the luminescent results in a compact way (Figure 2-68).

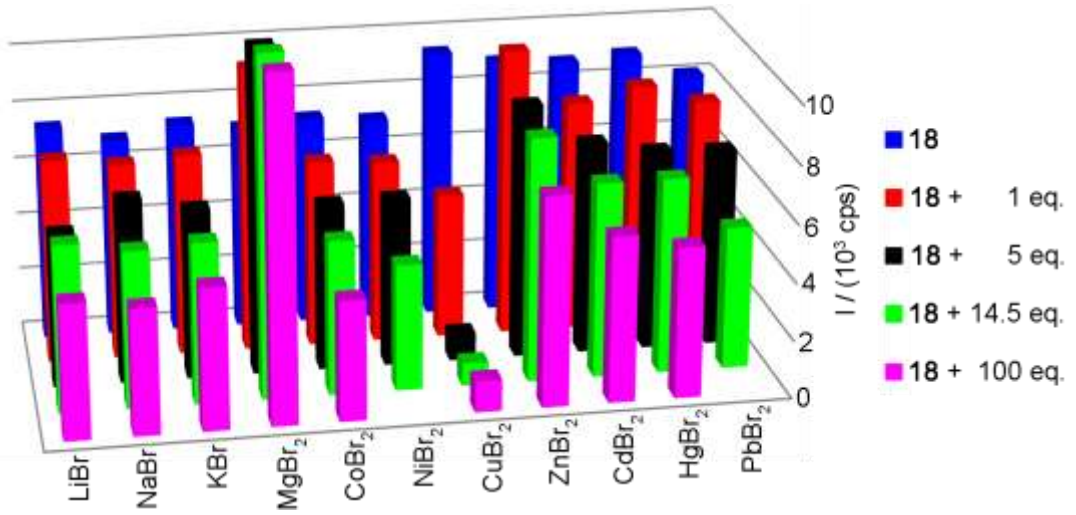

Figure 2-68: Representation of every tested combination between **18** and the respective metal bromide except from $FeBr_2$ and $AlBr_3$ in MeOH (10^{-5} M, λ_{ex} = 378 nm, emission depicted at 510 nm).

In this series of measurements the addition of many metal salts resulted again in a decreasing intensity caused by dilution. As explained before the added volume of the solvent had a larger impact on the luminescent changes than the amount of metal salt. This is true for lithium, sodium, potassium, cobalt, nickel, cadmium, mercury and lead bromide. Copper bromide once again quenches the luminescent emission by absorption of the incoming beam (Figure 2-10 right).

The overall intensity, consisting of several thousand cps, is relatively low, pointing to only little decomposition of **18** to **11**. The measurements were carried out from the left to the right side and the first six series up to nickel were recorded at the same day. Four days later the other metal salt additions started with copper bromide were measured. For this relatively long period of time only slight changes were observed indicated by the nearly constant blue bars among the measurements. This provides a hint that the composition of the stock solution is almost unchanged.

In Figure 2-68 the additions of aluminum and iron bromide are not shown. The luminescent changes of **18** towards their presence are displayed in Figure 2-69.

These two metal bromides are depicted separately because of their known acidic behavior (cf. section 2.2.11.3). In both cases the addition of 1 eq. metal salt caused nearly no changes but at 5 eq. an increase of emission is observed that can be assigned to the formation of **11**. From a raised concentration to 14.5 eq. differences between these two added metal bromides are obvious.

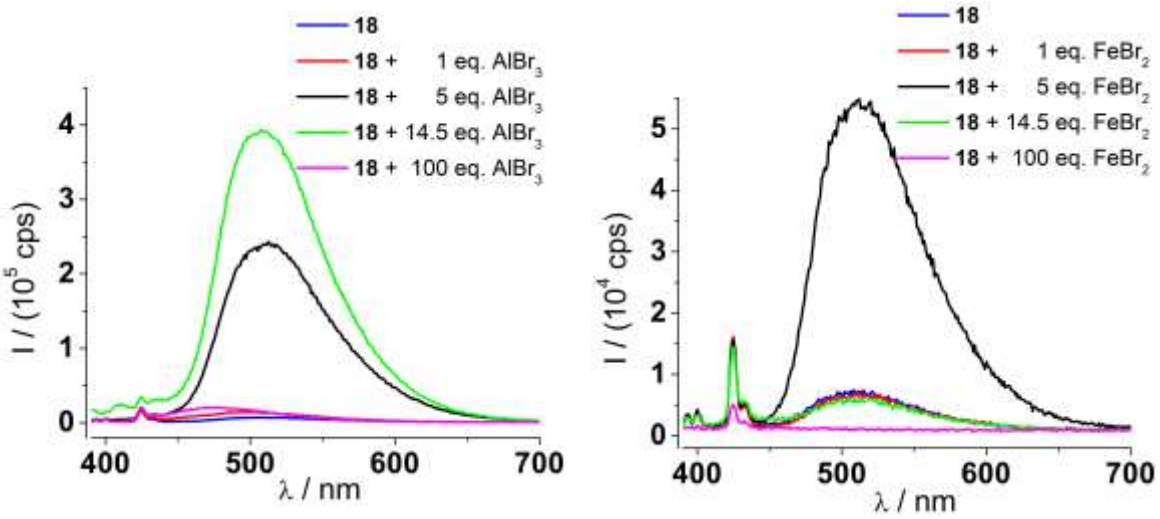

Figure 2-69: Emission properties of **18** after addition of aluminum bromide (left) and iron bromide (right) (10^{-5} M in MeOH, λ_{ex} = 378 nm).

Aluminum ions caused a further intensity increase while the same amount of iron decreased the emission because of the absorptive character of iron ions (Figure 2-10 left). At 100 eq., aluminum also quenches the luminescence due to the reaction of **11** with protons to non-luminescent derivatives discussed around Scheme 2-18.

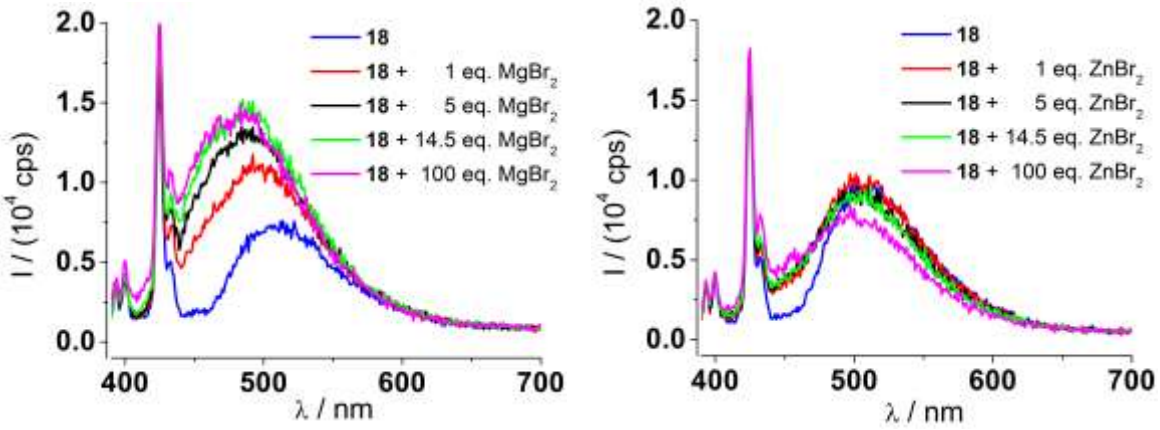

Figure 2-70: Emission properties of **18** after addition of magnesium bromide (left) and zinc bromide (right) (10^{-5} M in MeOH, λ_{ex} = 378 nm).

The only differences in the emissive behavior of **18** that may be caused by a metal-ligand interaction can be found after addition of magnesium and zinc in Figure 2-68. Both in Figure 2-70 displayed additions to **18** point to the same direction but magnesium ions reveal more pronounced changes. This time not a formation of **11** but a shift in wavelength even from 1 eq. on can be observed. Therefore, the reason of

protonation can be excluded and an interaction between **18** and magnesium ions is likely.
But the determined response of **18** is far too low to consider the application of this synthesized imine as a colorimetric sensor.

Furthermore, two series of measurements were applied like in section 2.2.5.5. Sodium hydroxide was added to deprotonate **18** and afterwards metal cations were injected to the sample successively. This procedure allowed to judge in a very compact way on the metal coordinative properties of **18** at elevated pH value.

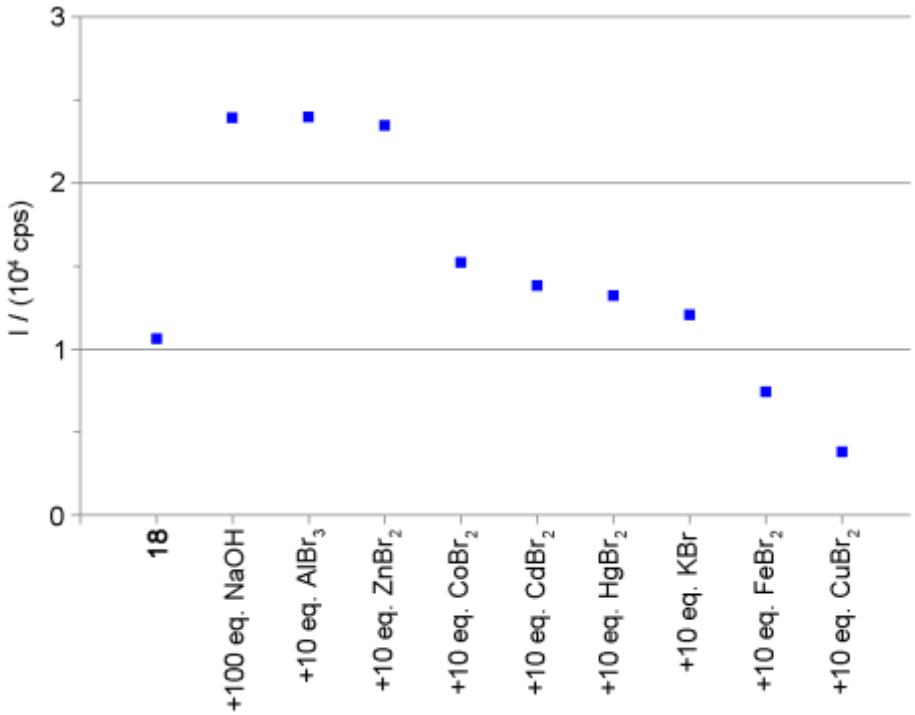

Figure 2-71: Overview about the emission of a solution including **18** to which 100 eq. NaOH and successively 10 eq. of different metal bromides were added (10^{-5} M, λ_{ex} = 378 nm, emission depicted at 510 nm).

In Figure 2-71 the emission at 510 nm is chosen to follow the intensity changes during the metal salt additions. The wavelength dependent information are displayed in Figure 5-49. After addition of sodium hydroxide a strong increase of intensity is visible that was also observed in the right part of Figure 2-67. Further injections caused decreasing emission whereat cobalt, iron and copper led to more pronounced quenching. The last two can be explained by absorption but the first one was unexpected and not observed without sodium hydroxide.

In a second experiment a larger excess of hydroxide was added to ensure an even higher pH. The wavelength dependent information belonging to Figure 2-72 are displayed in Figure 5-50.

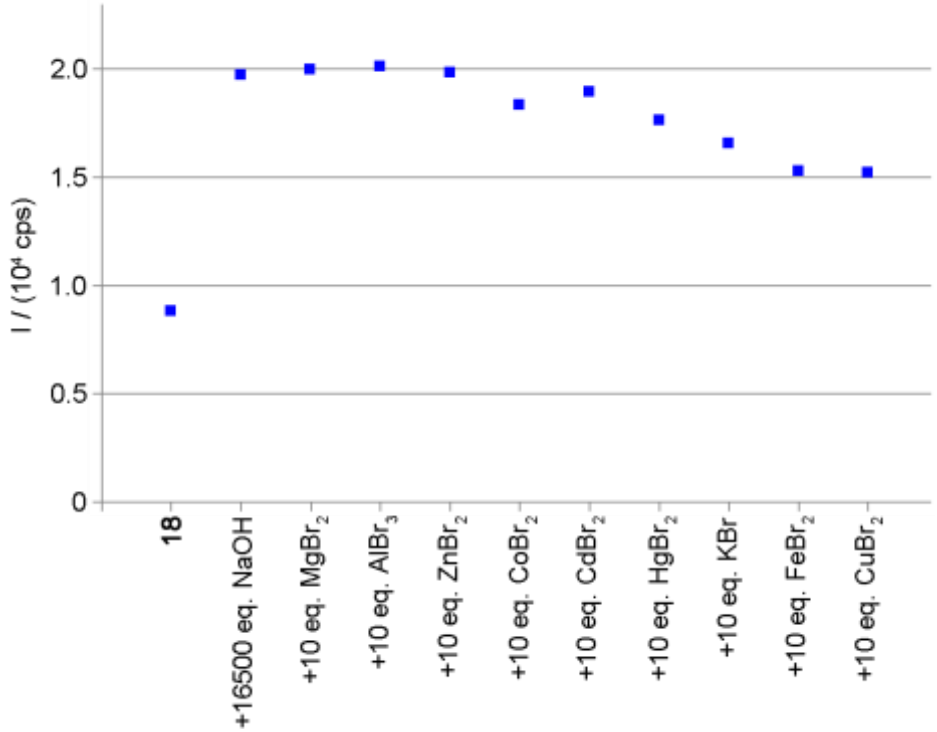

Figure 2-72: Overview about the emission of a solution including **18** to which 16500 eq. NaOH and successively 10 eq. of different metal bromides were added (10^{-5} M, λ_{ex} = 378 nm, emission depicted at 510 nm).

Even these stronger alkaline conditions had no distinct impact on the luminescence response of **18** after addition of metal bromides in methanol. Dilution is still the dominant ongoing process and as observed for **12** the large excess of sodium hydroxide prevents an effective quenching of iron and copper bromide.

So despite of the elevated pH value no metal coordination that affected the luminescent response of **18** was observed nor with 100 eq. neither with 16500 eq. added sodium hydroxide.

Because of the weak response of **18** towards metal cations, one series of experiments was set up with a less polar aprotic solvent. DCM was chosen because it dissolves zinc bromide in sufficient amounts. Two drawbacks of this solvent are its huge difference to the long-term aspired solvent water and, linked to this, the poor solubility of other metal bromides. The low solubility of other metal bromides disa-

bles comparison measurements in this solvent. Nevertheless, DCM was used to evaluate if the C=N isomerization would work in the absence of such a polar protic solvent like methanol.

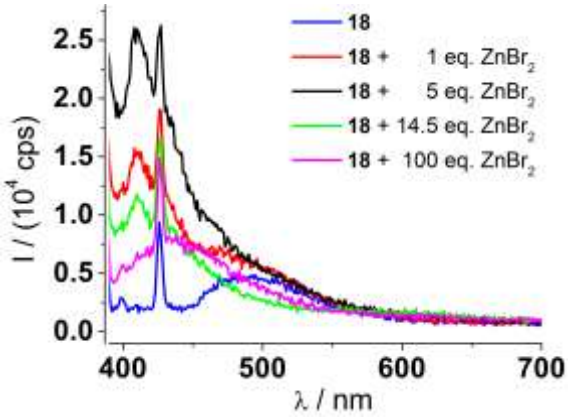

Figure 2-73: Emission properties of **18** after addition of zinc bromide, both dissolved in DCM (10^{-5} M, λ_{ex} = 378 nm).

In Figure 2-73 the results are shown after zinc bromide in DCM was added to a solution of **18** in DCM. The comparison to methanol (Figure 2-70 right) exhibits huge differences. In this less polar solvent even the addition of 1 eq. caused a threefold increase of intensity compared to the visible emission of **11** combined with an around 100 nm shift in wavelength. 5 eq. enhanced this trend of rising intensity but further additions resulted in a subsequent quenching and an accompanied small bathochromic shift. This indicates that the new formed luminescent species may not be sufficiently stable to build-up an easy detectable state.

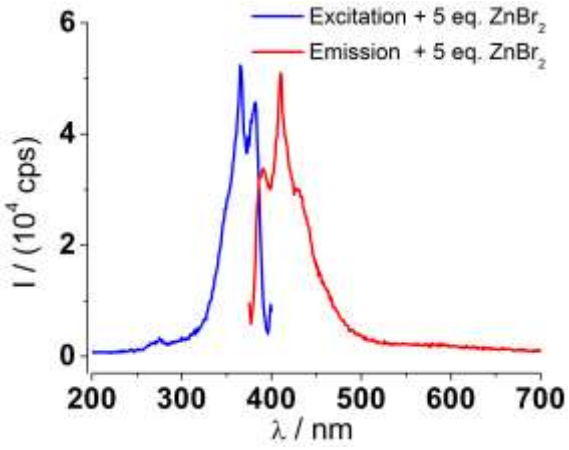

Figure 2-74: Excitation (blue, λ_{det} = 411 nm) and emission (red, λ_{ex} = 365 nm) spectra of **18** + 5 eq. $ZnBr_2$ (10^{-5} M in DCM).

This addition of zinc bromide was investigated in more detail by recording an excitation and emission spectrum at optimized detecting or exciting wavelength (Figure 2-74). When excited at a proper wavelength, this new formed luminescent species after zinc bromide addition to a solution of **18** in DCM emits around 50000 cps at its maximum of λ = 411 nm. Because the radiative relaxation of **18** was not observed at all a factor of increase cannot be determined.

Noticeable is the similarity to the response of **13** in methanol after addition of cadmium bromide (Figure 2-41). In that case also a new band around 400 nm arose and exhibited a vibrational structured signal with a similar intensity. So it seems likely that the immobilization of the C=N isomerization can be achieved in different solvents and results in a detectable luminescent output.

2.2.17 9-Anthracene(*o*-(*β*-hydroxyethoxy)benzyl)amine (19)

The last prepared and investigated potential sensor was 9-anthracene(*o*-(*β*-hydroxyethoxy)benzyl)amine (**19**). It was derived via reduction of **18** as established in the synthesis of the former produced amines **15** and **16**.

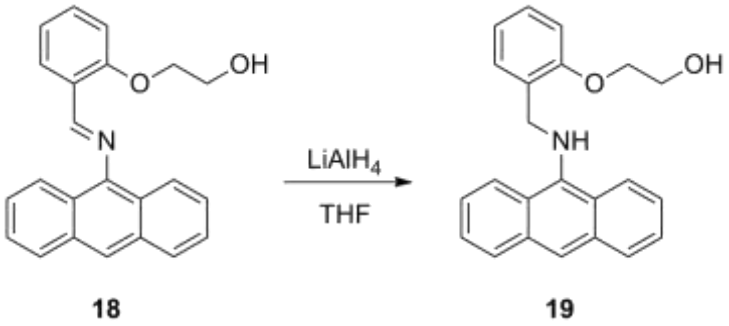

18 **19**

Scheme 2-24: Synthesis of **19** derived by reduction of **18**.

In the beginning a suitable reducing agent had to be identified for the reduction of **18** displayed in Scheme 2-24. $NaBH_4$ in THF was tested but resulted in tiny conversion only after stirring the reaction mixture overnight at room temperature. Even a subsequent stirring at the boiling point of THF (66 °C) for two days turned over just 10 % of **18** to **19**. Therefore, the more reactive reducing agent[107] $LiAlH_4$ (in THF) was chosen, which turned out to convert **18** nearly quantitatively to **19** after stirring the reaction mixture at room temperature overnight.

The separation of over-stoichiometric amounts of $LiAlH_4$ was the major challenge during the purification of **19**. Different attempts were tested but the best results were achieved by removal of the volatile components of the reaction mixture under reduced pressure followed by addition of ethylacetate and water. The insoluble components were filtered off and the two layers were separated. The crude product was recrystallized from hexane and ethylacetate to isolate **19** in a yield of 34 %. This could be optimized by a more efficient way to remove the excess of $LiAlH_4$. In this step of the purification process the work under inert conditions was interrupted and this may have caused the only moderate yield of **19**.

Nevertheless, **19** was isolated and its structure was confirmed by NMR spectroscopy, mass spectrometry as well as elemental analysis.

2.2.18 Luminescence properties of 9-anthracene(*o*-(*β*-hydroxyethoxy)benzyl)amine (19)

Several questions concerning the optical properties of **19** arose before it was investigated by UV/Vis absorption and luminescence spectroscopy. One interesting point was the long-term stability of **19** and a second was if its behavior in the presence of protons would be similar to both former synthesized amines **15** and **16**. Regarding the second point, it was questionable if the protonated state would be stable and reversible like in **15** or if protonation would decompose the anthracene derivative as seen in the case of **16**.

Also its metal coordinating properties were topic of investigation. Due to the additional donor atom in comparison to the previous prepared amines a higher affinity of **19** towards metal ions was expected.

2.2.18.1 UV/Vis absorption and luminescence emission of 9-anthracene(o-(β-hydroxyethoxy)benzyl)amie (19)

The absorptive behavior of **19** is once again discussed at first. Knowledge about this feature is important in subsequent investigations to choose a proper excitation wavelength and to open the possibility of comparison between the absorption and the excitation spectrum.

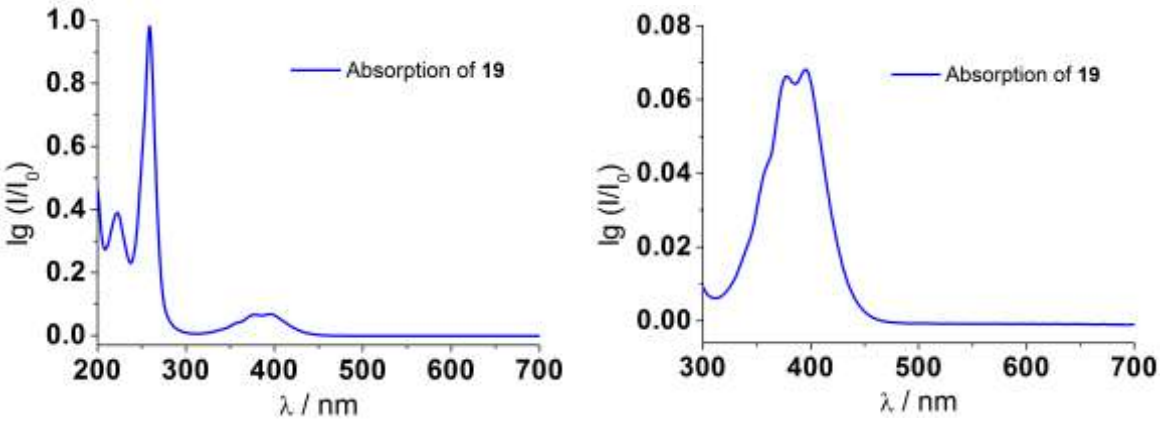

Figure 2-75: UV/Vis absorption spectra of **19**. Left: full spectrum; right: enlargement of the spectral region around 400 nm (10^{-5} M in MeOH).

Figure 2-75 displays the absorption of **19** in the spectral region between 200 and 700 nm and exhibits many similarities to **15** and **16**. All three prepared amines

show two maxima and a shoulder at the high energy side of the signal around 400 nm. The intensity is in between those of the two other amines as well as the curve form in general.

The excitation and emission of **18** is given in Figure 2-76.

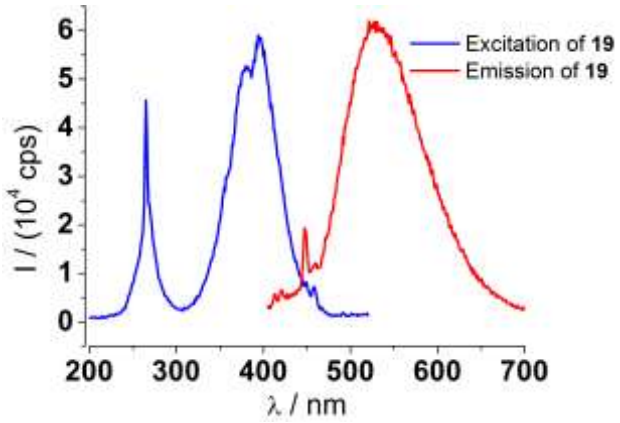

Figure 2-76: Excitation (blue, λ_{det} = 530 nm) and emission (red, λ_{ex} = 396 nm) spectra of **19** (10^{-5} M in MeOH).

Comparing the curve shape of the blue line in Figure 2-76 with the absorption spectrum of **19**, a very similar course is obvious. The maxima are almost at the same wavelength and differ only by a few nanometers. Also two maxima and one shoulder are visible in the band around 400 nm as well as a sharp peak around 250 nm. Because of these similarities it is very likely that only one species was observed during both experiments in contrast to the investigated imines where the absorption of the imine was detected but the emission was caused by traces of **11**.

But the analogies of **19** to **15** and **16** are clearly visible. These two anthracene derivatives show a broad band with two maxima as well as a shoulder in their excitation spectra. Furthermore, the emission of all three amines is characterized by one broad band without a vibrational structure. The maximum of this broad band (around 530 nm), illustrated in the red line of Figure 2-76, is nearly identical to **15** and deviates just by 5 nm from **16**.

Comparable is also the large STOKES shift of more than 100 nm between the maxima of the excitation and emission spectrum. This was also valid for the two earlier synthesized amines and may point towards a relatively long lifetime of the excited state.

A further important property is the stability of a potential sensor. While **16** turned out to be stable over several days in a 10^{-5} M solution, **15** decomposed to **11** within

hours. Therefore, the stability of **19** was monitored over time and its luminescence is compared to the relatively labile amine **15**.

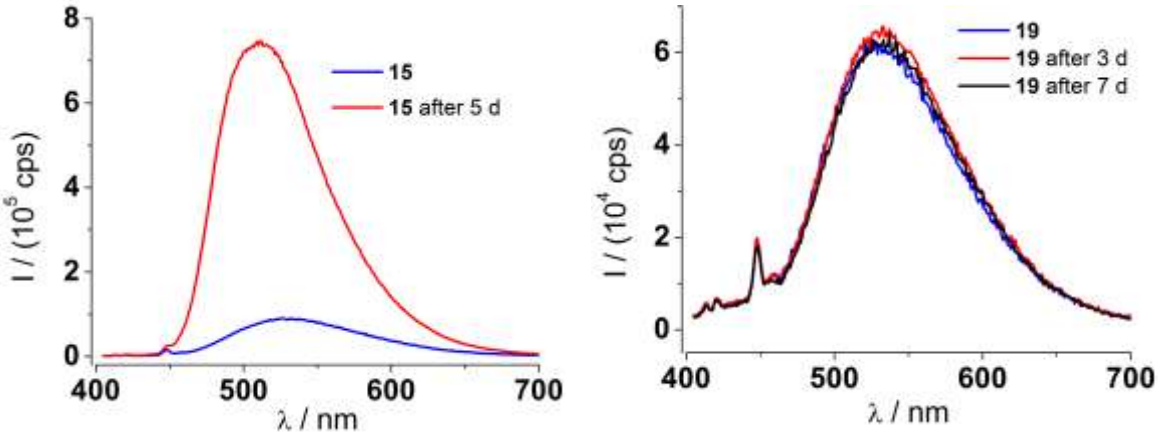

Figure 2-77: Emission spectra of **15** before and after a period of 5 days (left, λ_{ex} = 396 nm) and emission of **19** observed over 7 days (right, λ_{ex} = 396 nm).

On the first glance one can see the decomposition of **15** after 5 days and the stability of **19** even after 7 days. In the left part of Figure 2-77 the intensity increased very strongly and the maximum is shifted from 530 nm to 510 nm indicating the formation of **11**. In contrast the stock solution of **19** is characterized by its long-term durability indicated by the constant emission of **19** where no change in intensity or wavelength can be detected.

This is a great advantage of **19** regarding its use as a potential luminescent sensor.

2.2.18.2 Luminescence analysis after addition of acids and bases to 9-anthracene(o-(β-hydroxyethoxy)benzyl)amine (19)

The basic absorptive and emissive properties exhibit similarities to **15** and **16**. By addition of acid to **19** it was investigated if this derivative also points towards the application as a reversible colorimetric pH sensor like **15** or if it decomposes in the presence of protons like **16**. So to ensure comparability the same procedure was used to vary the pH value by addition of hydrochloric acid or sodium hydroxide.

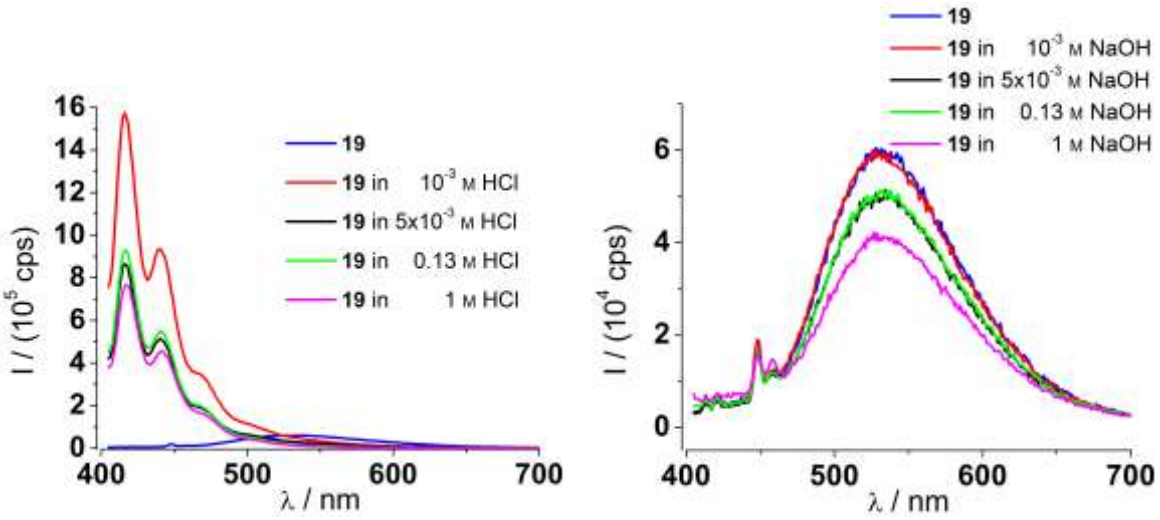

Figure 2-78: Emission spectra of **19** under acidic (left) and alkaline (right) conditions (λ_{ex} = 396 nm).

The in Figure 2-78 displayed difference in the response of **19** towards protons and hydroxide ions could not be more pronounced. While in the right part a classic example of dilution is presented, the left part shows one of the largest changes observed during this project.

This allows the conclusion that **19** is stable in basic solutions and does not change its emission at all but protons cause a very distinct switch of the radiative relaxation. The determination the factor of increasing intensity is not as straight forward as for examples where the maximum does not shift. Due to the huge shift in emission wavelength (114 nm), the emission maximum would most probably reach an even higher intensity at an appropriate excitation wavelength. To evaluate the maximum emission of the protonated **19**, excitation and emission spectra were recorded at suitable wavelengths and the corresponding spectra are shown in Figure 2-79.

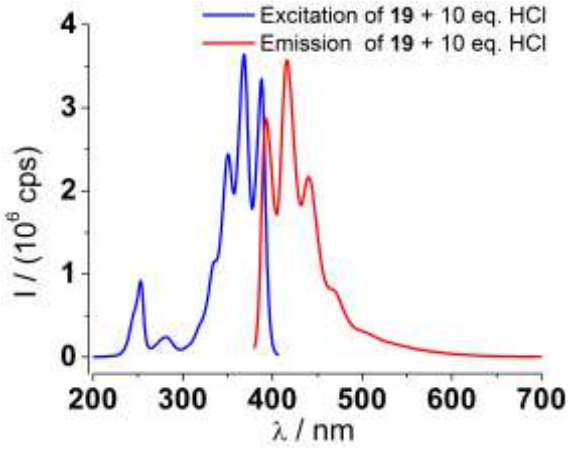

Figure 2-79: Excitation (blue, λ_{det} = 416 nm) and emission (red, λ_{ex} = 368 nm) spectra of **19** in methanol after addition of 10 eq. aqueous hydrochloric acid.

Comparing the excitation spectra of **19** and its protonated counterpart the expected change in wavelength is found. Like in the case of **15** a hypochromic shift can be noticed as well as a modified curve shape. While **19** showed in the blue line of Figure 2-76 two hardly separated maxima and one shoulder, the excitation spectrum displayed in Figure 2-79 exhibits a clearly vibrational structured band with three easily distinguishable maxima and one shoulder. But the major differences are visible comparing the emission of **19** and its protonated analog. Irradiating the protonated **19** at a proper wavelength as done in the red line of Figure 2-79, one can see an emission intensity of more than 3.5 million cps. This number could now be compared with the emission of **19** at 530 nm without protons but another inaccuracy has to be mentioned. The used detector in the spectrofluorometer can only report intensities up to 2 million cps[108] reliably so the determined 62-fold intensity increase also contains an error.

But more important than determining the factor of increasing intensity is the result that the emission maximum is shifted by 114 nm. This is a large value and allows an easy detection of this new luminescent species.

Besides this, the stability of the protonated state was observed over several minutes. Like in the case of **16**, the protonated counterpart of **19** proved to be stable during the experiment displayed in Figure 5-51. Therefore, both states of **19** before and after addition of acid are stable.

The next question was whether **19** can reversibly be switched between these states by protonation and deprotonation.

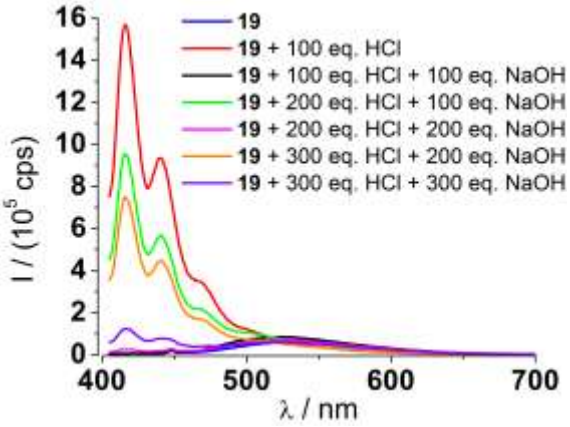

Figure 2-80: Emission of **19** in methanol before and after alternately added 100 eq. aqueous hydrochloric acid and 100 eq. aqueous sodium hydroxide (λ_{ex} = 396 nm).

Therefore, aqueous solutions of hydrochloric acid and sodium hydroxide were added alternately to a 10^{-5} M solution of **19** in methanol and the results are displayed in Figure 2-80. After addition of 100 eq. acid the striking change in intensity and wavelength occurs but this was completely reversed when the same amount of base was injected.

It was also possible to restore both states during two further cycles of protonation and subsequent deprotonation even though with decreasing intensity after each switch.

So up to this point **19** combines the advantages of **15** and **16**. Similarities to **15** are found in the response of **19** regarding protons that are characterized by a huge shift in wavelength, a very strong increase of intensity as well as their determined reversibility. These two derivatives resemble each other also in their high stability of the protonated state. But the durability among them differs. Whereas **15** decays in noticeable amounts to **11** over hours, the optical properties of the same solution containing **19** were constant even after one week. For the sake of long-term durability **19** is comparable to **16** that was also stable over the observed period of time.

These results induce the interest in the application of **19** as a colorimetric pH sensor.

2.2.18.3 Luminescence analysis after addition of metal salts to 9-anthracene(o-(β-hydroxyethoxy)benzyl)amine (19)

After this very promising behavior of **19** towards protons its response to metal salts was topic of the investigation throughout this section. The third introduced donor atom may enable a stronger interaction between the potential sensor and the metal cation. To check if an addition of a metal bromide results in clear changes the in section 2.1.8.1 discussed screening procedure was applied to **19**.

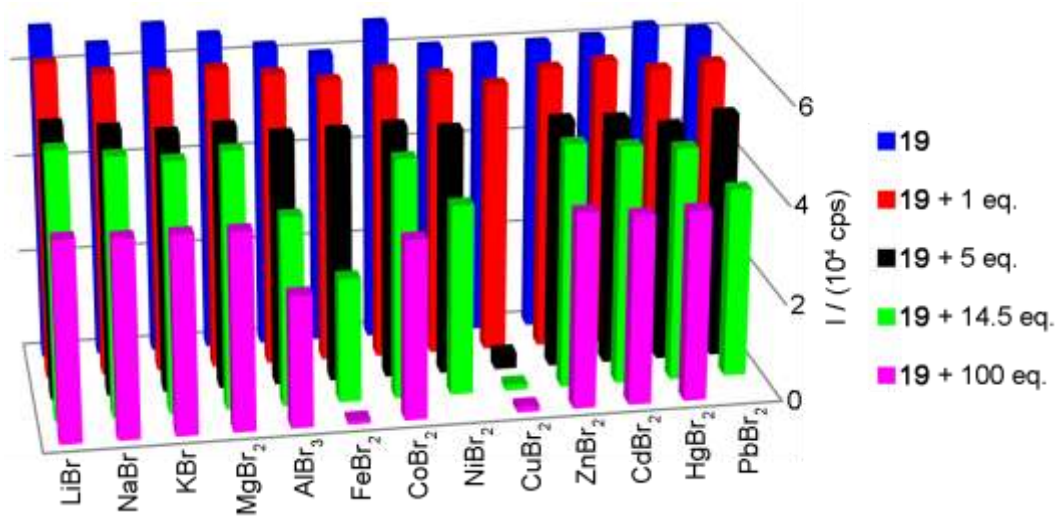

Figure 2-81: Representation of every tested combination between **19** and the respective metal bromide in MeOH (10^{-5} M, λ_{ex} = 396 nm, emission depicted at 530 nm).

In Figure 2-81 the addition of metal salts to a solution of **19** in methanol is displayed. Thereby many additions resulted in a similar development of intensity. The only exceptions were aluminum, iron, and copper bromide that were not dominated by dilution. In the other cases the added volume influenced the intensity to a larger extend than the amount of metal salt that was injected. The strong quenching after addition of copper salt was observed throughout this project and can be explained by its absorptive character initially discussed in section 2.1.8.4.

So despite of the third donor atom no clear interaction between one of the added metal bromides and **19** was determined.

The additions of aluminum and iron bromide resulted just in protonation and were not caused by an ion coordination of **19**. Their response is nevertheless displayed in Figure 2-82 to give a further example about the sensitivity of **19** towards protons.

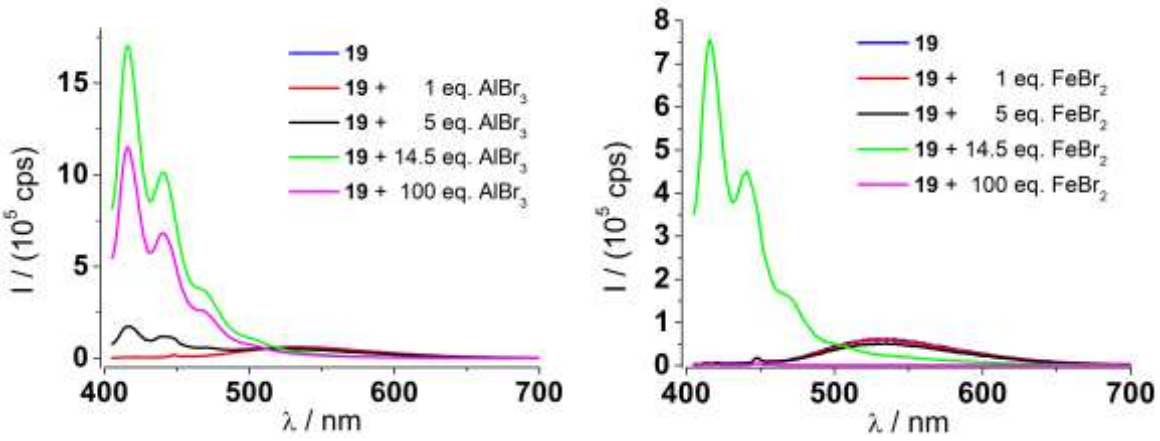

Figure 2-82: Emission properties of **19** after addition of aluminum bromide (left) and iron bromide (right) (10^{-5} M in MeOH, λ_{ex} = 396 nm).

As described before, iron(II) oxidizes under atmospheric conditions to iron(III) and hence in the metal bromide solution trivalent cations are present like in the case of aluminum. These three times charged ions are LEWIS acidic and can release protons from methanol or traces of water.

Therefore, the same changes as observed in the left side of Figure 2-78 occur when aluminum and iron bromide were added to **19** and the solvent water is not required for this distinct variation of the radiative relaxation.

The next series of experiments were performed after adding an excess of base. At first 100 eq. sodium hydroxide were added and successively 10 eq. of different metal bromides were injected to the same sample. The aspired behavior was to enhance the metal coordination affinity of **19** by deprotonation of the OH group at increased pH value.

Wavelength dependent information to Figure 2-83 are given in Figure 5-58.

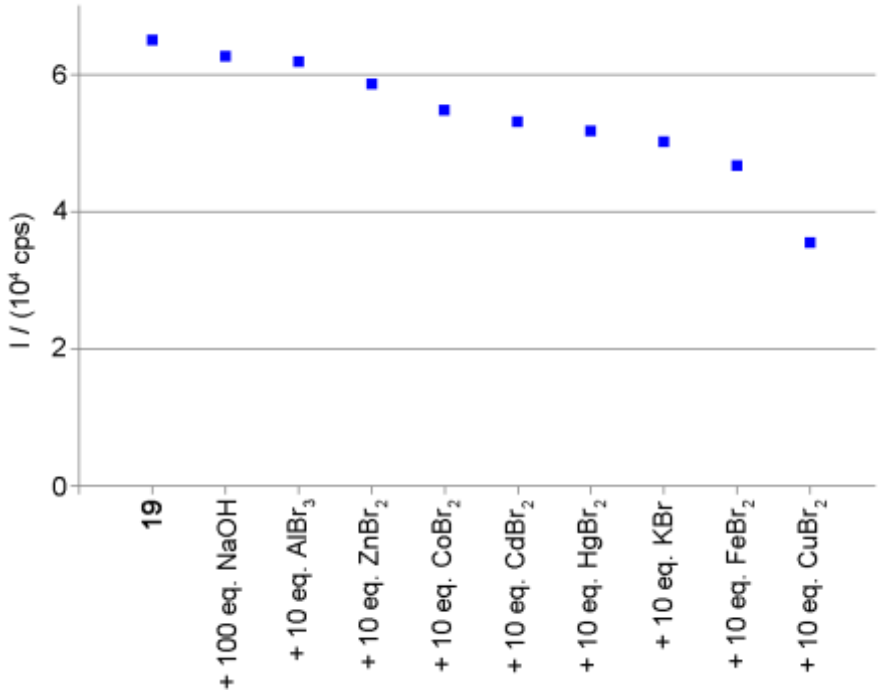

Figure 2-83: Overview about the emission of a solution including **19** to which 100 eq. NaOH and successively 10 eq. of different metal bromides were added (10^{-5} M, λ_{ex} = 396 nm, emission depicted at 530 nm).

Figure 2-83 was gained by observing an experiment, in which **19** was dissolved in methanol, subsequently an aqueous solution of sodium hydroxide was added first, followed by the successively injection of 10 eq. of each tested metal bromide in methanol.

The clear trend of evenly decreasing intensity at 530 nm points towards dilution because not the kind of metal was responsible for these slight changes but the added volume of solution. The only exception was copper bromide that led to a bit stronger decrease by its absorptive behavior.

A similar experiment was carried out but this time with a more pronounced excess of base (16500 eq.). The results are displayed in Figure 2-84 and exhibit the same

tendency. Even copper bromide caused here no deviation from the equally spaced decrease of intensity. Most likely this large amount of hydroxide coordinates the metal cations including copper and the absorption properties are altered.

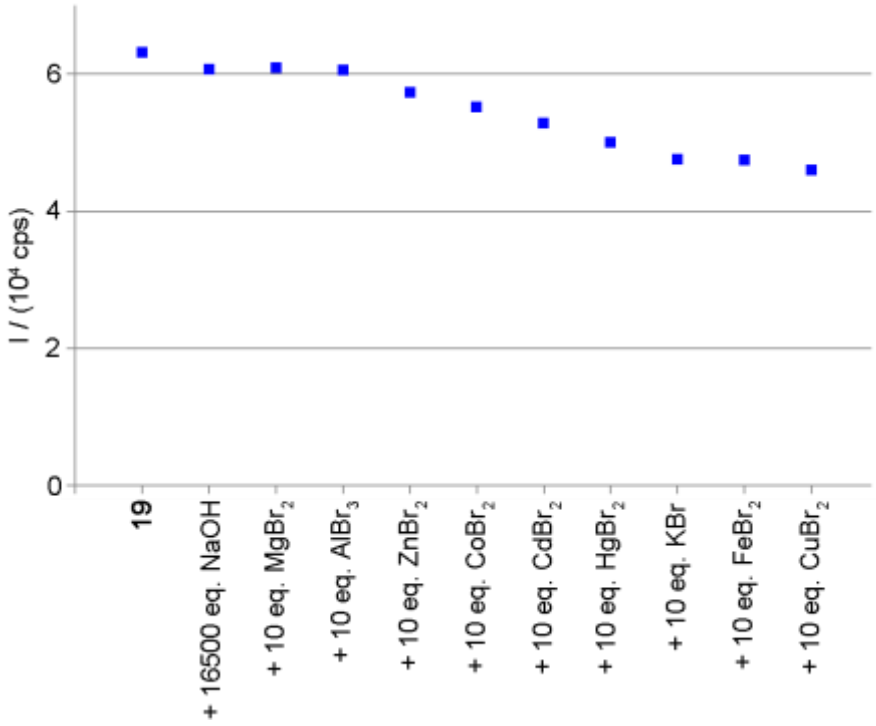

Figure 2-84: Overview about the emission of a solution including **19** to which 16500 eq. NaOH and successively 10 eq. of different metal bromides were added (10^{-5} M, λ_{ex} = 396 nm, emission depicted at 530 nm).

This type of experiment is a good example for the difficulties arising from the usage of additives to the investigated potential sensor. Many times they cause not only the desired effects like in this case deprotonation but their presence can also change the luminescent properties of the investigated potential sensor. Another possibility, as observed here after addition of copper ions, is the absence of these changes by unintentional side reactions like coordination of the analyte by the additive. This can also become a problem when buffer solutions are prepared to investigate the luminescent changes caused by a metal cation at defined pH value.

To conclude, the promising behavior of **19** towards acids, namely the colorimetric reversible detection of protons with two stable addressable luminescent states, was not found regarding metal bromides in methanol.

Therefore, the question arose if this build-up of the amine directly bond to the anthracene moiety is a proper scaffold not only for pH sensors but also for metal detection. In other words: which of the two possible reasons for the absence of luminescent variations is crucial? No coordination of metal cations by amines like **19** or no luminescent report of such coordination?

To answer this question the solvent was changed from the polar protic methanol to the less polar aprotic DCM. The narrow solubility of metal salts limited this test to zinc bromide as target species but allowed at least a direct comparison, because zinc bromide was added to **19** in methanol before and is depicted in the right part of Figure 2-85.

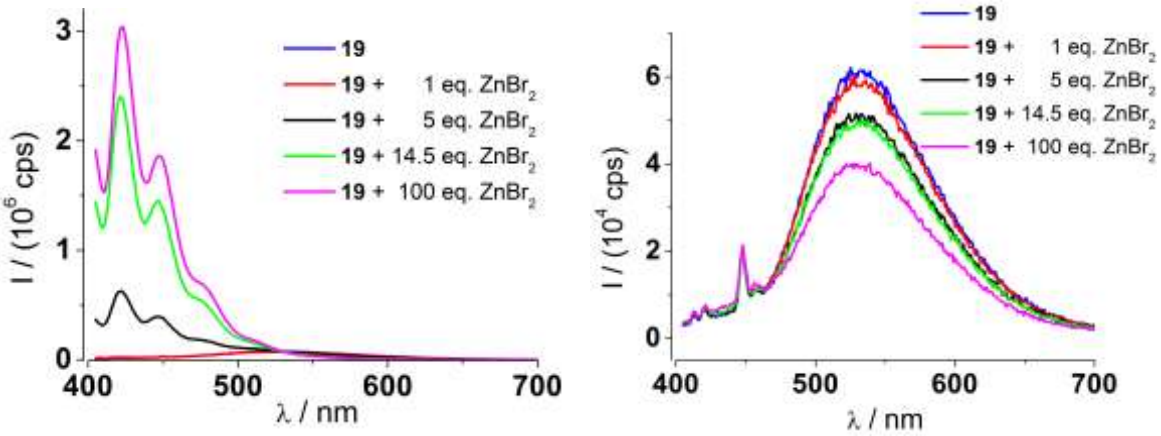

Figure 2-85: Emission properties of **19** after addition of zinc bromide in DCM (left) and methanol (right) (10^{-5} M, λ_{ex} = 396 nm).

The left part of Figure 2-85 displays the luminescent response after addition of zinc bromide to **19**, both dissolved in DCM. The changes are tremendous. Not only the increase in intensity but also a huge shift of the emitting wavelength is obvious. This argues for a new formed luminescent species generated by coordination of the zinc cations by **19**. After addition of 5 eq. the formation of a new structured band was recorded and further injections increased the emission intensity of this new luminescent derivative.

Especially the differences evoked by the solvents methanol and DCM are immense. While in methanol dilution was the only observed process, the clear variations in intensity and wavelength were observed by just changing the solvent.

This new structured signal is reminiscent to the one of protonated **19** but exhibited different maxima of the emission wavelength. For comparison the excitation and emission of this new luminescent species is displayed in Figure 2-86.

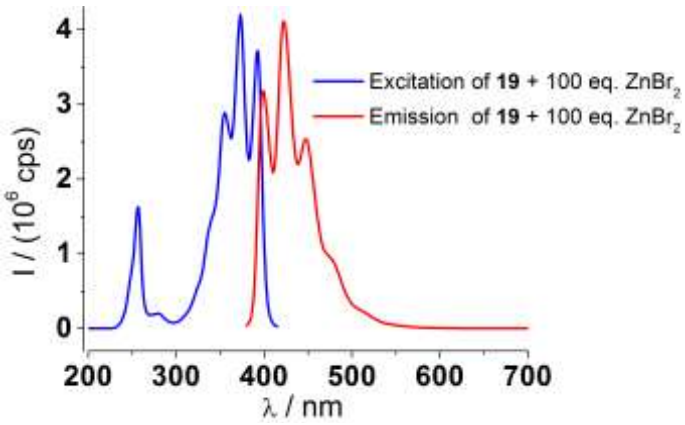

Figure 2-86: Excitation (blue, λ_{det} = 422 nm) and emission (red, λ_{ex} = 373 nm) spectra of **19** + 100 eq. $ZnBr_2$ (10^{-5} M in DCM).

Considering the emission maxima of **19** after addition of zinc bromide at λ = 399 nm, 422 nm and 447 nm as well as the shoulder around 477 nm, it is noticeable that they are shifted by 6 or 7 nm in regard to the protonated **19**. This bathochromic shift in the less polar solvent DCM is the opposite one would expect from a less pronounced solvent relaxation (cf. chapter 4.2.2).
Additionally, the excitation spectrum is shifted in the same direction by around 5 nm delivering a second hint that these variations are not introduced by the change of the solvent but by formation of another luminescent species.
So the response of **19** towards protons in a mixture of methanol and water is similar to the one caused by the coordination of zinc bromide by **19** in DCM but different excited species are present. This second response cannot be introduced by protons.

This last discussed experiment shows the potential of **19** not only to detect protons in a colorimetric reversible fashion but also to coordinate metal cations in the less polar solvent DCM. So the scaffold of anthracene as fluorophor and a directly bond amine receptor is able to report the presence of a metal cation by distinct colorimetric changes of the emission properties.

3 Summary and Outlook

Two main approaches were followed within this thesis to establish anthracene based colorimetric molecular sensors.
The first one, namely the synthesis and investigation of ansa-bridged anthracenes, turned out to be less promising due to their unspectacular luminescent behavior towards metal cations and varied pH value. One representative of this class was synthesized in high purity and characterized by NMR and fluorescence spectroscopy. However, the absence of a colorimetric response to any tested analyte does not seem to justify the high effort of preparing ansa-bridged anthracenes.

But the second approach, gathered under the headline of "anthracene derivatives without spacers", brought up various interesting findings reported in this thesis. The starting point was the optimized synthesis of **11** as the key intermediate throughout this thesis, especially with regard to its long-term storage capability and firstly determined solid state structure via X-ray diffraction.
Based thereon, a preparative route to a new subclass of substances was explored: imines of **11** with receptor units directly bonded to the fluorophore anthracene. All four representatives of this subclass were synthesized for the first time (**12**, **13**, **14** and **18**) and except of **14**, derived by the reaction of a ketone with **11**, in good to excellent yields (61, 90 and 93 %). Special care found the purification procedure because even the smallest impurities might have colossal impact on the fluorescent properties. These three imines, arised from aldehydes and **11**, were fully characterized by NMR spectroscopy, EI mass spectrometry as well as elemental analysis. In addition, the solid state structures of these anthracene derivatives were determined via X-ray diffraction.
Furthermore, their luminescent properties were investigated in detail. Generally, representatives of this new subclass showed no observable luminescence despite of detected absorption. The reason for this is their structural included C=N double bond. The isomerization between the *E* and *Z* diastereomers opens an effective non-radiative relaxation pathway. Therefore, they form tailor-made luminescent off-states. Despite of this favorable prerequisite, the second necessary condition for a

sensoric system, namely an interruption of the isomerization, worked only to a small extent. The majority of the added metal cations caused no sufficient changes of the luminescent properties in methanol. Exceptions are the responses of **13** and **14** towards cadmium bromide, the varied luminescent behavior of **18** upon addition of magnesium bromide in methanol as well as the changes of **18** caused by zinc bromide in DCM. Unfortunately, one of the mentioned interactions reached applicational interest due to only moderate variations.

Huge changes were observed after the addition of acids to each of the prepared imines. Therefore, the response of **12** towards protons was studied extensively to understand the ongoing processes.

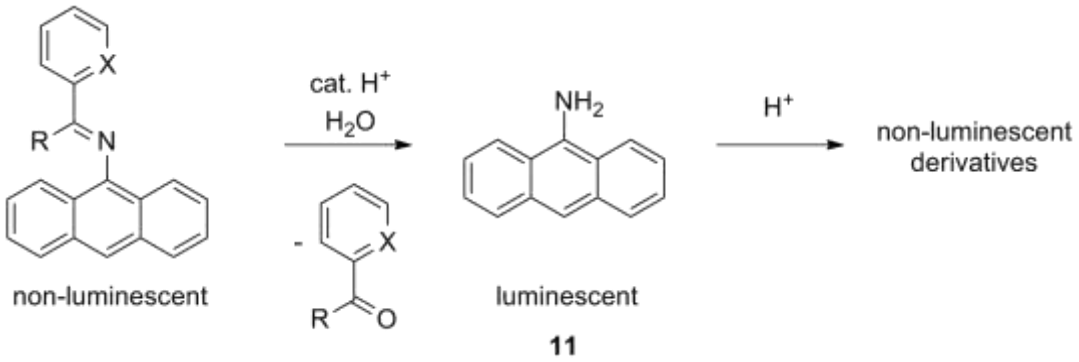

Scheme 3-1: Reaction of the non-luminescent imines **12** (X = COH, R = H), **13** (X = N, R = H), **14** (X = N, R = Me) and **18** (X = COC_2H_4OH, R = H) to the luminescent **11** and conversion to non-luminescent products.

The in Scheme 3-1 summarized procedure was developed by a comparison of the luminescent variations **11** and **12** undergo in the presence of protons. This procedure was confirmed by time dependent spectroscopic luminescence and NMR studies and the employment of X-ray diffraction gave an impression of the non-luminescent final products.

Aside, a second subclass of potential anthracene based colorimetric molecular sensors was established. The three first examples (**15**, **16** and **19**) thereof were received by reduction of the C=N double bond of the previously discussed imines. The solid state structures of **15** and **16** were determined via X-ray diffraction and all three derivatives were analyzed comprehensively.

In contrast to the prepared imines, the luminescence intensity of these amines is detectable, although their emission intensity is only moderate compared to the compounds **8** and **11**. The first striking luminescent result investigating these amines was the response of **15** towards acids. An enormous increase of intensity along with a shift of the emission wavelength maximum by more than 100 nm hints towards a promising sensor application targeting protons. Unfortunately, the stability of **15** in solution was not sufficient but the decomposition of this derivative was observed over a few days. Examining **16** in the presence of protons revealed its decomposition in acetic media but its high stability over days in solutions of methanol.
The third investigated amine, **19**, combined the advantages of both previously discussed amines. It exhibits stable protonated and non-protonated states as well as a reversible addressability of these. Furthermore, the huge increase of intensity and the remarkable shift of its emission wavelength provide an excellent system for the detection of protons (Figure 3-1 left).

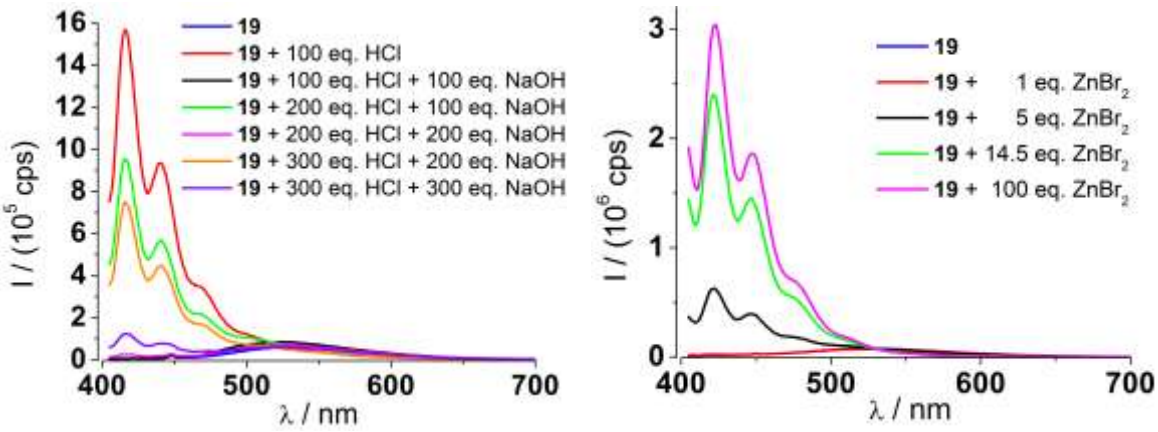

Figure 3-1: Left: Reversible response of **19** towards protons in a mixture of MeOH and H_2O.
Right: Response of **19** towards zinc bromide in DCM.

The responses of the three prepared amines towards various metal salts in methanol were only moderate compared to the astonishing behavior of the amines at varying pH value. Nevertheless, interactions between **16** and aluminum cations as well as **16** and copper cations resulted in monitorable luminescent changes.
Completely different results were obtained when **19** was investigated in DCM (Figure 3-1 right). The response after addition of zinc bromide turned out to be as massive as the changes after protonation of the amines. A striking shift of more than 100 nm combined with a huge intensity increase demonstrate, that anthracene de-

rivatives like **19** are not only capable to detect protons but also metal cations in a colorimetric fashion.

Perhaps the most important contribution to the field of luminescence sensors during this thesis is the established new route to two different types of them.

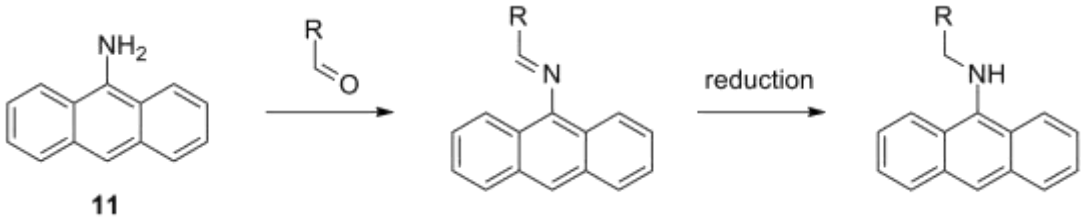

Scheme 3-2: Established synthetic route: Reaction of **11** with an aldehyde to an imine and further reduction to the corresponding amine.

All aldehydes tested during this thesis reacted to imines in good quantity and were purified to high quality. Similarly, every examined reduction to obtain the corresponding amine was successful after adjustment of the reaction and purification conditions. This suggests, that the established route shown in Scheme 3-2 can be used to obtain a variety of potential sensors working with either C=N isomerization (imines) or ICT (amines). The prepared amines seem to possess a higher potential in the application as colorimetric sensors due to their stability towards protonation. If the claimed standard of investigating potential sensors in polar protic solvents is retained, amines provide a better option than imines. Nevertheless, the synthesis of imines is an indispensable step towards the promising amines.

Following projects should focus on the introduction of different aldehydes to the established route.

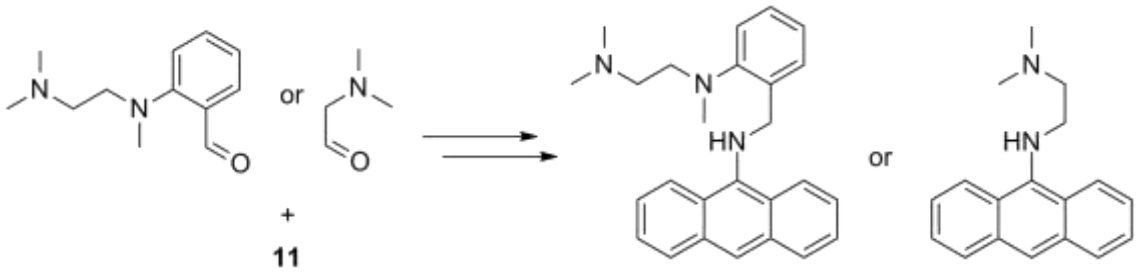

Scheme 3-3: Suggested aldehydes for the syntheses of potential sensors.

The two aldehydes shown in Scheme 3-3 are recommended for the syntheses of potential sensors. The left one exhibits an analog structure to **17**, which was the start-

ing material for the most promising compound of this project (**19**) and the right one was chosen due to its minor steric demand compared with the aldehydes already deployed. An additional reason for these two proposed receptors is their exclusively usage of amine donors that could favor the coordination of specific metal cations in comparison to ligands bearing both, oxygen and nitrogen donor atmos.

An even more challenging but probably also more rewarding approach would be the derivatization of **11** in its 1-position. The substitution of anthracene in 1-position is known[109] but has not been transferred to **11** yet.

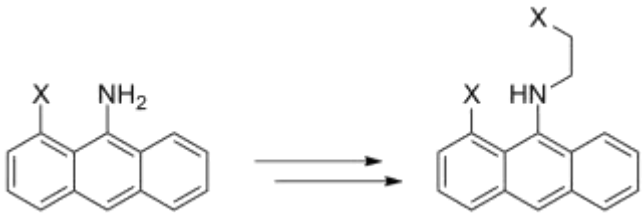

Scheme 3-4: Left: Suggested modification of 9-aminoanthracene with X = OMe or NMe_2. Right: Resulting potential sensor.

Derivatives bearing the structure shown in the right part of Scheme 3-4 offer an additional donor atom in close proximity to the amine in 9-position and should favor a coordination of metal cations by providing a rigid, pre-organized system as well as a energetically most favorable six-membered ring.

The implementation of either or both suggested modifications should allow a transfer of the promising colorimetric properties the amines exhibited during this project to polar protic solvents like methanol or even water.

4 Experimental information

4.1 General working procedure

Air and moisture sensitive reactions were carried out under SCHLENK[110] conditions in dried nitrogen or argon atmosphere and resulting sensitive substances were stored in an argon glovebox. The used solvents were purchased in high quality and dried due to standard laboratory techniques if necessary. The starting materials were received from the companies *ABCR*, *Acros Organics*, *Sigma Aldrich*, *Deutero* and *VWR*.

4.2 Fluorescence analysis

4.2.1 Spectrometer setup

For fluorescence analysis, a *FluoroMax-4* from the company *HORIBA Jobin Yvon* was used. Its detailed setup is shown in Figure 4-1.

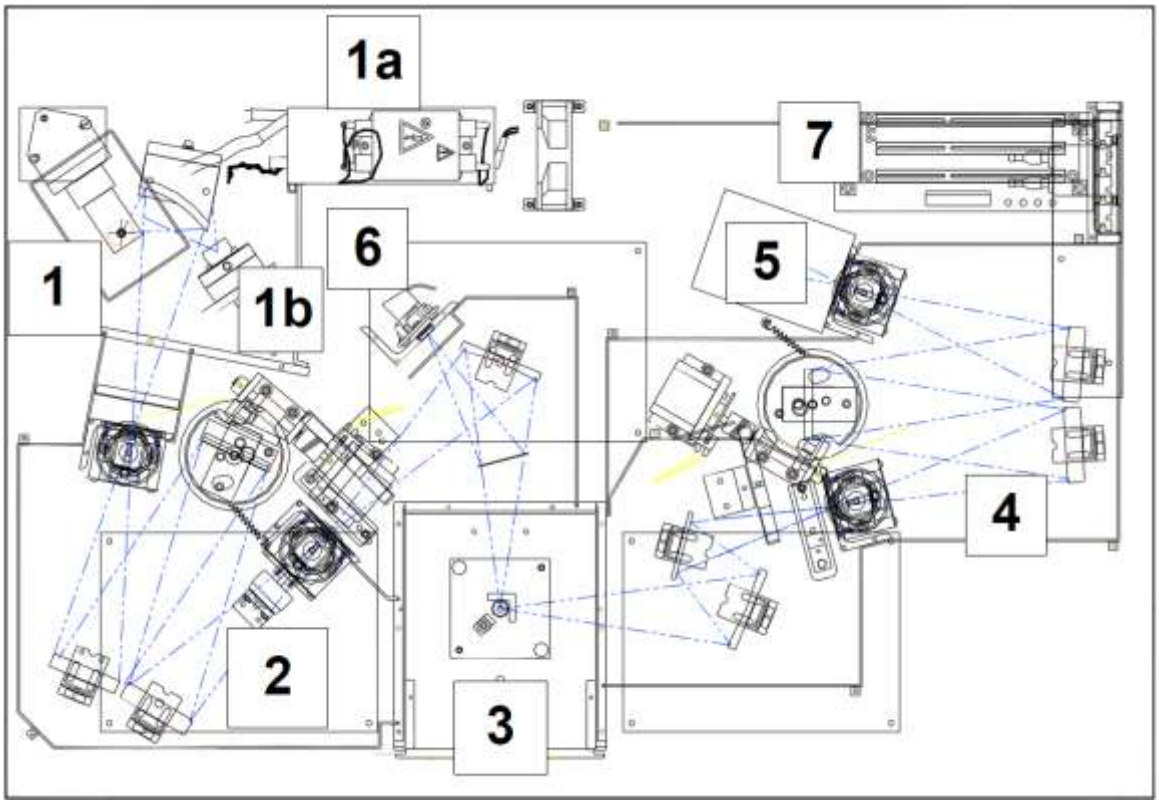

Figure 4-1: Schematic description of the used spectrofluorometer.[108]

The xenon arc-lamp (1) is applied as a continuous light source with a power of 150 W. Its power supply is termed 1a in the description. The xenon flash lamp (1b) is not installed in the used spectrometer but in the *FluoroMax-4P*, a version constructed especially for the detection of phosphorescence processes. The excitation (2) and emission monochromators (4) are based on the CZERNY-TURNER[111] all-reflective optics. The excitation beam is focused to the sample compartment (3) and about 8 % of the excitation light is split off to the reference photodiode (6). To monitor the signal, a photon-counting detector (5) is used. It consists of a photomultiplier tube with a spectral range of 180-850 nm. The linear range of photon counting is up to two million cps. The connection to the host computer is depicted as 7.[108]
The software *FluorEssence* v3.0 was applied to record fluorescence spectra as well as analyze the received data graphically.[112]

4.2.2 Basic phenomena

This chapter covers a series of basic phenomena observed during the performance of fluorescence measurements in this thesis. These observations were not caused by specific investigated molecules but are noteworthy due to their occurrence during many fluorescence analyses.
A basic consideration is the choice of the sample concentration. Too low concentrations lead to not detectable emission, whereas very high concentrations can also result in low emission due to collisional quenching or absorption of the whole incoming light in the first millimeters of the sample.[84]

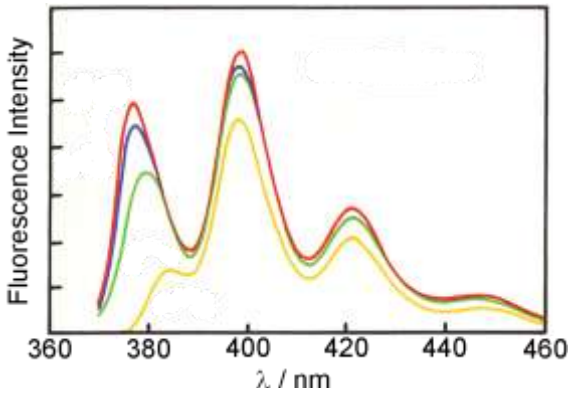

Figure 4-2: Fluorescence emission of anthracene at different concentrations (yellow: 10^{-3} M, green: 10^{-4} M, blue: 10^{-5} M, red: 10^{-6} M).[84]

Another possible consequence of too high sample concentrations is visualized in Figure 4-2. The inner filter effect reduces the emission of the energetically highest band of anthracene at high concentrations.[113] This can be understood by the reabsorption of the emitted light on its way to the detector through the sample. Molecules in the electronic ground state can be excited because of the very small STOKES shift anthracene exhibits. Proper sample concentrations of molecules investigated during this project turned out to be in the range of 10^{-5} M.

The second basic phenomenon discussed in this section is solvent relaxation. This can be illustrated by the help of a JABLOŃSKI diagram.

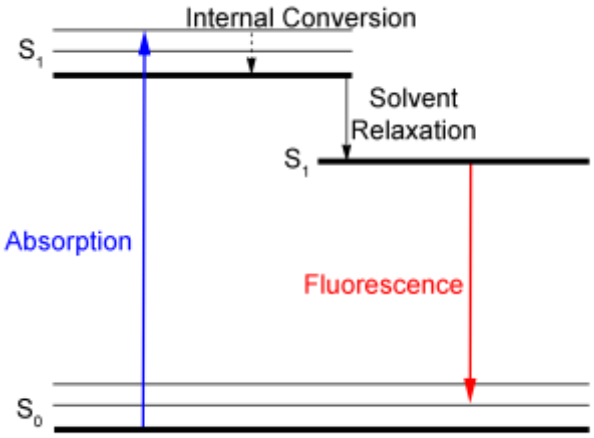

Figure 4-3: JABLOŃSKI diagram concerning solvent relaxation.

Many molecular substances display a larger dipole moment in their electronically excited state compared to their ground state. In the presence of a polar solvent, a reorientation of the solvent molecules around the excited species can lower its energy (Figure 4-3). The resulting fluorescent emission is consequentially shifted to lower energy. So the more polar the solvent around an excited species, the more pronounced bathochromic shift can be observed in its emission. Nevertheless, the absorption spectrum is much less affected by the solvent polarity due to the very fast absorption (typically 10^{-15} s), which does not allow any reorientation of the solvent. Solvent relaxation occurs typically in a 10^{-10} s range[24] and is often faster than fluorescence processes (approximately 10^{-6}-10^{-9} s[13]). Therefore, the STOKES shift is also dependent on the solvent and increases with its polarity.

Working with very weak emissive species (like the imines discussed in this thesis), RAMAN[114] bands of the solvent can be observable (Figure 4-4).

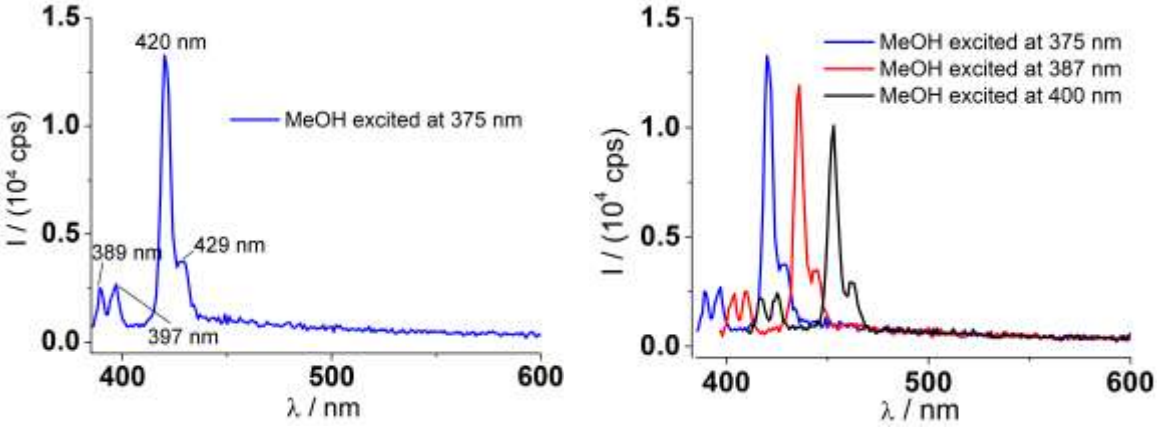

Figure 4-4: Left: Fluorescence spectrum of MeOH with depicted RAMAN signals of the solvent. Right: Shifted peaks due to variation of the excitation wavelength.

The emission wavelength of fluorophores is generally independent of the used excitation wavelength according to the rules of KASHA[115] and VAVILOV.[91] An excitation wavelength dependency on the emission wavelength can be noticed in the right part of Figure 4-4. This provides the first hint that the observed peaks may originate from RAMAN transitions and not from luminescence. By comparison with published RAMAN signals of methanol, an assignment of the peaks shown in the left part of Figure 4-4 is possible.

λ / nm	ῡ / cm^{-1}
389	960
397	1478
420	2857
429	3357

1 atm	assignment
1033 vs	C–O stretch
1106 w	CH_3 rock
1149 w	CH_3 bend
1448 s	
2832 vs	C–H sym str
2940 vs	C–H antisym str
3330 vw, br	O–H stretch

Figure 4-5: Left: Wavelengths and corresponding wavenumbers from Figure 4-4 left. Right: Published RAMAN signals of MeOH in cm^{-1} (vs = very strong, s = strong, w = weak, vw = very weak, br = broad) with associated types of vibration.[116]

By comparison of the observed peaks (Figure 4-5 left) with reported RAMAN signals of MeOH[116] (Figure 4-5 right), the measured signal at 389 nm can be assigned to a C—O stretching vibration. Another example is the good agreement of the very intense reported signals at 2832 cm^{-1} and 2940 cm^{-1} with the strongest observed peak at 420 nm corresponding to symmetric and antisymmetric C—H stretching vibrations.

4.3 Further applied analytical methods

4.3.1 Mass spectrometry

EI-MS[117]: Instrument *MAT 95* (70 eV); ESI-MS[118]: Instrument *HCT Ultra*. The mass to charge ratios of the molecular ions and the fragment ions are based on the isotopes bearing the highest natural abundances (^{1}H, ^{13}C, ^{14}N, ^{16}O, ^{28}Si, ^{32}S, $^{35}Cl/^{37}Cl$, $^{79}Br/^{81}Br$).

4.3.2 NMR spectroscopy

The spectra were mainly recorded on the *Bruker Avance III 300* instrument. Exceptions are the time dependent investigations of **12** in section 2.2.5.3 that were recorded on a *Bruker Avance III 400* instrument. The measurements were carried out at room temperature in 1-10 % solutions of deuterated solvents. The chemical shifts δ are given in ppm and the coupling constants *J* in Hz. The residual proton signals of the deuterated solvents were chosen as internal standards for ^{1}H NMR spectra. For ^{13}C spectra, the carbon resonances of the solvents were used for calibration, too. The assignment of the peaks was accomplished by two dimensional NMR techniques (^{1}H-^{1}H COSY[119], ^{1}H-^{13}C HSQC[120], ^{1}H-^{13}C HMBC[121]). The observed multiplicities are abbreviated as follows: s = singlet, d = doublet, t = triplet, q = quartet, m = multiplet. Combined abbreviations are derived from their components (e.g. dd = doublet of doublets).

4.3.3 UV/Vis spectroscopy

This spectroscopic method was chosen to gain information about non-radiative processes not observable by fluorescence spectroscopy. One fundamental difference between these techniques is the arrangement of irradiation source, sample and detector visualized in Figure 4-6.

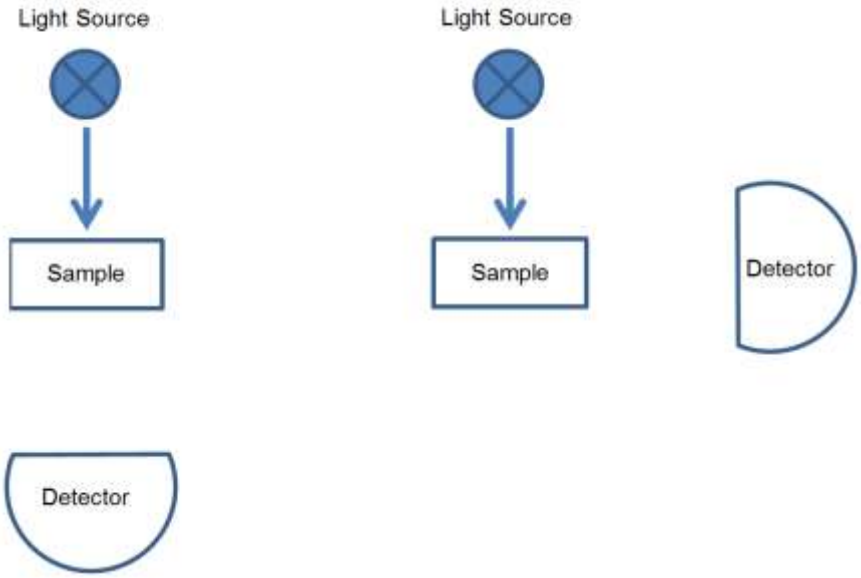

Figure 4-6: Different experimental setup for measurement of absorption (left) and fluorescence emission (right).

The detector is placed in a linear arrangement with regard to the light source and sample in order to determine the absorption of molecules (Figure 4-6 left). Analyzed species absorb a fraction of the incoming beam and the transmitting light is detected. In contrast, fluorescence measurements are carried out in a right angle setup. Thereby, the transmitted beam is not detected but only the fluorescence radiation that is emitted by the excited molecules in an isotropic fashion.

In this thesis presented UV/Vis spectra were recorded at a *Jasco V-650* double-beam spectrophotometer. In general, the measurements were corrected by subtraction of a identical cuvette bearing only the solvent methanol.

The type of designation $A_{218} = 0.22$ (e.g. in section 2.2.3.1) abbreviates an absorption of $\lg(I/I_0) = 0.22$ at 218 nm.

4.3.4 X-ray diffraction

Choice and application of crystals

Air sensitive crystals were extracted from SCHLENK flasks under a counterflow of argon and placed in perfluorinated polyether oil on a microscope slide.[122] A suitable single crystal was chosen with the help of a polarizing microscope and mounted, inside a droplet of oil, at the top of a MiTeGen loop. The loop was moved immediately to the diffractometer, where the droplet was frozen due to the nitrogen flow with a temperature of 100 K surrounding the crystal. The oil solidified in a glass-like manner and fixed the crystal during the data collection.

Data collection, structure solution and refinement

The majority of data sets were recorded at a *Bruker APEX II Quazar* bearing an *Incoatec Mo IμS* or an *APEX II Ultra* equipped with a *Bruker TXS Mo* source. Both diffractometers use monochromatic Mo-K_α-radiation (λ = 0.71073 Å). An exception was the measurement of **15**, where Cu-K_α-radiation (λ = 1.54178 Å) was applied to determine its solid state structure. The associated diffractometer was equipped with a *SMART6000* detector and a *Bruker TXS* source. The reflexes were detected by combined ω--and φ-scans with a step width of 0.3° or 0.5° in the respective directions.
The last used version of all programs is listed below, although different versions of them were applied over the last three years. The determination and refinement of the unit cells were accomplished by usage of APEX2 v2012/2[123]. Integration of the recorded frames was performed with SAINT v8.30C[124] and the resulting data underwent an empirical absorption correction with the help of SADABS v2014/1[125] followed by space group determination with XPREP v2014/1[126]. All structures were solved using the program SHELXT v2014/1[127] and refined with SHELXL v2013/4[128] in the graphical user interface shelXle v2013/6[129]. The positions of hydrogen atoms were refined using riding models[130] and their displacement parameters were constrained to their pivot atoms. Hydrogen atoms attached to heteroatoms (oxygen or nitrogen) have been found in the FOURIER-density-difference map and were refined with DFIX command to set the distance to tabulated values.

4.4 Synthesis and Characterization

4.4.1 Synthesis of 9,10-(dibromomethyl)anthracene (1)

Under inert conditions 5.00 g anthracene (1.00 eq., 28.05 mmol) were solved in a mixture of 100 mL 48 % aqueous hydrobromic acid and 25 mL acetic acid. After addition of 5.00 g trioxane (1.95 eq., 55.5 mmol) and 0.20 g tetradecyltrimethylammonium bromide (0.02 eq., 0.59 mmol) the solution was stirred for 23 h at room temperature. Another 5.00 g trioxane (1.95 eq., 55.5 mmol) were added and after stirring the reaction mixture at room temperature for additional 24 h another 5.00 g trioxane (1.95 eq., 55.5 mmol) were added. The reaction mixture was stirred for 5 d, the precipitate was filtered, washed with water and small amounts of ethanol. The crude reaction product was dried under reduced pressure and recrystallized from 500 mL chloroform to yield **1** as a yellow solid.

Molecular formula: $C_{16}H_{12}Br_2$

Molecular weight: 364.07 g/mol

Yield: 4.27 g (11.73 mmol, 42 %).

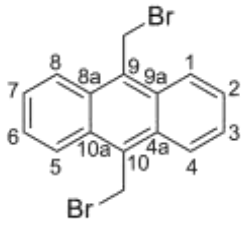

^{1}H-NMR

(300 MHz, $CDCl_3$): δ /ppm = 5.52 (s, 4 H, CH_2), 7.65-7.71 (m, 4 H, $H_{2,3,6,7}$), 8.35-8.41 (m, 4 H, $H_{1,4,5,8}$).

EI-MS

m/z (%): 364 (2) $[M]^+$, 285/283 (8/9) $[M - Br]^+$, 204 (100) $[M - 2\ Br]^+$.

Elemental analysis

in % (calculated) C: 52.97 (52.78), H: 3.32 (3.32), Br: 42.81 (43.89).

4.4.2 Synthesis of 1,4,7-tris(*p*-nitrobenzenesulfonyl)-1,4,7-triazaheptane (2)

A solution of 0.33 g triethylenediamine (1.00 eq., 3.17 mmol, 0.34 mL) in 25 mL DCM was added to a solution of 1.40 mL triethylamine (3.19 eq., 10.1 mmol, 1.02 g) and 2.04 g nosyl chloride (2.9 eq., 9.19 mL) in 10 mL DCM.

After stirring for 45 h under inert atmosphere, the precipitate was filtered, washed with a small amount of DCM, ammonium chloride solution and water.

The desired product was obtained as a white solid and contained less than two weight % NH_4Cl.

Molecular formula: $C_{22}H_{22}N_6O_{12}S_3$

Molecular weight: 658.64 g/mol

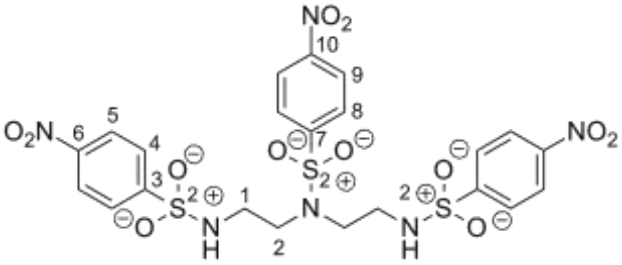

Yield: 0.769 g (1.14 mmol, 36 %).

^{1}H-NMR

(300 MHz, DMSO-d^6): δ /ppm = 2.96 (t, $^3J_{HH}$ = 6.7 Hz, 4 H, H_1), 3.23 (t, $^3J_{HH}$ = 6.7 Hz, 4 H, H_2), 7.99-8.06 (m, 6 H, $H_{4,8}$), 8,16 (s, 2 H, NH), 8.33-8.43 (m, 6 H, $H_{5,9}$).

^{13}C{^{1}H}-NMR

(75 MHz, DMSO-d^6): δ /ppm = 41.49 (s, 2 C, C_1), 48.39 (s, 2 C, C_2), 124.64 (s, 2 C, C_9), 124.73 (s, 4 C, C_5), 128.13 (s, 2 C, C_8), 128.54 (s, 4 C, C_4), 143.94 (s, 1 C, C_7), 145.74 (s, 2 C, C_3), 149.66 (s, 2 C, C_6), 149.88 (s, 1 C, C_{10}).

ESI-MS (-)

m/z (%): 657 (100) $[M-H]^-$.

Elemental analysis

in % (calculated) C: 40.33 (40.12), H: 3.78 (3.37), N: 12.05 (12.76), S: 13.86 (14.61).

4.4.3 Synthesis of sodium β-trimethylsilylethanesulfonate (5)

To a solution of 28.9 mL vinyltrimethylsilane (1.00 eq., 200 mmol, 20.0 g) and 1.15 mL tert-butylperbenzoate (0.03 eq., 6.02 mmol, 1.17 g) in 70 mL methanol 60 mL of a 40 % aqueous solution of sodium hydrogen sulfite (1.91 eq., 382 mmol, 39.8 g) was added. The reaction mixture was stirred for 48 h at 50 °C under inert conditions.

The mixture was concentrated and three times coevaporated with 25 mL methanol each to remove left water. The resulting dried solid was suspended in 200 mL methanol, stirred rapidly for 10 min and filtered over celite.

The filter cake was again suspended in 200 mL methanol, rapidly stirred for 10 min and again filtered. Tis procedure was repeated.

The resulting methanol layers were combined and dried to yield **5** as a white solid.

Molecular formula: $C_5H_{13}NaO_3SSi$

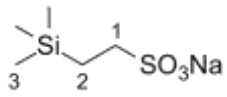

Molecular weight: 204.30 g/mol

Yield: 27.3 g (134 mmol, 67 %).

^{1}H-NMR

(300 MHz, DMSO-d^6): δ /ppm = - 0.03 (s, 9 H, H_3), 0.78-0.86 (m, 2 H, H_2), 2.29-2.36 (m, 2 H, H_1).

^{13}C{^{1}H}-NMR

(75 MHz, DMSO-d^6): δ /ppm = - 1.75 (s, 3 C, C_3), 11.92 (s, 1 C, C_2), 46.47 (s, 1 C, C_1).

4.4.4 Synthesis of β-trimethylsilylethanesulfonyl chloride (6)

Under inert atmosphere 80.0 mL thionyl chloride (8.24 eq., 1.10 mol, 131 g) were added dropwise to 27.3 g **5** (1.00 eq., 134 mmol) over 1 h in a reaction flask cooled to 0 °C. Evolution of SO_2 was monitored and after the addition of thionyl chloride was finished, 0.4 mL DMF (0.04 eq., 5.19 mmol, 0.38 g) were added dropwise, followed by a strong generation of SO_2.

The reaction mixture was stirred over night while the temperature rose to room temperature.

The excess thionyl chloride was distilled of and two times following procedure was done to remove remaining thionyl chloride: 50 mL hexane were added and removed under reduced pressure.

Additional 50 mL hexane were added, filtered over celite and the remaining solid was washed with 75 mL hexane. The volatile components were removed under reduced pressure and the crude product was vacuum distilled to yield **6** as an orange oil.

Molecular formula: $C_5H_{13}ClO_2SSi$

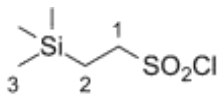

Molecular weight: 200.76 g/mol

Yield: 1.53 g (7.62 mmol, 5.7 %).

^{1}H-NMR

(300 MHz, DMSO-d^6): δ /ppm = - 0.11 (s, 9 H, H_3), 1.27-1.34 (m, 2 H, H_2), 3.56-3.64 (m, 2 H, H_1).

^{13}C{^{1}H}-NMR

(75 MHz, DMSO-d^6): δ /ppm = - 1.88 (s, 3 C, C_3), 12.06 (s, 1 C, C_2), 63.56 (s, 1 C, C_1).

4.4.5 Synthesis of 1,4,7-tris(*β*-trimethylsilylethanesulfonyl)-1,4,7-triazaheptane (7)

To a solution of 0.07 mL diethylenetriamine (1.00 eq., 0.62 mmol) and 0.43 mL triethylamine (5.00 eq., 3.11 mmol) in 0.63 mL DMF a solution of 0.47 mL **6** (4.00 eq., 2.49 mmol) in 0.63 mL DMF was added tropwise at 0 °C. The reaction mixture was stirred under inert conditions for 1.5 h at 0 °C and was poured into 3.75 mL water. The aqueous solution was three times extracted with 5 mL DCM and the combined organic fractions were washed with 10 mL conc. aqueous sodium chloride solution. The organic layer was dried with sodium sulfate, filtered and the volatile components were removed under reduced pressure. The crude product was purified by column chromatography (ethyl acetate and petroleum ether 20:1 → ethyl acetate).

Molecular formula: $C_{19}H_{48}N_3O_6S_3Si_3$

Molecular weight: 596.06 g/mol

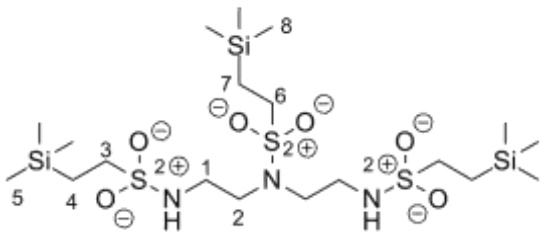

Yield: 73 mg (0.122 mmol, 20 %).

^{1}H-NMR

(300 MHz, DMSO-d^6): δ /ppm = 0.04 (s, 18 H, H_5), 0.05 (s, 9 H, H_8), 0.96-1.05 (m, 6 H, $H_{4,7}$), 2.92-3.05 (m, 6 H, $H_{3,6}$), 3.29-3.38 (m, 4 H, H_1), 3.40-3.47 (m, 4 H, H_2).

4.4.6 Synthesis of 2',5',8'-tris(β-trimethylsilylethanesulfonyl)-2',5',8'-triaza[9](9,10)anthracenophane (8)

To a mixture of 214 mg **7** (1.00 eq., 0.36 mmol) and 0.35 g caesium carbonate (3.00 eq., 1.07 mmol) in 7.5 mL DMF a suspension of 131 mg **1** (1.00 eq., 0.36 mmol) in 5.25 mL DMF was added. The reaction mixture was stirred under inert conditions for 48 h at room temperature.

The volatile components were removed at reduced pressure, 30 mL DCM and 30 mL water were added, the aqueous fraction was extracted with 30 mL DCM and the combined organic layers were washed with 30 mL conc. aqueous sodium chloride solution. The organic layer was dried with sodium sulfate and concentrated to dryness. The crude product was purified via column chromatography two times (1st: petroleum ether and ethyl acetate 5:1 → ethyl acetate; 2nd: petroleum ether and ethyl acetate 10:1 → ethyl acetate). **8** was isolated as a slightly yellow solid.

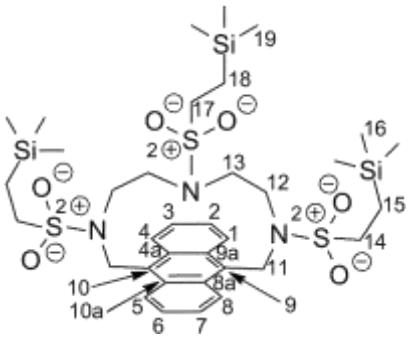

Molecular formula: $C_{35}H_{59}N_3O_6S_3Si_3$

Molecular weight: 798.31 g/mol

Yield: 31 mg (0.039 mmol, 11 %).

^{1}H-NMR

(300 MHz, DMSO-d^6): δ /ppm = - 0.08 (s, 9 H, H_{19}), 0.13 (s, 18 H, H_{16}), 0.58-0.66 (m, 2 H, H_{18}), 1.08-1.18 (m, 4 H, H_{15}), 1.41-1.57 (m, 4 H, H_{13}), 2.38-2.52 (m, 6 H, $H_{12,17}$), 3.00-3.09 (m, 4 H, H_{14}), 5.58 (s, 4 H, H_{11}), 7.66-7.74 (m, 4 H, $H_{2,3,6,7}$), 8.43-8.51 (m, 4 H, $H_{1,4,5,8}$).

^{13}C{^{1}H}-NMR

(75 MHz, DMSO-d^6): δ /ppm = - 1.88 (s, 3 C, C_{19}), - 1.72 (s, 6 C, C_{16}), 10.32 (s, 1 C, C_{18}), 10.42 (s, 2 C, C_{15}), 44.73 (s, 2 C, C_{12}), 45.65 (s, 2 C, C_{11}), 46.35 (s, 2 C, C_{14}), 46.66 (s, 2 C, C_{13}), 48.44 (s, 1 C, C_{17}), 124.83 (s, 4 C, $C_{2,3,6,7}$), 127.42 (s, 4 C, $C_{1,4,5,8}$), 127.91 (s, 2 C, $C_{9,10}$), 131.67 (s, 4 C, $C_{4a,8a,9a,10a}$).

4.4.7 Synthesis of 9-nitroanthracene (10)

To a suspension of 20.2 g anthracene (1.00 eq., 113 mmol) in 85 mL glacial acetic acid 8.60 mL nitric acid (1.10 eq., 124 mmol, 65 %) were added dropwise under inert conditions while stirring and keeping the reaction mixture at room temperature via a water bath. The mixture was stirred till an orange solution was formed (about 1 h) and a mixture of 100 mL concentrated hydrochloric acid and 100 mL glacial acetic acid was added. The yellow precipitate was filtered through a BÜCHNER funnel and washed many times with water till the washings became neutral.

The isolated 9-chloro-9,10-dihydro-10-nitroanthracene (**9**) was poured into a warm (around 70 °C) solution of sodium hydroxide (10 %) in water (200 mL). The solution became red and the yellow precipitate was filtered through a glass frit, washed many times with water till the washings became neutral and dried under reduced pressure. This procedure gave **10** as a yellow solid.

Molecular formula: $C_{14}H_9NO_2$

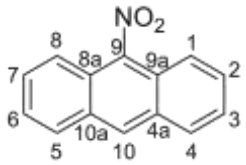

Molecular weight: 223.23 g/mol

Yield: 21.1 g (94.5 mmol, 84 %).

^{1}H-NMR

(300 MHz, DMSO-d^6): δ /ppm = 7.66-7.73 (m, 2 H, $H_{3,6}$), 7.76-7.83(m, 2 H, $H_{2,7}$), 7.90 (d, $^3J_{HH}$ = 8.7 Hz, 2 H, $H_{1,8}$), 8.30 (d, $^3J_{HH}$ = 8.7 Hz, 2 H, $H_{4,5}$), 9.01 (s, 1 H, H_{10}).

^{13}C{^{1}H}-NMR

(75 MHz, DMSO-d^6): δ /ppm = 120.45 (s, 2 C, $C_{1,8}$), 121.63 (s, 2 C, $C_{8a,9a}$), 126.56 (s, 2 C, $C_{3,6}$), 128.71 (s, 2 C, $C_{4,5}$), 129.73 (s, 2 C, $C_{2,7}$), 130.25 (s, 2 C, $C_{4a,10a}$), 131.03 (s, 1 C, C_{10}), 143.29 (s, 1 C, C_9).

EI-MS

m/z (%): 223 (100) $[M]^+$, 176 (68) $[M - NO_2]^+$.

4.4.8 Synthesis of 9-aminoanthracene (11)

Under inert conditions a suspension of 13.4 g 9-nitroanthracene (**10**) (1.00 eq., 60.0 mmol) in 270 mL conc. acetic acid was warmed to 80 °C while the solid was dissolving to an orange solution. Afterwards, a suspension of tin(II) chloride dihydrate (5.00 eq., 300 mmol, 67.8 g) in 200 mL conc. hydrochloric acid was added, attended by precipitation of a yellow solid. The suspension was stirred at 80 °C for 50 min and cooled to room temperature over 75 min.

The light yellow solid was filtered under inert atmosphere and washed many times with water till the washings became neutral. Thereby the pale yellow solid turned at first grey-black and then again pale yellow.

Afterwards the solid was dried under reduced pressure and was dissolved through the frit with dried, degased chloroform (9-times 10 mL) while a white solid was remaining. The volatile components were removed under reduced pressure and the crude product was recrystallized from hexane (25 mL, degased) and chloroform (20 mL, dried, degased). **11** was isolated in the form of an orange solid.

Molecular formula: $C_{14}H_{11}N$

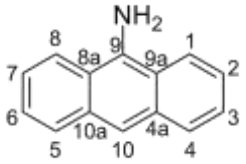

Molecular weight: 193.27 g/mol

Yield: 5.87 g (30.4 mmol, 51 %).

^{1}H-NMR

(300 MHz, DMSO-d^6): δ /ppm = 6.61 (s, 2 H, NH_2), 7.26-7.33 (m, 2 H, $H_{2,7}$), 7.35-7.42 (m, 2 H, $H_{3,6}$), 7.62 (s, 1 H, H_{10}), 7.85 (d, $^3J_{HH}$ = 8.6 Hz, 2 H, $H_{4,5}$), 8.35 (d, $^3J_{HH}$ = 8.6 Hz, 2 H, $H_{1,8}$).

^{13}C{^{1}H}-NMR

(75 MHz, DMSO-d^6): δ /ppm = 111.99 (s, 1 C, C_{10}), 116.70 (s, 2 C, $C_{8a,9a}$), 122.12 (s, 2 C, $C_{2,7}$), 123.12 (s, 2 C, $C_{1,8}$), 125.27 (s, 2 C, $C_{3,6}$), 128.04 (s, 2 C, $C_{4,5}$), 132.16 (s, 2 C, $C_{4a,10a}$), 141.24 (s, 1 C, C_9).

EI-MS

m/z (%): 193 (100) $[M]^+$, 165 (18) $[M\text{-}CNH_2]^+$.

Elemental analysis

in % (calculated) C: 86.68 (87.01), H: 5.58 (5.74), N: 7.20 (7.25).

4.4.9 Synthesis of 9-anthracenesalicylimine (12)

To a suspension of **11** (1.00 eq., 1.50 g, 7.76 mmol) in 30 mL ethanol (degased, dried) salicylaldehyde (1.50 eq., 11.6 mmol, 1.24 mL) was added under inert atmosphere. The reaction mixture was stirred firstly at 78 °C for 6 h and then overnight at room temperature.

The precipitated solid was filtered and washed with dried degased ethanol (3 · 4 mL) to yield **12** as a yellow solid.

Molecular formula: $C_{21}H_{15}NO$

Molecular weight: 297.35 g/mol

Yield: 2.14 g (7.20 mmol, 93 %).

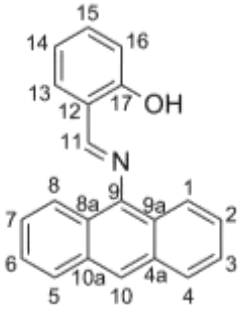

^{1}H-NMR

(300 MHz, DMSO-d^6): δ /ppm = 7.04-7.13 (m, 2 H, $H_{14,16}$), 7.48-7.60 (m, 5 H, $H_{2,3,6,7,15}$), 7.84 (dd, $^3J_{HH}$ = 7.7 Hz, $^4J_{HH}$ = 1.7 Hz, 1 H, H_{13}), 7.98 (d, $^3J_{HH}$ = 7.6 Hz, 2 H, $H_{1,8}$), 8.13 (d, $^3J_{HH}$ = 7.6 Hz, 2 H, $H_{4,5}$), 8.48 (s, 1 H, H_{10}), 8.95 (s, 1 H, H_{11}), 12.47 (s, 1 H, OH).

^{13}C{^{1}H}-NMR

(75 MHz, DMSO-d^6): δ /ppm = 116.81 (s, 1 C, C_{16}), 119.47 (s, 2 C, $C_{12,14}$), 122.01 (s, 2 C, $C_{8a,9a}$), 123.09 (s, 3 C, $C_{1,8,10}$), 125.75 (s, 2 C, $C_{3,6}$), 125.92 (s, 2 C, $C_{2,7}$), 128.30 (s, 2 C, $C_{4,5}$), 131.28 (s, 2 C, $C_{4a,10a}$), 132.08 (s, 1 C, C_{13}), 133.95 (s, 1 C, C_{15}), 142.95 (s, 1 C, C_9), 160.16 (s, 1 C, C_{17}), 168.83 (s, 1 C, C_{11}).

EI-MS

m/z (%): 297 (100) $[M]^+$, 204 (9) $[M\text{-}C_6H_4OH]^+$, 176 (10) $[C_{14}H_8]^+$.

Elemental analysis

in % (calculated) C: 84.65 (84.82), H: 5.05 (5.08), N: 4.73 (4.71).

4.4.10 Synthesis of 9-anthracenepicolylimine (13)

To a suspension of **11** (1.00 eq., 0.99 g, 5.12 mmol) in 20 mL ethanol (degased, dried) 2-pyridinecarboxaldehyde (1.50 eq., 0.73 ml, 7.68 mmol) was added under inert atmosphere. After stirring the reaction mixture at 78 °C for 2.5 h, the volatile components were removed under reduced pressure.

The crude reaction product was purified via recrystallization from hexane (15 mL) to yield **13** as an orange solid.

Molecular formula: $C_{20}H_{14}N_2$

Molecular weight: 282.34 g/mol

Yield: 1.30 g (4.60 mmol, 90 %).

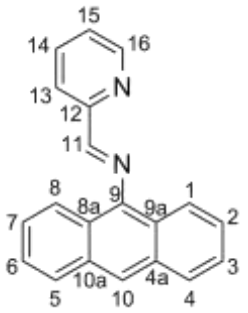

^{1}H-NMR

(300 MHz, DMSO-d^6): δ /ppm = 7.43-7.57 (m, 4 H, $H_{2,3,6,7}$), 7.66 (dd, $^3J_{HH}$ = 7.5 Hz, $^3J_{HH}$ = 4.8 Hz, 1 H, H_{15}), 7.97 (d, $^3J_{HH}$ = 8.9 Hz, 2 H, $H_{1,8}$), 8.07-8.14 (m, 3 H, $H_{4,5,14}$), 8.41 (s, 1 H, H_{10}), 8.50 (d, $^3J_{HH}$ = 7.9 Hz, 1 H, H_{12}), 8.65 (s, 1 H, H_{11}), 8.81 (d, $^3J_{HH}$ = 4.8 Hz, 1 H, H_{16}).

^{13}C{^{1}H}-NMR

(75 MHz, DMSO-d^6): δ /ppm = 121.04 (s, 2 C, $C_{8a,9a}$), 121.59 (s, 1 C, C_{13}), 122.41 (s, 1 C, C_{10}), 123.30 (s, 2 C, $C_{1,8}$), 125.47 (s, 2 C, $C_{2,7}$), 125.70 (s, 2 C, $C_{3,6}$), 126.27 (s, 1 C, C_{15}), 128.16 (s, 2 C, $C_{4,5}$), 131.31 (s, 2 C, $C_{4a,10a}$), 137.35 (s, 1 C, C_{14}), 144.49 (s, 1 C, C_9), 149.88 (s, 1 C, C_{16}), 153.49 (s, 1 C, C_{12}), 166.39 (s, 1 C, C_{11}).

EI-MS

m/z (%): 282 (100) $[M]^+$, 204 (73) $[M\text{-}C_5H_4N]^+$, 176 (18) $[C_{14}H_8]^+$.

Elemental analysis

in % (calculated) C: 84.91 (85.08), H: 5.06 (5.00), N: 10.01 (9.92).

4.4.11 Synthesis of 9-anthracene-(α-methylpicolyl)imine (14)

3 mL 2-acetylpyridine (8.77 eq., 26.7 mmol) were added to **11** (1.00 eq., 0.59 g, 3.05 mmol) under inert atmosphere. The reaction mixture was stirred for 7 d at 85 °C accompanied by a color change from red to black.

The remaining 2-acetylpyridine was removed under reduced pressure and elevated temperature (110 °C) for 5 h.

The crude product was dissolved under inert conditions in 20 mL acetonitrile and was 3-times extracted with 20 mL hexane respectively. The combined hexane phases where once extracted with 20 mL acetonitrile. The two acetonitrile phases where together concentrated to its half volume and further 4-times extracted by each 20 mL hexane. These combined 80 mL hexane where once again extracted with 20 mL acetonitrile.

The volatile components of all combined hexane phases (140 mL in total) where removed under reduced pressure and the desired imine was obtained as an orange oil and contained less than two percent anthraquinone.

Molecular formula: $C_{21}H_{16}N_2$

Molecular weight: 296.13 g/mol

Yield: 322 mg (1.09 mmol, 36 %).

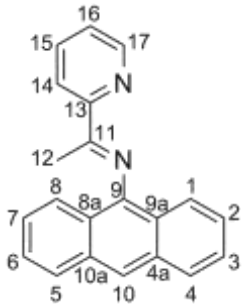

^{1}H-NMR

(300 MHz, DMSO-d^6): δ /ppm = 2.06 (s, 3 H, H_{12}), 7.40-7.56 (m, 4 H, $H_{2,3,6,7}$), 7.66 (ddd, $^3J_{HH}$ = 7.6 Hz, $^3J_{HH}$ = 4.9 Hz, $^4J_{HH}$ = 1.1 Hz, 1 H, H_{16}), 7.72 (d, $^3J_{HH}$ = 8.8 Hz, 2 H, $H_{1,8}$), 8.07 (ddd, $^3J_{HH}$ = 8.0 Hz, $^3J_{HH}$ = 7.6 Hz, $^4J_{HH}$ = 1.8 Hz, 1 H, H_{15}), 8.10 (d, $^3J_{HH}$ = 8.5 Hz, 2 H, $H_{4,5}$), 8.35 (s, 1 H, H_{10}), 8.56 (d, $^3J_{HH}$ = 8.0 Hz, 1 H, H_{14}) 8.79 (d, $^3J_{HH}$ = 4.9 Hz, 1 H, H_{17}).

$^{13}C\{^{1}H\}$-NMR

(75 MHz, DMSO-d^6): δ /ppm = 17.42 (s, 1 C, C_{12}), 119.59 (s, 2 C, $C_{8a,9a}$), 121.07 (s, 1 C, C_{10}), 121.36 (s, 1 C, C_{14}), 123.28 (s, 2 C, $C_{1,8}$), 125.22 (s, 2 C, $C_{2,7}$), 125.70 (s, 2 C, $C_{3,6}$), 125.84 (s, 1 C, C_{16}), 128.37 (s, 2 C, $C_{4,5}$), 131.37 (s, 2 C, $C_{4a,10a}$), 137.17 (s, 1 C, C_{15}), 143.22 (s, 1 C, C_9), 148.94 (s, 1 C, C_{17}), 155.19 (s, 1 C, C_{13}), 170.03 (s, 1 C, C_{11}).

EI-MS

m/z (%): 296 (100) $[M]^+$, 281 (16) $[M\text{-}CH_3]^+$, 217 (27) $[M\text{-}C_5H_5N]^+$, 176 (18) $[C_{14}H_8]^+$.

4.4.12 Synthesis of 9-anthracenesalicylamine (15)

To a suspension of $NaBH_4$ (5.00 eq., 6.73 mmol, 0.25 g) in 20 mL dried THF a yellow solution of **12** (1.00 eq., 1.35 mmol, 0.40 g) in 20 mL dried THF was added. The reaction mixture was stirred for 18 h under inert atmosphere at room temperature.

The volatile components were removed under reduced pressure and the residue was dissolved in chloroform (25 mL) and water (20 mL). The aqueous layer was once again extracted with chloroform (20 mL) and the combined organic phases were washed with water (30 mL). After drying the organic layer with magnesium sulfate and filtration the volatile components were removed under reduced pressure.

The crude product was recrystallized from hexane (10 mL, degased) and chloroform (3.5 mL, dried, degased) to isolate **15** as a yellow solid.

Molecular formula: $C_{21}H_{17}NO$

Molecular weight: 299.37 g/mol

Yield: 0.30 g (1.00 mmol, 74 %).

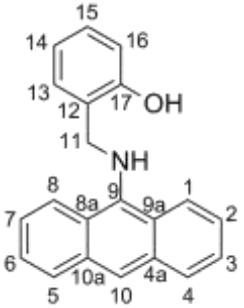

^{1}H-NMR

(300 MHz, DMSO-d^{6}): δ /ppm = 4.42 (d, $^{3}J_{HH}$ = 7.3 Hz, 2 H, H_{11}), 5.58 (t, $^{3}J_{HH}$ = 7.3 Hz, 1 H, NH), 6.76 (td, $^{3}J_{HH}$ = 7.7 Hz, $^{4}J_{HH}$ = 1.1 Hz, 1 H, H_{14}), 6.85 (dd, $^{3}J_{HH}$ = 7.7 Hz, $^{4}J_{HH}$ = 1.1 Hz, 1 H, H_{16}), 7.09 (td, $^{3}J_{HH}$ = 7.7 Hz, $^{4}J_{HH}$ = 1.6 Hz, 1 H, H_{15}), 7.35-7.49 (m, 5 H, $H_{2,3,6,7,13}$), 8.00 (d, $^{3}J_{HH}$ = 8.0 Hz, 2 H, $H_{4,5}$), 8.15 (s, 1 H, H_{10}), 8.39 (d, $^{3}J_{HH}$ = 8.3 Hz, 2 H, $H_{1,8}$), 9.69 (s, 1 H, OH).

^{13}C{^{1}H}-NMR

(75 MHz, DMSO-d^{6}): δ /ppm = 50,70 (s, 1 C, C_{11}), 114.87 (s, 1 C, C_{16}), 118.84 (s, 1 C, C_{14}), 119.97 (s, 1 C, C_{10}), 123.66 (s, 2 C, $C_{1,8}$), 124.24 (s, 2 C, $C_{2,7}$), 124.75 (s, 2 C, $C_{8a,9a}$), 125.26 (s, 2 C, $C_{3,6}$), 126.48 (s, 1 C, C_{12}), 127.98 (s, 1 C, C_{15}), 128.51 (s, 2 C, $C_{4,5}$), 129.15 (s, 1 C, C_{13}), 131.92 (s, 2 C, $C_{4a,10a}$), 142.63 (s, 1 C, C_{9}), 155.14 (s, 1 C, C_{17}).

EI-MS

m/z (%): 299 (17) $[M]^{+}$, 193 (100) $[M\text{-}C_7H_5OH]^{+}$, 176 (18) $[C_{14}H_8]^{+}$.

Elemental analysis

in % (calculated) C: 82.96 (84.25), H: 5.39 (5.72), N: 4.55 (4.68).

4.4.13 Synthesis of 9-anthracenepicolylamine (16)

To a solution of **13** (1.00 eq., 0.78 g, 2.76 mmol) in 15 mL toluene (dried) a 1 M solution of $Na[BEt_3H]$ (2.50 eq., 6.91 mmol, 6.91 mL) in toluene was added. The reaction mixture was stirred under inert atmosphere for 20 h at room temperature.

The volatile components were removed under reduced pressure and the residue was dissolved in ethylacetate (20 mL) and water (50 mL). The aqueous layer was twice extracted with ethylacetate (20 mL each) and the combined organic layers were dried with magnesium sulfate. After filtration the volatile components were once again removed under reduced pressure and the crude product was purified via column chromatography (pentane and ethylacetate 20:1 → pentane and ethylacetate

2:1) and recrystallization from hexane (10 mL) and ethylacetate (2 mL). **16** was isolated as an orange solid.

Molecular formula: $C_{20}H_{16}N_2$

Molecular weight: 284.35 g/mol

Yield: 0.18 g (0.63 mmol, 23 %).

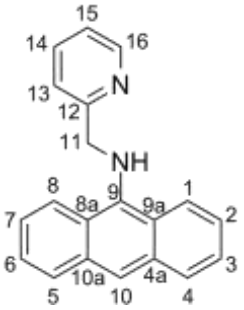

^{1}H-NMR

(300 MHz, DMSO-d^6): δ /ppm = 4.61 (d, $^3J_{HH}$ = 6.8 Hz, 2 H, H_{11}), 6.11 (t, $^3J_{HH}$ = 6.8 Hz, 1 H, NH), 7.29 (dd, $^3J_{HH}$ = 7.5 Hz, $^3J_{HH}$ = 5.2 Hz, 1 H, H_{15}), 7.38-7.49 (m, 4 H, $H_{2,3,6,7}$), 7.57 (d, $^3J_{HH}$ = 7.5 Hz, 1 H, H_{13}), 7.77 (td, $^3J_{HH}$ = 7.5 Hz, $^4J_{HH}$ = 1.8 Hz, 1 H, H_{14}), 8.00 (d, $^3J_{HH}$ = 7.5 Hz, 2 H, $H_{4,5}$), 8.15 (s, 1 H, H_{10}), 8.39 (d, $^3J_{HH}$ = 7.8 Hz, 2 H, $H_{1,8}$), 8.57 (d, $^3J_{HH}$ = 5.2Hz, 1 H, H_{16}).

^{13}C{^{1}H}-NMR

(75 MHz, DMSO-d^6): δ /ppm = 56.20 (s, 1 C, C_{11}), 119.92 (s, 1 C, C_{10}), 122.00 (s, 1 C, C_{13}), 122.22 (s, 1 C, C_{15}), 123.65 (s, 2 C, $C_{1,8}$), 124.27 (s, 2 C, $C_{2,7}$), 124.35 (s, 2 C, $C_{8a,9a}$), 125.27 (s, 2 C, $C_{3,6}$), 128.53 (s, 2 C, $C_{4,5}$), 131.92 (s, 2 C, $C_{4a,10a}$), 136.66 (s, 1 C, C_{14}), 142.35 (s, 1 C, C_9), 148.83 (s, 1 C, C_{16}), 159.42 (s, 1 C, C_{12}).

EI-MS

m/z (%): 284 (87) $[M]^+$, 192 (100) $[M\text{-}C_6H_6N]^+$, 165 (31) $[C_{13}H_9]^+$.

Elemental analysis

in % (calculated) C: 84.00 (84.48), H: 5.39 (5.67), N: 9.87 (9.85).

4.4.14 Synthesis of *o*-(*β*-hydroxyethoxy)benzaldehyde (17)

To a solution of sodium hydroxide (1.00 eq., 13.5 mmol, 0.54 g) in 13.5 mL degased water salicylaldehyde (1.00 eq., 13.5 mmol, 1.41 mL) was added drop wise over a period of 15 min under inert conditions. Also 2-chloroethanol (1.00 eq., 13.5 mmol, 0.91 mL) was added drop wise and the reaction mixture was stirred at 100 °C for 16 h.

After cooling to room temperature a solution of sodium hydroxide was added up to a pH of 10. The aqueous solution was extracted 4-times with DCM (15 mL each), the organic layers were combined and dried with magnesium sulfate. The filtration was followed by removal of volatile components under reduced pressure and the crude reaction product was purified via column chromatography of petroleum ether and ethylacetate (10:1 → 1.1). **17** was isolated as light yellow oil.

Molecular formula: $C_9H_{10}O_3$

Molecular weight: 166.17 g/mol

Yield: 0.95 g (5.74 mmol, 42 %).

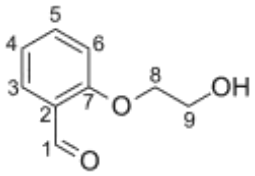

^{1}H-NMR

(300 MHz, DMSO-d^6): δ /ppm = 3.78 (q, $^3J_{HH}$ = 5.2 Hz, 2 H, H_9), 4.15 (t, $^3J_{HH}$ = 5.2 Hz, 2 H, H_8), 4.97 (t, $^3J_{HH}$ = 5.2 Hz, 1 H, OH), 7.06 (d, $^3J_{HH}$ = 7.5 Hz, 1 H, H_4), 7.22 (d, $^3J_{HH}$ = 8.4 Hz, 1 H, H_6), 7.59-7.72 (m, 2 H, $H_{3,5}$), 10.46 (s, 1 H, H_1).

^{13}C{^{1}H}-NMR

(75 MHz, DMSO-d^6): δ /ppm = 59.47 (s, 1 C, C_9), 70.56 (s, 1 C, C_8), 113.75 (s, 1 C, C_6), 120.64 (s, 1 C, C_4), 124.42 (s, 1 C, C_2), 127.28 (s, 1 C, C_3), 136.35 (s, 1 C, C_5), 161.25 (s, 1 C, C_7), 189.73 (s, 1 C, C_1).

EI-MS

m/z (%): 166 (12) $[M]^+$, 192 (47) $[M\text{-}H_2O]^+$, 121 (100) $[M\text{-}C_2H_5OH]^+$, 105 (18) $[M\text{-}OC_2H_5OH]^+$, 77 (21) $[C_6H_5]^+$.

4.4.15 Synthesis of 9-anthracene(*o*-(*β*-hydroxyethoxy)benzyl)-imine (18)

To a suspension of **11** (1.00 eq., 5.28 mmol, 1.02 g) in 5 mL ethanol a solution of **17** (2.46 eq., 13.0 mmol, 2.16 g) in 5 mL ethanol was added under inert atmosphere. The reaction mixture was stirred while heated to 78 ° over 19 h. Afterwards the reaction flask was cooled at -33 °C for 3 d and the crystallized solid was filtered under inert atmosphere, washed with cooled ethanol (three times 4 mL) and dried under reduced pressure.

The crystalline solid was dissolved in 12 mL ethylacetate and the volatile components were removed under reduced pressure. The crude product was recrystallized from hexane (20 mL) and ethylacetate (1 mL) to result in the yellow solid **18**.

Molecular formula: $C_{23}H_{19}NO_2$

Molecular weight: 341.40 g/mol

Yield: 1.11 g (3.25 mmol, 61 %).

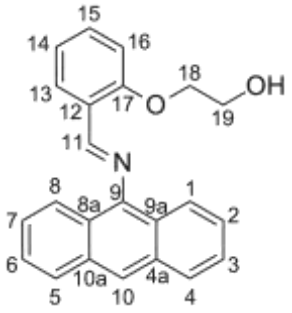

^{1}H-NMR

(300 MHz, DMSO-d^6): δ /ppm = 3.63 (q, $^3J_{HH}$ = 5.2 Hz, 2 H, H_{19}), 4.09 (t, $^3J_{HH}$ = 5.2 Hz, 2 H, H_{18}), 4.80 (t, $^3J_{HH}$ = 5.2 Hz, 1 H, OH), 7.17-7.26 (m, 2 H, $H_{14,16}$), 7.42-7.56 (m, 4 H, $H_{2,3,6,7}$), 7.62 (t, $^3J_{HH}$ = 7.9 Hz, 1 H, H_{15}), 7.93 (d, $^3J_{HH}$ = 8.6 Hz, 2 H, $H_{1,8}$), 8.09 (d, $^3J_{HH}$ = 8.3 Hz, 2 H, $H_{4,5}$), 8.35-8.40 (m, 2 H, $H_{10,13}$), 9.01 (s, 1 H, H_{11}).

^{13}C{^{1}H}-NMR

(75 MHz, DMSO-d^6): δ /ppm = 59.39 (s, 1 C, C_{19}), 70.42 (s, 1 C, C_{18}), 113.24 (s, 1 C, C_{16}), 120.92 (s, 1 C, C_{14}), 121.42 (s, 1 C, C_{10}), 121.57 (s, 2 C, $C_{8a,9a}$), 123.59 (s, 2 C, $C_{1,8}$), 123.74 (s, 1 C, C_{12}), 125.19 (s, 2 C, $C_{2,7}$), 125.69 (s, 2 C, $C_{3,6}$), 126.98 (s, 1 C, C_{13}), 128.13 (s, 2 C, $C_{4,5}$), 131.40 (s, 2 C, $C_{4a,10a}$), 133.83 (s, 1 C, C_{15}), 146.30 (s, 1 C, C_9), 159.15 (s, 1 C, C_{17}), 161.50 (s, 1 C, C_{11}).

EI-MS

m/z (%): 341 (98) $[M]^+$, 296 (29) $[M\text{-}C_2H_5OH]^+$, 193 (100) $[C_{14}H_{11}N]^+$, 119 (44) $[C_7H_5NO]^+$.

Elemental analysis

in % (calculated) C: 79.75 (80.92), H: 5.30 (5.61), N: 3.81 (4.10).

4.4.16 Synthesis of 9-anthracene(*o*-(*β*-hydroxyethoxy)benzyl)-amine (19)

To a suspension of $LiAlH_4$ (5.00 eq., 8,05 mmol, 306 mg) in THF (26 mL) a solution of **18** (1.00 eq., 1,61 mmol, 0.55 g) in THF (26 mL) was added drop wise. The reaction mixture was stirred for 18 h at room temperature under inert atmosphere.

The volatile components were removed under reduced pressure and ethylacetate (15 mL) and water (15 mL) were added. The insoluble constituents were filtered off and washed with ethylacetate and water followed by phase separation. After extraction of the aqueous phase with ethylacetate the combined organic layers were dried with magnesium sulfate, filtered and the volatile components were removed under reduced pressure.

The crude product was recrystallized from hexane (10 mL) and ethylacetate (10 mL) to isolate the orange solid **19**.

Molecular formula: $C_{23}H_{21}NO_2$

Molecular weight: 343.42 g/mol

Yield: 0.19 g (0.55 mmol, 34 %).

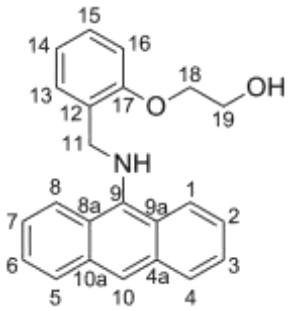

^{1}H-NMR

(300 MHz, DMSO-d^{6}): δ /ppm = 3.75 (q, $^{3}J_{HH}$ = 5.2 Hz, 2 H, H_{19}), 4.05 (t, $^{3}J_{HH}$ = 5.2 Hz, 2 H, H_{18}), 4.44 (d, $^{3}J_{HH}$ = 7.4 Hz, 2 H, H_{11}), 4.92 (t, $^{3}J_{HH}$ = 5.2 Hz, 1 H, OH), 5.60 (t, $^{3}J_{HH}$ = 7.4 Hz, 1 H, NH), 6.87 (td, $^{3}J_{HH}$ = 7.8 Hz, $^{4}J_{HH}$ = 0.9 Hz, 1 H, H_{14}), 7.00 (d, $^{3}J_{HH}$ = 7.8 Hz, 1 H, H_{16}), 7.23 (td, $^{3}J_{HH}$ = 7.8 Hz, $^{4}J_{HH}$ = 1.5 Hz, 1 H, H_{15}), 7.37 (d, $^{3}J_{HH}$ = 7.8 Hz, 1 H, H_{13}), 7.38-7.49 (m, 4 H, $H_{2,3,6,7}$), 8.00 (d, $^{3}J_{HH}$ = 7.1 Hz, 2 H, $H_{4,5}$), 8.16 (s, 1 H, H_{10}), 8.38 (d, $^{3}J_{HH}$ = 8.2 Hz, 2 H, $H_{1,8}$).

^{13}C{^{1}H}-NMR

(75 MHz, DMSO-d^{6}): δ /ppm = 50.76 (s, 1 C, C_{11}), 59.63 (s, 1 C, C_{19}), 69.72 (s, 1 C, C_{18}), 111.46 (s, 1 C, C_{16}), 120.12 (s, 1 C, C_{10}), 120.18 (s, 1 C, C_{14}), 123.73 (s, 2 C, $C_{1,8}$), 124.27 (s, 2 C, $C_{2,7}$), 124.97 (s, 2 C, $C_{8a,9a}$), 125.24 (s, 2 C, $C_{3,6}$), 128.32 (s, 2 C, $C_{12,15}$), 128.46 (s, 2 C, $C_{4,5}$), 129.11 (s, 1 C, C_{13}), 131.87 (s, 2 C, $C_{4a,10a}$), 142.47 (s, 1 C, C_{9}), 156.56 (s, 1 C, C_{17}),

EI-MS

m/z (%): 343 (100) $[M]^{+}$, 192 (58) $[M\text{-}CH_2C_6H_4OC_2H_4OH]^{+}$, 165 (24) $[C_{13}H_9]^{+}$, 151 (22) $[CH_2C_6H_4OC_2H_4OH]^{+}$, 133 (43) $[CH_2C_6H_4OC_2H_3]^{+}$ 107 (27) $[CH_2C_6H_4OH]^{+}$.

Elemental analysis

in % (calculated) C: 78.83 (80.44), H: 6.14 (6.16), N: 3.88 (4.08).

5 Supplement

5.1 Fluorescence information

5.1.1 Solubility of metal salts

As described in chapter 2.1.8.1, the solubility of different metal bromides in various organic solvents was investigated. Therefore 0.01 M solutions of the metal salts should be prepared. The results are shown in Table 5-1 and Table 5-2. The results for lithium, cobalt and zinc bromide were determined less accurate because of their hygroscopic behavior.

Table 5-1: Solubility of several metal salts in different solvents.

+: Completely soluble; —: Not completely soluble.

	H_2O	**MeOH**	**MeCN**	**THF**	**DCM**
LiBr	+	+	+	+	+
NaBr	+	+	—	—	—
KBr	+	+	—	—	—
$MgBr_2$	+	+	—	—	—
$FeBr_2$	+	+	—	+	—
$CoBr_2$	+	+	+	+	+
CuBr	—	—	+	—	—
$CuBr_2$	+	+	+	—	—
$ZnBr_2$	+	+	+	+	+
AgBr	—	—	—	—	—
$HgBr_2$	—	+	+	+	—

Table 5-2: Solubility of several metal salts in different solvents.

+: Completely soluble; —: Not completely soluble.

	DMSO	EtOH
NaBr	+	+
KBr	+	—
$MgBr_2$	+	+
$CuBr_2$	+	+
AgBr	—	—

5.1.2 Excitation and emission spectra of anthraquinone

For comparison, the excitation and emission properties of a common impurity and oxidation product in anthracene chemistry, namely anthraquinone, was measured.

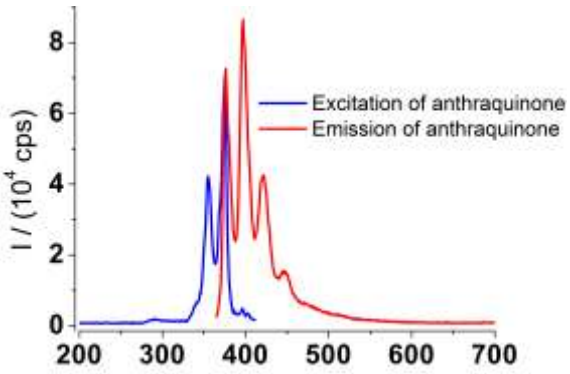

Figure 5-1: Excitation (blue, λ_{det} = 421 nm) and emission (red, λ_{ex} = 355 nm) spectra of anthraquinone in MeOH.

5.1.3 Further luminescence properties of 2',5',8'-tris(*β*-trimethylsilyl-ethanesulfonyl)-2',5',8'-triaza[9](9,10)anthracenophane (8)

Detailed information about the wavelength dependent fluorescence intensity of **8** after addition of metal bromides (summarized in Figure 2-9) are presented in this chapter.

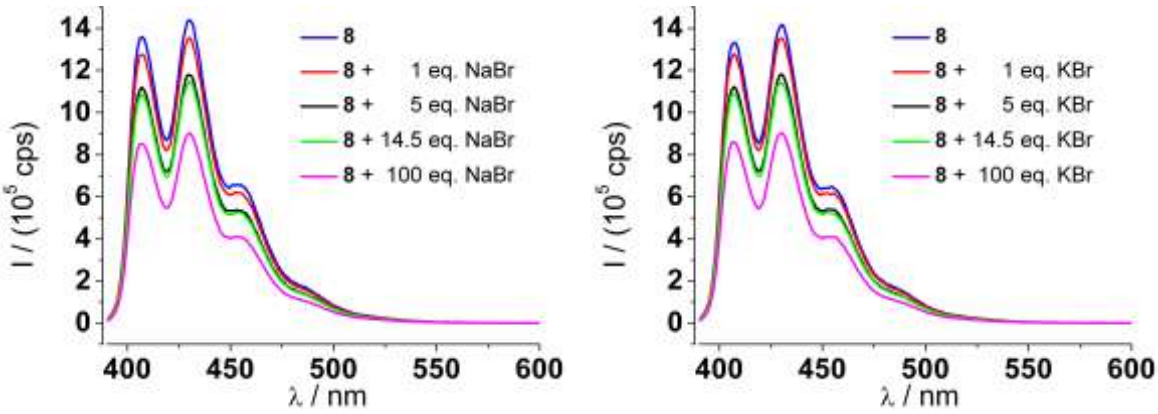

Figure 5-2: Emission properties of **8** after addition of sodium bromide (left) and potassium bromide (right) (10^{-5} M in MeOH, λ_{ex} = 380 nm).

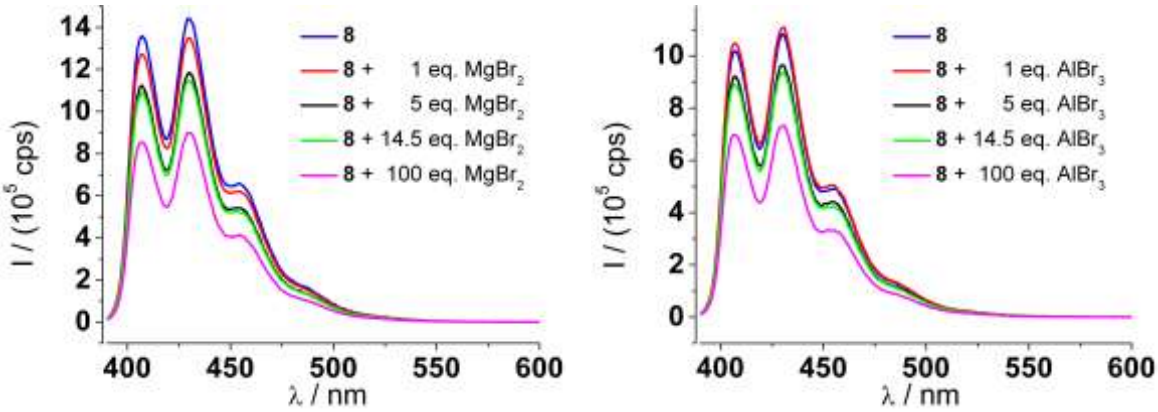

Figure 5-3: Emission properties of **8** after addition of magnesium bromide (left) and aluminum bromide (right) (10^{-5} M in MeOH, λ_{ex} = 380 nm).

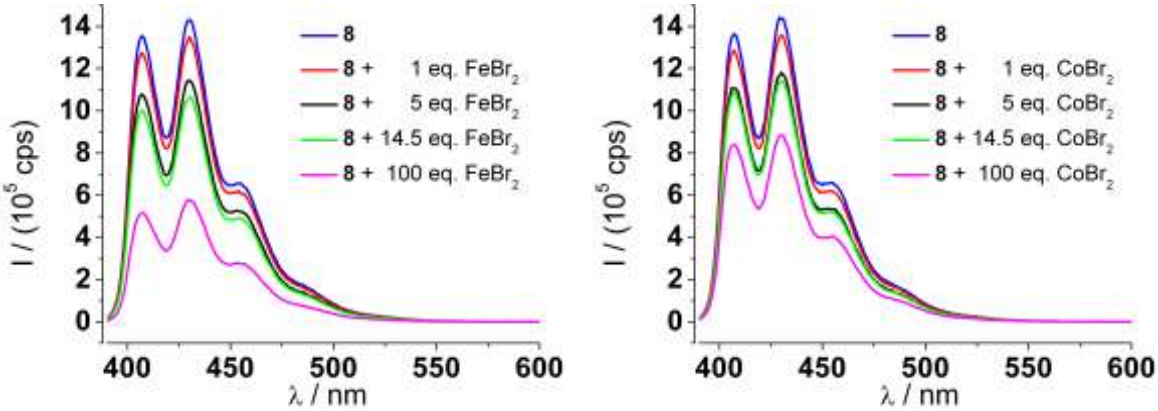

Figure 5-4: Emission properties of **8** after addition of iron bromide (left) and cobalt bromide (right) (10^{-5} M in MeOH, λ_{ex} = 380 nm).

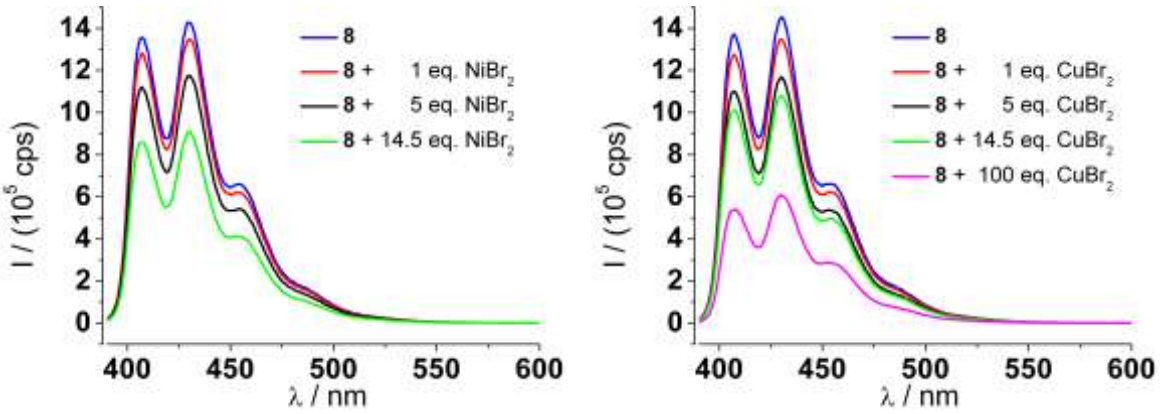

Figure 5-5: Emission properties of **8** after addition of nickel bromide (left) and copper bromide (right) (10^{-5} M in MeOH, λ_{ex} = 380 nm).

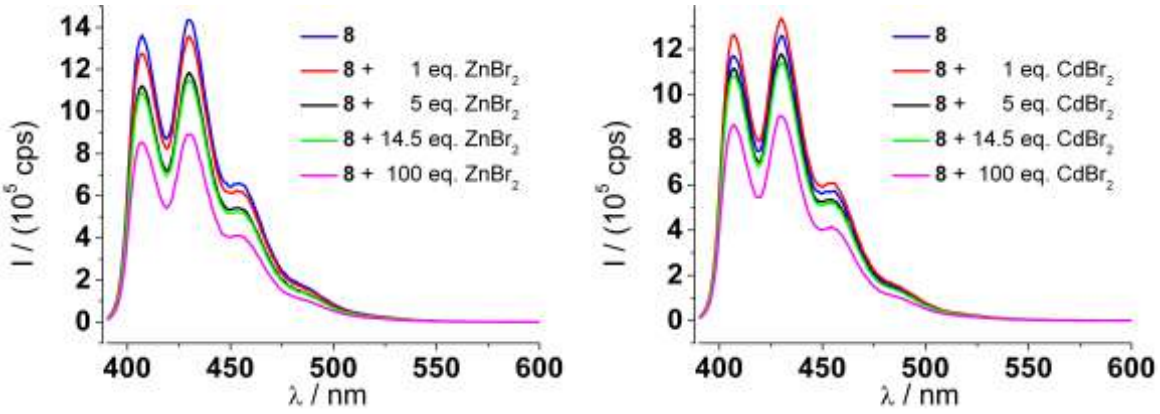

Figure 5-6: Emission properties of **8** after addition of zinc bromide (left) and cadmium bromide (right) (10^{-5} M in MeOH, λ_{ex} = 380 nm).

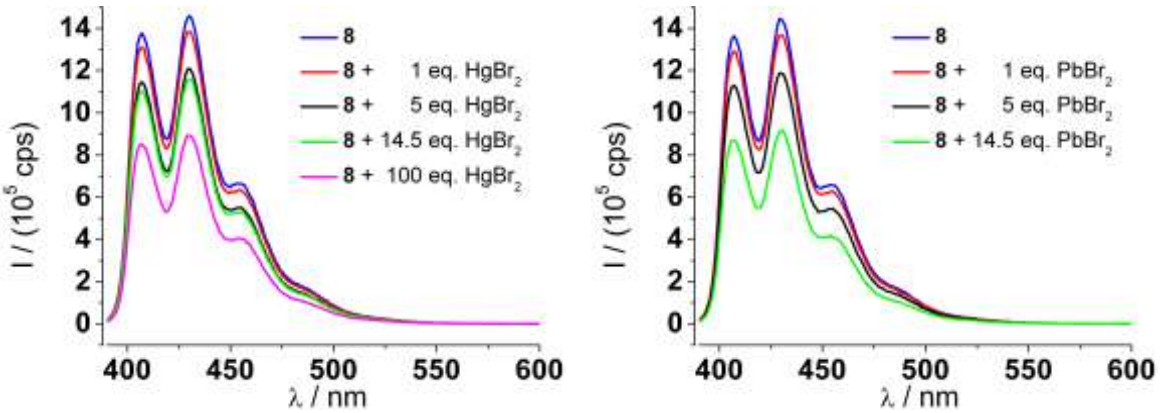

Figure 5-7: Emission properties of **8** after addition of mercury bromide (left) and lead bromide (right) (10^{-5} M in MeOH, λ_{ex} = 380 nm).

5.1.4 Lifetime measurement of 9-aminoanthracene (11)

The experimental results shown in Figure 5-8 were obtained during a workshop of the company HORIBA SCIENTIFIC in Essen 2014 and were measured at an exhibited spectrometer (DeltaFlex series).

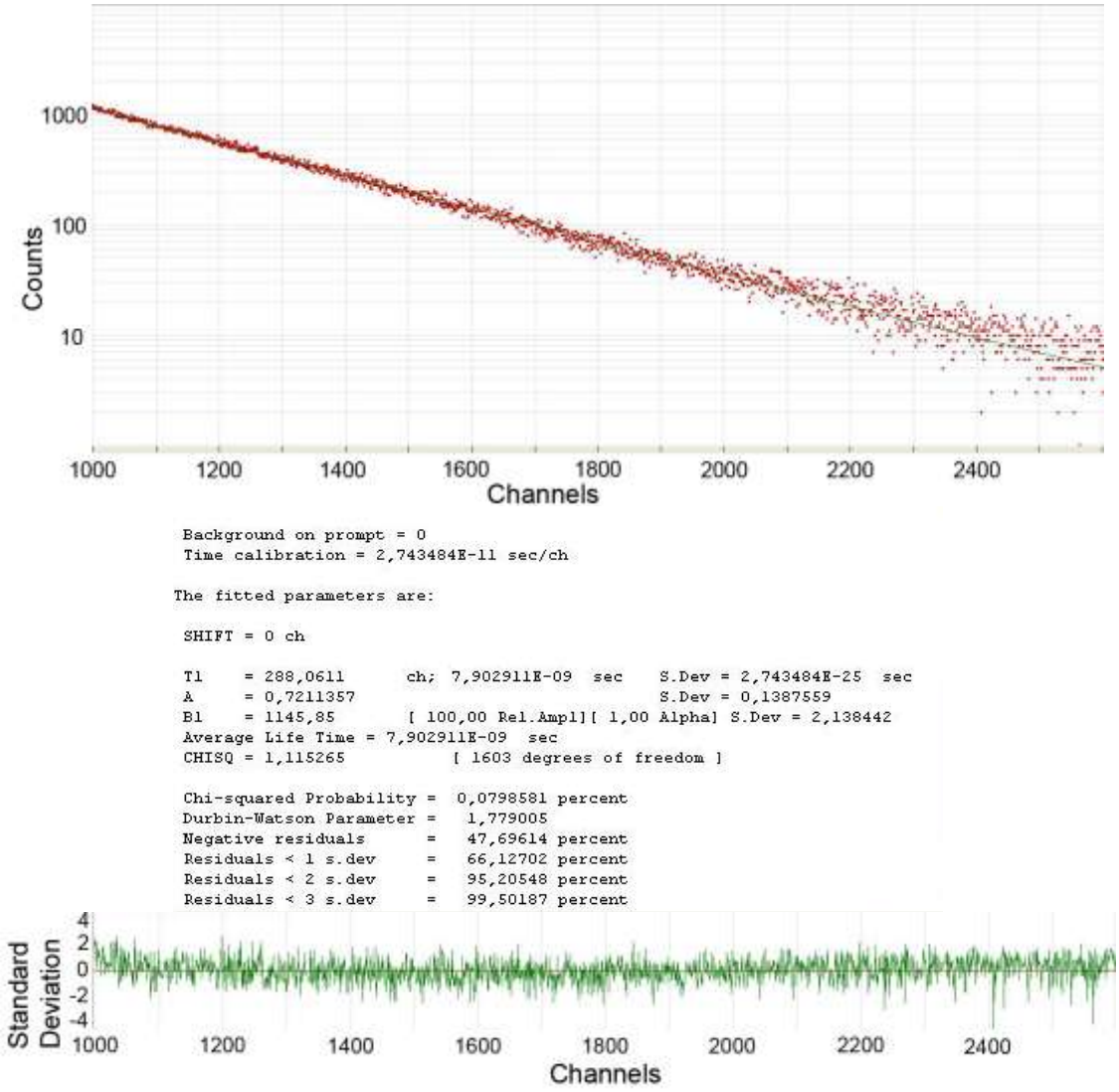

Figure 5-8: Lifetime measurement of **11** (10^{-5} M in MeOH).

5.1.5 Further luminescence properties of 9-anthracenesalicylimine (12)

Detailed information about the wavelength dependent fluorescence intensity of **12** after addition of metal bromides (summarized in Figure 2-30) are presented in this chapter.

Additionally, the behavior of **12** towards metal bromides after a previous addition of sodium hydroxide in two different concentrations is displayed in Figure 5-15 (cf. Figure 2-32) and Figure 5-16 (cf. Figure 2-33).

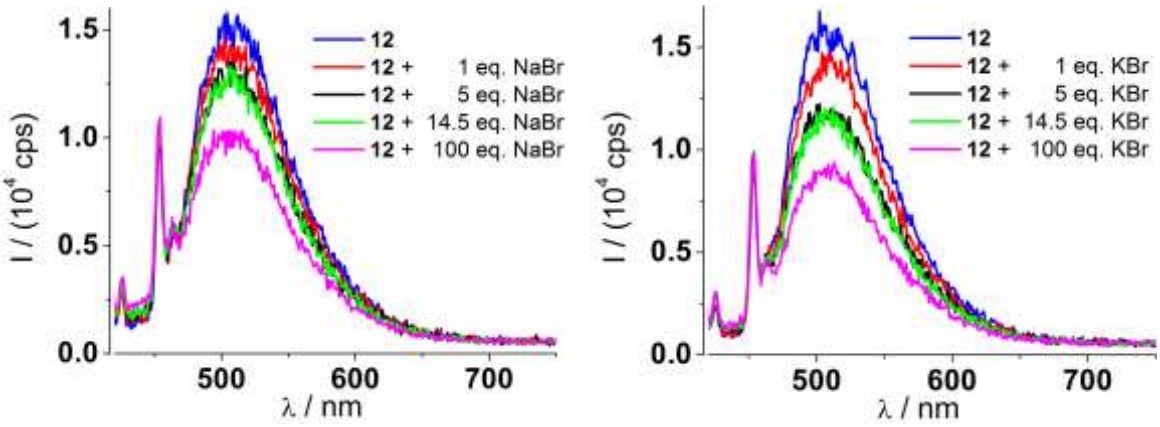

Figure 5-9: Emission properties of **12** after addition of sodium bromide (left) and potassium bromide (right) (10^{-5} M in MeOH, λ_{ex} = 400 nm).

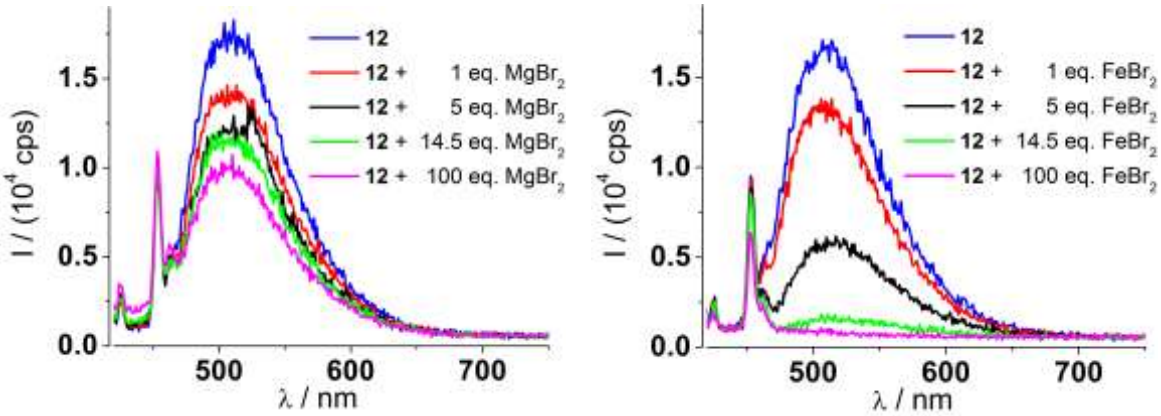

Figure 5-10: Emission properties of **12** after addition of magnesium bromide (left) and iron bromide (right) (10^{-5} M in MeOH, λ_{ex} = 400 nm).

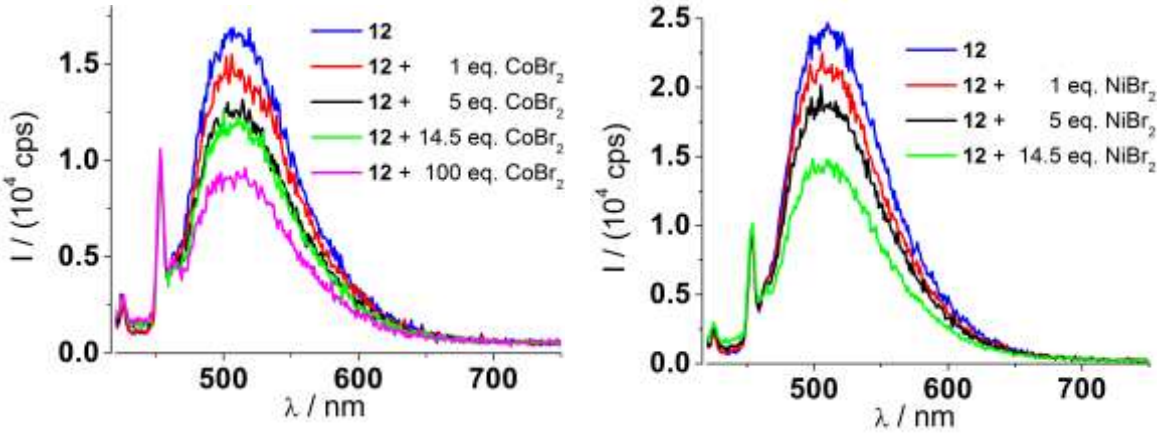

Figure 5-11: Emission properties of **12** after addition of cobalt bromide (left) and nickel bromide (right) (10^{-5} M in MeOH, λ_{ex} = 400 nm).

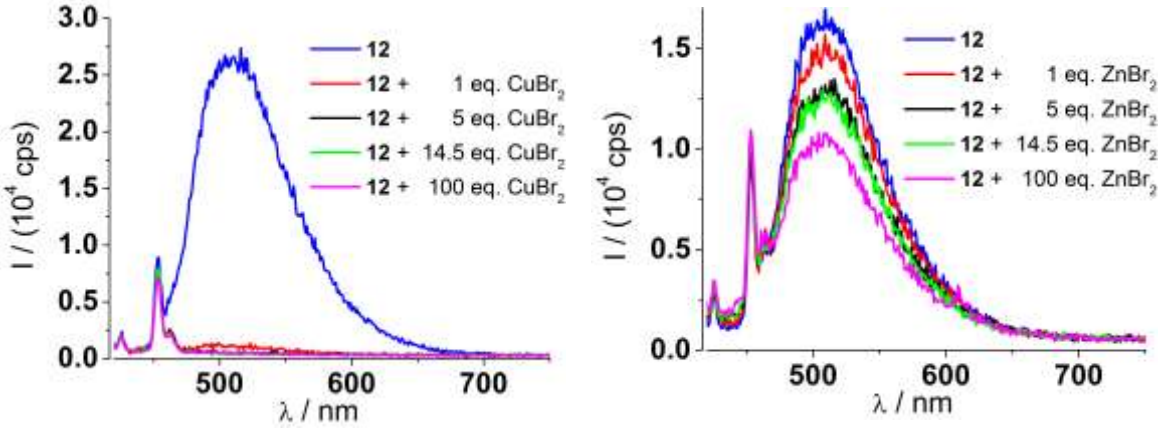

Figure 5-12: Emission properties of **12** after addition of copper bromide (left) and zinc bromide (right) (10^{-5} M in MeOH, λ_{ex} = 400 nm).

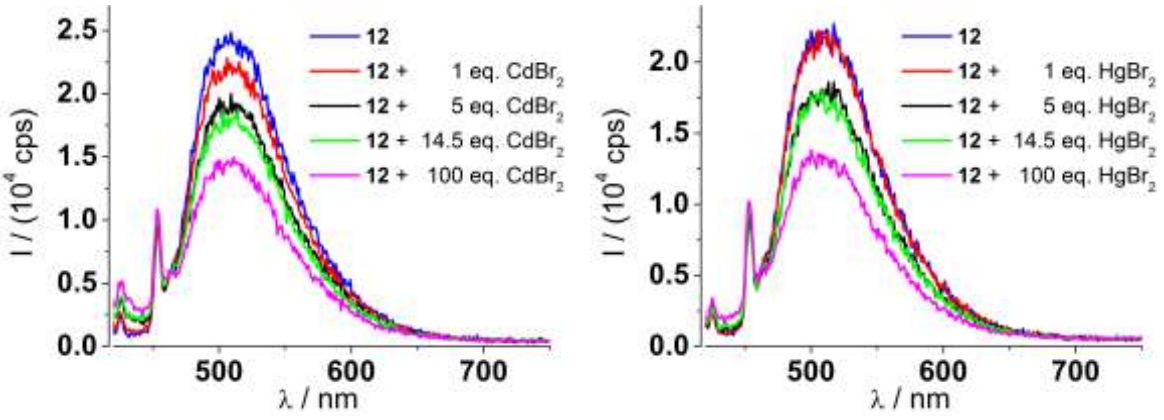

Figure 5-13: Emission properties of **12** after addition of cadmium bromide (left) and mercury bromide (right) (10^{-5} M in MeOH, λ_{ex} = 400 nm).

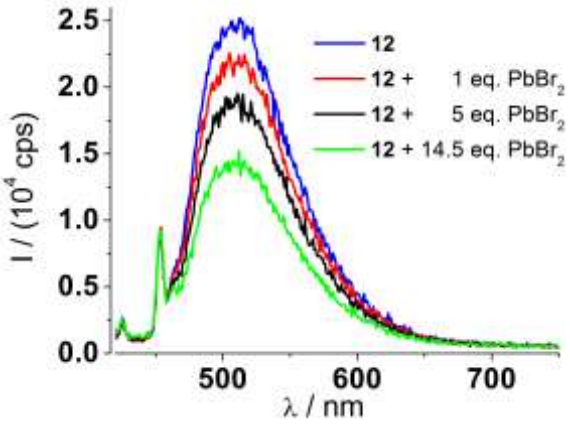

Figure 5-14: Emission properties of **12** after addition of led bromide (10^{-5} M in MeOH, λ_{ex} = 400 nm).

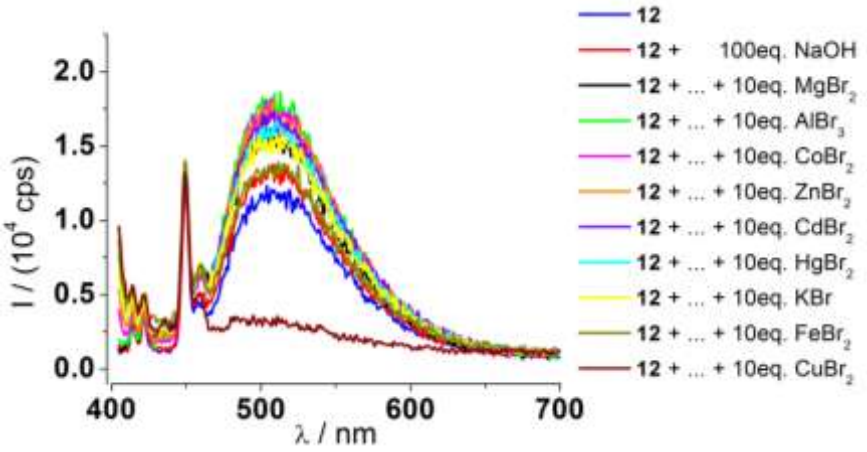

Figure 5-15: Stacked spectra of **12** before and after successive addition of 100 eq. NaOH and several metal bromides in MeOH (10^{-5} M, λ_{ex} = 397 nm).

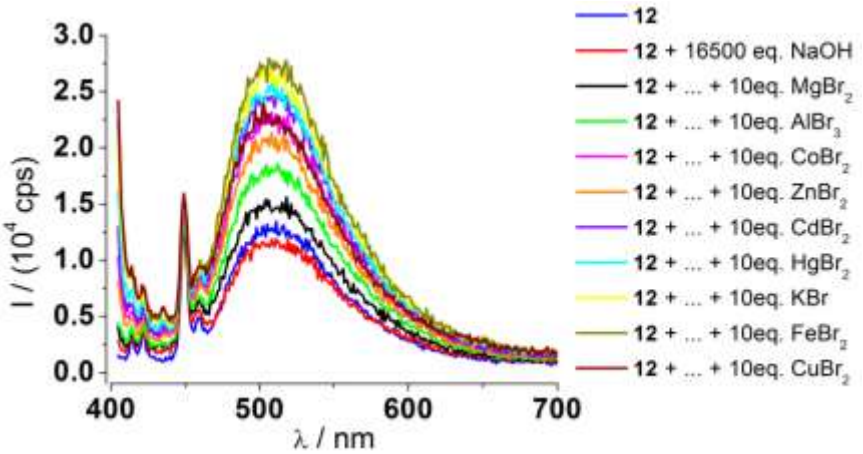

Figure 5-16: Stacked spectra of **12** before and after successive addition of 16500 eq. NaOH and several metal bromides in MeOH (10^{-5} M, λ_{ex} = 397 nm).

5.1.6 Further luminescence properties of 9-anthracenepicolylimine (13)

Detailed information about the wavelength dependent fluorescence intensity of **13** after addition of metal bromides (summarized in Figure 2-39) are presented in this chapter.

Additionally, time dependent changes of **13** with hydrochloric acid (Figure 5-17 left) and aluminum bromide (Figure 5-17 right) are displayed.

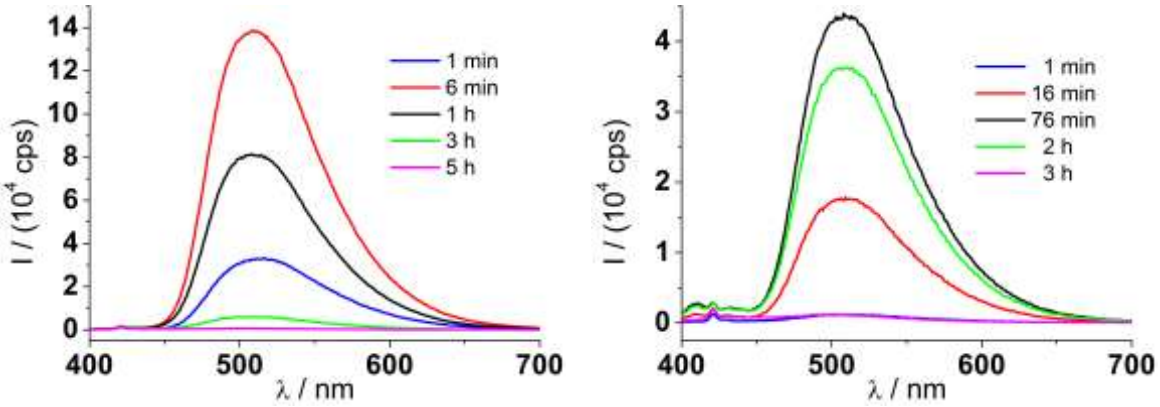

Figure 5-17: Emission spectra of **13** after addition of 10 eq. HCl (left) and 10 eq. $AlBr_3$ (right) (λ_{ex} = 375 nm).

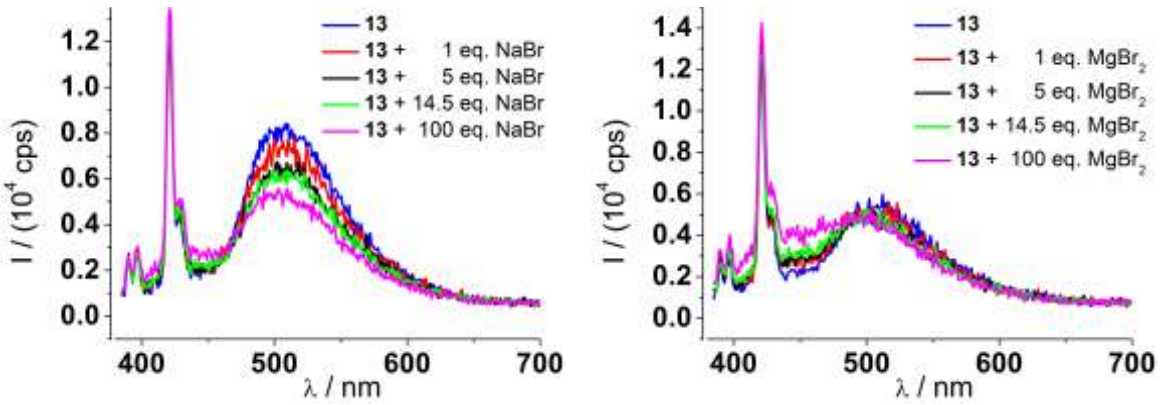

Figure 5-18: Emission properties of **13** after addition of sodium bromide (left) and magnesium bromide (right) (10^{-5} M in MeOH, λ_{ex} = 375 nm).

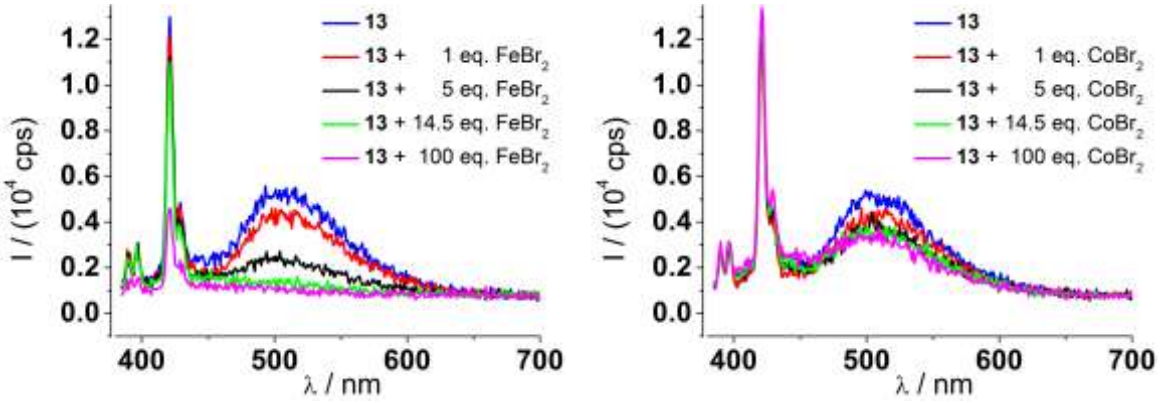

Figure 5-19: Emission properties of **13** after addition of iron bromide (left) and cobalt bromide (right) (10^{-5} M in MeOH, λ_{ex} = 375 nm).

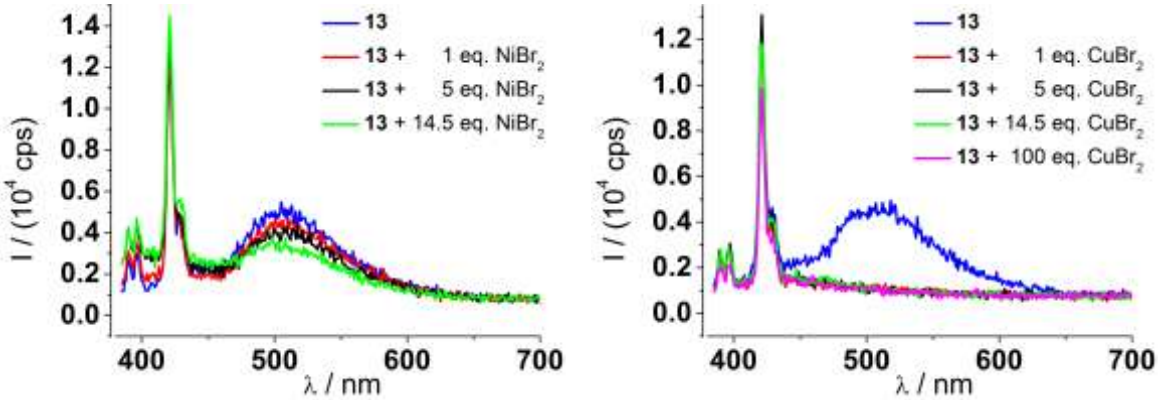

Figure 5-20: Emission properties of **13** after addition of nickel bromide (left) and copper bromide (right) (10^{-5} M in MeOH, λ_{ex} = 375 nm).

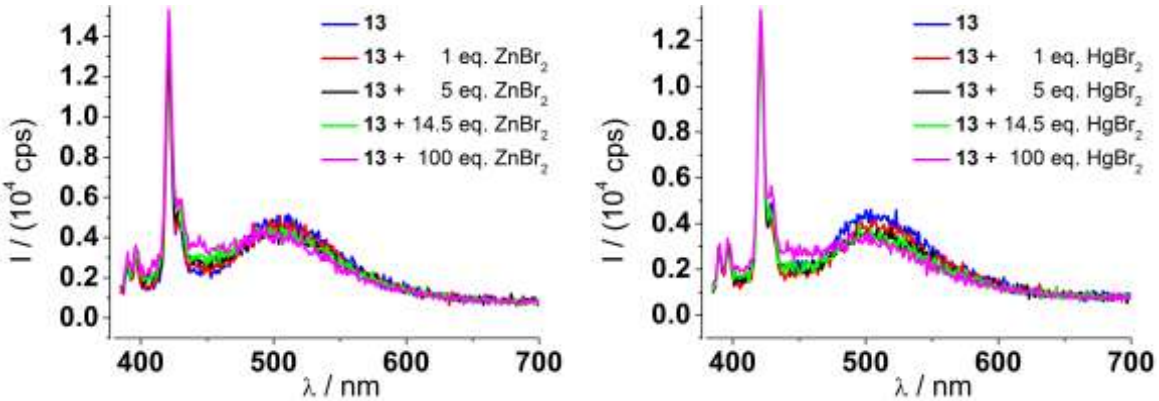

Figure 5-21: Emission properties of **13** after addition of zinc bromide (left) and mercury bromide (right) (10^{-5} M in MeOH, λ_{ex} = 375 nm).

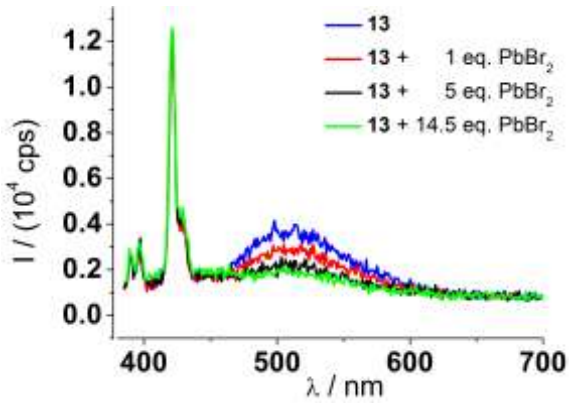

Figure 5-22: Emission properties of **13** after addition of lead bromide (10^{-5} M in MeOH, λ_{ex} = 375 nm).

5.1.7 Further luminescence properties of 9-anthracene-(*α*-methyl-picolyl)imine (14)

Detailed information about the wavelength dependent fluorescence intensity of **14** after addition of metal bromides (summarized in Figure 2-46) are presented in this chapter.

Additionally, time dependent changes of **14** with hydrochloric acid (Figure 5-23 left and Figure 5-24 left) and aluminum bromide (Figure 5-24 right) are displayed as well as the stability of **14** after 3 days (Figure 5-23 right).

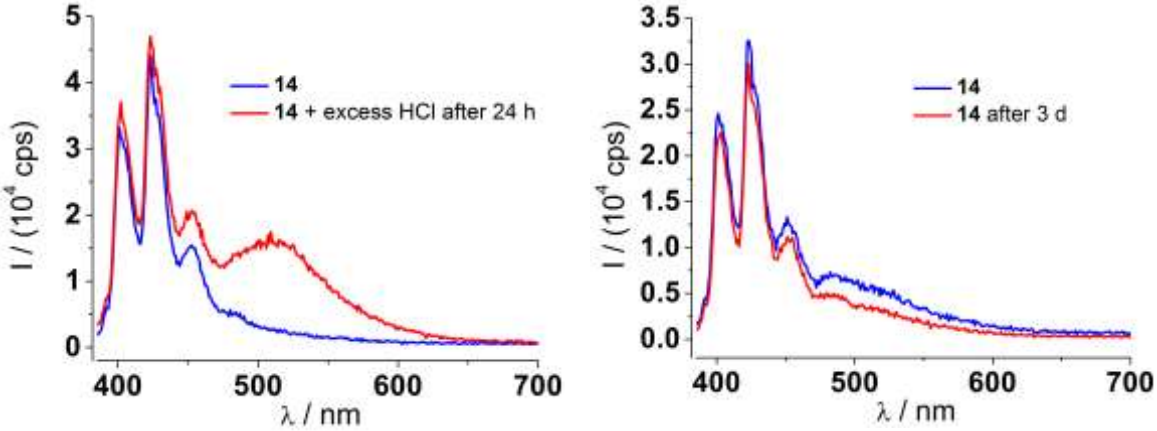

Figure 5-23: Emission spectra of **14** before and after reacting with an excess of HCl for 24 h (left, λ_{ex} = 376 nm) and emission of **14** before and after a period of 3 days(right, λ_{ex} = 376 nm).

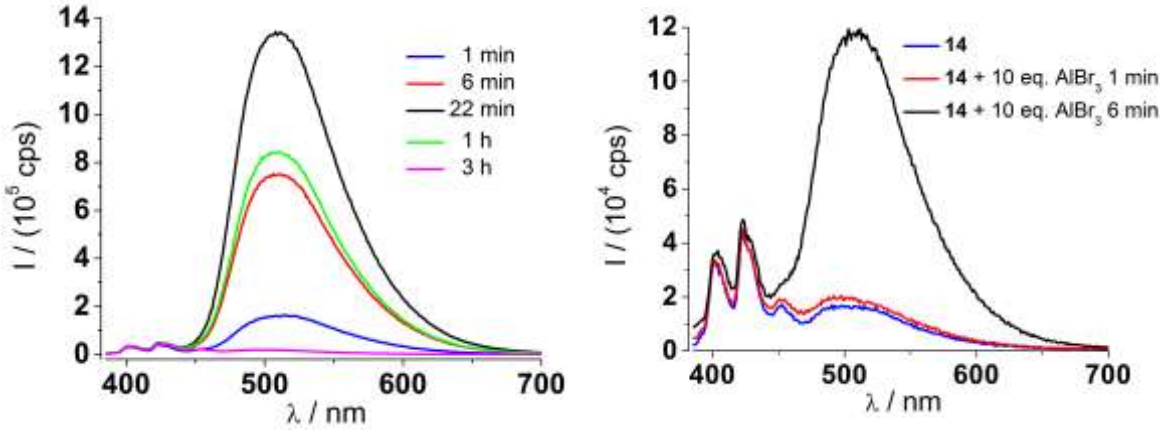

Figure 5-24: Emission spectra of **14** after addition of 10 eq. HCl (left) and 10 eq. $AlBr_3$ (right) (λ_{ex} = 376 nm).

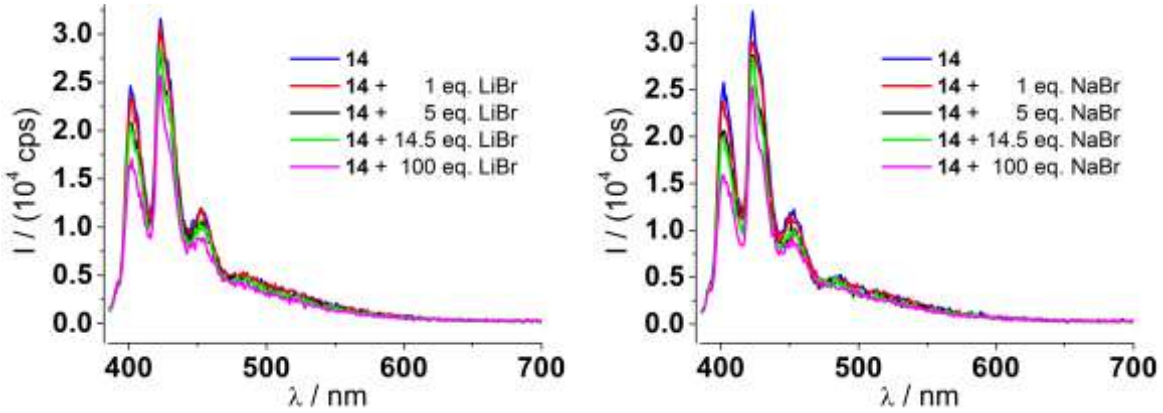

Figure 5-25: Emission properties of **14** after addition of lithium bromide (left) and sodium bromide (right) (10^{-5} M in MeOH, λ_{ex} = 376 nm).

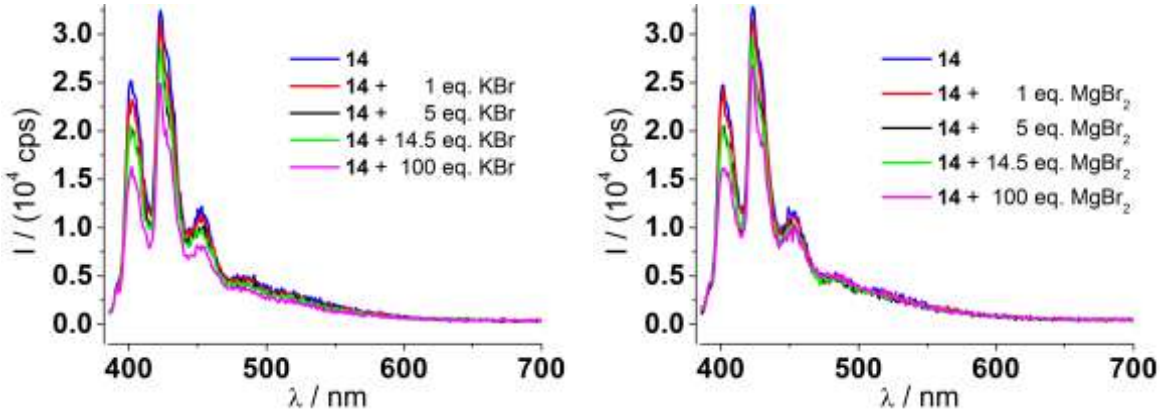

Figure 5-26: Emission properties of **14** after addition of potassium bromide (left) and magnesium bromide (right) (10^{-5} M in MeOH, λ_{ex} = 376 nm).

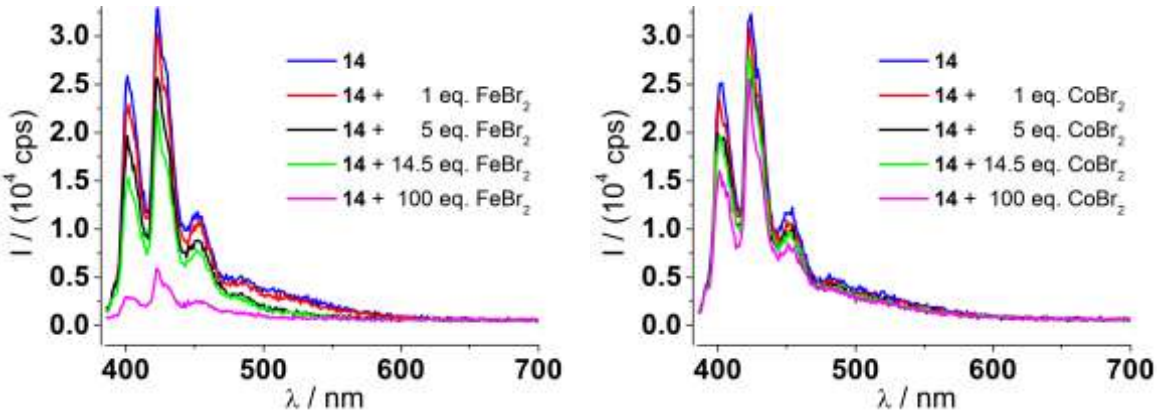

Figure 5-27: Emission properties of **14** after addition of iron bromide (left) and cobalt bromide (right) (10^{-5} M in MeOH, λ_{ex} = 376 nm).

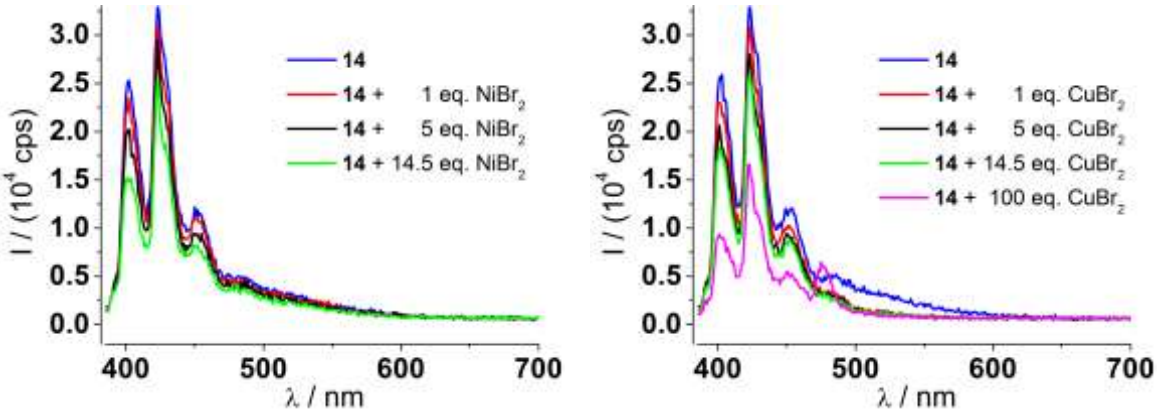

Figure 5-28: Emission properties of **14** after addition of nickel bromide (left) and copper bromide (right) (10^{-5} M in MeOH, λ_{ex} = 376 nm).

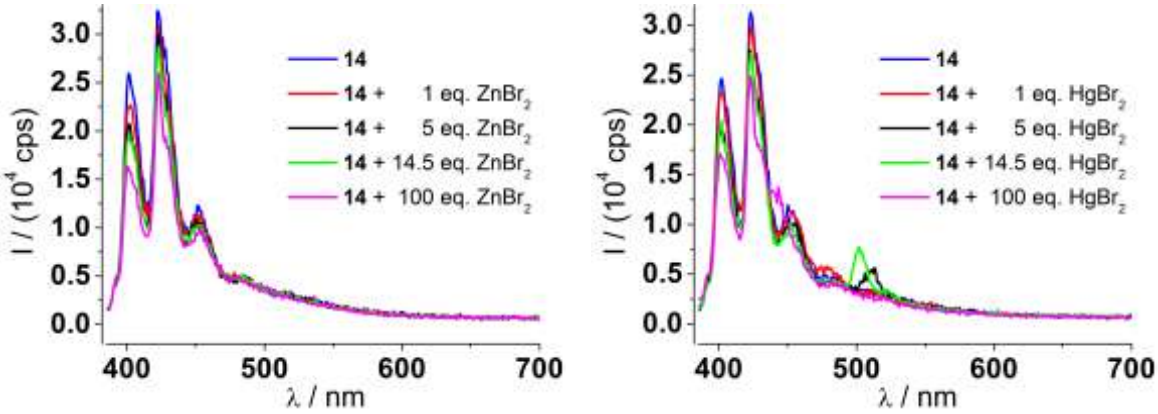

Figure 5-29: Emission properties of **14** after addition of zinc bromide (left) and mercury bromide (right) (10^{-5} M in MeOH, λ_{ex} = 376 nm).

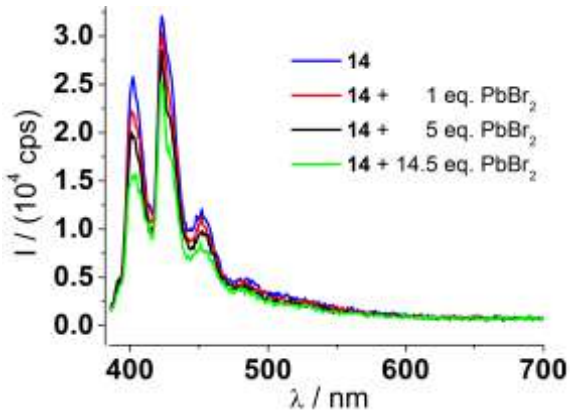

Figure 5-30: Emission properties of **14** after addition of lead bromide (10^{-5} M in MeOH, λ_{ex} = 376 nm).

5.1.8 Further luminescence properties of 9-anthracenesalicylamine (15)

Detailed information about the wavelength dependent fluorescence intensity of **15** after addition of metal bromides (summarized in Figure 2-53) are presented in this chapter.

Additionally, the stability of **15** as well as its protonated counterpart is shown in Figure 5-31.

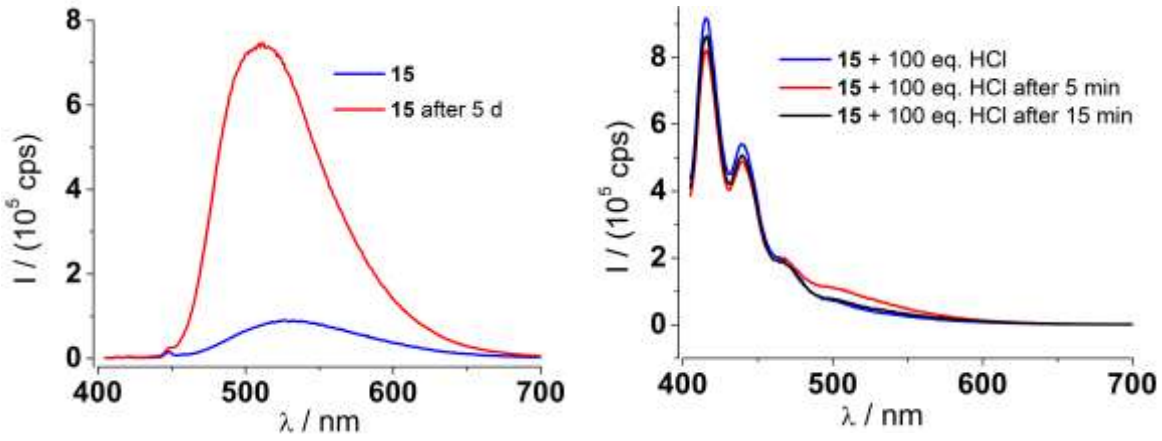

Figure 5-31: Emission spectra of **15** before and after a period of 5 days (left, λ_{ex} = 396 nm) and emission of **15** in the presence of HCl over 15 minutes (right, λ_{ex} = 396 nm).

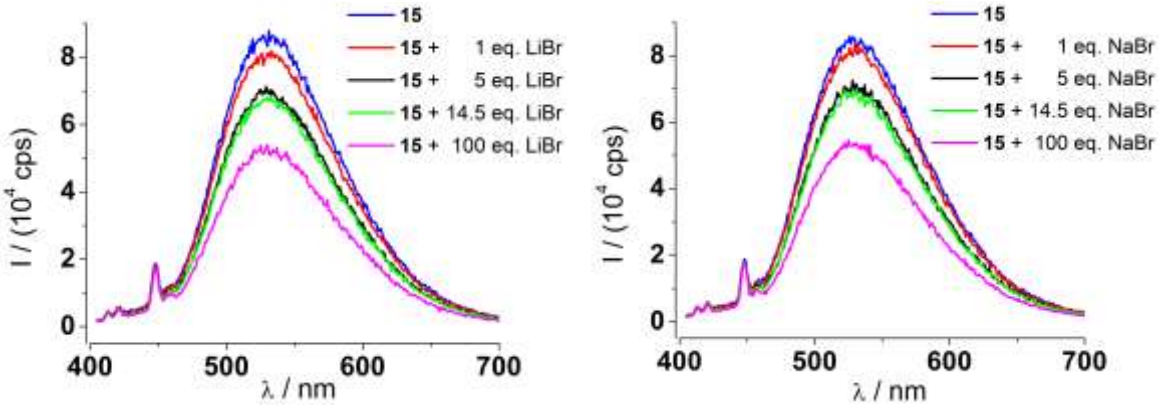

Figure 5-32: Emission properties of **15** after addition of lithium bromide (left) and sodium bromide (right) (10^{-5} M in MeOH, λ_{ex} = 396 nm).

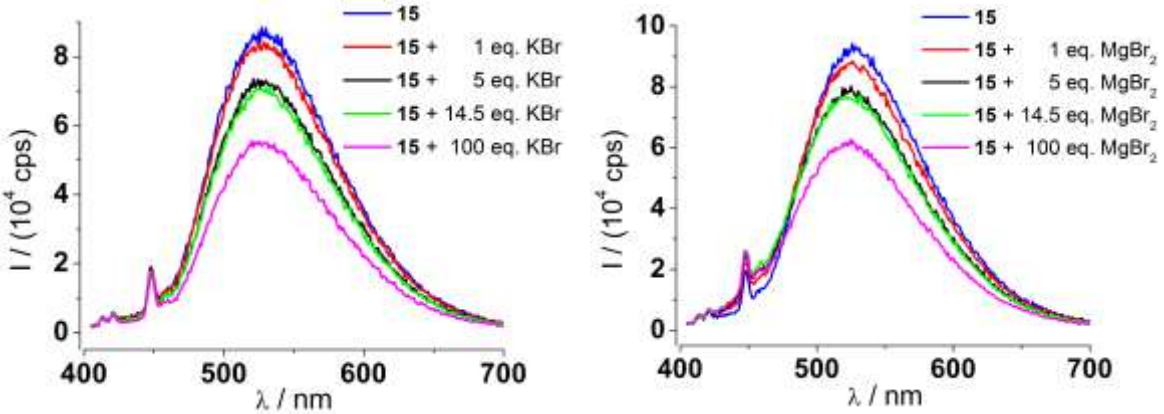

Figure 5-33: Emission properties of **15** after addition of potassium bromide (left) and magnesium bromide (right) (10^{-5} M in MeOH, λ_{ex} = 396 nm).

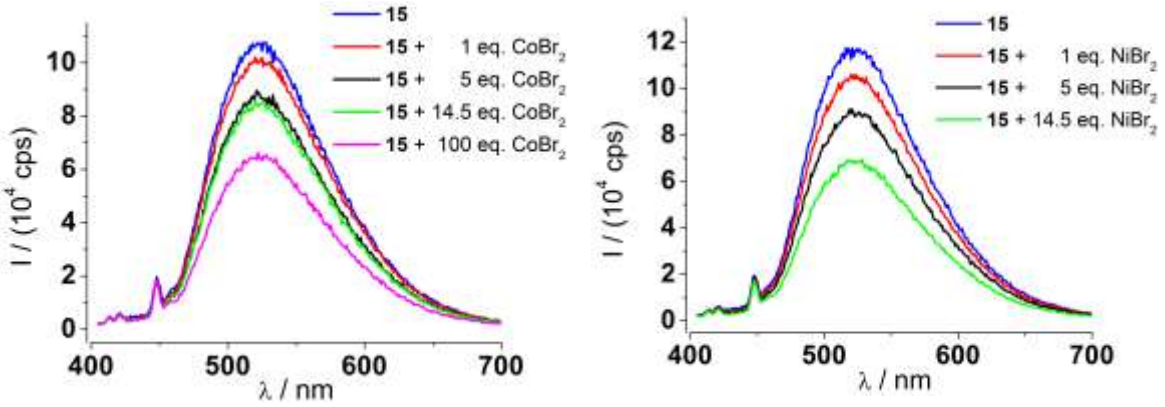

Figure 5-34: Emission properties of **15** after addition of cobalt bromide (left) and nickel bromide (right) (10^{-5} M in MeOH, λ_{ex} = 396 nm).

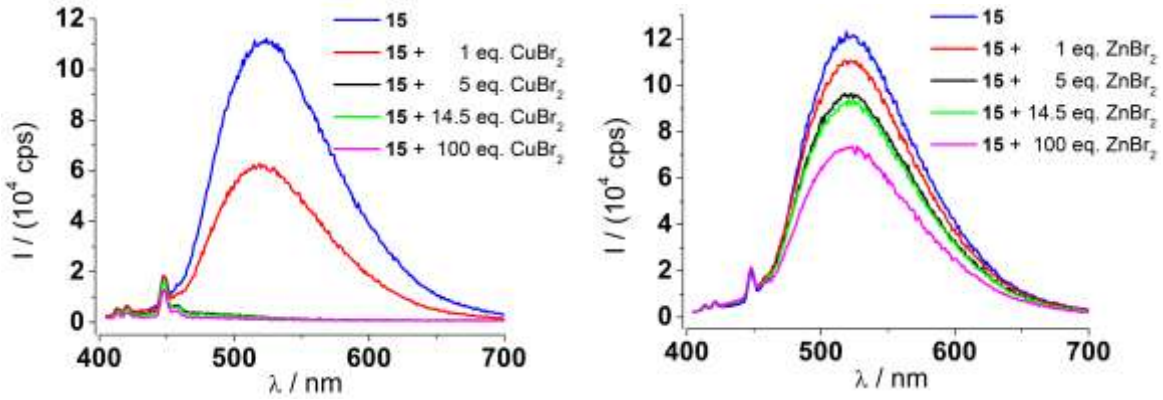

Figure 5-35: Emission properties of **15** after addition of copper bromide (left) and zinc bromide (right) (10^{-5} M in MeOH, λ_{ex} = 396 nm).

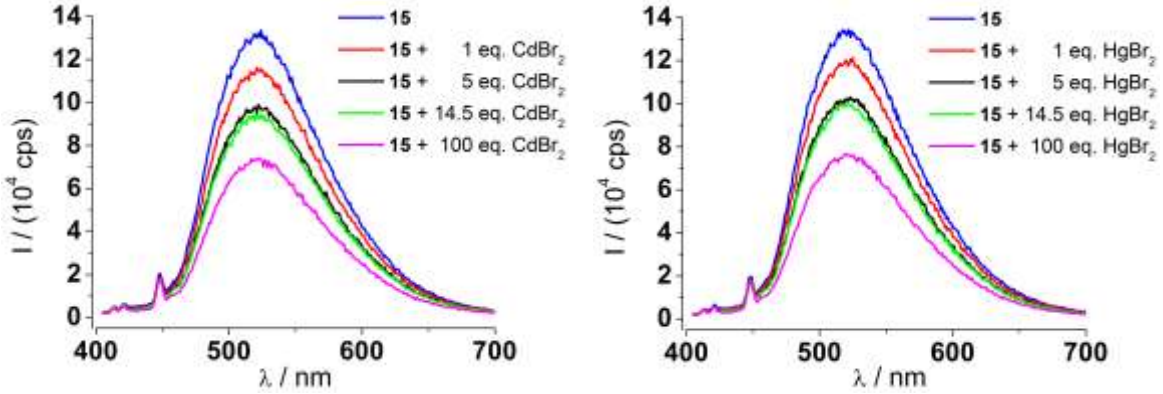

Figure 5-36: Emission properties of **15** after addition of cadmium bromide (left) and mercury bromide (right) (10^{-5} M in MeOH, λ_{ex} = 396 nm).

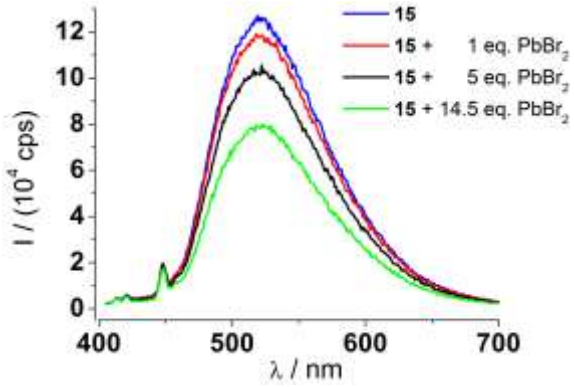

Figure 5-37: Emission properties of **15** after addition of lead bromide (10^{-5} M in MeOH, λ_{ex} = 396 nm).

5.1.9 Further luminescence properties of 9-anthracenesalicylamine (16)

Detailed information about the wavelength dependent fluorescence intensity of **16** after addition of metal bromides (summarized in Figure 2-59) are presented in this chapter.

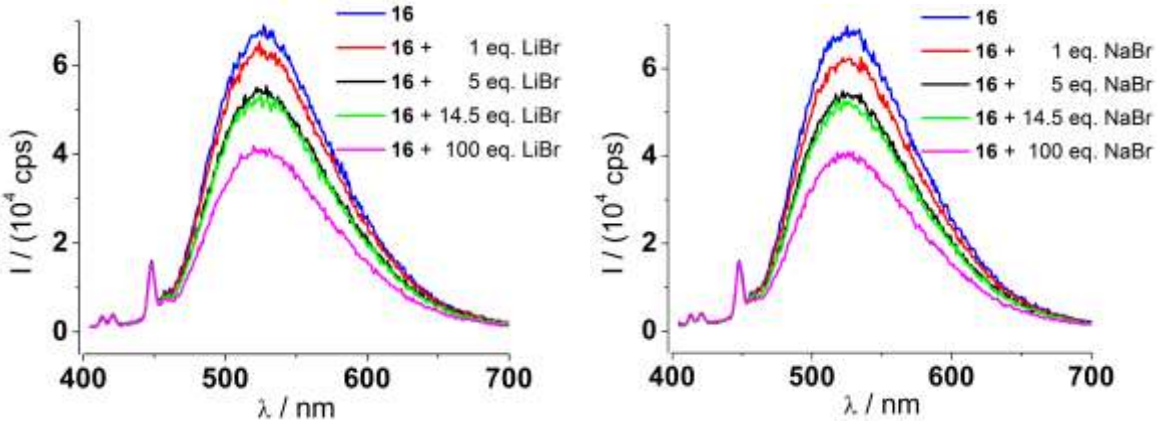

Figure 5-38: Emission properties of **16** after addition of lithium bromide (left) and sodium bromide (right) (10^{-5} M in MeOH, λ_{ex} = 396 nm).

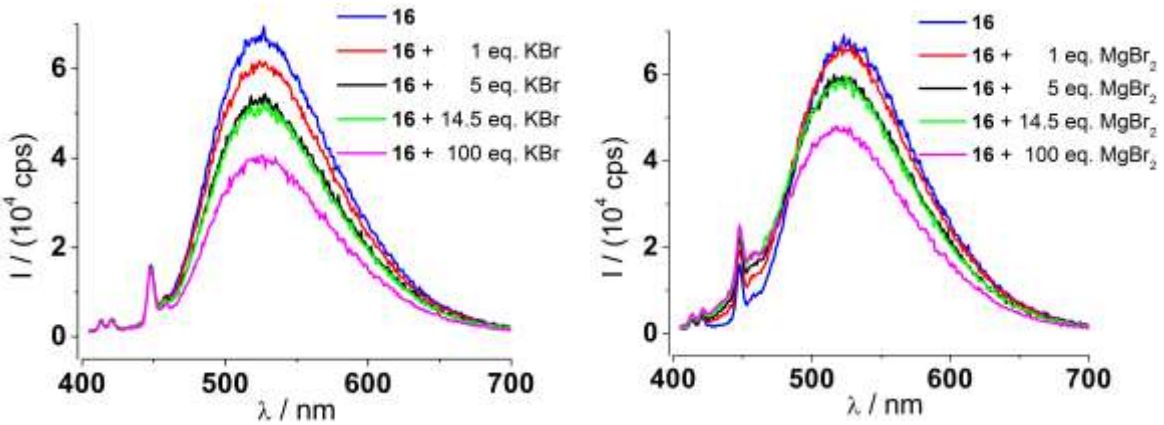

Figure 5-39: Emission properties of **16** after addition of potassium bromide (left) and magnesium bromide (right) (10^{-5} M in MeOH, λ_{ex} = 396 nm).

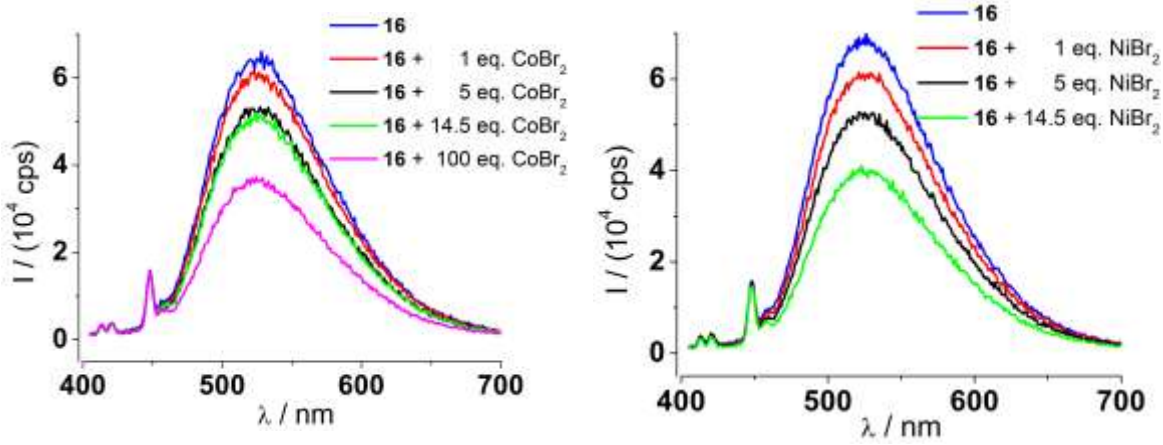

Figure 5-40: Emission properties of **16** after addition of cobalt bromide (left) and nickel bromide (right) (10^{-5} M in MeOH, λ_{ex} = 396 nm).

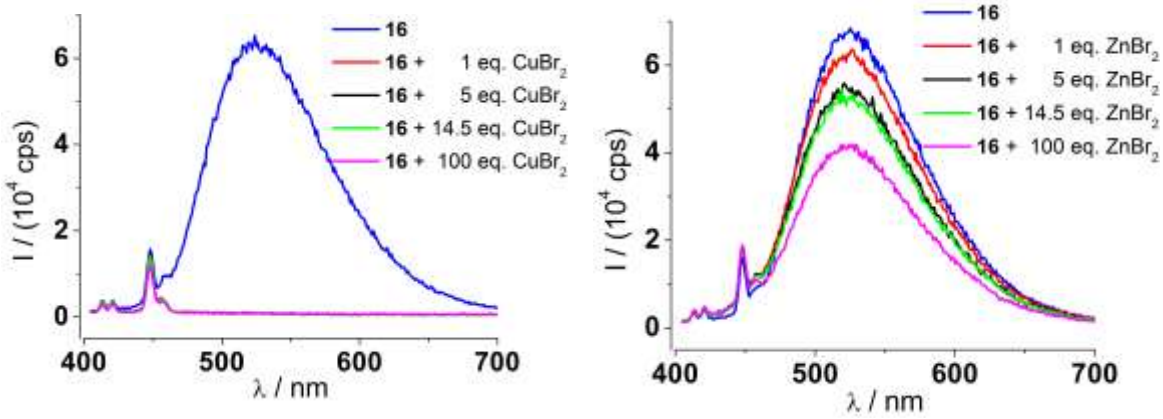

Figure 5-41: Emission properties of **16** after addition of copper bromide (left) and zinc bromide (right) (10^{-5} M in MeOH, λ_{ex} = 396 nm).

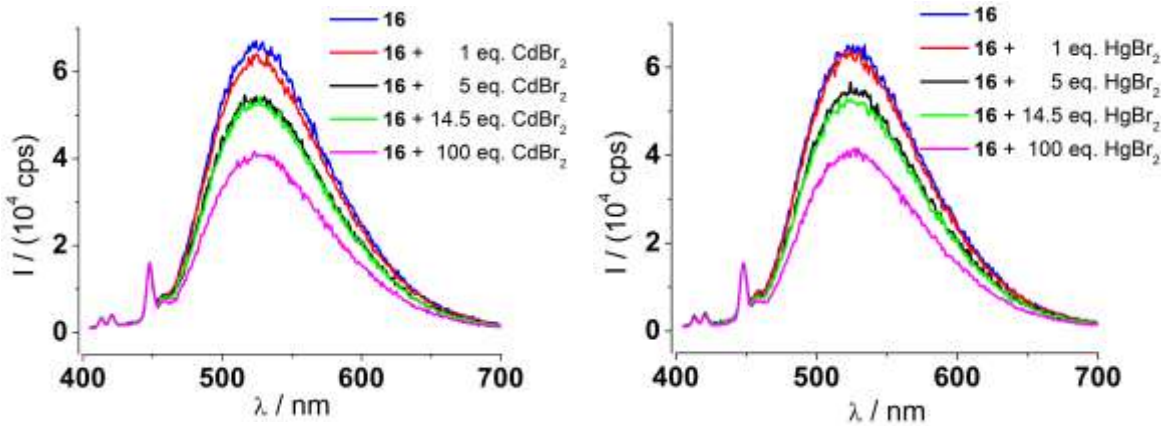

Figure 5-42: Emission properties of **16** after addition of cadmium bromide (left) and mercury bromide (right) (10^{-5} M in MeOH, λ_{ex} = 396 nm).

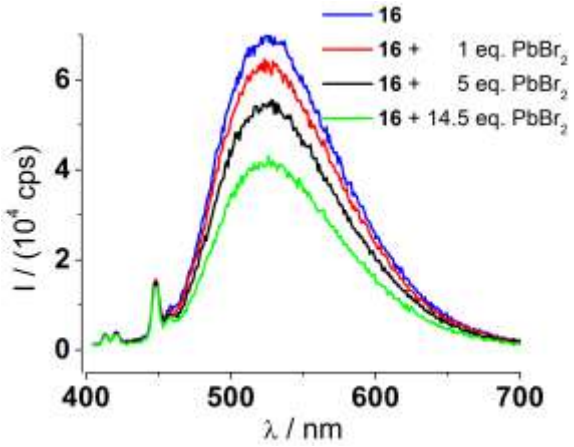

Figure 5-43: Emission properties of **16** after addition of lead bromide (10^{-5} M in MeOH, λ_{ex} = 396 nm).

5.1.10 Further luminescence properties of 9-anthracene(*o*-(*β*-hydroxyethoxy)benzyl)imine (18)

Detailed information about the wavelength dependent fluorescence intensity of **18** after addition of metal bromides (summarized in Figure 2-68) are presented in this chapter.

Additionally, the behavior of **18** towards metal bromides after a previous addition of sodium hydroxide in two different concentrations is displayed in Figure 5-49 (cf. Figure 2-71) and Figure 5-50 (cf. Figure 2-72).

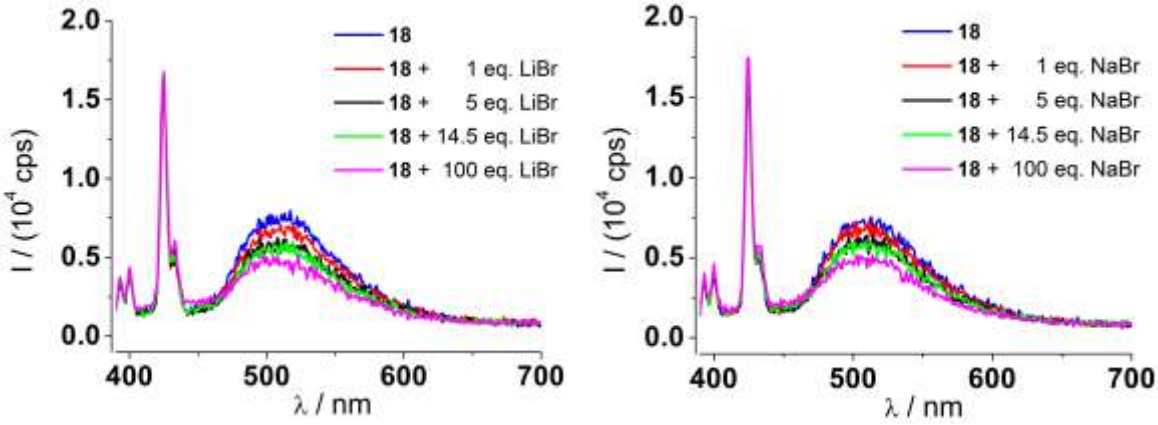

Figure 5-44: Emission properties of **18** after addition of lithium bromide (left) and sodium bromide (right) (10^{-5} M in MeOH, λ_{ex} = 378 nm).

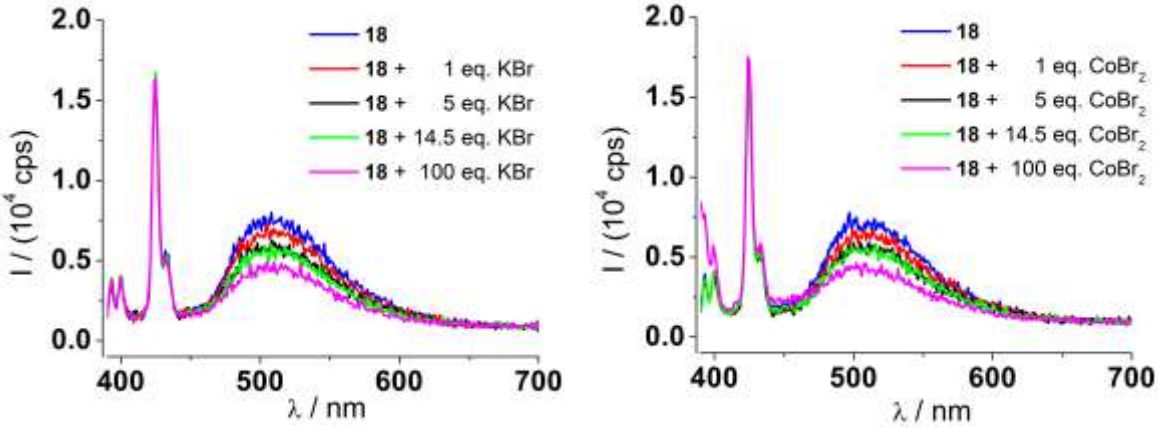

Figure 5-45: Emission properties of **18** after addition of potassium bromide (left) and cobalt bromide (right) (10^{-5} M in MeOH, λ_{ex} = 378 nm).

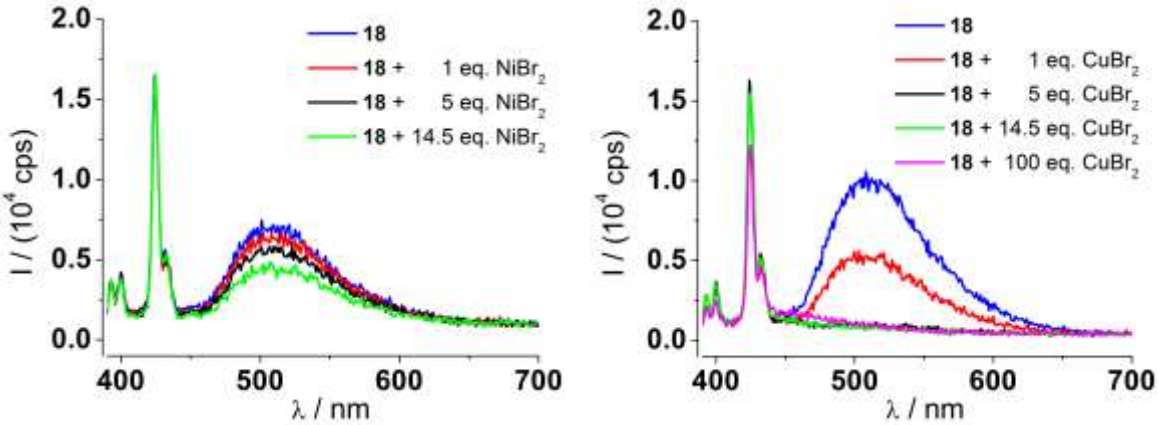

Figure 5-46: Emission properties of **18** after addition of nickel bromide (left) and copper bromide (right) (10^{-5} M in MeOH, λ_{ex} = 378 nm).

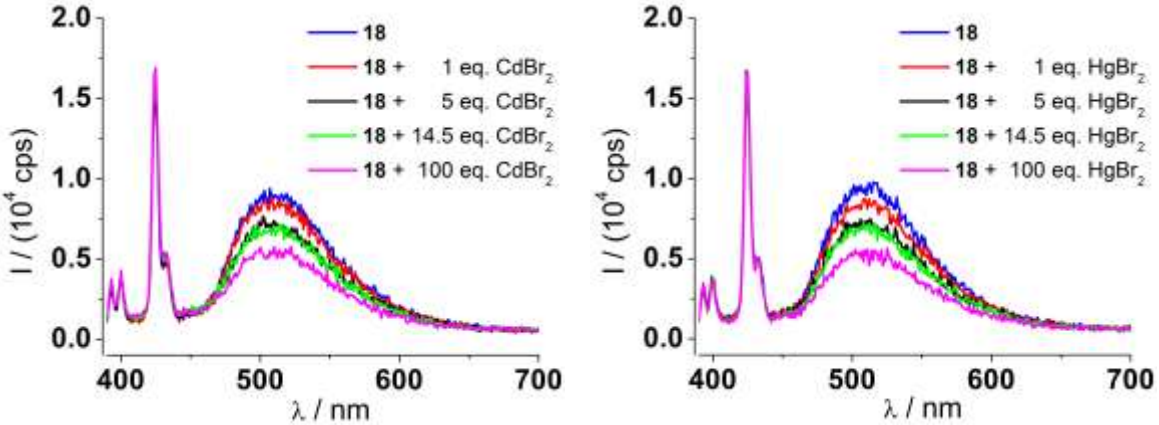

Figure 5-47: Emission properties of **18** after addition of cadmium bromide (left) and mercury bromide (right) (10^{-5} M in MeOH, λ_{ex} = 378 nm).

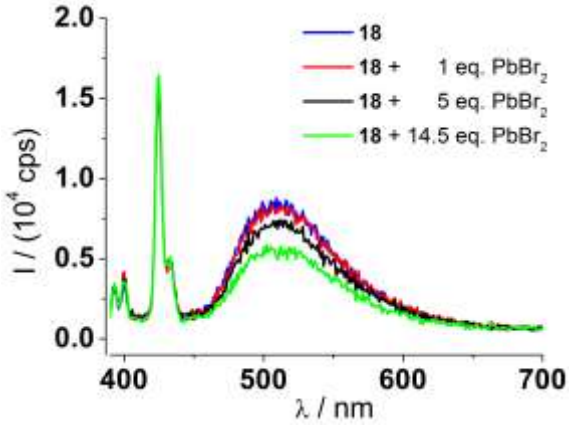

Figure 5-48: Emission properties of **18** after addition of lead (10^{-5} M in MeOH, λ_{ex} = 378 nm).

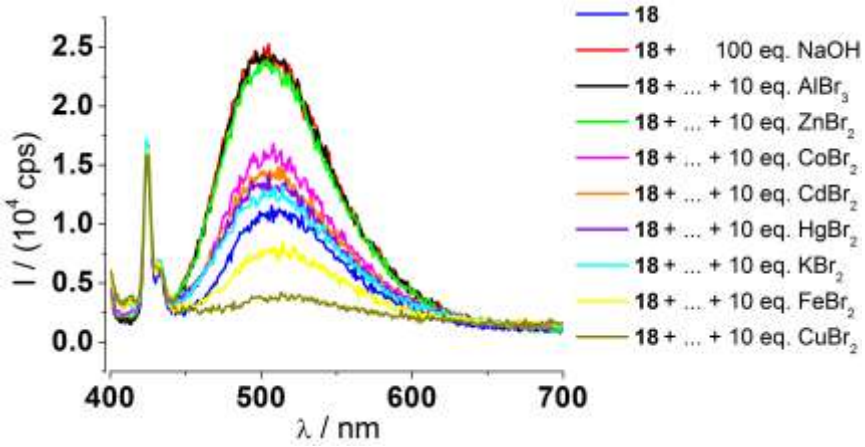

Figure 5-49: Stacked spectra of **18** before and after successive addition of 100 eq. NaOH and several metal bromides in MeOH (10^{-5} M, λ_{ex} = 378 nm).

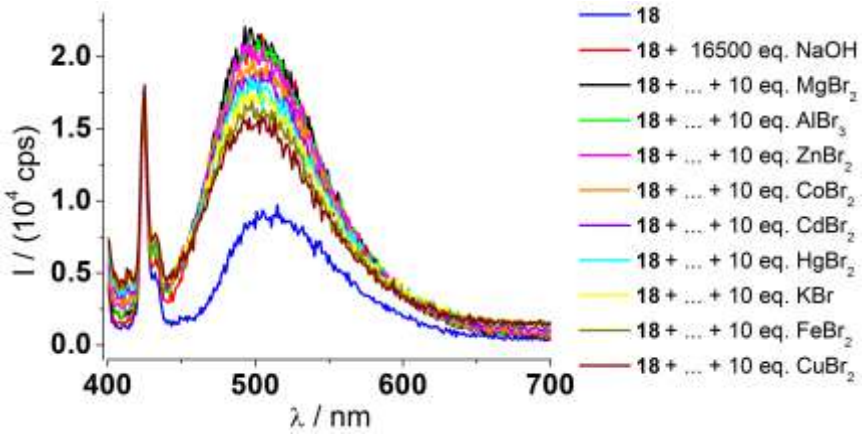

Figure 5-50: Stacked spectra of **18** before and after successive addition of 16500 eq. NaOH and several metal bromides in MeOH (10^{-5} M, λ_{ex} = 378 nm).

5.1.11 Further luminescence properties of 9-anthracene(*o*-(*β*-hydroxyethoxy)benzyl)amine (19)

Detailed information about the wavelength dependent fluorescence intensity of **19** after addition of metal bromides (summarized in Figure 2-81) are presented in this chapter. The stability of **19** after protonation is shown in Figure 5-51.

Additionally, the behavior of **19** towards metal bromides after a previous addition of sodium hydroxide in two different concentrations is displayed in Figure 5-58 (cf. Figure 2-83) and Figure 5-59 (cf. Figure 2-84).

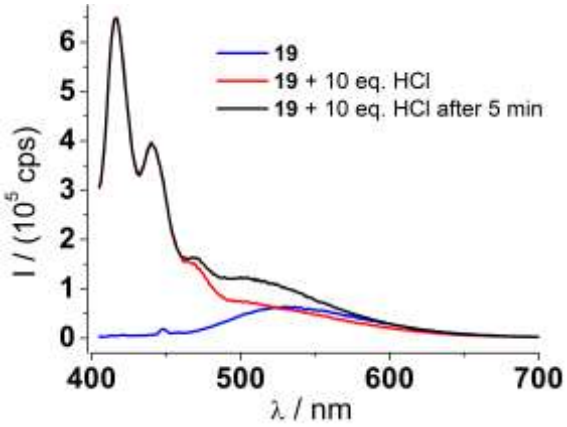

Figure 5-51: Emission of **19** before and after the addition of 10 eq. HCl over 5 minutes (right, λ_{ex} = 396 nm).

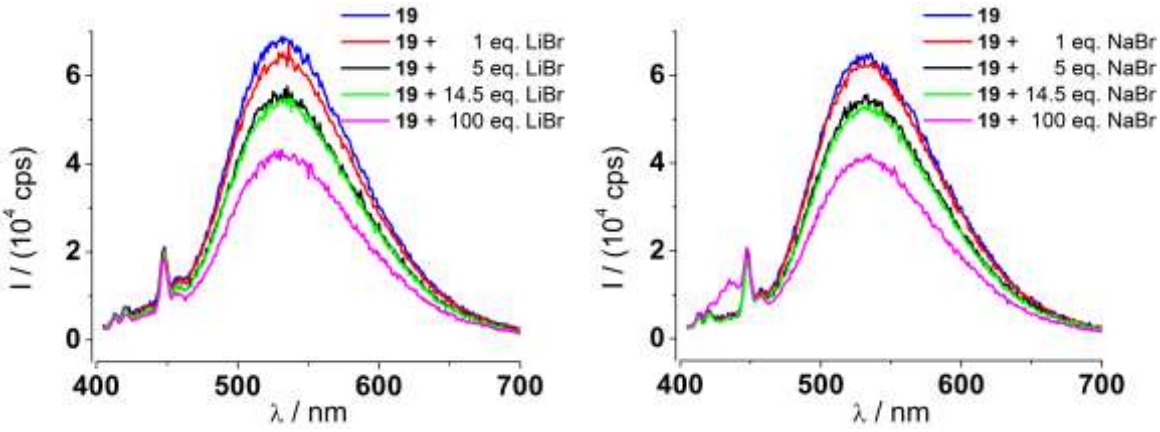

Figure 5-52: Emission properties of **19** after addition of lithium bromide (left) and sodium bromide (right) (10^{-5} M in MeOH, λ_{ex} = 396 nm).

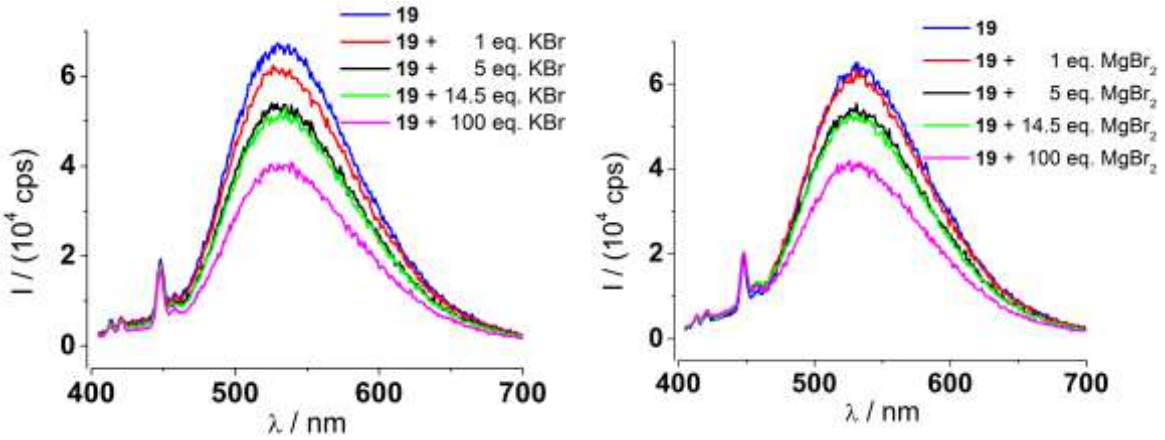

Figure 5-53: Emission properties of **19** after addition of potassium bromide (left) and magnesium bromide (right) (10^{-5} M in MeOH, λ_{ex} = 396 nm).

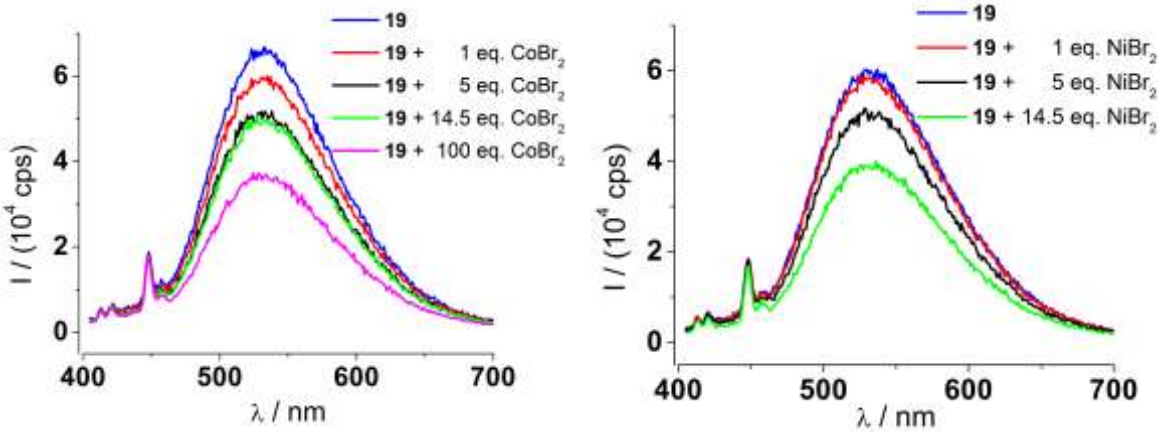

Figure 5-54: Emission properties of **19** after addition of cobalt bromide (left) and nickel bromide (right) (10^{-5} M in MeOH, λ_{ex} = 396 nm).

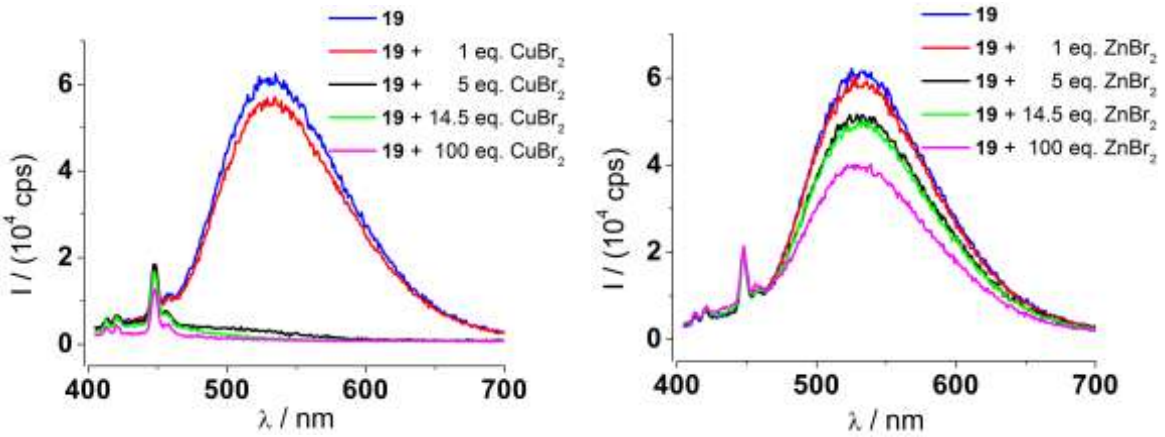

Figure 5-55: Emission properties of **19** after addition of copper bromide (left) and zinc bromide (right) (10^{-5} M in MeOH, λ_{ex} = 396 nm).

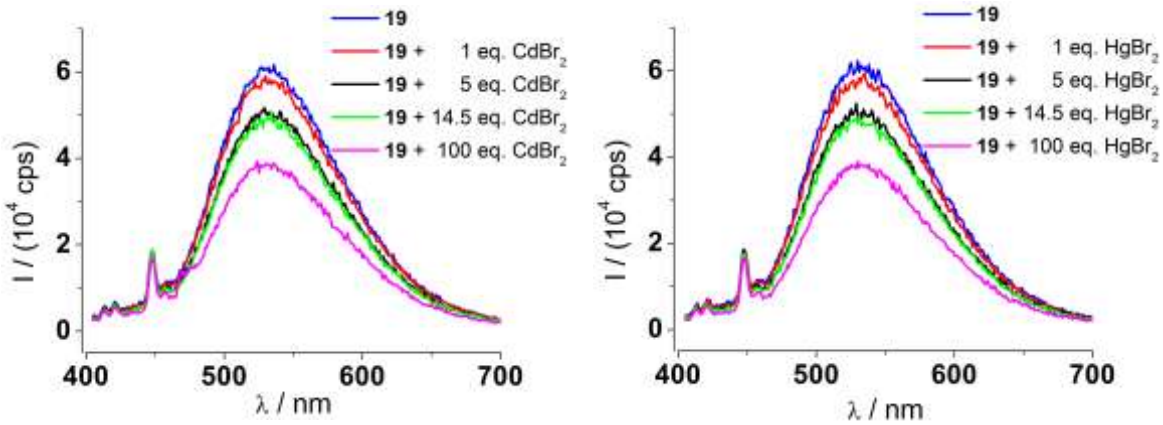

Figure 5-56: Emission properties of **19** after addition of cadmium bromide (left) and mercury bromide (right) (10^{-5} M in MeOH, λ_{ex} = 396 nm).

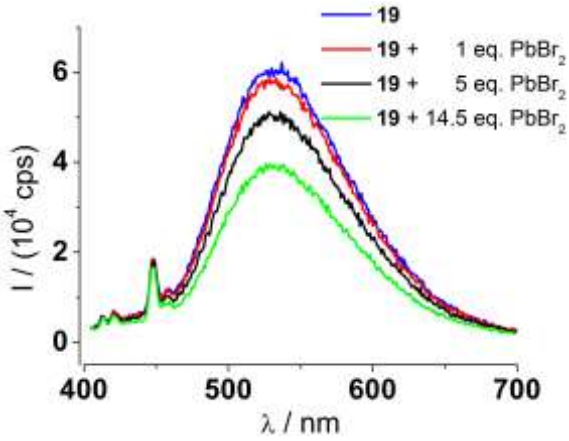

Figure 5-57: Emission properties of **19** after addition of lead bromide (10^{-5} M in MeOH, λ_{ex} = 396 nm).

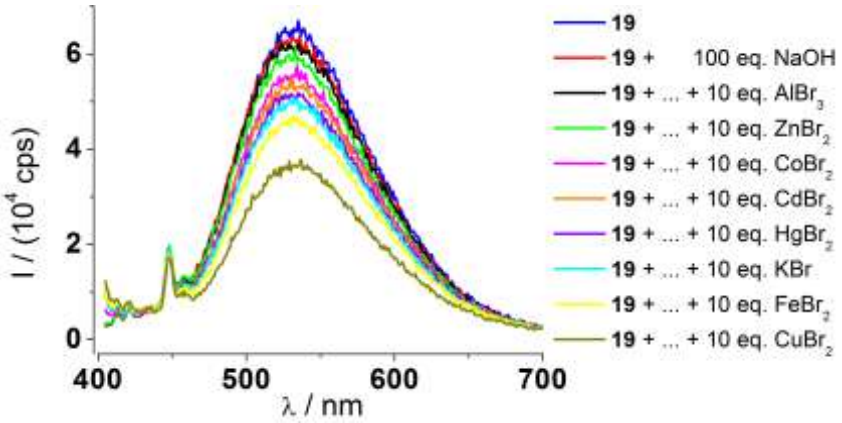

Figure 5-58: Stacked spectra of **19** before and after successive addition of 100 eq. NaOH and several metal bromides in MeOH (10^{-5} M, λ_{ex} = 396 nm).

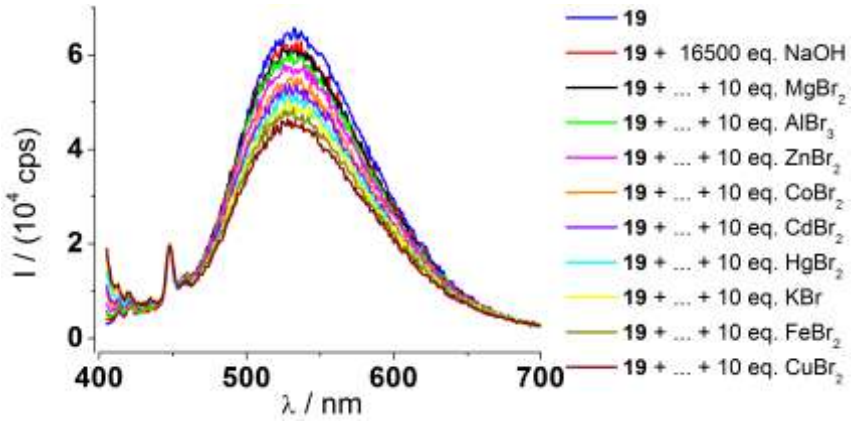

Figure 5-59: Stacked spectra of **19** before and after successive addition of 16500 eq. NaOH and several metal bromides in MeOH (10^{-5} M, λ_{ex} = 396 nm).

5.2 Crystallographic information

5.2.1 9-Chloro-9,10-dihydro-10-nitroanthracene (9)

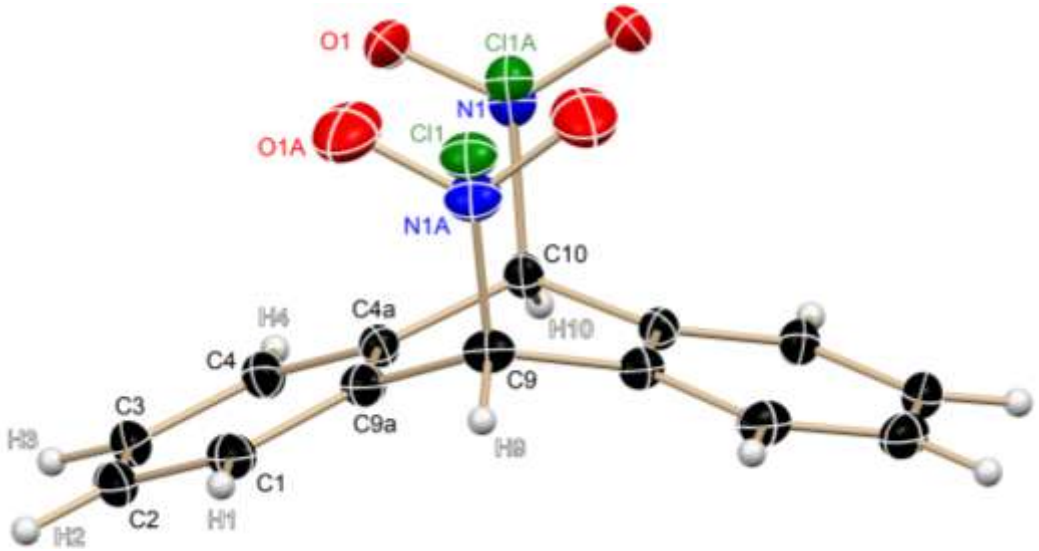

Figure 5-60: Solid state structure of **9**. Anisotropic displacement parameters are displayed at the 50 % probability level. Only the labeled part represents the asymmetric unit. The molecule is completed by a mirror plane containing the atoms C9, C10, Cl1 and N1. The positional disorder between the chlorine atom and the nitro group exhibits a side occupation factor of 7 %.

Table 5-3: Crystallographic information of 9-chloro-9,10-dihydro-10-nitroanthracene (**9**).

Structure code	SW_ClHAnNO$_2$H	Volume	1162.5(5) Å^3
Empirical formula	$C_{14}H_{10}ClNO_2$	Z	4
Formula weight	259.68 g/mol	Absorption coefficient	0.320 / mm
Temperature	101(2) K	F(000)	536
Wavelength	0.71073 Å	Crystal size	0.20 · 0.15 · 0.10 mm
Crystal system	Orthorhombic	θ range	2.316 to 33.751 °
Space group	*Cmc*2$_1$	Reflections collected	42650
Unit cell dimensions		Independent reflections	2398 [*R*(int) = 0.0291]
	a = 14.907(3) Å	Completeness to θ = 25.242°	100.0 %
	b = 10.890(2) Å	Restraints / parameters	49 / 102
	c = 7.161(2) Å	Goodness-of-fit on F^2	1.071
	α = 90 °	*R*1 [I>2σ(I)]	0.0282
	β = 90 °	*wR*2 (all data)	0.0806
	γ = 90 °	Largest diff. peak / hole	0.357 / -0.213 e Å^{-3}

5.2.2 9-Aminoanthracene (11)

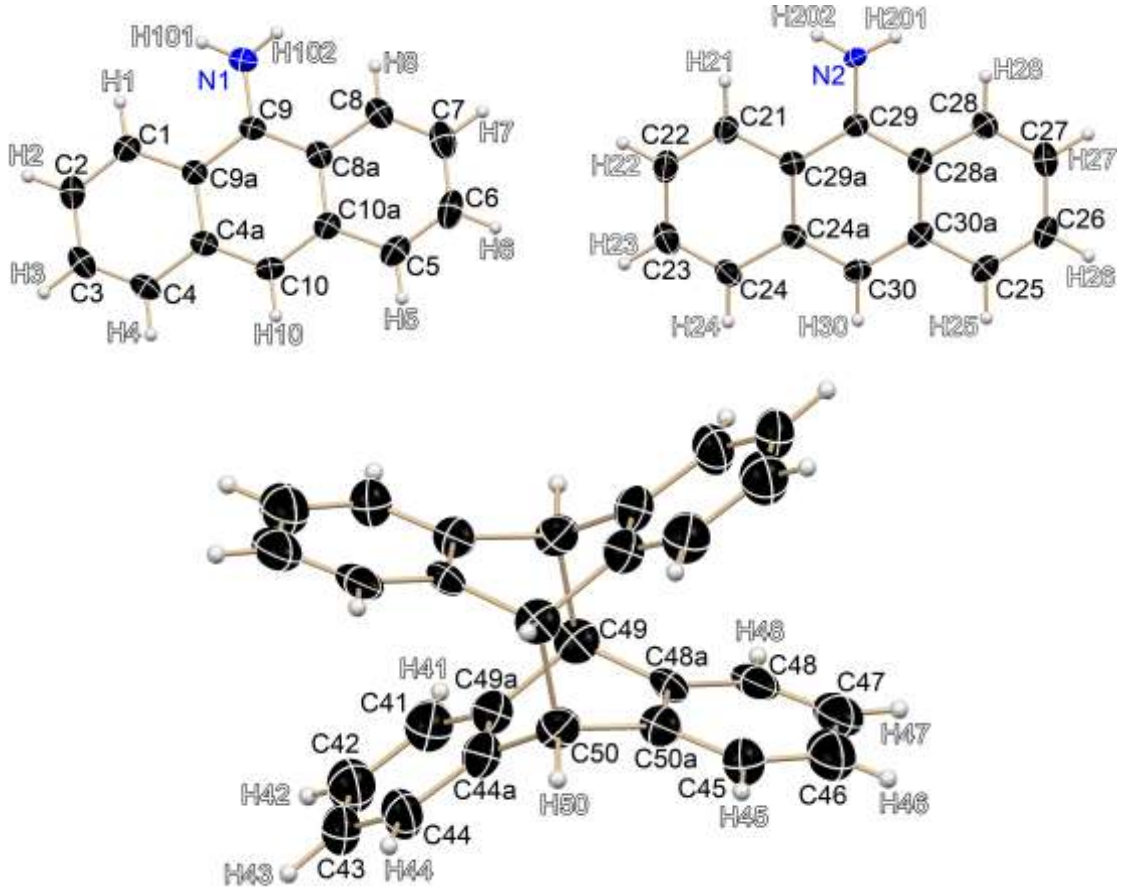

Figure 5-61: Solid state structure of **11**. Anisotropic displacement parameters are displayed at the 50 % probability level. The fragment at the bottom is present at the position of the upper right fragment with a side occupation factor of 9.5 %.

The asymmetric unit consists of two 9-aminoanthracene molecules. One of them (displayed in Figure 5-61 upper left) is completely present, whereas the other molecule (displayed in Figure 5-61 upper right) shows a 2-times disorder. At first, half of the dimer shown in the bottom of Figure 5-61 is present at that position with a side occupation factor of 9.5 %. The other (non-labeled) half of that dimer is created by a center of inversion and belongs to the next asymmetric unit.

Secondly, the amino group of the 9-aminoanthracene is subject of a positional disorder (not shown in Figure 5-61 for clarity) at C30 with a side occupation factor of 14.7 %.

Table 5-4: Crystallographic information of 9-aminoanthracene (**11**).

Structure code	SW_9-AA	Volume	972.0(4) Å^3
Empirical formula	$C_{14}H_{11}N$	Z	4
Formula weight	192.46 g/mol	Absorption coefficient	0.077 / mm
Temperature	101(2) K	F(000)	406
Wavelength	0.71073 Å	Crystal size	0.10 · 0.10 · 0.10 mm
Crystal system	Triclinic	θ range	1.771 to 27.511 °
Space group	$P\bar{1}$	Reflections collected	32397
Unit cell dimensions		Independent reflections	4450 [R(int) = 0.0345]
	a = 8.331(2) Å	Completeness to θ = 25.242°	99.8 %
	b = 10.169(2) Å	Restraints / parameters	1345 / 423
	c = 11.993(3) Å	Goodness-of-fit on F^2	0.985
	α = 73.51(2) °	R1 [I>2σ(I)]	0.0565
	β = 88.84(2) °	wR2 (all data)	0.1615
	γ = 86.10(2) °	Largest diff. peak / hole	0.301 / -0.227 e Å^{-3}

5.2.3 9-Anthracenesalicylimine (12)

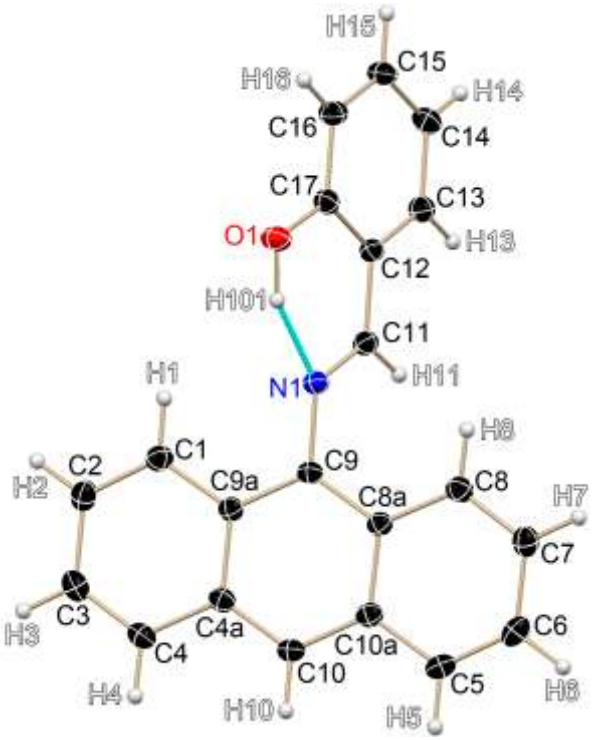

Figure 5-62: Solid state structure of **12**. Anisotropic displacement parameters are displayed at the 50 % probability level.

Table 5-5: Crystallographic information of 9-anthracenesalicylimine (**12**).

Structure code	SW_ASI	Volume	732.5(3) Å^3
Empirical formula	$C_{21}H_{15}NO$	Z	2
Formula weight	297.34 g/mol	Absorption coefficient	0.083 / mm
Temperature	100(2) K	F(000)	312
Wavelength	0.71073 Å	Crystal size	0.291 · 0.169 · 0.163 mm
Crystal system	Triclinic	θ range	2.092 to 30.025 °
Space group	$P\bar{1}$	Reflections collected	19830
Unit cell dimensions		Independent reflections	4212 [R(int) = 0.0307]
	a = 8.735(2) Å	Completeness to θ = 25.242°	99.8 %
	b = 9.539(2) Å	Restraints / parameters	0 / 212
	c = 9.781(3) Å	Goodness-of-fit on F^2	1.089
	α = 86.23(3) °	R1 [I>2σ(I)]	0.0459
	β = 84.56(2) °	wR2 (all data)	0.1365
	γ = 64.58(2) °	Largest diff. peak / hole	0.425 / -0.254 e Å^{-3}

5.2.4 Anthraquinone monoimine and photodimer of 9-amino-anthracene

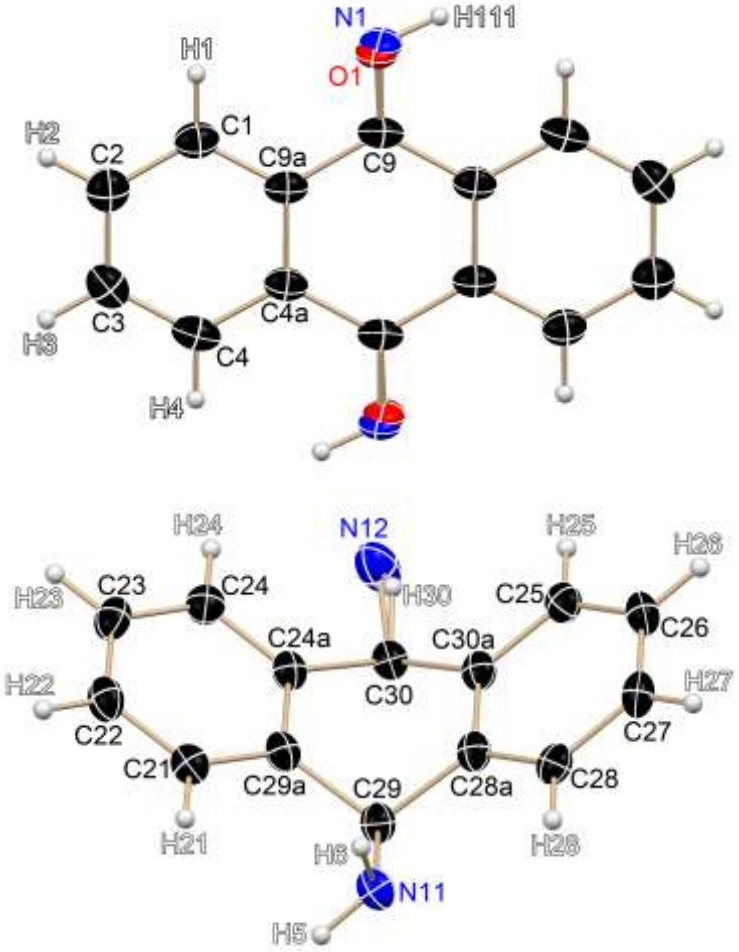

Figure 5-63: Solid state structure of: anthraquinone monoimine (top) and photodimer of 9-aminoanthracene (bottom, without symmetry generated half of the molecule). Anisotropic displacement parameters are displayed at the 50 % probability level.

The asymmetric unit consists of one half of the upper molecule and the shown half of the lower one. In the first derivative O1 and N1 show a side occupation factor of 0.5 whereas in the second derivative a positional disorder causes a side occupation factor of 0.95 for N11. That is why no protons were found bond to N12.

Table 5-6: Crystallographic information of anthraquinone monoimine and photodimer of 9-aminoanthracene.

Structure code	SW_Zers1	Volume	718.6(3) Å^3
Empirical formula	$C_{42}H_{31}N_3O$	Z	1
Formula weight	593.42 g/mol	Absorption coefficient	0.083 / mm
Temperature	100(2) K	F(000)	312
Wavelength	0.71073 Å	Crystal size	0.220 · 0.060 · 0.010 mm
Crystal system	Triclinic	θ range	2.232 to 25.365 °
Space group	$P\bar{1}$	Reflections collected	34143
Unit cell dimensions		Independent reflections	2631 [R(int) = 0.0714]
	a = 8.453(2) Å	Completeness to θ = 25.242°	99.8 %
	b = 9.391(2) Å	Restraints / parameters	78 / 237
	c = 10.424(3) Å	Goodness-of-fit on F^2	1.105
	α = 64.44(2) °	R1 [I>2σ(I)]	0.0444
	β = 74.30(2) °	wR2 (all data)	0.1209
	γ = 82.89(2) °	Largest diff. peak / hole	0.198 / -0.196 e Å^{-3}

5.2.5 9,9'-Dihydro-10,10'-diiminio-9,9'-bianthracene

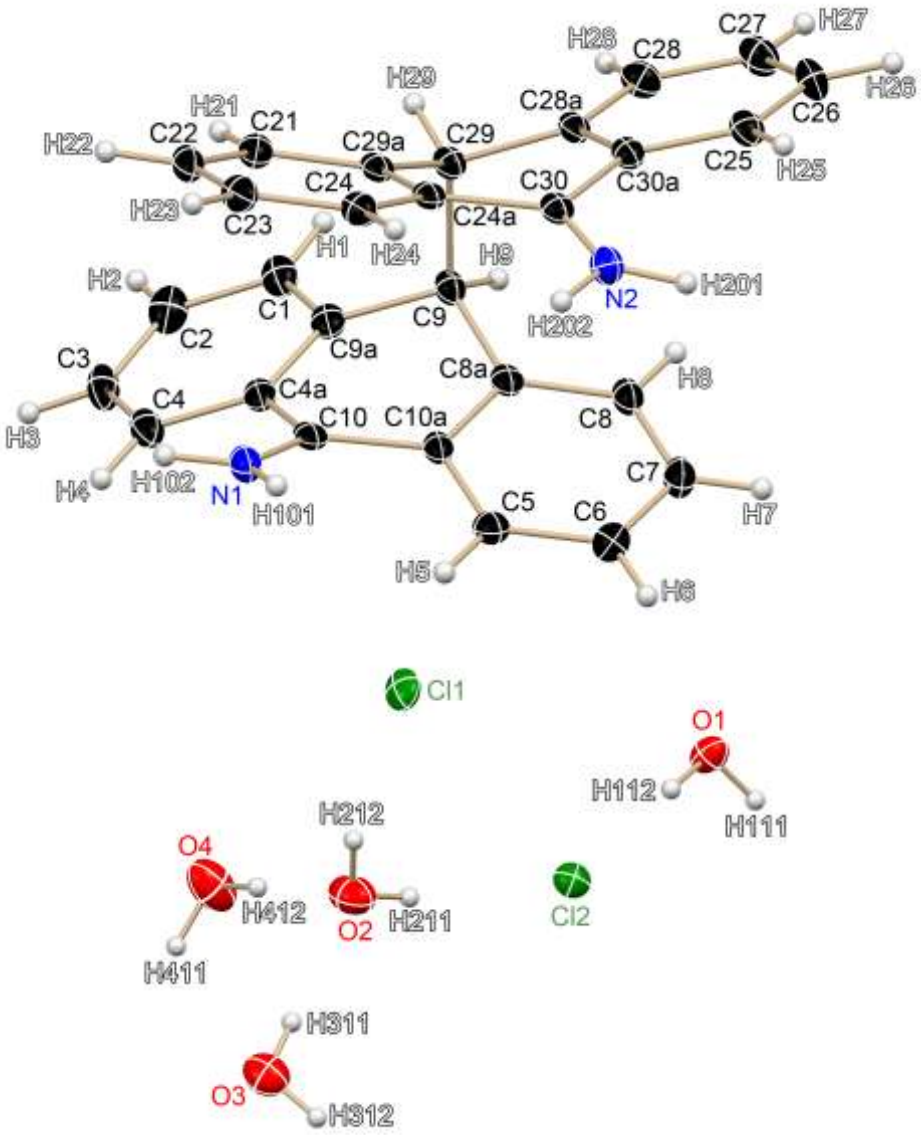

Figure 5-64: Solid state structure of: 9,9'-dihydro-10,10'-diiminio-9,9'-bianthracene (top) and cocrystallized water and chloride (bottom). Anisotropic displacement parameters are displayed at the 50 % probability level.

Besides 9,9'-dihydro-10,10'-diiminio-9,9'-bianthracene (discussed in chapter 2.2.5.4) the obtained single crystal contained two chloride atoms and four water molecules in the asymmetric unit. O4 and its bond hydrogen atoms H411 and H412 exhibit a side occupation factor of 0.45. Multiple hydrogen bonds are present among water molecules, between water and chloride, between the iminium salt and water and between the iminium salt and chloride.

Table 5-7: Crystallographic information of 9,9'-dihydro-10,10'-diiminio-9,9'-bianthracene.

Structure code	SW_Zers2	Volume	2563.1(8) Å^3
Empirical formula	$C_{28}H_{30}Cl_2N_2O_4$	Z	4
Formula weight	519.53 g/mol	Absorption coefficient	0.288 / mm
Temperature	100(2) K	F(000)	1090
Wavelength	0.71073 Å	Crystal size	0.118 · 0.066 · 0.051 mm
Crystal system	Orthorhombic	θ range	2.063 to 28.366 °
Space group	$Pna2_1$	Reflections collected	46344
Unit cell dimensions		Independent reflections	6395 [R(int) = 0.0462]
	a = 13.709(2) Å	Completeness to θ = 25.242°	100.0 %
	b = 14.221(3) Å	Restraints / parameters	42 / 373
	c = 13.147(2) Å	Goodness-of-fit on F^2	1.022
	α = 90 °	R1 [I>2σ(I)]	0.0306
	β = 90 °	wR2 (all data)	0.0701
	γ = 90 °	Largest diff. peak / hole	0.237 / -0.164 e Å^{-3}

5.2.6 9-Anthracenepicolylimine (13)

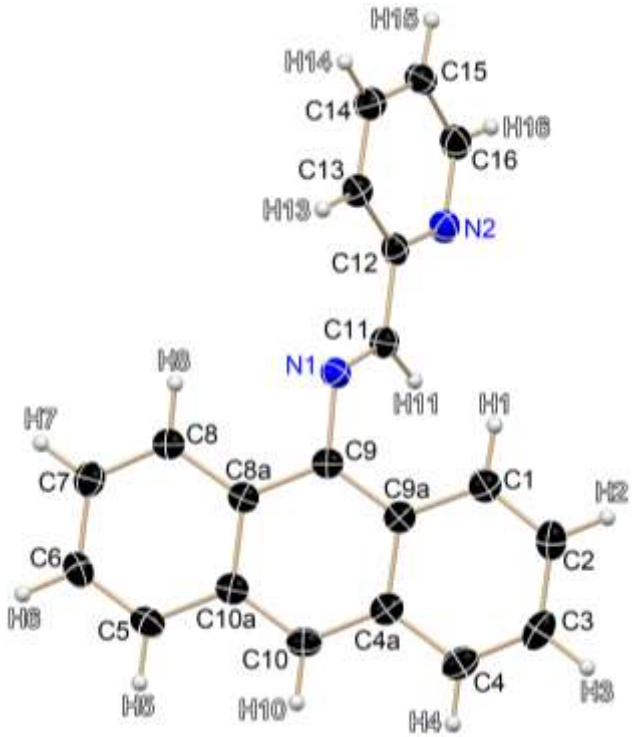

Figure 5-65: Solid state structure of **13**. Anisotropic displacement parameters are displayed at the 50 % probability level.

Table 5-8: Crystallographic information of 9-anthracenepicolylimine (**13**).

Structure code	SW_API	Volume	1438.5(6) Å^3
Empirical formula	$C_{20}H_{14}N_2$	Z	4
Formula weight	282.33 g/mol	Absorption coefficient	0.077 / mm
Temperature	100(2) K	F(000)	592
Wavelength	0.71073 Å	Crystal size	0.173 · 0.122 · 0.097 mm
Crystal system	Monoclinic	θ range	1.767 to 26.376 °
Space group	$P2_1/c$	Reflections collected	12479
Unit cell dimensions		Independent reflections	2944 [R(int) = 0.0303]
	a = 5.781(2) Å	Completeness to θ = 25.242°	99.8 %
	b = 10.796(2) Å	Restraints / parameters	1 / 203
	c = 23.090(3) Å	Goodness-of-fit on F^2	1.062
	α = 90 °	$R1$ [I>2σ(I)]	0.0420
	β = 93.46(3) °	$wR2$ (all data)	0.1150
	γ = 90 °	Largest diff. peak / hole	0.209 / -0.189 e Å^{-3}

5.2.7 9-Anthracenesalicylamine (15)

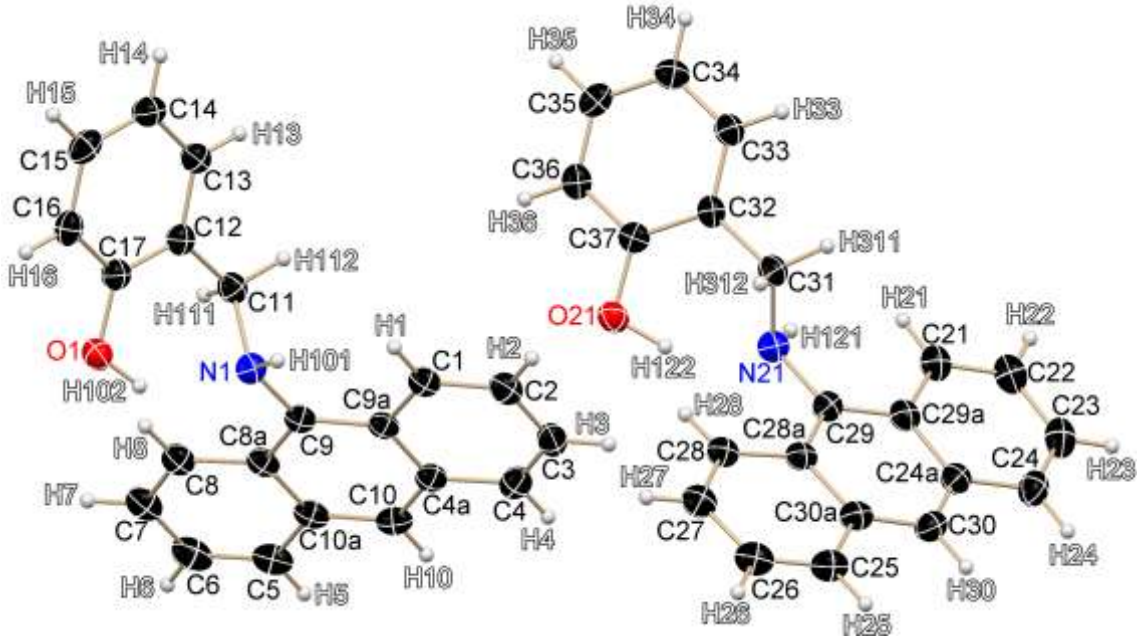

Figure 5-66: Solid state structure of **15**. Anisotropic displacement parameters are displayed at the 50 % probability level.

Table 5-9: Crystallographic information of 9-anthracenesalicylamine (**15**).

Structure code	SW_ASA	Volume	12080(4) Å^3
Empirical formula	$C_{42}H_{34}N_2O_2$	Z	16
Formula weight	598.71 g/mol	Absorption coefficient	0.629 / mm
Temperature	100(2) K	F(000)	5056
Wavelength	1.54178 Å	Crystal size	0.220 · 0.060 · 0.010 mm
Crystal system	Orthorhombic	θ range	2.448 to 68.230 °
Space group	*Fdd*2	Reflections collected	24842
Unit cell dimensions		Independent reflections	4968 [*R*(int) = 0.0476]
	a = 27.698(3) Å	Completeness to θ = 67.679°	96.8 %
	b = 72.197(5) Å	Restraints / parameters	1 / 431
	c = 6.041(2) Å	Goodness-of-fit on F^2	1.058
	α = 90 °	*R*1 [I>2σ(I)]	0.0418
	β = 90 °	*wR*2 (all data)	0.1085
	γ = 90 °	Largest diff. peak / hole	0.234 / -0.182 e Å^{-3}
Absolute structure parameter	-0.09(15)		

5.2.8 9-Anthracenepicolylamine (16)

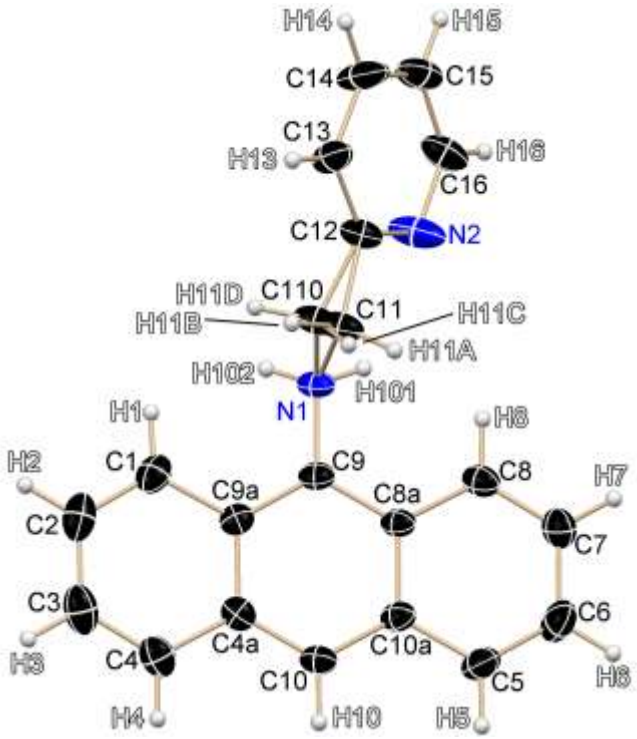

Figure 5-67: Solid state structure of **16**. Anisotropic displacement parameters are displayed at the 50 % probability level.

Table 5-10: Crystallographic information of 9-anthracenepicolylamine (**16**).

Structure code	SW_APA	Volume	1483.0(7) Å^3
Empirical formula	$C_{20}H_{16}N_2$	Z	4
Formula weight	284.35 g/mol	Absorption coefficient	0.075 / mm
Temperature	100(2) K	F(000)	600
Wavelength	0.71073 Å	Crystal size	0.198 · 0.108 · 0.081 mm
Crystal system	Monoclinic	θ range	1.943 to 30.516 °
Space group	*C*2	Reflections collected	13580
Unit cell dimensions		Independent reflections	4014 [*R*(int) = 0.0226]
	a = 18.064(3) Å	Completeness to θ = 25.242°	100.0 %
	b = 7.834(2) Å	Restraints / parameters	9 / 211
	c = 12.895(3) Å	Goodness-of-fit on F^2	1.037
	α = 90 °	*R*1 [I>2σ(I)]	0.0375
	β = 125.64(3) °	*wR*2 (all data)	0.1000
	γ = 90 °	Largest diff. peak / hole	0.257 / -0.207 e Å^{-3}

5.2.9 9-Anthracene(*o*-(*β*-hydroxyethoxy)benzyl)imine (18)

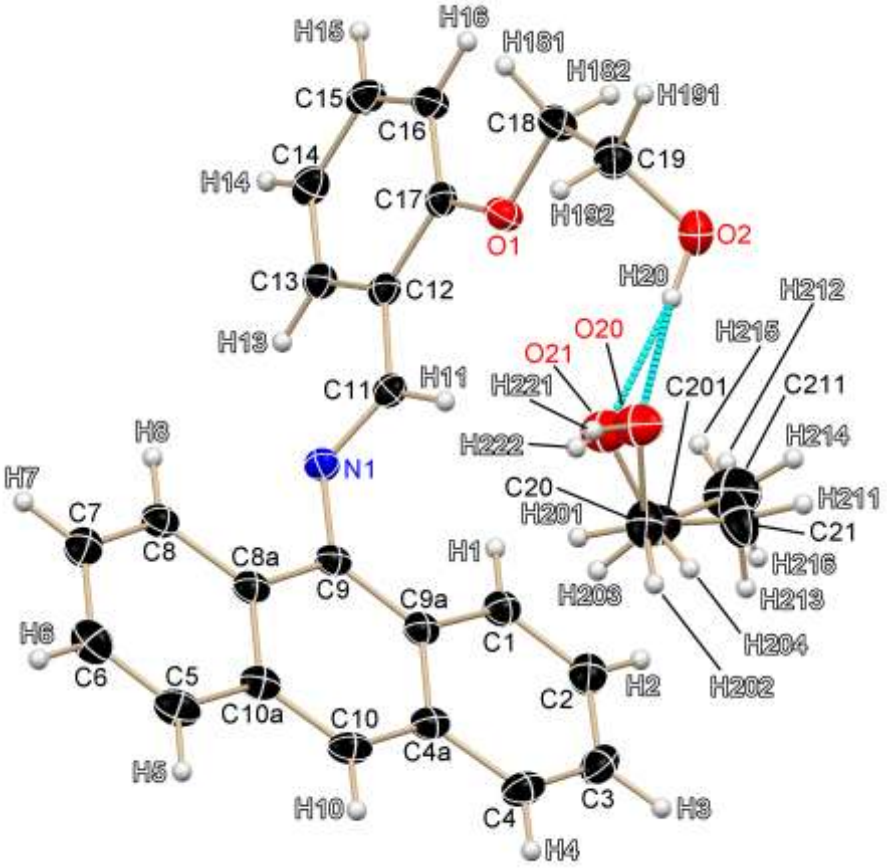

Figure 5-68: Solid state structure of **18**. Anisotropic displacement parameters are displayed at the 50 % probability level.

Table 5-11: Crystallographic information of 9-anthracene(*o*-(*β*-hydroxyethoxy))benzylimine (**18**).

Structure code	SW_AHI	Volume	2076.9(7) Å^3
Empirical formula	$C_{25}H_{25}NO_3$	Z	4
Formula weight	387.46 g/mol	Absorption coefficient	0.081 / mm
Temperature	100(2) K	F(000)	824
Wavelength	0.71073 Å	Crystal size	0.302 · 0.086 · 0.084 mm
Crystal system	Monoclinic	θ range	1.185 to 26.740 °
Space group	$P2_1/c$	Reflections collected	32877
Unit cell dimensions		Independent reflections	4385 [R(int) = 0.0367]
	a = 17.218(3) Å	Completeness to θ = 25.242°	99.7 %
	b = 14.760(2) Å	Restraints / parameters	20 / 293
	c = 8.188(2) Å	Goodness-of-fit on F^2	1.082
	α = 90 °	R1 [I>2σ(I)]	0.0383
	β = 93.56(3) °	wR2 (all data)	0.1015
	γ = 90 °	Largest diff. peak / hole	0.190 / -0.208 e Å^{-3}

6 References

[1] B. Valeur, M. N. Berberan-Santos, *J. Chem. Educ.* **2011**, *88*, 731-738.

[2] A. U. Acuña, F. Amat-Guerri, *Fluorescence of Supermolecules, Polymers, and Nanosystems, Vol. 4*, Springer, Berlin, Heidelberg, **2008**, 3-20.

[3] W. E. Safford, *Ann. Rep. Smithsonian Inst.* **1915**, 271-298.

[4] F. H. Garrison, *An Introduction to the History of Medicine,* 2nd ed., W.B. Saunders Company, Philadelphia, **1917**, 283.

[5] R. Boyle, *Experiments and Considerations touching Colours,* 1st ed., London, **1664**, 199-216.

[6] I. Newton, *Opticks: or, a Treatise of the Reflections, Refractions, Inflections and Colours,* 4th corrected ed., W. Innys, London, **1730**, 162.

[7] I. Newton, *Phil. Trans.* **1671**, *6*, 3075-3087.

[8] A. U. Acuña, F. Amat-Guerri, P. Morcillo, M. Liras, B. Rodríguez, *Org. Lett.* **2009**, *11*, 3020-3023.

[9] J. F. W. Herschel, *Phil. Trans. R. Soc. London* **1845**, *135*, 143-145.

[10] G. G. Stokes, *Phil. Trans. R. Soc. London* **1852**, *142*, 463-562.

[11] G. G. Stokes, *Phil. Trans. R. Soc. London* **1853**, *143*, 385-396.

[12] J. Hölsä, *Elec. Soc. Interface* **2009**, *18*, 42-45.

[13] N. J. Turro, V. Ramamurthy, J. C. Scaiano, *Modern Molecular Photochemistry of Organic Molecules,* 1st ed., University Science Books, Sausalito, **2010**, 33-36.

[14] A. Jabłoński, *Z. Physik* **1935**, *94*, 38-46.

[15] B. Bowers, *Proc. IEEE* **2002**, *90*, 1696-1698.

[16] P. W. Atkins, J. de Paula, *Physikalische Chemie,* 4th. ed., WILEY-VCH, Weinheim, **2006**, 552-553.

[17] a) E. Condon, *Phys. Rev.* **1926**, *28*, 1182-1201; b) J. Franck, E. G. Dymond, *Trans. Faraday Soc.* **1926**, *21*, 536-542.

[18] N. J. Turro, V. Ramamurthy, J. C. Scaiano, *Modern Molecular Photochemistry of Organic Molecules,* 1st ed., University Science Books, Sausalito, **2010**, 128-129.

[19] a) J. Dumas, *Ann. Pharm.* **1833**, *5*, 5-20; b) A. Laurent, *Liebigs Ann. Chem.* **1840**, *34*, 287-296.

[20] E. de Barry Barnett, M. A. Matthews, *Ber. Dtsch. Chem. Ges.* **1926**, *59*, 1429-1438.

[21] a) D. Stern, *Fluoreszenzchemosensoren auf Basis des Anthracen-Fluorophors,* Georg-August University Göttingen, Dissertation, **2009**; b) D. Stern, N. Finkelmeier, K. Meindl, J. Henn, D. Stalke, *Angew. Chem.* **2010**, *122*, 7021-7024; *Angew. Chem. Int. Ed.* **2010**, *49*, 6869-6872; c) D. Stern, N. Finkelmeier, D. Stalke, *Chem. Commun.* **2011**, *47*, 2113-2115.

[22] K. P. C. Vollhardt, N. E. Schore, *Organische Chemie,* 4th ed., WILEY-VCH, Weinheim, **2005**, 644.

[23] a) E. J. Bowen, E. Mikiewicz, *Nature* **1947**, *159*, 706; b) W. H. Wright, *Chem. Rev.* **1967**, *67*, 581-597.

[24] J. R. Lakowicz, *Principles of Fluorescence Spectroscopy,* 3rd ed., Springer, New York, **2006**, 6-11.

[25] N. J. Turro, V. Ramamurthy, J. C. Scaiano, *Modern Molecular Photochemistry of Organic Molecules,* 1st ed., University Science Books, Sausalito, **2010**, 202.

[26] L. J. Kricka, P. Fortina, *Clin. Chem.* **2009**, *55*, 670-683.
[27] A. M. Breul, M. D. Hager, U. S. Schubert, *Chem. Soc. Rev.* **2013**, *42*, 5366-5407.
[28] D. Yokoyama, *J. Mater. Chem.* **2011**, *21*, 19187-19202.
[29] S. W. Hell, E. Rittweger, *Nature* **2009**, *461*, 1069-1070.
[30] A. P. de Silva, *J. Phys. Chem. Lett.* **2011**, *2*, 2865-2871.
[31] Y. Li, T. Liu, H. Liu, M.-Z. Tian, Y. Li, *Acc. Chem. Res.* **2014**, *47*, 1186-1198.
[32] S. Das*, et al.*, *Dalton Trans.* **2013**, *42*, 4757-4763.
[33] Y.-J. Huang, Y.-B. Jiang, S. D. Bull, J. S. Fossey, T. D. James, *Chem. Commun.* **2010**, *46*, 8180-8182.
[34] T. Saha, A. Sengupta, P. Hazra, P. Talukdar, *Photochem. Photobiol. Sci.* **2014**, *13*, 1427-1433.
[35] W. Retting, R. Lapouyade, *Topics in Fluorescence Spectroscopy: Probe Design and Chemical Sensing, Vol. 4*, Plenum Press, New York, **1994**, 109.
[36] A. P. de Silva, D. B. Fox, A. J. M. Huxley, N. D. McClenaghan, J. Roiron, *Coord. Chem. Rev.* **1999**, *185–186*, 297-306.
[37] a) C. Lodeiro, J. L. Capelo, J. C. Mejuto, E. Oliveira, H. M. Santos, B. Pedras, C. Nunez, *Chem. Soc. Rev.* **2010**, *39*, 2948-2976; b) J. Wu, W. Liu, J. Ge, H. Zhang, P. Wang, *Chem. Soc. Rev.* **2011**, *40*, 3483-3495.
[38] Z. Liu, H.-L. Wang, M. Cotlet, *Chem. Mater.* **2014**, *26*, 2900-2906.
[39] L. Yuan, W. Lin, K. Zheng, S. Zhu, *Acc. Chem. Res.* **2013**, *46*, 1462-1473.
[40] R. A. Bissel, A. P. de Silva, H. Q. N. Gunaratne, P. L. M. Lynch, G. E. M. Maguire, C. P. McCoy, K. R. A. S. Sandanayake, *Top. Curr. Chem., Vol. 168*, Springer, Berlin, Heidelberg, **1993**, 229-230.
[41] M. E. Huston, K. W. Haider, A. W. Czarnik, *J. Am. Chem. Soc.* **1988**, *110*, 4460-4462.
[42] K. Kubo, *Topics in Fluorescence Spectroscopy, Vol. 9*, Springer US, **2005**, 219-247.
[43] T. Gunnlaugsson, H. Ali, M. Glynn, P. Kruger, G. Hussey, F. Pfeffer, C. G. dos Santos, J. Tierney, *J Fluoresc* **2005**, *15*, 287-299.
[44] R. A. Bissell*, et al.*, *J. Chem. Soc., Perkin Trans. 2* **1992**, 1559-1564.
[45] D. C. Magri, A. P. de Silva, *New J. Chem.* **2010**, *34*, 476-481.
[46] J. K. Tusa, H. He, *J. Mater. Chem.* **2005**, *15*, 2640-2647.
[47] A. P. de Silva, T. P. Vance, M. E. S. West, G. D. Wright, *Org. Biomol. Chem.* **2008**, *6*, 2468-2480.
[48] A. P. de Silva, H. Q. N. Gunaratne, T. Gunnlaugsson, A. J. M. Huxley, C. P. McCoy, J. T. Rademacher, T. E. Rice, *Chem. Rev.* **1997**, *97*, 1515-1566.
[49] J. T. Hutt, J. Jo, A. Olasz, C.-H. Chen, D. Lee, Z. D. Aron, *Org. Lett.* **2012**, *14*, 3162-3165.
[50] J. B. Briks, *Photophysics of Aromatic Molecules,* 1st ed., Wiley - Interscience, London, New York, Sydney, Toronto, **1970**, 301-371.
[51] J. B. Birks, L. G. Christophorou, *Spectrochimica Acta* **1963**, *19*, 401-410.
[52] M. Kołaski, C. R. Arunkumar, K. S. Kim, *J. Chem. Theory Comput.* **2012**, *9*, 847-856.
[53] S. Karuppannan, J.-C. Chambron, *Chem. Asian J.* **2011**, *6*, 964-984.
[54] B. Ma, F. Zeng, X. Li, S. Wu, *Chem. Commun.* **2012**, *48*, 6007-6009.
[55] T. Förster, *Ann. Phys.* **1948**, *437*, 55-75.
[56] K. E. Sapsford, L. Berti, I. L. Medintz, *Angew. Chem.* **2006**, *118*, 4676-4704; *Angew. Chem. Int. Ed.* **2006**, *45*, 4562-4589.

[57] D. Geißler, S. Linden, K. Liermann, K. D. Wegner, L. J. Charbonnière, N. Hildebrandt, *Inorg. Chem.* **2013**, *53*, 1824-1838.
[58] E. M. W. M. van Dongen, L. M. Dekkers, K. Spijker, E. W. Meijer, L. W. J. Klomp, M. Merkx, *J. Am. Chem. Soc.* **2006**, *128*, 10754-10762.
[59] A. R. Clapp, I. L. Medintz, H. Mattoussi, *ChemPhysChem* **2006**, *7*, 47-57.
[60] J.-F. Zhu, H. Yuan, W.-H. Chan, A. W. M. Lee, *Org. Biomol. Chem.* **2010**, *8*, 3957-3964.
[61] J.-S. Wu, W.-M. Liu, X.-Q. Zhuang, F. Wang, P.-F. Wang, S.-L. Tao, X.-H. Zhang, S.-K. Wu, S.-T. Lee, *Org. Lett.* **2007**, *9*, 33-36.
[62] Y. Ma, H. Liu, S. Liu, R. Yang, *Analyst* **2012**, *137*, 2313-2317.
[63] a) S. Kim, J. Y. Noh, K. Y. Kim, J. H. Kim, H. K. Kang, S.-W. Nam, S. H. Kim, S. Park, C. Kim, J. Kim, *Inorg. Chem.* **2012**, *51*, 3597-3602; b) C.-H. Chen, D.-J. Liao, C.-F. Wan, A.-T. Wu, *Analyst* **2013**, *138*, 2527-2530; c) A. Kumar, V. Kumar, K. K. Upadhyay, *Analyst* **2013**, *138*, 1891-1897.
[64] H. Xu, Z. Liu, L. Sheng, M. Chen, D. Huang, H. Zhang, C. Song, S. Chen, *New J. Chem.* **2013**, *37*, 274-277.
[65] H.-Y. Lin, P.-Y. Cheng, C.-F. Wan, A.-T. Wu, *Analyst* **2012**, *137*, 4415-4417.
[66] A. K. Mandal, M. Suresh, P. Das, E. Suresh, M. Baidya, S. K. Ghosh, A. Das, *Org. Lett.* **2012**, *14*, 2980-2983.
[67] Y.-Q. Sun, P. Wang, J. Liu, J. Zhang, W. Guo, *Analyst* **2012**, *137*, 3430-3433.
[68] I. B. Berlman, *Handbook of Fluorescence Spectra of Aromatic Molecules,* 2nd ed., Academic Press, New York, **1971**, 356.
[69] a) S. Rosenfeld, *J. Org. Chem.* **1993**, *58*, 7572-7575; b) H. Wolf, D. Leusser, R. V. J. Mads , R. Herbst-Irmer, Y.-S. Chen, E.-W. Scheidt, W. Scherer, B. B. Iversen, D. Stalke, *Chem.-Eur. J.* **2014**, *20*, 7048-7053.
[70] T. Inoue, T. Kaneda, S. Misumi, *Tetrahedron Lett.* **1974**, *15*, 2969-2972.
[71] a) J. E. Richman, T. J. Atkins, *J. Am. Chem. Soc.* **1974**, *96*, 2268-2270; b) T. J. Atkins, J. E. Richman, W. F. Oettle, *Org. Synth.* **1978**, *58*, 86-95.
[72] B. Altava, M. Isabel Burguete, B. Escuder, S. V. Luis, E. García-España, M. Carmen Muñoz, *Tetrahedron* **1997**, *53*, 2629-2640.
[73] R. C. Hoye, J. E. Richman, G. A. Dantas, M. F. Lightbourne, L. S. Shinneman, *J. Org. Chem.* **2001**, *66*, 2722-2725.
[74] M. I. Burguete, B. Escuder, E. García-España, S. V. Luis, J. F. Miravet, *Tetrahedron* **2002**, *58*, 2839-2846.
[75] T. J. Kealy, P. L. Pauson, *Nature* **1951**, *168*, 1039-1040.
[76] C. Elschenbroich, *Organometallchemie,* 6th ed., Teubner, Wiesbaden, **2008**, 452.
[77] T. Gunnlaugsson, A. P. Davis, J. E. O'Brien, M. Glynn, *Org. Biomol. Chem.* **2005**, *3*, 48-56.
[78] a) K. S. Peters, S. Gasparrini, L. R. Heeb, *J. Am. Chem. Soc.* **2005**, *127*, 13039-13047; b) I.-H. Um, S.-W. Min, J. M. Dust, *J. Org. Chem.* **2007**, *72*, 8797-8803; c) K. B. Jose, J. Cyriac, J. T. Moolayil, V. S. Sebastian, M. George, *J. Phys. Org. Chem.* **2011**, *24*, 714-719.
[79] S. M. Weinreb, C. E. Chase, P. Wipf, S. Venkatraman, *Org. Synth.* **1998**, *75*, 161-164.
[80] H. Jork, W. Funk, W. Fischer, H. Wimmer, *Physikalische und chemische Nachweismethoden: Grundlagen, Reagenzien I,* 1th corrected ed., VCH, Weinheim, **1990**.

[81] E. Lax, C. Synowietz, *Taschenbuch für Chemiker und Physiker,* 3rd ed., Springer, Berlin, Heidelberg, New York, **1967**, 375, 377, 449, 453.
[82] E. Pretsch, P. Bühlmann, M. Badertscher, *Spektroskopische Daten zur Strukturaufklärung organischer Verbindungen,* 5th ed., Springer, Heidelberg, Dordrecht, London, New York, **2010**, 424.
[83] S. Wandtke, *Fluoreszenzuntersuchungen an Anthracenderivaten,* Georg-August University Göttingen, Master thesis, **2011**.
[84] J. R. Lakowicz, *Principles of Fluorescence Spectroscopy,* 3rd ed., Springer, New York, **2006**, 57.
[85] M. Hesse, H. Meier, B. Zeeh, *Spektroskopische Methoden in der organischen Chemie,* 7th ed., Thieme, Stuttgart, New York, **2005**, 16-17.
[86] M. Shellaiah, Y.-H. Wu, A. Singh, M. V. Ramakrishnam Raju, H.-C. Lin, *J. Mat. Chem. A* **2013**, *1*, 1310-1318.
[87] K. Hirano, S. Urban, C. Wang, F. Glorius, *Org. Lett.* **2009**, *11*, 1019-1022.
[88] C. E. Braun, C. D. Cook, C. Merritt, J. E. Rousseau, *Org. Synth.* **1951**, *31*, 77-79.
[89] P. Rademacher, *Strukturen organischer Moleküle,* 1st ed., VCH, Weinheim, **1987**, 56.
[90] J. Clayden, N. Greeves, S. Warren, *Organic Chemistry,* 2nd ed., Oxford University Press, New York, **2012**, 144.
[91] N. J. Turro, V. Ramamurthy, J. C. Scaiano, *Modern Molecular Photochemistry of Organic Molecules,* 1st ed., University Science Books, Sausalito, **2010**, 301-302.
[92] F. A. Cotton, G. Wilkinson, C. A. Murillo, M. Bochmann, *Advanced Inorganic Chemistry,* 6th ed., John Wiley & Sons inc., New York, Chichester, **1999**, 187.
[93] T. T. Tidwell, *Angew. Chem.* **2008**, *120*, 1032-1036; *Angew. Chem. Int. Ed.* **2008**, *47*, 1016-1020.
[94] T. Steiner, *Angew. Chem.* **2002**, *114*, 50-80; *Angew. Chem. Int. Ed.* **2002**, *41*, 48-76.
[95] E. Pretsch, P. Bühlmann, M. Badertscher, *Spektroskopische Daten zur Strukturaufklärung organischer Verbindungen,* 5th ed., Springer, Heidelberg, Dordrecht, London, New York, **2010**, 208.
[96] Bruker, *Almanac 2014,* 1st ed., **2014**, T2.
[97] C. K. Bradsher, D. J. Beavers, *J. Org. Chem.* **1956**, *21*, 1067-1068.
[98] O. L. Chapman, K. Lee, *J. Org. Chem.* **1969**, *34*, 4166-4168.
[99] E. Riedel, *Anorganische Chemie,* 6th ed., Walter de Gruyter, Berlin, New York, **2004**, 105-107.
[100] T. C. Bruice, T. H. Fife, J. J. Bruno, N. E. Brandon, *Biochemistry* **1962**, *1*, 7-12.
[101] E. Müller, *Angew. Chem.* **1920**, *33*, 303-305.
[102] R. S. Cahn, C. Ingold, V. Prelog, *Angew. Chem.* **1966**, *78*, 413-447; *Angew. Chem. Int. Ed.* **1966**, *5*, 385-415.
[103] H. D. Flack, *Acta Cryst. A* **1983**, *39*, 876-881.
[104] A. F. Holleman, N. Wiberg, E. Wiberg, *Lehrbuch der Anorganischen Chemie,* 102th ed., Walter de Gruyter, Berlin, New York, **2007**, 672-673.
[105] H. Brintzinger, H. Erlenmeyer, *Helv. Chim. Acta* **1965**, *48*, 826-830.
[106] J. He, J. Zheng, J. Liu, X. She, X. Pan, *Org. Lett.* **2006**, *8*, 4637-4640.
[107] K. P. C. Vollhardt, N. E. Schore, *Organische Chemie,* 4th ed., WILEY-VCH, Weinheim, **2005**, 342.
[108] HORIBA, *FluoroMax-4 Spectrofluorometer Operation Manual,* **2006**, 2.2-2.6.

[109] R. Camenzind, B. Rickborn, *J. Org. Chem.* **1986**, *51*, 1914-1916.
[110] a) W. Schlenk, A. Thal, *Ber. Dtsch. Chem. Ges.* **1913**, *46*, 2840-2854; b) T. T. Tidwell, *Angew. Chem.* **2001**, *113*, 343-349; *Angew. Chem. Int. Ed.* **2001**, *40*, 331-337; c) Georg-August-University, *Virtuelles Labor*, www.stalke.chemie.uni-goettingen.de/virtuelles_labor/de.html, access at 11/8/2014.
[111] M. Czerny, A. F. Turner, *Z. Physik* **1930**, *61*, 792-797.
[112] HORIBA, *FluorEssence v3.0*, Edison, **2008**.
[113] S. Kao, A. N. Asanov, P. B. Oldham, *Instrum. Sci. Technol.* **1998**, *26*, 375-387.
[114] C. V. Raman, *Indian J. Phys.* **1928**, *2*, 387-398.
[115] M. Kasha, *Discuss. Faraday Soc.* **1950**, *9*, 14-19.
[116] J. F. Mammone, S. K. Sharma, M. Nicol, *J. Phys. Chem.* **1980**, *84*, 3130-3134.
[117] H. J. Svec, *Int. J. Mass Spectrom. Ion Processes* **1985**, *66*, 3-29.
[118] J. F. d. l. Mora, G. J. Van Berkel, C. G. Enke, R. B. Cole, M. Martinez-Sanchez, J. B. Fenn, *J. Mass Spectrom.* **2000**, *35*, 939-952.
[119] W. P. Aue, E. Bartholdi, R. R. Ernst, *J. Chem. Phys.* **1976**, *64*, 2229-2246.
[120] G. Bodenhausen, D. J. Ruben, *Chem. Phys. Lett.* **1980**, *69*, 185-189.
[121] A. Bax, M. F. Summers, *J. Am. Chem. Soc.* **1986**, *108*, 2093-2094.
[122] a) H. Hope, *Acta Cryst. B* **1988**, *44*, 22-26; b) T. Kottke, D. Stalke, *J. Appl. Cryst.* **1993**, *26*, 615-619; c) D. Stalke, *Chem. Soc. Rev.* **1998**, *27*, 171-178.
[123] Bruker AXS Inc., *APEX2 v2012/2*, WI, USA, Madison, **2012**.
[124] Bruker AXS Inc., *SAINT v8.30C*, WI, USA, Madison, **2013**.
[125] G. M. Sheldrick, *SADABS 2014/1*, Göttingen, **2014**.
[126] G. M. Sheldrick, *XPREP in SHELXTL 2014/2*, WI, USA, Madison, **2014**.
[127] G. M. Sheldrick, *Acta Cryst. A* **2014**, *70*, C1437.
[128] G. M. Sheldrick, *Acta Cryst. A* **2008**, *64*, 112-122.
[129] C. B. Huebschle, G. M. Sheldrick, B. Dittrich, *J. Appl. Cryst.* **2011**, *44*, 1281-1284.
[130] R. Srinivasan, N. R. Jagannathan, *Acta Cryst. B* **1982**, *38*, 2093-2095.

7 Curriculum Vitae

Personal Data

Name	Sebastian Wandtke
Date of birth	04.10.1985
Place of birth	Zweibrücken
Address	Weißdornweg 8
	37077 Göttingen, Germany
Phone number	+49 551 2006301
Email address	Sebastian_Wandtke@web.de
Nationality	German
Marital status	married with Claudia Wandtke

School, Scholastics and Ph.D.

11/2011 – today	Ph.D. thesis "*Anthracene Based Colorimetric Molecular Sensors*" in charge of Prof. Dr. Stalke at the Institute of Inorganic Chemistry Georg-August-University Göttingen, within the Ph.D. program Georg-August-University School of Science (GAUSS)
10/2009 – 09/2011	**Master of Science in Chemistry at Georg-August-University Göttingen;** M. Sc. degree, final mark 1.2, predicate "with honors"
03/2011 – 09/2011	Master's thesis "*Fluoreszenzuntersuchungen an Anthracenderivaten*" in charge of Prof. Dr. Stalke (mark 1.0)
10/2006 – 08/2009	**Bachelor of Science in Chemistry at Georg-August-University Göttingen;** B. Sc. degree, final mark 1.9
04/2009 – 08/2009	Bachelor's thesis "*Bis(dimethylamino)anthracenylphosphane und –phosphorane*" in charge of Prof. Dr. Stalke (mark 1.0)
06/2006 – 08/2006	Social internship at the Christian guesthouse MZ Hanstedt 1; mainly manual and accompanying activities
09/2005 – 05/2006	Community service the Christian guesthouse MZ Hanstedt 1
09/1998 – 06/2005	**Abitur at the Gymnasium Winsen/Luhe**; equivalent to A-level, final mark 2.0

Experience in University

03/2011 – today	**Scientific researcher** In charge of Prof. Dr. Stalke at the Institute of Inorganic Chemistry Georg-August-University, Göttingen
10/2009 – today	**Non-independent teaching of undergraduates** • Supervision and organization of practical and theoretical lab work of main subject chemistry students • Tutor for first year main subject chemistry students as well as minor subject chemistry students as part of their Bachelor of Science

Personal Skills

Languages	German, native English, fluent
Computer applications	Advanced knowledge in crystallographic programs (Bruker APEXII, SHELXTL, ShelXle, Mercury) Advanced knowledge in office programs (MS Word, MS Excel, MS Powerpoint) Advanced knowledge in chemistry referred programs (Chemdraw, MestreNova, Origin)
Expertise	According to §5 Chemikalienverbotsordnung
Management skills	Workshop: *Führungsexzellenz durch Diversity Management*

Personal Interests and Voluntary Activities

Table Tennis

08/2010 – 08/2012	Team captain of the 2nd men's team ESV Rot-Weiß Göttingen
1995 - today	Practice and competition matches in the sports clubs MTV Pattensen, TSV Auetal and ESV Rot-Weiß Göttingen

Christian Campus Group

2009 – today	Member of the planning and realization team
2008 – today	Regular participation in church services and events

Congress and Workshop Participation

- **9th Workshop of Center for Materials Crystallography**, 09. – 10.10.2014 in Aarhus, Denmark (participation)

- **8th Workshop of Center for Materials Crystallography**, 27.03.2014 in Göttingen, Germany (participation)

- **Central European Conference on Photochemistry 2014**, 09. – 13.02.2014 in Bad Hofgastein, Austria (poster presentation: *Fluorescence Sensing Properties of 9-Anthraceneimines*)

- **Midterm Review Center for Materials Crystallography**, 27. – 28.06.2013 in Aarhus, Denmark (poster presentation: *A New Combination: Anthracene Fluorophore and C=N-Isomerization)*

- **6th Chemie-Forum**, **Jungchemiker-Forum**, 05.06.2013 in Göttingen, Germany (poster presentation: *9-Anthracenesalicylimine and 9-Anthracenepicolylimine as Potential Fluorescence Chemosensors*)

- **6th Workshop of Center for Materials Crystallography**, 22.11.2012 in Göttingen, Germany (participation)

- **4th Workshop of Center for Materials Crystallography**, 10. – 11.11.2011 in Göttingen, Germany (participation)